2012

Efficacy and Mechanistic Evaluation of Tic10, A Novel Antitumor Agent

Joshua Edward Allen
University of Pennsylvania, joshjea@gmail.com

Efficacy and Mechanistic Evaluation of Tic10, A Novel Antitumor Agent

Abstract

TNF-related apoptosis-inducing ligand (TRAIL; Apo2L) is an endogenous protein that selectively induces apoptosis in cancer cells and is a critical effector in the immune surveillance of cancer. Recombinant TRAIL and TRAIL-agonist antibodies are in clinical trials for the treatment of solid malignancies due to the cancer-specific cytotoxicity of TRAIL. Recombinant TRAIL has a short serum half-life and both recombinant TRAIL and TRAIL receptor agonist antibodies have a limited capacity to perfuse to tissue compartments such as the brain, limiting their efficacy in certain malignancies. To overcome such limitations, we searched for small molecules capable of inducing the TRAIL gene using a high throughput luciferase reporter gene assay. We selected TRAIL-inducing compound 10 (TIC10) for further study based on its induction of TRAIL at the cell surface and its promising therapeutic index. TIC10 is a potent, stable, and orally active antitumor agent that crosses the blood-brain barrier and transcriptionally induces TRAIL and TRAIL-mediated cell death in a p53-independent manner. TIC10 induces a sustained upregulation of TRAIL in tumors and proximal cells that may contribute to the antitumor activity of TIC10 through a bystander effect. Expression profiling of TIC10-induced transcriptional changes revealed changes in FOXO target genes. We found that Foxo3a undergoes a TIC10-induced nuclear translocation, binds to the TRAIL gene promoter in response to TIC10, and is responsible for TIC10-induced cell death and TRAIL production in vitro and in vivo. TIC10 activates Foxo3a through the dual inactivation of Akt and ERK, which normally phosphorylate and inactivate Foxo3a. The induction of TRAIL by TIC10 can be recapitulated using pharmacological inhibitors of Akt and ERK signaling pathways or siRNA. These mechanistic data provide a clear therapeutic strategy for targeting the TRAIL gene and suggest that Foxo3a-mediated TRAIL induction is responsible for the synergy between PI3K/Akt and MAPK pathway inhibitors. TIC10 is a potentially first-in-class antitumor therapy that utilizes the tumor microenvironment to produce TRAIL, acts as a pharmacological delivery vehicle to improve the therapeutic properties of TRAIL, and highlights Foxo3a activation as an attractive opportunity to induce TRAIL-mediated apoptosis that can be harnessed through dual inhibition of the MAPK and PI3K/Akt pathway.

Degree Type

Dissertation

Degree Name

Doctor of Philosophy (PhD)

Graduate Group

Biochemistry & Molecular Biophysics

First Advisor

Wafik S. El-Deiry

Keywords

Foxo3a, small molecule, targeted therapy, TIC10, TRAIL

Subject Categories

Oncology

EFFICACY AND MECHANISTIC EVALUATION OF TIC10,

A NOVEL ANTITUMOR AGENT

Joshua E. Allen

A DISSERTATION

in

Biochemistry and Molecular Biophysics

in

Partial Fulfillment of the Requirements for the

Degree of Doctor of Philosophy

2012

Supervisor of Dissertation:

_____

Wafik S. El-Deiry, M.D. Ph.D.
Adjunct Professor of Medicine
Rose Dunlap Professor and Chief, Hematology/Oncology, Penn State Hershey Medical Center

Graduate Group Chairperson:

_____

Kathryn M. Ferguson, Ph.D.
Associate Professor, Physiology

Dissertation Committee:

Trevor Penning, Ph.D., Professor, Pharmacology

Charles Abrams, M.D., Professor and Associate Chief, Hematology-Oncology

Ronen Marmorstein, Ph.D., Professor, Wistar Institute

Xiaolu Yang, Ph.D., Professor, Cancer Biology

DEDICATION

To my mother who inspired me to pursue this career path and to relentlessly persevere.

ACKNOWLEDGMENTS

I thank my advisor, Wafik El-Deiry, for his enduring support and the opportunities that he has provided me to form the foundation of my career. I would also like to thank all of my previous mentors and teachers throughout my education, as each step has been essential in allowing me to become who I am today. I thank the past and present members of the El-Deiry lab, particularly Dave, who have made my journey possible and pleasant. I would also like to thank Nicole, my family, and my friends who keep my days bright. I would also like to thank my thesis committee members for their feedback and enlightening perspectives.

ABSTRACT

EFFICACY AND MECHANISTIC EVALUATION OF TIC10, A NOVEL ANTITUMOR AGENT

Joshua E. Allen

Wafik S. El-Deiry, M.D. Ph.D.

TNF-related apoptosis-inducing ligand (TRAIL; Apo2L) is an endogenous protein that selectively induces apoptosis in cancer cells and is a critical effector in the immune surveillance of cancer. Recombinant TRAIL and TRAIL-agonist antibodies are in clinical trials for the treatment of solid malignancies due to the cancer-specific cytotoxicity of TRAIL. Recombinant TRAIL has a short serum half-life and both recombinant TRAIL and TRAIL receptor agonist antibodies have a limited capacity to perfuse to tissue compartments such as the brain, limiting their efficacy in certain malignancies. To overcome such limitations, we searched for small molecules capable of inducing the TRAIL gene using a high throughput luciferase reporter gene assay. We selected TRAIL-inducing compound 10 (TIC10) for further study based on its induction of TRAIL at the cell surface and its promising therapeutic index. TIC10 is a potent, stable, and orally active antitumor agent that crosses the blood-brain barrier and transcriptionally induces TRAIL and TRAIL-mediated cell death in a p53-independent manner. TIC10 induces a sustained upregulation of TRAIL in tumors and proximal cells that may contribute to the antitumor activity of TIC10 through a bystander effect. Expression profiling of TIC10-induced transcriptional changes revealed changes in FOXO target genes. We found that Foxo3a undergoes a TIC10-induced nuclear translocation, binds to the TRAIL gene promoter in response to TIC10, and is responsible for TIC10-induced cell death and TRAIL production in vitro and in vivo. TIC10 activates Foxo3a through the dual inactivation of Akt and ERK, which normally phosphorylate and inactivate Foxo3a. The induction of TRAIL by TIC10 can be recapitulated using pharmacological inhibitors of Akt and ERK signaling pathways or siRNA. These mechanistic data provide a clear therapeutic

strategy for targeting the TRAIL gene and suggest that Foxo3a-mediated TRAIL induction is responsible for the synergy between PI3K/Akt and MAPK pathway inhibitors. TIC10 is a potentially first-in-class antitumor therapy that utilizes the tumor microenvironment to produce TRAIL, acts as a pharmacological delivery vehicle to improve the therapeutic properties of TRAIL, and highlights Foxo3a activation as an attractive opportunity to induce TRAIL-mediated apoptosis that can be harnessed through dual inhibition of the MAPK and PI3K/Akt pathway.

TABLE OF CONTENTS

APPENDICES

List of Figures:

CHAPTER 1:

CHAPTER 2:

CHAPTER 3:

CHAPTER 1

INTRODUCTION

1.1 TRAIL Biology

Overview

TNF-related apoptosis-inducing ligand (TRAIL) was initially identified by its sequence homology with other Tumor Necrosis Factor (TNF) family members (Pitti et al., 1996; Wiley SR, 1995). At physiological conditions, TRAIL is capable of binding to four distinct transmembrane receptors in humans: the proapoptotic receptors DR4 and DR5 or the two decoy receptors DcR1 and DcR2. Both TRAIL and its receptors form homotrimers in complex upon binding (Cha et al., 1999; Hymowitz et al., 1999). In mice, TRAIL-R is the only cognate death receptor (Wu et al., 1999). TRAIL also binds two decoy receptors, DcR1 (Degli-Esposti et al., 1997b; Mongkolsapaya et al., 1998; Pan et al., 1997a) that lacks an intracellular domain and DcR2 (Degli-Esposti et al., 1997a; Marsters et al., 1997; Pan et al., 1998) which contains a truncated intracellular domain. The two decoy receptors compete for TRAIL binding with the death receptors with similar binding affinities (Degli-Esposti et al., 1997a; Degli-Esposti et al., 1997b). Additionally, TRAIL binds the soluble receptor osteoprotegerin that negatively regulates osteoclastogenesis and bone resorption, though the interaction is much weaker than that of the other TRAIL receptors (Emery et al., 1998).

TRAIL has received considerable attention, primarily due to its apoptosis-inducing capability demonstrated in several human cancer cell lines (Walczak et al., 1997). TRAIL is expressed in a variety of human fetal and adult tissues including spleen, thymus, prostate, small intestine, and placenta (Wiley SR, 1995). Contrary to other TNF-family members, membrane-bound TRAIL is conditionally expressed in immunological cells such as natural killer (NK) cells, B cells, monocytes, and dendritic cells following cytokine stimulation (Fanger et al., 1999; Griffith et al., 1999; Kemp et al., 2004; Zamai et al., 1998). Intracellular stores of TRAIL have also been found in polymorphonuclear neutrophils (Cassatella et al., 2006; Kemp et al., 2005; Koga et al., 2004; Ludwig et al., 2004; Tecchio et al., 2004) which are released after a variety of stimuli (Kemp et al., 2005; Simons et al., 2008; Simons et al., 2007).

The X-ray crystallographic structures of trimeric soluble TRAIL revealed a single zinc atom bound between the three monomers that is important for the integrity and activity of TRAIL

(Bodmer et al., 2000; Cha et al., 1999; Eimon et al., 2006; Hymowitz et al., 1999; Mongkolsapaya et al., 1999). Upon binding TRAIL, the two human proapoptotic death receptors DR4 (Pan et al., 1997a) and DR5 (MacFarlane et al., 1997; Pan et al., 1998; Pan et al., 1997d; Walczak et al., 1997; Wu et al., 1997) initiate cell death signaling through colocalization of their intracellular death domains (DD) that occurs after ligand binding (Tartaglia et al., 1993).

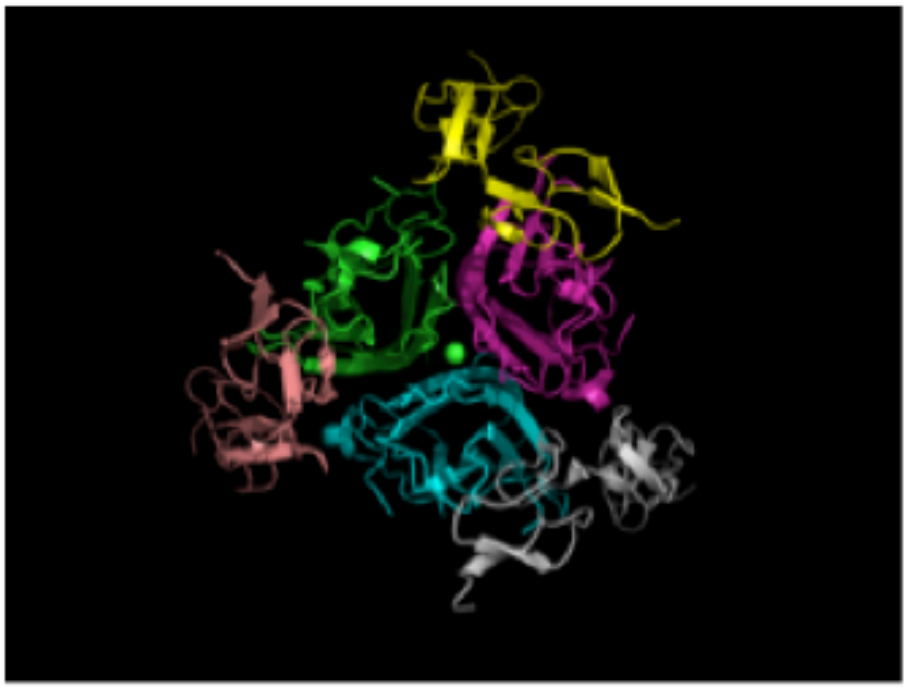

Figure 1.1. Crystal structure of TRAIL:DR5 complex. Homotrimeric DR5 (grey, light pink, and yellow) bound to homotrimeric TRAIL (cyan, green, and magenta). Zinc atom (green) is displayed in the center of the complex. Figure was generated by Joshua Allen using PyMOL software with Protein Data Bank (PBD) accession number 1D4V (Mongkolsapaya et al., 1999).

TRAIL signaling

TRAIL binding to DR4 or DR5 also triggers the internalization of the receptor:ligand complex by dynamin-mediated endocytosis and can attenuate TRAIL signaling (Austin et al., 2006; Kohlhaas et al., 2007). Following ligand binding, the colocalized DDs of DR4 or DR5 recruit Fas-associated death domain (FADD) and procaspase-8 to form the death inducing signaling complex (DISC). Caspase-10 is also recruited to this DISC and is activated at the same rate as caspase-8 (Kischkel et al., 2001; Sprick et al., 2002; Wang et al., 2001). Mice lack a homologue of caspase-10, suggesting that caspase-8 and caspase-10 may be functionally redundant. However, the ability of these two caspases to substitute for each other in TRAIL-mediated apoptosis in mammalian cells is unclear due to conflicting reports. The anti-apoptotic protein cellular FLICE-like inhibitory protein (c-FLIP) can also be recruited to DISC to inhibit binding activation of caspase-8 and -10 by directly competing for binding to FADD (Micheau et al., 2002; Thome and Tschopp, 2001).

At the DISC, procaspase-8 is activated by autocatalytic cleavage to yield caspase-8, which can cleave the effector caspases-3, -6, and -7 to induce apoptosis by the intrinsic death pathway. Cells that undergo cell death via this pathway are known as type I cells. Activation of caspase-8 in type II cells, however, is not sufficient to trigger the caspase cascade. In type II cells, caspase-8 cleaves Bid to form tBid, which primarily interacts with Bax and Bak at the mitochondrial membrane to promote cytochrome c release (Li et al., 1998; Luo et al., 1998). In the cytosol, cytochrome c binds to apoptotic peptidase activating factor 1 (Apaf-1) and caspase -9 to form the apoptosome, which initiates the caspase cascade. Permeabilization of the mitochondrial membrane also releases Smac/DIABLO, which inhibits X-linked inhibitor of apoptosis protein (XIAP) to allow for complete activation of the effector caspases (Albeck et al., 2008; Jost et al., 2009; Maas et al., 2010; Sun et al., 2002).

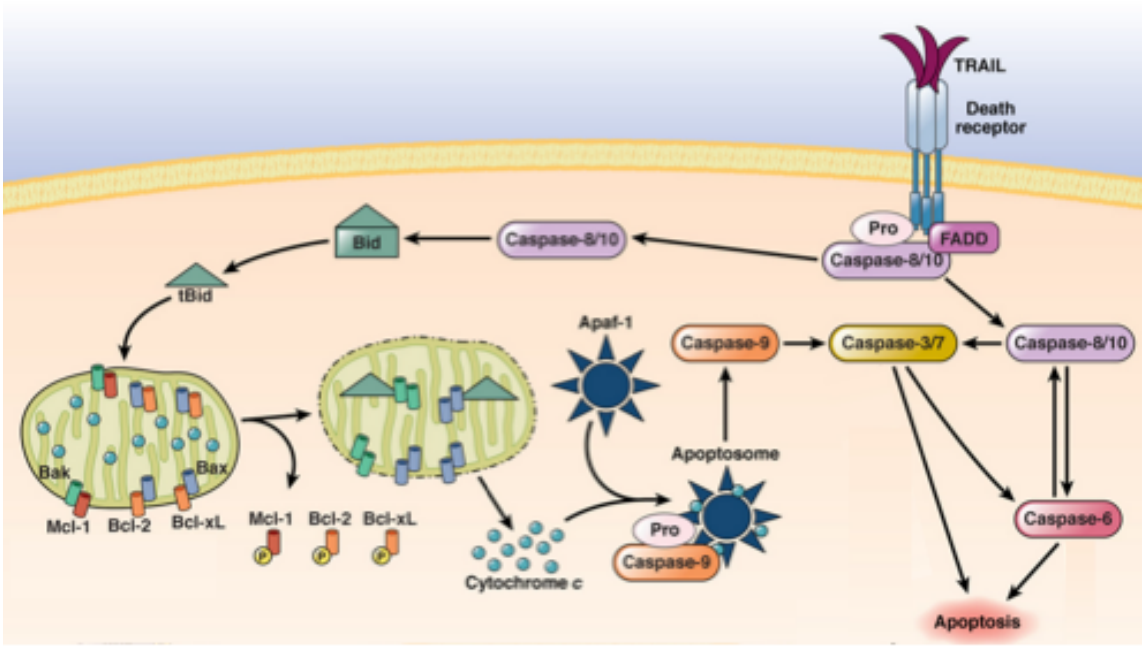

Figure 1.2. Apoptotic signaling induced by TRAIL. TRAIL initiates cell death by binding to the proapoptotic death receptors DR4 or DR5 that colocalizes their intracellular death domains. This clustering recruits the Fas-associated death domain (FADD) and pro-caspase-8 that results in its activation through autocatalytic cleavage. In type II cells, active caspase-8 cleaves Bid to a truncated form, tBID, which subsequently interacts with proapoptotic Bcl-2 family members Bax and Bak. This interaction leads to permeabilization of the mitochondrial membrane and release of cytochrome c. Cytosolic cytochrome c then combines with Apaf-1 and ATP to form the apoptosome that activates caspase-9 to trigger apoptosis through the caspase cascade. The stress-activated kinase JNK can phosphorylate the antiapoptotic Bcl-2 family members such as Bcl-xL to dissociate their interactions with the proapoptotic Bcl-2 family members Bax and Bak. These previously sequestered proapoptotic proteins are then free to oligomerize and porate the mitochondrial membrane to induce apoptosis. Figure was adapted with permission from the publisher (Elsevier) (Allen and El-Deiry, 2011).

Cancer cell mechanisms of resistance to TRAIL

While many cancer cells are sensitive to TRAIL, there are a significant number of cancer cell lines that are resistant to TRAIL-mediated cell death. Mechanisms of TRAIL resistance and sensitization through combinatorial therapy have been intensely studied because of the impetus to develop recombinant human TRAIL (rhTRAIL) as an antitumor agent. The most obvious mechanism of resistance is downregulation of the proapoptotic receptors, which has been described in head and neck cancer and small cell lung cancer. The El-Deiry lab found that tumor cell lines with evolved resistance to rhTRAIL downregulated surface DR4 and DR5, though the total cellular expression level was unchanged (Jin et al., 2004). Mutations in the DR5 gene have also been noted in its death domain in head and neck cancer (Pai et al., 1998), metastatic breast cancer (Shin et al., 2001), NSCLC (Lee et al., 1999), and non-Hodgkin's lymphoma (Lee et al., 2001). Upregulation of decoy receptors has also been proposed as a culprit in some settings: DcR1 in gastrointestinal tract tumors (M Saeed Sheikh, 1999), DcR2 in human breast cancer cell lines (Sanlioglu et al., 2005) and human lung and prostate tumor cells (Aydin et al., 2007; Sanlioglu et al., 2007). The ratio of DR4 to DcR1 and DcR2 has also been linked to TRAIL sensitivity in primary tumor cells (C Büneker, 2009). However, given that TRAIL signaling involves many molecules that can transduce, amplify, or inhibit apoptotic signaling it is perhaps unsurprising that TRAIL receptor expression levels alone are insufficient to explain TRAIL sensitivity in most cases (Griffith and Lynch, 1998; Lincz et al., 2001).

Aside from c-FLIP that confers resistance at the receptor level, several downstream regulators of apoptosis have been identified as potent determinants of TRAIL sensitivity. Of particular importance is the Bcl-2 family of proteins that regulator mitochondrial-mediated cell death and contain pro-apoptotic (Bax, Bak, Bad, and Bok) and anti-apoptotic (Bcl-2, Bcl-XL Mcl-1, and Bcl-w). The pro-apoptotic Bcl-2 family members induce cell death by oligomerization, which causes pores in the mitochondrial membrane, leading to cytochrome-c release and eventually caspase-mediated apoptosis. Accordingly, downregulation of pro-apoptotic Bcl-2 members such as Bax (Burns and El-Deiry, 2001) or upregulation of anti-apoptotic members

such as Bcl-2 (Meng et al., 2007; Sun et al., 2001) have been sufficient to cause cancer cell resistance to TRAIL. Other proteins that inhibit apoptosis such cIAP, XIAP, and survivin have also been identified as important regulators of TRAIL sensitivity (Chawla-Sarkar et al., 2004; Cummins et al., 2004).

A more recently described mechanism of modulating TRAIL sensitivity is post-translation modifications to DR4 and DR5 such as glycosylation and palmitoylation. Enzymes involved in O-linked glycosylation such as GALNT14, GALNT3, FUT3, and FUT6 have been strongly correlated with TRAIL sensitivity in several cancer cell lines (Wagner et al., 2007). Biochemical analysis of DR5 provided direct evidence that this glycosylation event increases sensitivity to TRAIL-mediated cell death. Such post-translational modification appears to be specific to TRAIL receptors rather than other receptors of the TNF family such as Fas. The unique glycosylation sites in the extracellular domains of DR4 and DR5 that are not shared by other family members may explain this. N-linked glycosylation appears to also affect DR4 at a unique site that is not conserved in DR5 (Pan et al., 1997a; Sheridan et al., 1997; Yoshida et al., 2007). DR4 is also palmitoylated at three intracellular sites that results in inhibition of signaling through the extrinsic death pathway (Rossin et al., 2009).

Nevertheless, TRAIL induces rapid apoptosis in several solid and hematological malignant cell lines as a monotherapy (Ashkenazi et al., 1999b; Gazitt, 1999; Kelley et al., 2001; Marini et al., 2005; Pollack et al., 2001) and in combination with chemotherapy and radiotherapy whit enhances antineoplastic efficacy (Chinnaiyan et al., 2000; Gliniak and Le, 1999; Keane et al., 1999a; Keane et al., 1999b; Mizutani et al., 1999; Nimmanapalli et al., 2001). This therapeutic synergy may be due to upregulation of p53 in response to chemotherapy and radiation, which induces DR4 and DR5 expression (El-Deiry, 2000; Liu et al., 2004).

Non-apoptotic TRAIL signaling

The notion that cancer cells are more sensitive to TRAIL, a tumor suppressor that is a pro-apoptotic ligand, is counterintuitive as the genesis and progression of cancer typically involves loss of function associated with tumor suppressors. While this disparity is still unclear, it seems

that in certain settings TRAIL signaling can be converted to prosurvival signaling through mechanisms that involve IKK, JNK, and p38 MAPK. Among these events, IKK-mediated activation of NFκB is the most reported alternative signaling pathway triggered by TRAIL stimulation. Signal transduction through this axis involves an association of receptor-interacting protein-1 (RIP1), TNF receptor-associated factor 2 (TRAF2), NF-kappa-B essential modulator (NEMO), TNF-R1-associated death domain (TRADD), and caspase-10 into a complex called Complex II (Jin and El-Deiry, 2006; Varfolomeev et al., 2005). Formation of Complex II is dependent on FADD and caspase-8, though these proteins are not associated with the complex. Within Complex II, NEMO appears to activate IKK whereas RIP1 and TRAF2 are important for activating JNK and p38 MAPK (Lin et al., 2000).

While the functional significance or physiological relevance of activating of these prosurvival signaling pathways by TRAIL stimulation is still under investigation, the phenomenon has been described for other TNF family members. Some reports found that inactivation of NFκB sensitizes cells to TRAIL-mediated cell death (Beraza et al., 2009; Lluis et al., 2010; Luo et al., 2004), which supports the notion that NFκB activation acts as a negative feedback to dampen proapoptotic signaling induced by TRAIL. Alternatively, NFκB inactivation has been reported to decrease sensitivity to TRAIL in certain cell types (Chen et al., 2003; Ou et al., 2005) and NFκB activation can also recruit phagocytes through upregulation of chemokines (Varfolomeev et al., 2005). TRAIL has also been reported to induce autophagy in certain cells types (Han et al., 2008; Herrero-Martin et al., 2009; Hou et al., 2008; Mills et al., 2004; Park et al., 2007) and DR5 has been linked to anoikis (Laguinge et al., 2008; Samara et al., 2007), a form of programmed cell death that involves detachment of adherent cells.

Physiological roles for TRAIL

TRAIL is expressed on the surface of immune effector cells such as natural killer cells, macrophages, dendritic cells, and cytotoxic T-cells in response to cytokines, in particular interferon-gamma that contains a response element in the TRAIL gene promoter (Gong and Almasan, 2000). TRAIL-knockout mice or zebrafish do not display any gross developmental

defects (Cretney et al., 2002; Eimon et al., 2006), though the mice are more susceptible to carcinogen-induced sarcomas and metastasis (Cretney et al., 2002). TRAIL-knockout mice also do not induce thymocyte apoptosis, which is deregulated in autoimmune diseases (Lamhamedi-Cherradi et al., 2003). Clinical observations have also suggested a role for TRAIL in autoimmune diseases; patients with systemic lupus erythmatosus or multiple sclerosis have elevated serum levels of soluble TRAIL (Lub-de Hooge et al., 2005; Wandinger et al., 2003). TRAIL has also been implicated in cardiovascular problems such as atherosclerosis (Michowitz et al., 2005; Schoppet et al., 2006) and diabetes (Corallini et al., 2007). The El-Deiry lab also created the first TRAIL-R knockout mouse that developed normally but had an enlarged thymus and decreased radiation-induced apoptosis in several tissues (Finnberg et al., 2005).

1.2 TRAIL-based Therapies as Antitumor Agents

Overview

Due to the potent and cancer-selective apoptotic activity of TRAIL, rhTRAIL has been intensely studied and developed for use as a novel treatment for human cancer. Most studies have found TRAIL to have no effects on normal cells, which boded well for the safety profile of rhTRAIL. Concerns were raised when reports surfaced that rhTRAIL induced cell death in hepatocytes, though this was later found to likely be specific to the version and preparation of a particular His-tagged rhTRAIL (Higuchi et al., 2002; Jo et al., 2000; Lawrence et al., 2001; Walczak et al., 1999b). Various forms of rhTRAIL have been described with a polyhistidine tag (Pitti et al., 1996), Flag tag (Pascal, 2000), leucine zipper (Ganten et al., 2006; Walczak et al., 1999a), or isoleucine zipper. Comparisons of these preparations suggested that leucine or isoleucine zipper rhTRAIL was effective and was not toxic to hepatocytes (Ganten et al., 2006). rhTRAIL was found to be safe in cynomolgous monkeys and have a terminal plasma half-life of approximately 30 minutes (Ashkenazi et al., 1999a). Non-human primates were used in these safety studies as rodents are resistant to the toxicity of TNF, which is in the same family of proteins as TRAIL. A phase I study with intravenous rhTRAIL in humans reported no dose-limiting toxicities, 17/32

patients with stable disease, and one patient with a chondrosarcoma had a partial response (Herbst et al., 2006; Herbst et al., 2010a).

Several TRAIL-receptor agonist antibodies have been developed that target either DR4 or DR5 with benefits of having longer serum half-lives and the absence of binding to the decoy receptors, DcR1 and DcR2. Human Genome Sciences has developed two pro-apoptotic death receptor agonist antibodies: lexatumumab and mapatumumab that target DR5 and DR4, respectively. These antibodies exhibited a promising spectrum of activity in preclinical studies and are currently in clinical trials in several settings.

Lexatumumab

Lexatumumab is one of the most developed DR5-agonist antibodies. A phase I study with lexatumumab given as a single intravenous dose every 21 days in previously treated advanced solid malignancies reported a maximum-tolerated dose (MTD) of 10 mg/kg. The terminal serum half-life was reported as ~16 days and roughly a third of enrolled patients experienced stable disease (Plummer et al., 2007). Another phase I study reported 10 mg/kg lexatumumab to be safe at a more frequent interval of one dose every 14 days (Wakelee et al., 2010).

As with rhTRAIL, several preclinical studies have suggested the use of lexatumumab in combination with other therapies to increase efficacy such as lapatinib (Dolloff et al., 2011) radiation (Marini et al., 2006), paclitaxel (Gong et al., 2006), bortezomib (Luster et al., 2009; Saulle et al., 2007; Smith et al., 2007), HDAC inhibitors (Nawrocki et al., 2007), doxorubicin (Wu et al., 2007), and cisplatin (Wu and Kakehi, 2009). Phase Ib studies evaluated lexatumumab in combination with gemcitabine, pemetrexed, doxorubicin, or FOLFIRI (B. I. Sikic, 2007). Tumor regression was noted in patient cohorts receiving the combination of lexatumumab and doxorubicin or FOLFIRI. Severe adverse events were noted, with anemia, fatigue, and dehydration cited as potentially attributable to lexatumumab among the combined therapies.

Conatumumab

Conatumumab (AMG 665) is a fully humanized agonist antibody against DR5 that has been developed by Amgen. (Kaplan-Lefko et al., 2010). A link between the increase in serum caspase-3/7 activity and M30 level, a keratin cleavage product, in the activation of the extrinsic apoptotic pathway by conatumumab in a preclinical cancer model, which could be used as cell death biomarkers (Kaplan-Lefko et al., 2010). A first-in-man study with conatumumab reported no dose-limiting toxicity (DLT) when administered at 20 mg/kg once every 14 days. This safety was corroborated with the same dosing schedule in Japanese patients (Doi et al., 2011). No maximum tolerated dose was reached but there were tumor reduction seen in a few patients receiving 0.3 mg/kg, which including NSCLC and colorectal cancer (Herbst et al., 2010b). An interim analysis of a phase Ib/II study combining conatumumab with panatumumab in metastatic colorectal cancer reported safety but no sign of efficacy in that setting. Another phase Ib/II study combining conatumumab and doxorubicin in advanced unresectable soft tissue sarcomas also reported safety but no additional efficacy over doxorubicin alone (Demetri et al., 2012). Encouragingly, a recent report found that conatumumab in combination with FOLFIRI significantly increased progression-free survival (PFS) and objective response rate compared FOLFIRI combined with placebo or the type I IGF receptor antagonist antibody ganitumab (Cohn et al., 2012).

Drozitumab

Drozitumab (Apomab, PRO95780) is another DR5-agonist antibody developed by Genentech that exhibited activity in preclinical models including rhabdomyosarcoma (Adams et al., 2008; Kang et al., 2011). The first phase I study reported safety at up to 20 mg/kg given once every 14 days and a terminal serum half-life of ~9 to 19 days (Camidge et al., 2007). A phase Ib with drozitumab and first-line FOLFOX plus bevacizumab in patients with metastatic CRC reported that the combination was well tolerated and no adverse interactions were found between drozitumab and the chemotherapy (C. S. Rocha Lima, 2011). In another phase Ib study, drozitumab was combined with cetuximab plus irinotecan or with FOLFIRI with or without bevacizumab in previously treated metastatic CRC patients. This trial also reported no adverse interactions between drozitumab and the chemotherapy (A. D. Baron, 2011).

Mapatumumab

Mapatumumab (HGS-ETR1) is the only DR4-targeted antibody currently in clinical trials. Mapatumumab exhibited preclinical antitumor activity against several cancer cell lines but no objective response was found when used as a single agent in a phase I study [14]. Most studies showed that TRAIL-receptor agonist antibodies are not very effective when used as monotherapy in patients with gastrointestinal (GI) cancer. Combining TRAIL with other therapeutic agents may overcome resistance mechanisms, such as combination of TRAIL-based therapies with c-FLIP inhibitors or the multi-kinase inhibitor sorafenib, which downregulates Bcl-xL, cIAP2, and Mcl1 (Ricci et al., 2007). Mapatumumab has been studied in three phase II trials that included patients with non-Hodgkin's lymphoma (NHL), colorectal cancer, and NSCLC (Greco et al., 2008) (Trarbach et al., 2010). No dose limiting toxicity was noted in these studies and clinical response or stable disease was observed in 14 or 17 patients with follicular NHL. Mapatumumab has also demonstrated clinical efficacy in combination with gemcitabine and cisplatin (Mom et al., 2009) as well as paclitaxel and carboplatin (Leong et al., 2009). In collaboration with Anaphore, we have been involved in the development of DR4-agonist Atrimers, which are trimeric peptide scaffolds engineered to mimic the natural ligand TRAIL, that demonstrate promising preclinical efficacy and safety (Allen et al. manuscript submitted, 2012).

TRAIL delivery by gene therapy

An alternative therapeutic method of overcoming limitations of rhTRAIL is using gene delivery methods such as adenoviruses to deliver the antitumor protein. Ad5-TRAIL is a replication-deficient adenovirus that encodes for the human TRAIL gene and has demonstrated efficacy in preclinical models of prostate cancer (Griffith and Broghammer, 2001). Several preclinical studies have demonstrated the utility of overexpressing the TRAIL gene by viral methods and have also noted bystander effects by normal cells that cause tumor-specific cell death (He et al., 2004; Lee et al., 2002). Interestingly, one study found that adenoviral TRAIL has a greater spectrum of activity than soluble TRAIL (Seol et al., 2003). The problem of delivering TRAIL across the blood-

brain barrier has also been overcome in preclinical studies by using viral-mediated overexpression of TRAIL on mesenchymal stem cells that migrate toward gliomas (Sasportas et al., 2009).

1.3 Regulation of the human TRAIL Gene

The TRAIL gene is tightly regulated, potentially due to its considerable apoptotic potential and its involvement in some immune responses. The first report to clone the TRAIL gene promoter characterized a ~1.6kB promoter region, which is 97 bp upstream of the start of translation (Wang et al., 2000). This report identified several putative transcription factor binding sites in the TRAIL gene promoter: NHF3, GKLF, AP-1, CEBP, NFAT, GATA, and Inteferon-γ-activated sequence (GAS), GSP1, GSP2, and GSP4. Sequential deletions of the human TRAIL gene promoter driving luciferase reporters in Caco-2 cells suggested that the regions between -1371 to -819 and -165 to -35 contain key elements that are responsible for basal TRAIL transcriptional activity. TRAIL gene transcription has been reported to respond to several transcription factors, cytokines, and small molecules (Figure 1.3) and in some cases have been mapped to transcription factors with consensus binding sequences found in the TRAIL gene promoter (Figure 1.4).

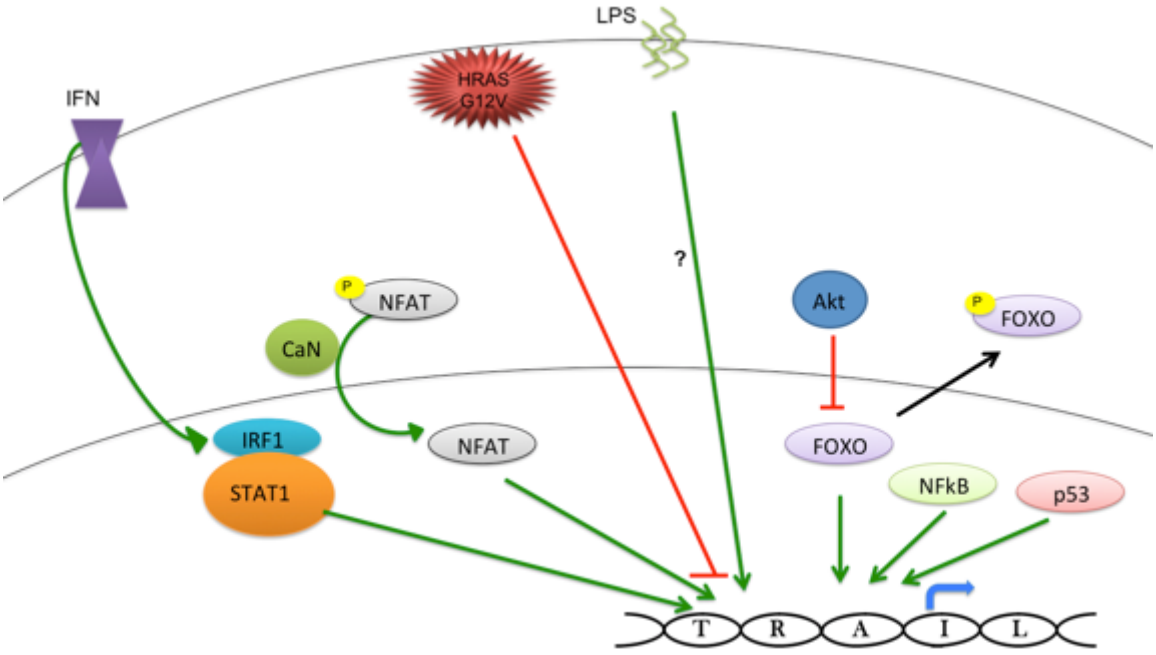

Figure 1.3. Molecules that alter human TRAIL gene transcription. Interferons (IFN) activate TRAIL gene transcription through ISRE and IRFE sequences in the promoter region. Mutant HRAS (G12V) silences TRAIL expression through hypermethylation of CpG islands in the TRAIL gene promoter. Green arrows indicate activating relationships, red arrows lines indicate inhibitory relationships, and blue arrow indicates start of transcription site.

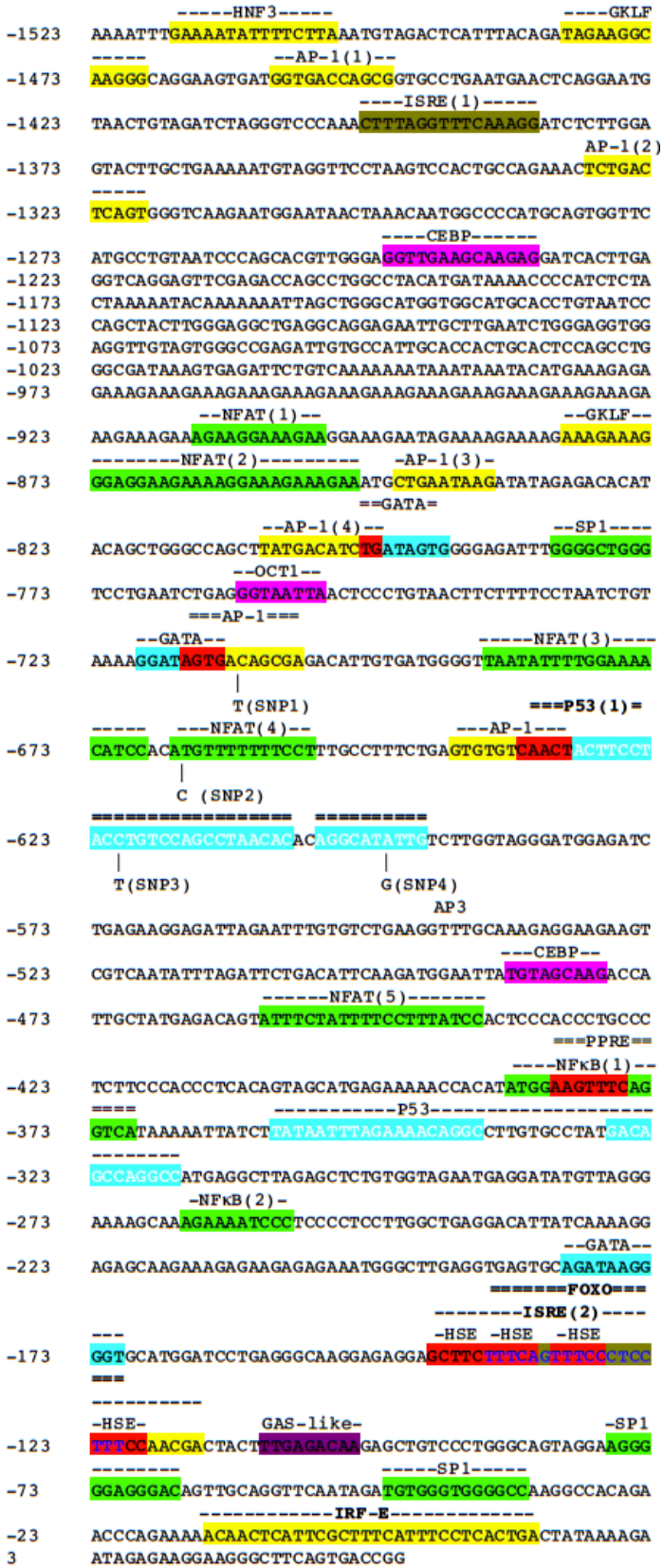

Figure 1.4. Sequence analysis of the human TRAIL gene promoter. Putative binding sites indicated by highlights above the appropriate sequences. Nucleotides contained in two or more putative binding sites are highlighted in red. Binding sites that have been empirically demonstrated to affect TRAIL promoter activity in experiment are bolded. Vertical lines below the sequence indicate SNPs. TRAIL sequence obtained from Accession No. AF178756.

Interferons

Luciferase reporter experiments found that interferon-γ was capable of inducing TRAIL promoter activity by two-fold in a region between 165 and -35 (Wang et al., 2000), which explained a previous report that showed rapid induction of TRAIL following incubation with IFN-γ (Griffith et al., 1999). STAT1 and IRF1 are thought to directly mediate the effects of IFN-γ on the TRAIL promoter. IFN-γ has also been shown to induce FasL- and TRAIL-dependent apoptosis in lung cancer cells (Kim et al., 2002) and is responsible for IL18- and TLR3-induced TRAIL expression in NK cells (Tu et al., 2011).

There are reports that suggest type I interferons (IFN-α and -β) induce the TRAIL gene more strongly that IFN-γ (Gong and Almasan, 2000). IFN-α and -β potently induce TRAIL in $CD4^+$ and $CD8^+$ peripheral blood T-cells following CD3-stimulation (Kayagaki et al., 1999) as well as Jurkat T cells. IFN-α has also been shown to induce TRAIL in macrophages (Solis et al., 2006) and in lymphoma cells in a JNK-dependent manner (Yanase et al., 2005). IFN-β induces TRAIL in colorectal cancer cell lines by a Stat-1-dependent mechanism (Choi et al., 2003). Taking the evidence together, IFN- α, -β, -γ have been shown to induce TRAIL gene transcription, though the robustness of TRAIL induction among them seems to be context-dependent.

NFAT

TRAIL is also positively regulated by the transcription factor NFAT, which is activated by calcineurin-mediated dephosphorylation. Wang et al. investigated the role of NFAT regulation of the TRAIL gene promoter due to the two putative binding sites that they previously noted in addition to three other newly found potential NFAT binding sites (Wang et al., 2000; Wang et al.,

2011c). Among the 5 NFAT family members, NFATc1 was by far the most potent positive regulator of the TRAIL transcription. Interestingly, NFAT-dependent TRAIL was not affected by deletion of their putative binding sites in luciferase reporters but instead was abrogated by deletion of the -165 to -35 region. Chromatin-immunoprecipitation and electrophoretic mobility shift assay (EMSA) experiments revealed that NFATc1 antagonizes SP-1 binding to the TRAIL promoter. This reports highlights a mechanism that immune cells such as cytotoxic T-cells might utilize to upregulate TRAIL and also underscores the need to directly test binding sites to accurately delineate transcriptional regulation. These observations also suggested that SP-1 may negatively regulate the TRAIL gene promoter.

SP-1

The study that described NFAT regulation of the TRAIL promoter also found that SP-1 represses TRAIL gene transcription, at least in human intestinal cells (Wang et al., 2011c). However, a recent study reported a positive regulation of TRAIL gene transcription by SP-1 in vascular smooth muscle cells but appears to involve SP-1 phosphorylated at Thr453 (Chan et al., 2010). Phosphorylation of SP-1 at Thr453 and Thr739 by p38 appears to be essential for its positive regulation of the VEGF gene (Lin et al., 2011). Future studies need to further examine if these differences are due to difference in cell types or if this phosphorylation event modulates the relationship between SP-1 and TRAIL gene regulation. The mechanism of HDACi-induced upregulation of TRAIL appeared to involve SP-3 (Nebbioso et al., 2005).

NFκB

Inhibition of NFκB in Jurkat T cells and primary T lymphocytes revealed that NFκB positively regulates TRAIL expression in a manner that depends on the NFκB binding site 1 (Baetu et al., 2001) (Fig. 1.4). NFκB also upregulates FasL and together, these proapoptotic ligands may be responsible for tumor-cell elimination in immune surveillance and/or attenuation of T-cell activation to prevent autoimmunity. NFκB is also responsible for constitutive TRAIL expression in human T-cell leukemia virus type I (HTLV-1)-induced leukemia, though other concomitant effects

of NFκB seem to cause resistance to TRAIL-mediated apoptosis (Matsuda et al., 2005). In accordance with a positive regulatory role for NFκB with respect to TRAIL, the prostaglandin 15d-PGJ2 represses TRAIL transcription by inhibiting the binding of NFκB to the NFκB binding site 1 (Fig. 1.4). This study also identified the transcription factor HSF-1 as a negative regulator of the TRAIL gene that is involved in 15d-PGJ2-induced TRAIL repression. This negative regulation of HSF-1 is completely dependent on its DNA binding domain and is in contrast to its positive regulation of the FasL gene (Cippitelli et al., 2003). Cnb, the regulatory subunit of calcineurin, was recently shown to active NFκB-mediated TRAIL expression through direct binding to the integrin CD11b (Su et al., 2012).

P53

The El-Deiry lab identified two potential p53 binding sites in the TRAIL promoter following observations that p53-inducing chemotherapies such as 5-FU and doxorubicin elevated TRAIL promoter activity (Kuribayashi et al., 2008). One of these binding sites was at -630 was shown to mediate p53-induced TRAIL promoter activity using luciferase reporters. Radiation has been reported to induce TRAIL expression and it has been hypothesized that TRAIL plays role in the bystander effects observed following radiation (Shareef et al., 2007; Unnithan and Macklis, 2004). The role of p53 in radiation-induced TRAIL expression should be explored since it is well accepted that ionizing radiation robustly induces p53.

FOXO

Overexpression of Foxo3a in prostate cancer cells was found to induce TRAIL by gene expression profiling (Modur et al., 2002). In silico analysis revealed a binding site in the TRAIL gene promoter between -121 and -138 that was validated by luciferase reporter construct mutations and EMSAs to be completely responsible for Foxo3a-induced TRAIL promoter activity. This study also revealed that TRAIL expression is significantly decreased in metastatic prostate cancer. Foxo3a-driven TRAIL upregulation has been recently described as the apoptotic

mechanism responsible for memory B cell loss that results from chronic HIV infection (van Grevenynghe et al., 2011).

Unexplored binding sites

Clearly there are several putative transcription factor-binding sites within the TRAIL gene promoter that have been unexplored. It is worth noting that only a few of the examined binding sites for a given transcription factor have turned out to be functionally important, as in the case of NFκB, AP-1, and SP-1, which have multiple putative binding sites in the TRAIL promoter. Oct-1 is involved in regulating several housekeeping genes and has a putative binding site on the TRAIL promoter. Interestingly, HDACi have been found to induce Gadd45 expression through Oct-1 (Hirose et al., 2003). This observation along with the report that HDACi induces the TRAIL gene suggests that the direct examination of Oct-1 binding to the TRAIL promoter may be worth further investigation. The role of the heat shock elements in the proximal region of the TRAIL promoter may also be worth investigation as heat shock has already been linked to protection from TRAIL-mediated cell death (Ozoren and El-Deiry, 2002).

The MAPK pathway

Cells transformed with $HRAS_{G12V}$ were reported to have silenced expression of TRAIL due to hypermethylation of CpG islands in the TRAIL gene promoter that lie ~2,000bp upstream of the start of transcription (Lund et al., 2011). TRAIL could still be induced by interferon-γ in these transformed cells and the silencing could be reversed with decitabine, a DNA methyltransferase inhibitor. Mutations in *KRAS* during colon cancer progression are a common event in colon cancer (Bos et al., 1987; Forrester et al., 1987; Vogelstein et al., 1988). This may explain the silencing of TRAIL expression that has been noted in colon cancer, particularly during the progression from adenoma to carcinoma (Koornstra et al., 2003). Oncogenic *RAS* sensitizes cells to TRAIL-mediated apoptosis, potentially through MEK-dependent upregulation of DR4 and DR5 (Nesterov et al., 2004). Thus, concomitant silencing of TRAIL expression may be required to prevent induction of TRAIL-mediated apoptosis during Ras transformation.

Other inducers

A recent report found that pigment epithelium-derived factor (PEDF) induced the expression of TRAIL on the surface of macrophages (Ho et al., 2011). Further analysis revealed that PEGF also induces peroxisome proliferator-activated receptor-gamma (PPARγ), which binds to the TRAIL promoter to upregulate transcription at a PPAR-response element (PPRE). This represents yet another mechanism utilized by immune cells to induce the expression of TRAIL. Other molecules have been reported to induce TRAIL gene transcription but the underlying direct transcriptional mechanism has not been elucidated. Lipopolysaccharide (LPS), which is a component of gram-negative bacteria, has been reported to induce TRAIL at higher concentrations (Halaas et al., 2000), though an early report did not observe TRAIL-induction by LPS at lower doses (Griffith et al., 1999).

Regulation of TRAIL activity by isoforms

The human TRAIL gene spans ~20 kb and contains 5 exons and 4 introns that contain typical splice acceptor-AG/GT-splice donor consensus sites at their boundaries (Gong and Almasan, 2000; Shapiro and Senapathy, 1987). The first exon encodes for the 21 amino acid transmembrane domain and the 17 amino acid cytoplasmic domain. Exons 4 and 5 encode for the amino acids in the extracellular domain that are responsible for the interaction of TRAIL with its receptors. Exon 5 also encodes for the C-terminal amino acids along with containing the 3'-UTR and poly-A tail.

TRAIL is well known for its potent and cancer-selective apoptotic activity. However, it seems that this activity is unique to only one specific isoform of TRAIL among the 9 variants that have been reported to date (Figure 1.5). The first report of TRAIL isoforms identified three variants that involved variable inclusion of exons 2 and 3: the full length TRAILα, TRAILβ that lacks exon 3, and TRAILγ that lacks exons 2 and 3 (Krieg et al., 2003). Computational analysis of exons 2 and 3 revealed that both exons were flanked by consensus splice donor and splice acceptor sequences that are involved in post-translational alternative splicing. Interestingly, TRAILα and TRAILβ where localized to the cytoplasm whereas TRAILγ was associated with the

nuclear and cell surface membrane. A sequence analysis of TRAIL mRNA in granulosa tumor cells resulted in the identification of TRAILδ, which lacks exons 3 and 4 (Woods et al., 2008). The truncated TRAIL isoforms do not induce apoptosis like the full-length TRAIL (TRAILα) and it has been suggested that these variants are negative regulators of their full-length counterpart. No TRAIL variants other than the full length TRAIL detected in murine cells.

Recently, 7 alternatively spliced TRAIL variants were identified that were all truncated versions incapable of potentiating apoptosis: AK, E2, E3, E4, DA, BX424, and BX439 (Wang et al., 2011b). All of these isoforms contain common N-terminal sequences and possess the transmembrane helix but vary in the C-terminal region. The DA isoform lacks exon 3 and encodes for the same protein as TRAILβ and BX424 lacks exons 3 and 4, yielding the same protein as TRAILδ. BX439 completely lacks exons 2-4 but posses the same exons 1 and 5 as the full length TRAIL. AK and DA contain a unique exon not shared by any other reported isoforms. E2, E3, and E4 contain exons 1–2, 1–3, and 1–4, respectively, with an extended sequence at C-terminus. All of these variants, however, activated NFκB and the authors note the possibility that truncated TRAIL can play intracellular roles. Future studies should directly examine the ability of these various TRAIL isoforms to bind to TRAIL receptors.

The abundance of these isoforms varied significantly across the tested cancer cell lines with THP-1 human leukemia cell line and BT-325 human glioma cell line expressing most of these variants. A notable exception among the cell line panel was the human colon cancer cell line HCT116 that only expressed the full length isoform.

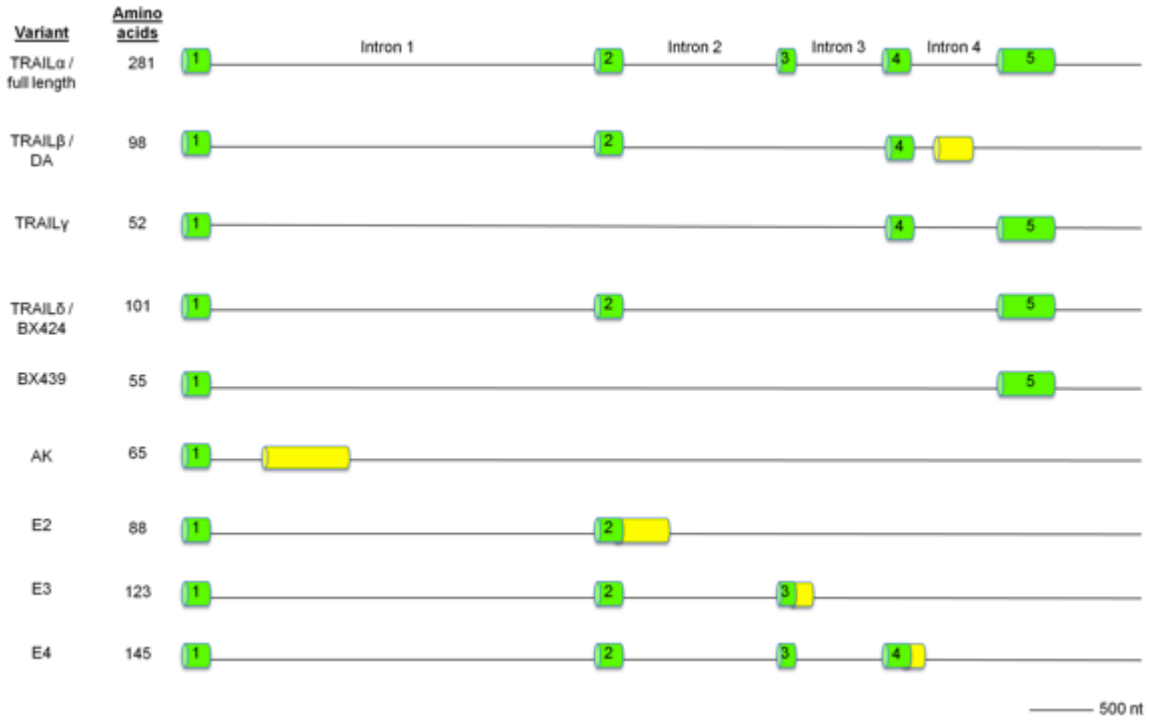

Figure 1.5. Genomic structure of human TRAIL variants. Exonic sequences of the full-length TRAIL are shown in green whereas novel sequences are shown in yellow.

SNPs in the TRAIL gene

Due to the altered expression of TRAIL in various disease settings, there have been multiple efforts to identify single nucleotide polymorphisms (SNPs) in various patient populations. SNP analysis of peripheral blood samples found that having a T instead of a C at position -723 was significantly associated with sporadic breast cancer and decreased TRAIL mRNA levels (SNP1) (Pal et al., 2011) (Fig. 1.4). Luciferase assays in cell lines indicated that this mutation from C to T indeed repressed TRAIL transcriptional activity. *In silico* analysis found that this mutation is predicted to create an SP-1 binding site. The authors propose that SP3 is negatively regulating this SP1 site, though future studies will need to validate the mutation-induced putative binding site and address this possibility.

Another SNP analysis of the TRAIL gene promoter revealed 4 SNPs that were highly polymorphic in healthy individuals (Weber et al., 2004). However, these SNPs were not

significantly associated with changes in TRAIL mRNA levels or with multiple sclerosis as a diagnostic or prognostic marker. The authors of the study note that SNP(1) is in an AP1 binding site, though they do not comment about other binding sites predicted at the other SNPs. Interestingly, both SNP3 and SNP4 each lie in p53 response element half-sites that the El-Deiry lab has previously reported and shown to be important for TRAIL induction in response to chemotherapy (Kuribayashi et al., 2008). While these SNPs were not associated with basal TRAIL levels in this population, it would be interesting to determine if these SNPs affect p53-induced TRAIL and response in chemotherapy-treated cancer patients.

A SNP at the -716 position of the TRAIL gene promoter was identified but not associated with prostate cancer. Other TRAIL gene promoter SNP associations have been identified in other disease settings but have not been evaluated for its functional effects on TRAIL transcription: -1525/-1595 and fatty liver disease (Yan et al., 2009). Other SNPs have been identified in coding regions such as position 1595 in exon 5 being linked with multiple sclerosis (Kikuchi et al., 2005). A small cohort study of healthy volunteers found 5 SNPs in TRAIL exons: 3 in the 3'-UTR at 1525, 1588, and 1595 whereas the other two were in in exon 1 and 2 at positions 192 and 912 (Gray et al., 2001). These two polymorphisms in the coding region did not result in any change in amino acid sequence. Another SNP study in bronchial asthma patients found 5 SNPs in the TRAIL gene with 1 SNP being in a coding region at 825 and 5 SNPs being in the 3'UTR at 1053, 1202, 1438, 1501, and 1508 (Unoki et al., 2000).

TRAIL expression in disease and physiology

Altered expression levels of TRAIL been noted in several diseases relative to healthy controls. For instance, TRAIL mRNA levels are elevated in patients with multiple sclerosis (Huang et al., 2000). Patients with systemic lupus erythematous or multiple sclerosis have elevated serum levels of soluble TRAIL (Lub-de Hooge et al., 2005; Wandinger et al., 2003). These clinical observations support a critical role for TRAIL in preventing autoimmune disorders, which may be explained by observation that TRAIL-knockout mice cannot induce thymocyte apoptosis (Lamhamedi-Cherradi et al., 2003). Breast cancer patients with brain metastases have

downregulated TRAIL mRNA levels (Bos et al., 2009). TRAIL expression silencing has also been noted in metastatic prostate cancer (Modur et al., 2002) and colon cancer (Koornstra et al., 2003). A role for TRAIL has been implicated in particular types of cellular differentiation such as colonic epithelial cells through a reciprocal expression relationship with PKCε (Gobbi et al., 2012). The El-Deiry lab has also implicated TRAIL-receptor signaling in the DNA damage response to radiation as well as the late effects of radiation (Finnberg et al., 2005; Finnberg et al., 2008).

1.4 Regulation of Foxo3a Activity

Overview

FOXO is a subfamily of the Forkhead transcription factors that regulates genes involved in numerous cellular processes that include metabolism, longevity, tumor suppression, and development (Calnan and Brunet, 2008). The subfamily includes 4 mammalian members: Foxo1, Foxo3a, Foxo4, and Foxo6. Among the FOXO family, Foxo1 and Foxo3a have been the most studied with Foxo3a being previously described as a direct regulator of the TRAIL gene through a FOXO binding site in the TRAIL gene promoter (Modur et al., 2002). The tumor suppressor role is ascribed to FOXOs based on their ability to induce target genes such as p21, TRAIL, and Bim that induce cell cycle arrest, apoptosis, and/or autophagy. FOXO proteins bind to the consensus sequence: TTGTTTAC (Furuyama et al., 2000; Xuan and Zhang, 2005). FOXOs are regulated predominantly by post-translation modifications (PTMs) that currently include phosphorylation, acetylation, and ubiquitination. These modifications often affect FOXO subcellular localization, typically involving 14-3-3 proteins and the nuclear localization and nuclear export sequences that are conserved among FOXOs. Altering FOXO protein levels through changes in transcription or causing protein degradation by polyubiquitination can also regulate FOXOs. FOXO members often associate with other proteins that can alter their affinity for particular target genes, alter the activity of the interacting protein, or can directly or indirectly mediate post-translational modifications (PTMs) to FOXOs. Together, these mechanisms allow for fine-tuned responses to a variety of external stimuli that can be transduced through FOXOs. While these interactions are

variable among FOXOs, we will primarily focus on Foxo3a due to its intimate involvement with TRAIL gene regulation (Figure 1.6).

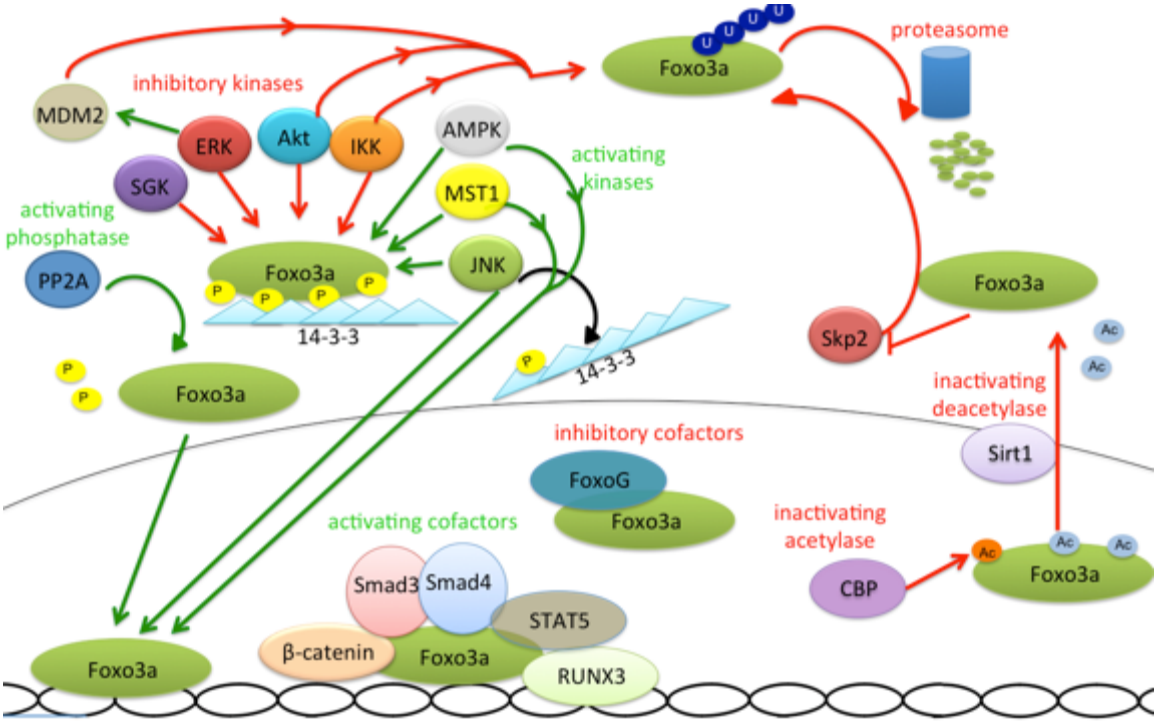

Figure 1.6. Multi-modal regulation of FOXO activity. Foxo3a localization can be regulated by phosphorylation events that dock the transcription factor to 14-3-3 proteins in the cytoplasm. These kinases include Akt, SGK, ERK, and IKK. Conversely, the kinases AMPK and MST1 phosphorylate Foxo3a and result in its activation. In addition to inhibitory phosphorylation, ERK also activates MDM2 to ubiquitinate Foxo3a and cause its proteasomal degradation. Akt and IKK can also induce the proteasomal degradation of Foxo3a. JNK is capable of phosphorylating 14-3-3ζ at Ser184, which interrupts its cytoplasmic interaction with Foxo3a. The phosphatase PP2A reverses Akt-mediated Foxo3a inactivation by dephosphorylating Foxo3a. Acetylation of Foxo3a occurs by CBP in its DNA-binding domain, which reduces its transcriptional activity. The deacetylase Sirt1 can also decrease Foxo3a activity, perhaps by deacetylating different residues than those that CBP affects. Sirt1 also causes the Skp2-dependent ubiquitination and proteasomal of Foxo3a, though Foxo3a decreases the transcription of Skp2. Foxo3a activity and gene specificity can also be positively regulated and tuned by association with β-catenin, STAT5,

and Smad3 and Smad4. FoxoG can directly bind and attenuate Foxo3a activity, particularly with respect to the complex formed between Foxo3a, Smad3, and Smad4.

FOXO regulation by kinases

Akt is a potent regulator that phosphorylates 3 residues that are conserved among FOXOs (Biggs et al., 1999; Brunet et al., 1999; Kops et al., 1999; Nakae et al., 1999). Interestingly, Foxo6 lacks one of the 3 residues phosphorylated by Akt and is not regulated by changes in localization (Jacobs et al., 2003). These Akt-mediated phosphorylation events create docking sites for 14-3-3 proteins on FOXOs, expose their nuclear export sequences, and affects the accessibility of their nuclear localization sequences (Brunet et al., 2002; Obsilova et al., 2005). Serum glucocorticoid kinase (SGK) is also capable of phosphorylating FOXOs at the same residues as Akt. Several other FOXO residues are phosphorylated to facilitate its interaction with the nuclear export proteins Ran and Crm1 (Rena et al., 2002; Zhao et al., 2004). Some phosphorylation sites are within the DNA binding domain and decrease binding affinity through electrostatic repulsion (Matsuzaki et al., 2005). The stress-activated kinases JNK and MST1 phosphorylate Foxo3a (Lehtinen et al., 2006) and Foxo4 (Essers et al., 2004; Oh et al., 2005), respectively, which results in their nuclear translocation. These events are independent of and antagonize the Akt-mediated phosphorylation events. AMPK phosphorylates Foxo3a at two sites and results in a distinct response that activates transcription of FOXO target genes specifically involved in energy metabolism and stress resistance (Greer et al., 2007).

Regulation of FOXO activity by transcription cofactors

FOXO is also controlled and fine-tuned by numerous transcription cofactors in response to various stimuli in a highly context-dependent manner. For instance, while Foxo1 function is inhibited by CBP-mediated acetylation, this allows for recruitment of the CBP coactivator complex to transcribe particular genes. FOXO proteins also bind β-catenin during oxidative stress, which increases FOXO target gene transcription and decreases TCF target gene transcription involved in Wnt signaling, which requires β-catenin as a cofactor for transcription (Almeida et al., 2007).

Foxo1 also interacts with the PPARγ co-activator PGC-1 in a manner that is disrupted during insulin signaling through Akt, allowing PGC-1 to interact with PPARγ (Li et al., 2007; Schilling et al., 2006). FOXO also interacts with Sirt1, a histone deacetylase, in a manner than increases transcription of cell cycle arrest gene and decreases apoptotic gene transcription by an undefined mechanism (Brunet et al., 2004; Daitoku et al., 2004; van der Horst et al., 2004).

Association with particular transcription factors also controls tuning of FOXO target gene transcription. One example is the association of Foxo3a and the transcription factor RUNX3 to bind the BIM promoter (Yamamura et al., 2006). FOXOs also interact with SMAD3 and SMAD4 to induce $p21^{waf1}$ transcription (Seoane et al., 2004) and Stat5 to induce Cited 2 (Bakker et al., 2004). FoxG (Seoane et al., 2004), PPARγ (Dowell et al., 2003), and the androgen receptor (Li et al., 2003) also interact with FOXOs but antagonize their transcriptional activity. Differential FOXO transcriptional activity can be further modulated by competition or cooperation with other transcription factors such as p53 (Nemoto et al., 2004) or Notch (Kitamura et al., 2007) for mutual target genes.

Other regulators of FOXO

Activation of cytoplasmic FOXO may be accomplished through inactivation of the phosphorylating kinases that antagonize FOXO activity and/or activation of phosphatases. Protein phosphatase 2A (PP2A) may be a culprit phosphatase as it was immunoprecipitated in a complex with Foxo3a (Singh et al., 2010). The localization of FoxO4 is also controlled by monoubiquitination triggered by oxidative stress via an unclear mechanism (van der Horst et al., 2006). Acetylation is another mode of regulating subcellular localization that can occur in response to oxidative stress and is carried out by CBP and PCAF (Senf et al., 2011; Yoshimochi et al., 2010) (Brunet et al., 2004; Daitoku et al., 2004; Fukuoka et al., 2003). The acetylation of Foxo3a by CBP actually decreases transcriptional activity, which is unexpected given that transcription factor acetylation is typically activating. The crystal structure of DNA-bound Foxo3a revealed that the CBP acetylation events occur in the DNA binding domain and likely interrupts the protein:DNA interaction (Tsai et al., 2007). Acetylation can also affect the localization of FoxO proteins in the nucleus, as

demonstrated by the increased association of Foxo1 to PML following acetylation (Kitamura et al., 2005).

Controlling FOXO proteins levels through degradation or changes in transcription is another mode of FOXO activity regulation. One avenue of controlling FOXO protein levels is through protein degradation, which is caused by FOXO phosphorylation by Akt in addition to localization changes (Matsuzaki et al., 2003; Plas and Thompson, 2003). In the case of Foxo1, this degradation is caused by polyubiquitination executed by the SCF^{skp2} complex (Huang et al., 2005). Skp2 has been recently shown to polyubiquitinate Foxo3a (Wang et al., 2011a), though this relationship is complicated by direct negative regulation of Skp2 mediated by direct binding of Foxo3a to its gene promoter (Wu et al., 2012). Foxo3a is also degraded following phosphorylation by IkappaB kinase (Hu et al., 2004a) or Akt (Plas and Thompson, 2003).

1.5 Scope of This Thesis Research

The El-Deiry lab began working on the TRAIL pathway with the initial cloning and discovery of DR5 as a p53 target gene that was uncovered by subtractive hybridization screening probing doxorubicin-induced transcripts (Wu et al., 1997). Other groups simultaneously discovered and cloned DR5 as a TRAIL receptor through structure-based methods (Pan et al., 1997a; Sheridan et al., 1997). Follow up studies from the El-Deiry lab found DR5 to also be induced by genotoxic stress and TNFα (Sheikh et al., 1998) and identified loss of function mutations within the DR5 gene in head and neck cancers. The murine homologue of DR5, TRAIL-R, in mice was also identified by the El-Deiry lab (Wu et al., 1999). The lab later generated the first TRAIL-$R^{-/-}$ transgenic mouse in an effort to potentially identify an oncogenic phenotype (Finnberg et al., 2005; Finnberg et al., 2008). While the TRAIL-$R^{-/-}$ mice exhibited apoptotic defects, they also showed signs of bronchopneumonia and others symptoms that were reminiscent of the late effects of gamma radiation, a poorly understood phenomenon that is a devastating clinical problem where patients develop severe lung inflammation several weeks following radiation.

These findings generated the hypothesis that increased TRAIL signaling may suppress inflammation and that upregulating TRAIL may ameliorate the late effects of gamma radiation.

The lab has described a number of determinants of TRAIL sensitivity such as FLIP (Kim et al., 2000), Bcl-XL, Bcl-2 (Burns and El-Deiry, 2001), Mcl-1, cIAPs, and myc (Ricci et al., 2004; Ricci et al., 2007). Induction of the TRAIL gene was also described by the lab in response to interferon-beta (Choi et al., 2003) and chemotherapy through a p53 binding site in the TRAIL gene promoter (Kuribayashi et al., 2008). Taking these studies together, the lab has a rich history of studying TRAIL gene regulation, its proapoptotic biology, and cellular determinants of TRAIL sensitivity. Due to role of TRAIL signaling as a suppressor of tumors and inflammation, we sought to identify small molecules that could upregulate endogenous TRAIL production as a potentially novel antitumor therapy and to potentially rescue the late effects of gamma radiation.

Recombinant TRAIL has been intensely developed as an antitumor agent due to its potent and cancer-selective cytotoxicity. These studies aim to identify a small molecule inducer of the TRAIL gene that functions via a p53-independent mechanism and overcomes therapeutic limitations of recombinant TRAIL due to its drug properties. While gene regulation of DR4 and DR5 has been well described, the regulation of the TRAIL gene has received less attention. We aimed to identify TRAIL-inducing compounds to develop novel anticancer drugs in addition to elucidating the molecular mechanism responsible for induction of the TRAIL gene to perhaps enhance the understanding of TRAIL gene regulation. To accomplish these goals, we performed a series of studies as outlined by the following research aims that capitulate the scope of this thesis research.

Research Aim I

Identify TRAIL-inducing compounds (TICs) that induce TRAIL gene transcription and cancer-specific cell death

Research Aim II

Evaluate the lead TIC as a TRAIL-inducer and antitumor agent in vitro and in vivo

Research Aim III

Elucidate the molecular mechanism of TIC-induced TRAIL gene transcription

In summary, these studies have led us to the identification of a potentially first-in-class agent TIC10, a small molecule TRAIL-inducing compound. We demonstrate TIC10's direct effector mechanisms, novel bystander effects involving normal cells, and upstream signaling pathways that specifically control its therapeutic effects. TRAIL is a natural effector mechanism for suppressing cancer that has evolved to allow for the immune surveillance of cancer and consequently lends itself as an attractive endogenous drug target in cancer treatment. We describe advantages over current TRAIL-based therapies that have important clinical implications, such as extending the use of this pathway in brain malignancies and overcoming administration barriers that potentially limit efficacy. We clearly delineate how the TRAIL gene is induced in response to TIC10 and upstream mechanisms that cause those changes. It is important to note that these novel TRAIL-mediated anti-tumor mechanisms allow for the promising safety and efficacy profile of TIC10 that is demonstrated with tumor response and overall survival endpoints in subcutaneous, orthotopic, and transgenic mouse models of cancer. The mechanism of action for TIC10 has implications beyond the molecule itself, suggesting that Akt and ERK are particularly critical regulators of Foxo3a and supports the combination of Akt and ERK inhibitors to gain Foxo3a- and TRAIL-dependent efficacy. This mechanism also provides insight as to the underlying mechanism of synergy observed between inhibitors of the MAPK and PI3K/Akt pathways that have been previously noted in the literature (Ebi et al., 2011; Sos et al, 2009; Edwards et al, 2006).

CHAPTER 2

IDENTIFICATION OF TIC10 AS A SMALL MOLECULE INDUCER OF TRAIL

2.1 Abstract

Recombinant TRAIL is a potent inducer of apoptosis but possesses efficacy-limiting properties such as a short half-life and poor biodistribution. We performed a high-throughput screen for small molecules capable of upregulating a TRAIL gene transcription reporter using a section of the human TRAIL gene promoter that excludes the previously identified p53 binding site. Out of the resulting "hit" compounds, we selected TRAIL-inducing compound 10 (TIC10) as the lead compound for further studies based on its ability to induce TRAIL at the cell surface and cell death in cancer cells but not normal cells. We found that TIC10 causes a dose-dependent increase in luciferase reporter gene activity for TRAIL transcription and TRAIL mRNA in p53-deficient HCT116 cells. This transcriptional upregulation results in an elevated amount of TRAIL on the surface of tumors as measured by flow cytometry in a panel of several human cancer cell lines. The induction of TRAIL occurred reproducibly in many cancer cell lines but was only evident after 48 hours of incubation or longer. Interestingly, short-term incubation with TIC10 was still sufficient to induce TRAIL at the later time point in the absence of drug. Together, these data indicate that TIC10 upregulates TRAIL transcription in a p53-independent manner and causes a sustained upregulation of TRAIL on the surface of tumor cells.

2.2 Introduction

While current TRAIL-based therapies are costly to produce for clinical applications and may be limited by stability and/or biodistribution, endogenous TRAIL is a robust and selective tumor suppressor. Endogenous TRAIL naturally lends itself as a drug target to restore anti-tumor immunity, the utility of which has been recently highlighted by the FDA approval of ipilimumab, a CTLA-4 targeted monoclonal antibody with unparalleled efficacy in metastatic melanoma (Ji et al., 2011). We hypothesized that upregulation of TRAIL gene expression by a small molecule would lead to a potent and novel anti-tumor mechanism by improving the biodistribution and pharmacokinetic properties of TRAIL such as increasing its effective half-life as well as increasing its concentration within the tumor microenvironment.

As a natural tumor suppressor, TRAIL is an attractive anti-neoplastic agent due to its

favorable safety and activity profile, which results from its ability to selectively induce apoptosis in cancer cells. Despite promising preclinical activity, clinical trials with rhTRAIL in human cancer patients have been met by limited success. Molecular properties that may lower the efficacy of TRAIL include protein instability, short serum half-life (~30 minutes), inability to cross the blood-brain barrier, and loss of activity associated with the recombinant protein compared to the endogenous protein due to differences in PTMs that differ across cellular expression systems such as bacteria.

There are practical issues associated with the use of therapeutics that are recombinant proteins such as high cost of production and intravenous administration. Some of these limitations have been recognized by the field and have resulted in circumventing innovations. Some of the most developed examples of this are the TRAIL-receptor agonist antibodies (reviewed in Chapter 1) such as mapatumumab and lexatumumab that have prolonged half-lives and are being explored in clinical trials (Abdulghani and El-Deiry, 2010). However, these antibodies can only bind one of the two pro-apoptotic receptors and tend to bind bivalently unlike TRAIL. In conclusion, TRAIL is a potent cancer cell-specific inducer of apoptosis that has demonstrated some efficacy in clinical trials as a recombinant protein but may be therapeutically hindered by several molecular and practical limitations that include stability, half-life, biodistribution, expense, and administration route.

TRAIL gene induction by a few small molecules has been previously reported such as histone deacetylase (HDAC) inhibitors (Nebbioso et al., 2005) and the Bcr-Abl tyrosine kinase inhibitor imatinib has been reported (Kikuchi et al., 2007). However, these small molecules clearly have other targets and intended functions that may yield different efficacy and safety profiles than a small molecule with fewer targets that specifically induces TRAIL and TRAIL-mediated apoptosis. Thus, we screened for small molecules capable of inducing the endogenous TRAIL gene to overcome limitations of current TRAIL-based therapeutics with the goal of developing a new class of TRAIL-based therapies possessing superior antitumor properties.

2.3 Materials and Methods

Cell Culture

All cell lines were obtained from ATCC except HCT116 Bax$^{-/-}$ and HCT116 p53$^{-/-}$ cells that were a gift from Bert Vogelstein (Johns Hopkins University, Baltimore, MA) and glioblastoma cell lines that were kindly provided by Akiva Mintz (Wake Forrest University, Winston-Salem, NC). Cells were maintained at 5% CO_2, 95% air, 37°C in water-jacketed incubators (Forma Scientific). Cell culture media was typically obtained from Gibco and mixed with 10% sterile-filtered fetal bovine serum and 1% penicillin/streptomycin. Parental cell lines were maintained in canted neck, tissue culture treated flasks (BD Falcon). For most experiments, cells were propagated in 6-well culture plates (Corning Incorporated) and allowed to adhere for a minimum of 12 hours prior to drug treatment in fresh media. Cells were enumerated using a Cellometer Auto T4 (Nexcelom Biosciences).

Reagents

D-luciferin (Gold BioTechnology, Inc.) was reconstituted in PBS and stored at -80°C. Propidium iodide was suspended in dH_2O and stored at -20°C.

High throughput Screening

We performed cell-based screening for TRAIL-inducing using a luciferase reporter assay. The reporter for the screen was luciferase under transcriptional control of the first 504 base pairs of the human TRAIL gene promoter. This construct was transfected into HCT116 Bax$^{-/-}$ that were seeded into 384-well black plates (Corning) at a density of 5×10^4 cells per well. Compounds were added to the well at concentrations of 20, 200, 500, and 1000 nM using robotically controlled pin tools (Biomek). Treatments were carried out in duplicate and plates were treated in duplicate to allow for readout of the reporter as well as a cell viability assay. Reporter activity and cell viability was imaged at 12, 24, 36, and 48 hours following treatment using an IVIS imaging system (Xenogen). The luciferase reporter signal was normalized to cell viability for data interpretation.

RT-qPCR analysis

Total RNA was extracted using RNeasy Minikit (Qiagen) by following the manufacturer's instructions. cDNA was generated using SuperScript II (Invitrogen) with 1 µg of RNA and oligodT. Primers were: TRAIL forward (CAGAGGAAGAAGCAACACATT), TRAIL reverse (GGTTGATGATTCCCAGGAGTTTATTTTG), GAPDH forward (CCACATCGCTCAGACACCAT), GAPDH reverse (GGCAACAATATCCACTTTACCAGAGT). PCR amplification was performed with the Applied Biosystems 7900HT Fast Real-time Detection System. Samples were standardized to 10 ng/µl and 20 ng of cDNA per sample was then utilized as a template for real-time PCR using a SYBR Green Master Mix (Qiagen Corp, USA). Quantitation used the $2\Delta\Delta$Ct method of crossing thresholds (Livak and Schmittgen, 2001) with GAPDH as the endogenous control for normalization. Reactions were performed in 384 well optical plates in a 7900HT instrument (Applied Biosystems), with 10ul reaction volumes. Data analysis used the ABI PRISM 7900 Sequence Detection System 2.2 software. To exclude the possibility of genomic DNA contamination, control PCR reactions with no cDNA template and No-RT control samples were also performed for each gene-specific primer set. Replicates of each PCR reaction were performed and the resultant data was averaged.

Surface TRAIL expression by flow cytometry

Cells were harvested by trypsinization and rinsed once in PBS. Cells were then fixed in 1mL of 4% paraformaldehyde in PBS for 20 minutes at room temperature. Cells were then rinsed twice in PBS and incubated with the anti-TRAIL primary antibody (Abcam) at 1:200 in PBS overnight at 4°C. Cells were rinsed twice and incubated with anti-Rabbit Alexafluor 488 (Invitrogen) at 1:250 for 1 hour at room temperature protected from light. Cells were rinsed in PBS, resuspended in 300 µL PBS, and analyzed by flow cytometry.

Cell cycle/Sub-G1 analysis

Cells were harvested from log-phase growth in cell culture in 6-well plates under indicated treatment conditions using brief trypsinization and collecting both adherent and floating cells. Cells were centrifuged for 5 minutes at 1100RPM, rinsed in PBS, and resuspended in .5mL of PBS. 5mL of chilled 80% ethanol was added dropwise while vortexing. Cells were then stored at 4°C for 30 minutes and further processed or stored at 4°C for analysis later. Cells were then centrifuged, washed in 2mL of PBS, and resuspended in 1mL of PBS. .5mL of phosphate-citric acid (.2M Na_2HPO_4, 4μM citric acid, pH 7.8) was added and the solution was incubated for 5 minutes followed by centrifugation. Cells were then resuspended in 300μL of PI/RNase staining solution (50 μg/mL PI and 250 μg/mL RNase A in PBS) and analyzed by flow cytometry. Data was processed using WinMDI version 2.8 software.

Mass spectrometry

Samples were analyzed on an Acquity Ultra Performance Liquid Chromatography (UPLC) system coupled to a Waters SYNAPT qTOF mass spectrometer. The column, which was kept at 40°C, was a Waters UPLC C18 2.1×50 mm with 1.7 μm particles. The binary solvent system included A. water containing 0.1% formic acid and 10mM ammonium formate and B. acetonitrile containing 0.1% formic acid. The gradient started from 10% A with a linear gradient to 50% B. The total run time including re-equilibration step was 8 min with a flow rate of 0.200 ml/min. The temperature of the sample organizer was set at 8°C. Approximately 2pmol of compound was injected. The compound was analyzed by electrospray ionization in positive ion mode. The data were collected at mass range of m/z 50–1000 with a scan duration of 0.2 sec. The source temperature was set at 120°C and nitrogen was used as desolvation gas (700 L/h) at 400°C. The voltages of the sampling cone and capillary were 35 V and 3.5 kV, respectively. Leukine Enkephalin was used as the lockspray reference compound (10 μl/min; 10 sec scan frequency). Tandem mass spectrometry was used for the generation of fragment ions. MS/MS was performed with a collision energy ramp from 20 to 50V. Elemental composition and assignment of structures to observed fragment ions were performed using MarkerLynx software.

Production of Recombinant TRAIL

30mL of LB with ampicillin (100µg/mL) was inoculated at 1:10,000 with bacteria transformed with the His-tagged TRAIL construct and incubated overnight in the shaker. The next day, the overnight culture was diluted 100 fold in LB with ampicillin and incubated for 2 hours in the shaker. IPTG was added at .5 mM working concentration and grown for 2.5 hours in the shaker. 1mL samples were taken before and after induction with IPTG. Cells were pelleted at 7000 RPM for 10 minutes and resuspended in 8mL of binding buffer (50 mM HaH_2PO_4, 300mM NaCl, 10mM imidazole, 10mM β-mercaptoethanol, pH 8.0). Lysozymes was added at 1mg/mL and incubated on ice for 30 minutes. The mixture was sonicated (3M, setting 2.5, 20s X 4) and centrifuged at 17,000 RPM for 30 minutes. The supernatant was removed and 1mL of Ni-NTA slurry (Invitrogen) was added and mixed at 4°C while rotating for 1 hour. The beads were centrifuged at 1000 RPM for 5 minutes at room temperature and 50uL was removed for subsequent analysis. The beads were resuspended in 2mL of Washing Buffer (50mM NaH_2PO_4, 300mM NaCl, 20mM imidazole, 10mM β-mercaptoethanol, pH 8.0) and loaded into a small empty column. After the beads were packed, the outlet was unstopped, and the column was washed with 2 column volumes of Washing Buffer. The protein was eluted with 700µL of Elution buffer (50mM NaH_2PO_4, 300mM NaCl, 250mM imidazole, 10mM β-mercaptoethanol, pH 8.0) for 3 times and collected as separate fractions. The induction and purity of fractions were determined by standard SDS-PAGE. Dialysis was performed twice in 1L of PBS containing 30% glycerol and 10mM β-mercaptoethanol for 1 hour at 4°C. The protein concentration was determined by BioRad protein assay according to the manufacturer's protocol.

Statistical Analyses. For pair-wise comparisons, we analyzed data by the Student's two-tailed *t* test using Excel (Microsoft).

2.4 Results

Selection of TIC10 as a lead TRAIL-inducing compound

To identify small molecule inducers of the human TRAIL gene, we screened for small molecules capable of upregulating TRAIL gene transcription using the NCI Diversity Set II library of 2000 synthetic compounds. As readout for the screen, we used a luciferase reporter activity in TRAIL-resistant HCT116 $Bax^{-/-}$ human colon cancer cells under transcriptional controls of the first 504 base pairs upstream of the start of transcription in the human TRAIL gene promoter. This region excludes the p53 DNA-binding response element that we previously identified (Kuribayashi et al., 2008). This TRAIL-resistant cell was selected for screening so that TRAIL upregulation would not induce cell death, which would attenuate the bioluminescent signal. Gen Sheng Wu constructed the luciferase reporter and Gabriel Krigsfeld and Patrick Mayes conducted the primary screen. This screen yielded 9 small molecules that were capable of reproducibly upregulating the reporter by greater than 2-fold at or below a dose of 1 μM (Figure 2.1). TIC3 is not discussed, as the compound was not available for further study. The majority of the TRAIL-inducing compounds (TICs) upregulated reporter activity at 1μM with the exception of TIC6, which increased reporter activity 3-fold at doses ranging 20 nM to 1 μM. The peak reporter activity was 4-fold induction by TIC4 at 24 hours and a dose of 1 μM. We then validated the TRAIL-induction observed with the luciferase reporter assay by RT-qPCR and found that TIC4, TIC8, TIC9, and TIC10 caused a significant increase in TRAIL mRNA levels at a dose of 5 μM (Figure 2.2A). Interestingly, only TIC9 and TIC10 induced an upregulation of TRAIL at the cell surface (Figure 2.2B).

We sought to select a lead TIC that was capable of inducing cancer-specific cell death in addition to TRAIL gene transcription. We tested the ability of TICs to induce Sub-G1 content in HCT116 $p53^{-/-}$ cells, which are a human colon carcinoma cell line, and HFF cells, which are normal untransformed human foreskin fibroblasts. We found that TIC9 induced the most cell death of HCT116 $p53^{-/-}$ cells with >50% Sub-G1 content but that the compound also induced cell death in normal cells as well (Figure 2.3). TIC10 induced the second highest amount of Sub-G1 content of the HCT116 $p53^{-/-}$ cells without cell death induction in the normal cells. Although the amount of Sub-G1 content was modest, we reasoned that perhaps higher doses of TICs might

result in higher amount of cell death. Indeed 5 μM doses of TICs induced higher levels of Sub-G1 content for almost all TICs but TIC9 and TIC10 where again clearly the most potent compounds, inducing Sub-G1 levels of >50% (Figure 2.4). Thus, we selected TIC10 for further study based on its selective cytotoxic activity against cancer cells.

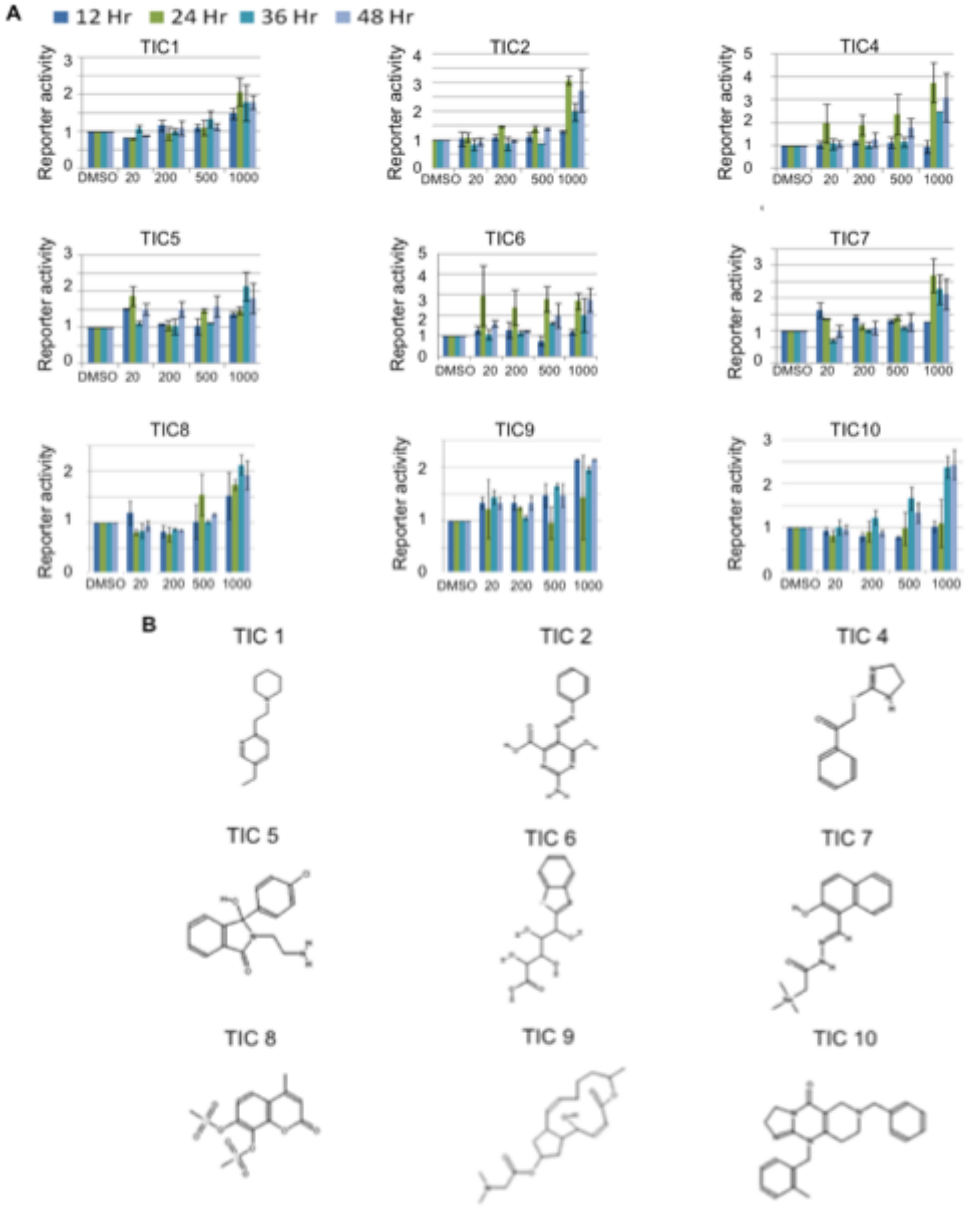

Figure 2.1. Identification of TRAIL-inducing compounds. (**A**) Activity of luciferase reporter in HCT116 Bax$^{-/-}$ cells under transcriptional control of the first 504 base pairs of the human TRAIL gene promoter upstream of the start of transcription (n=3). Working concentrations of TICs indicated on the x-axis in nanomolar. Data is normalized to cell viability under the same

conditions and relative to DMSO-treated conditions for each time point. Error bars indicate s.d. of replicates. (**B**) Structure of TRAIL-inducing compounds.

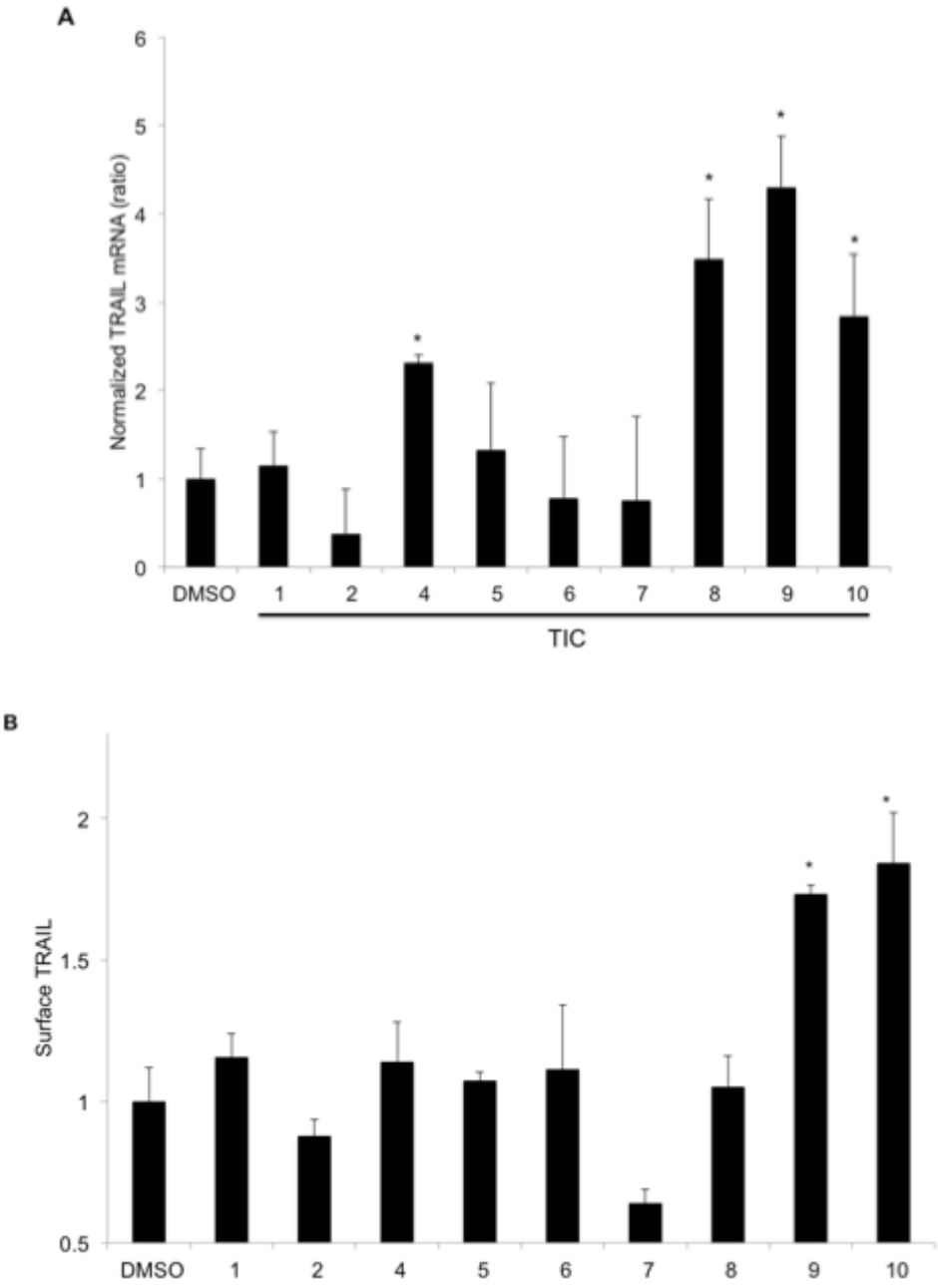

Figure 2.2. Validation of TIC-induced TRAIL. (**A**) RT-qPCR analysis of TRAIL mRNA levels in HCT116 $p53^{-/-}$ cells incubated with TICs (5 μM, 48 hr, n=3). Data is normalized to GAPDH mRNA levels. (**B)** Surface TRAIL analysis of HCT116 $p53^{-/-}$ cells incubated with TICs (5 μM, 72 hr, n=3). Error bars indicate s.d. of replicates. *$P < 0.05$ between the indicated condition and controls.

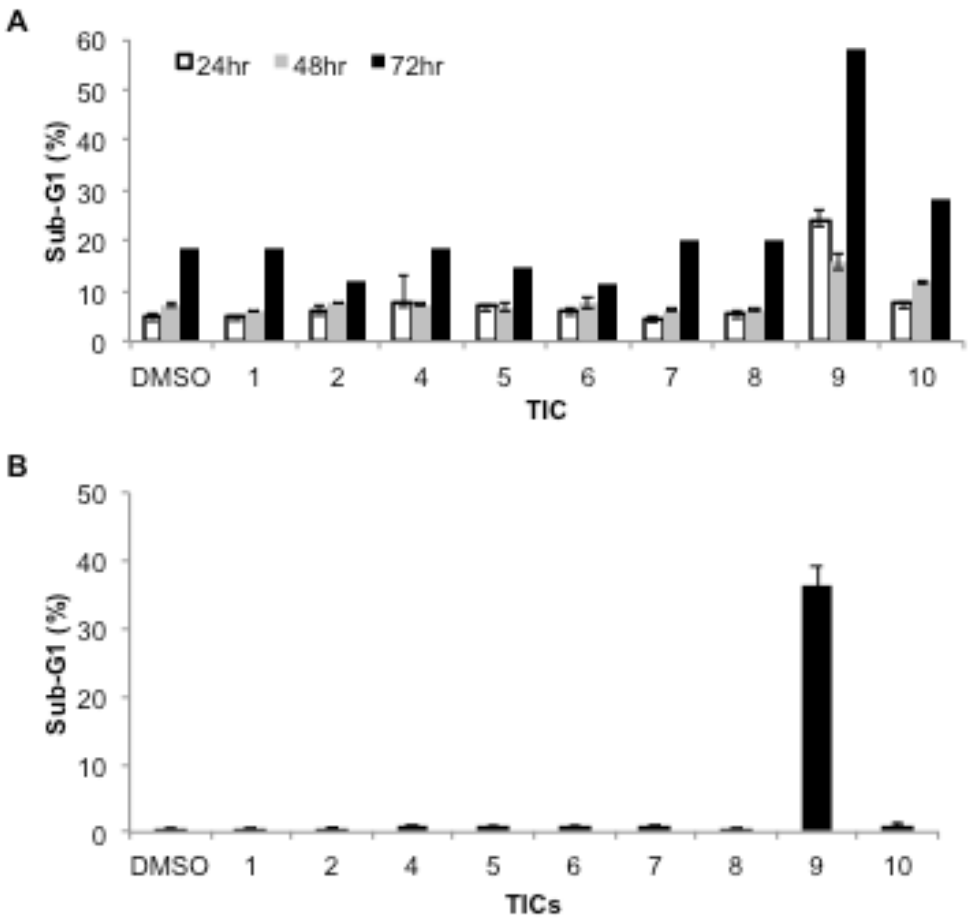

Figure 2.3. Cell death levels in normal and tumor cells with TIC treatment. (A) Sub-G1 content of HCT116 $p53^{-/-}$ treated with TICs (1 μM) for indicated time point (n=3). **(B)** Sub-G1 content of HFFs treated with TICs (1 μM) for 72 hours (n=3). Error bars indicate s.d. of replicates.

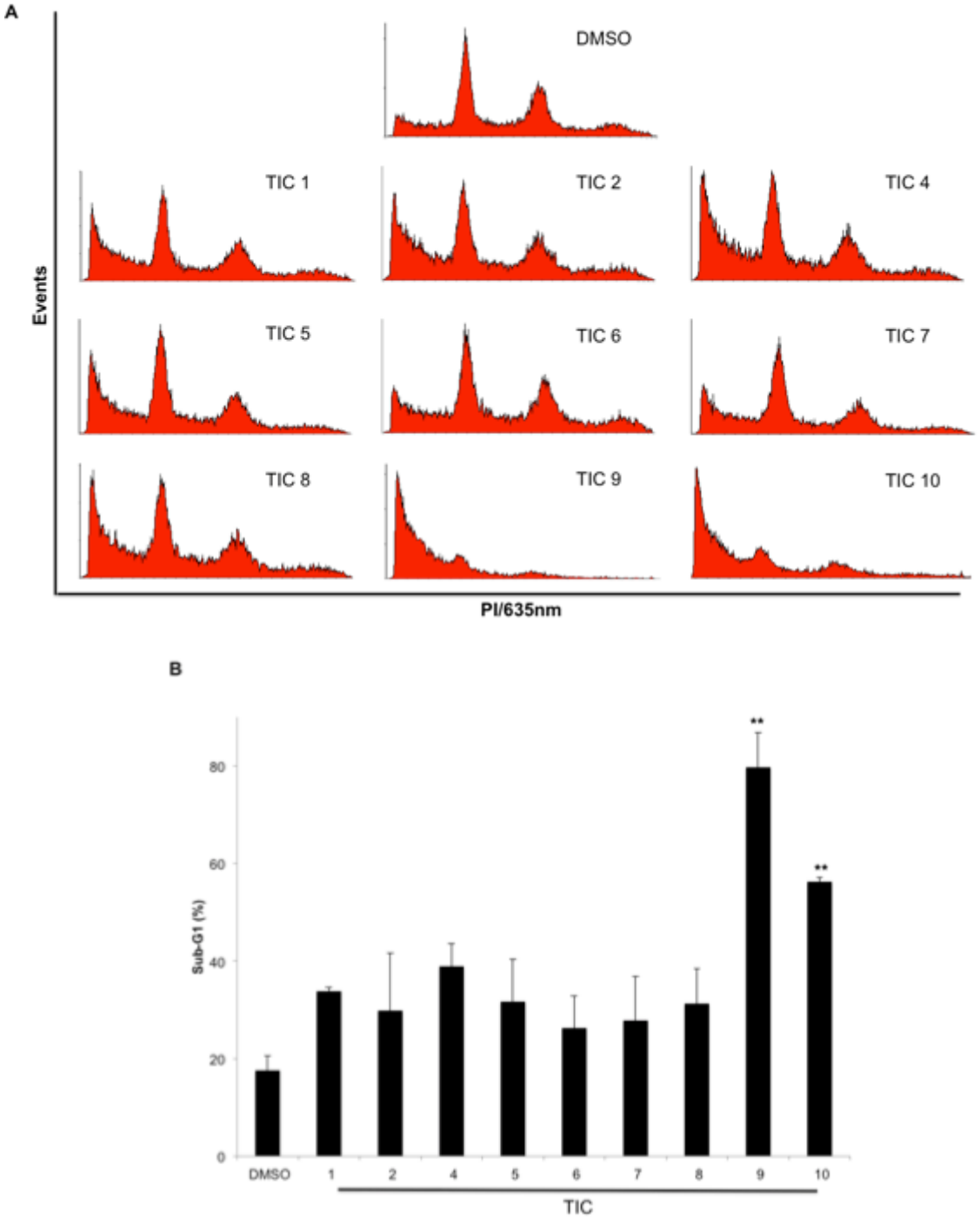

Figure 2.4. Cancer cell death induced by TICs. (A) Exemplary cell cycle profiles of HCT116 p53$^{-/-}$ treated with TICs (5 μM, 72 hr). **(B)** Sub-G1 quantification of HCT116 p53$^{-/-}$ treated with TICs (5 μM, 72 hr, n=3). Error bars indicate s.d. of replicates. ***P* < 0.005 between the indicated condition and controls.

TIC10 causes a sustained and p53-independent induction of TRAIL

TIC10 induced TRAIL promoter-dependent transcriptional activity of a luciferase reporter construct under regulatory control of the first 504 base pairs in a time- and dose-dependent manner in HCT116 $Bax^{-/-}$ cells (Figure 2.5A). Interestingly, the reporter activity was not upregulated by TIC10 prior to 48 hours. In accordance with this result, TIC10 caused a dose-dependent increase in TRAIL mRNA (Figure 2.5B-C) in p53-deficient HCT116 cells. We then tested if the TIC10-induced TRAIL transcription results in an increase in the amount of TRAIL localized to the cell surface of cancer cells. TIC10 indeed elevated surface TRAIL in a panel of several cancer cell lines that include human colon and breast cancers. (Figure 2.5D). This increase in surface TRAIL was also found to be p53-independent.

In accordance with the reporter assays, a time course analysis found that TRAIL was localized to the cell surface as a late event, peaking at 72 hours post-treatment in a dose-dependent manner (Figure 2.6A). We next tested if this induction of TRAIL as a late event requires continuous incubation with TIC10 or if this induction still occurs with short-term exposure to the molecule. We found that incubating with TIC10 for only 24 hours will still induce TRAIL on the cell surface at 48 hours following removal of the drug (Figure 2.6B). However, the longer the cells were incubated with TIC10, the larger the magnitude of TRAIL induction at 72 hours.

Thus TIC10 exposure leads to a significant and sustained presence of TRAIL on the cell surface of cancer cells in a time- and dose-dependent manner.

Based on the *in vitro* tumor-selective activity of TIC10 and its ability to induce the TRAIL in a p53-independent manner in several cancer cell lines, we selected TIC10 for further efficacy, safety, and mechanistic studies. We next confirmed the proposed structure of TIC10 using mass spectrometry. The observed mass and predicted elemental composition of the compound matched the expected mass and elemental composition (Figure 2.7). The fragmentation of TIC10 yielded several fragments that fit within the parent structure and fragment ions that fit with multiple regions of the parent compound that represent potential fragments.

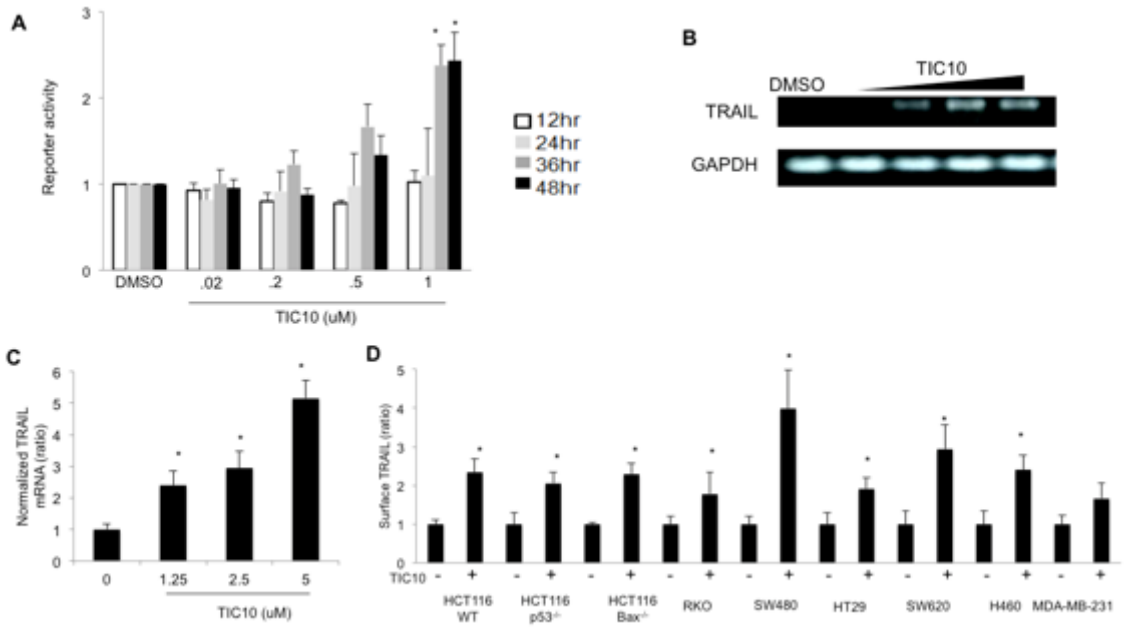

Figure 2.5. TIC10 induces TRAIL in a p53-independent manner. (A) Activity of luciferase reporter in HCT116 Bax$^{-/-}$ cells under transcriptional control of the first 504 base pairs of the human TRAIL gene promoter upstream of the start of transcription (n=3). Data is normalized to cell viability under the same conditions and relative to DMSO-treated conditions for each time point. (**B**) Semiquantitative RT-PCR analysis of TIC10-induced TRAIL messenger RNA in HCT116 p53$^{-/-}$ cells (48 hr) following treatment with DMSO or TIC10 (.5, 1, 5, and 10 μM from left to right). **(C)** RT-qPCR analysis of TIC10-treated HCT116 p53$^{-/-}$ cells (48 hr, n=4). (**D**) Surface TRAIL levels induced by TIC10 in a panel of cancer cells (10 μM, 72 hr, n=3). Error bars indicate s.d. of replicates. *P < 0.05 between the indicated condition and controls.

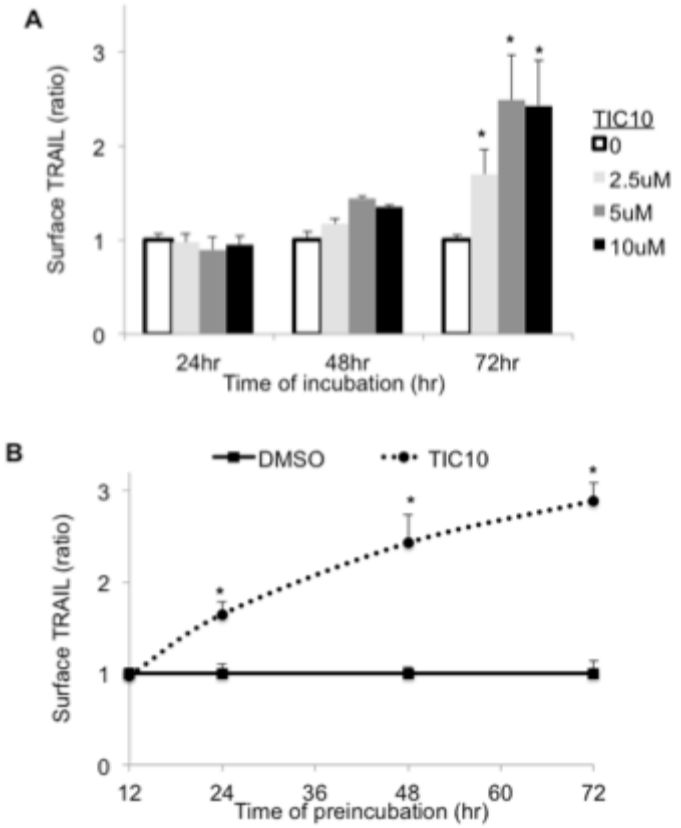

Figure 2.6. TIC10 causes a sustained induction of TRAIL on the surface of tumor cells. (A) Surface TRAIL levels in HCT116 $p53^{-/-}$ cells following TIC10 treatment at indicated conditions and time points (n=3). **(B)** HCT116 $p53^{-/-}$ TRAIL surface levels by flow cytometry at 72 hr following TIC10 treatment initiation (5 μM, n=3). Cells were treated for the indicated time of pre-incubation and then drug-free media was exchanged for the remaining time period until analysis at 72 hr. Error bars indicate s.d. of replicates. *P < 0.05 between the indicated condition and controls.

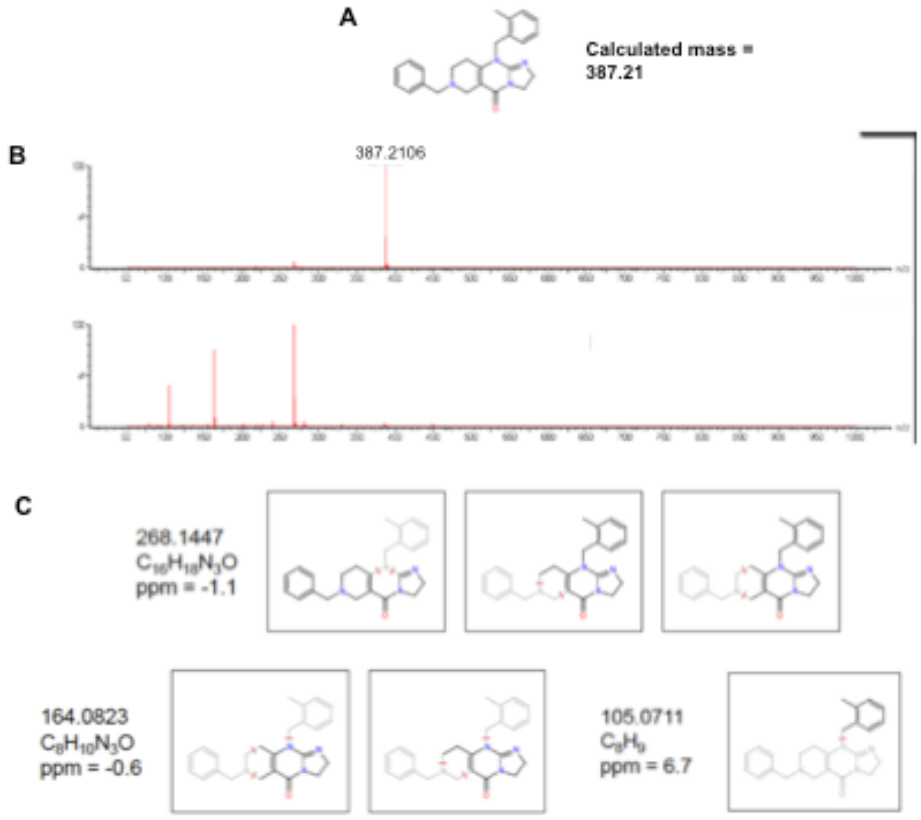

Figure 2.7. Validation of TIC10 structure by mass spectrometry. (A) Structure and mass of TIC10. **(B)** Mass spectrometry analysis of TIC10 showing the parent compound (top panel) and major fragments (bottom panel). **(C)** Potential structures of major fragments.

2.5 Discussion

The top 10 TICs represent a class of structurally diverse molecules that are potentially capable of upregulating TRAIL gene transcription at or below 1 μM, which is a potentially achievable dose *in vivo*. Interestingly, TIC9 was breflate, which is the prodrug of brefeldin A that is a classical inducer of endoplasmic reticulum (ER) stress and has been reported to induce high levels of p53-independent cell death (Shao et al., 1996). These observations raise the possibility that ER stress induces the TRAIL gene, though this observation will have to be validated with other classical ER stressors such as tunicamycin and thapsigargin and directly tested with appropriate molecular studies in the future. ER stress has been previously linked to the TRAIL pathway though induction of the TRAIL gene itself has not been described: (1) tunicamycin induces DR5 through IRE1α and

ATF6 (Jimbo et al., 2003); (2) ER stress triggers the intrinsic cell death pathway in a caspase-8-dependent manner (Jiang et al., 2007); (3) the acetic acid analogue α-TEA induces DR5 in a JNK/CHOP-dependent manner (Tiwary et al., 2010); (4) proteasome inhibitor-induced DR5 through CHOP (Yoshida et al., 2005); (5) direct positive regulative of the DR5 gene by CHOP binding to its promoter (Yamaguchi and Wang, 2004; Zou et al., 2008).

Only TIC9 and TIC10 were capable of elevating TRAIL expression on the cell surface. The lack of surface TRAIL induction by the other TICs despite elevation of TRAIL mRNA suggests that the TICs may differ in mechanism and potentially cause differential induction of TRAIL secretion and/or isoforms. Differences in TRAIL subcellular localization with different isoforms have been reported (Krieg et al., 2003).

TIC9 and TIC10 induced cell death of cancer cells much more strongly than the other TICs. The unique ability of TIC9 and TIC10 to cause a significant amount of cancer cell death may be related to their apparently unique ability to induce TRAIL at the cell surface. The structural diversity, variable kinetics of TRAIL induction, and differences in TRAIL localization induced by TICs suggest that these molecules may utilize different molecular mechanisms to induce the TRAIL gene. TIC9 but not TIC10 induced cell death of normal fibroblasts, suggesting that TIC10 may have a more favorable therapeutic index than TIC9. Thus, TIC10 was chosen as a lead TIC for further study based on its ability to induce TRAIL on the surface of tumors cells and its ability to potentiate significant levels of cancer-specific cell death.

In accordance with the design of the luciferase reporter screen, TIC10 induced TRAIL gene transcription in cells that lack p53. This is an important setting given the high frequency of p53 inactivation in human cancer by mutation or gene deletion, which often causes resistance to chemotherapy (Bunz et al., 1999). Another favorable observation for TIC10 as a therapeutic is its ability to induce TRAIL in cells that are p53-mutant (SW480) or -null (e.g. HCT116 $p53^{-/-}$), EGFR-null (SW620 cells), Her-2-null (MDA-MB-231 cells), cells that have mutant KRAS (e.g. SW480), or other oncogenic genetic aberrations. The ability of TIC10 to induce TRAIL in a sustained manner has important implications for its in vivo activity. Our data suggests that TRAIL can continue to be produced even after TIC10 is eliminated from the tumor environment.

CHAPTER 3

TIC10-INDUCED CYTOTOXICITY AND TRAIL-DEPENDENCY IN VITRO AND IN VIVO

3.1 Abstract

We tested the efficacy of TIC10 *in vitro* and *in vivo* to determine its utility as an antitumor agent. TIC10 induces a dose-dependent decrease in the cell viability of HCT116 cells and decreases the clonogenic survival of several different human cancer cell lines. Furthermore, TIC10 induced cell death in a p53-independent and Bax-dependent manner, as does rhTRAIL. The spectrum of activity for TIC10 is very broad and does not correlate with that of recombinant TRAIL, possibly due to the mechanism of TIC10. TIC10 induced Sub-G1 content, elevated levels of active caspase-3, and induced cell death that was inhibited by the pan-caspase inhibitor zVAD-fmk, which was suggestive of apoptosis. We then tested the contribution of TRAIL to the activity of TIC10 and found that suppression of TRAIL by shRNA, antibody-mediated sequestration, or overexpression of an inactivated death receptor (DR5) construct was sufficient to significantly inhibit TIC10-induced cell death. TIC10 caused potent antitumor effects *in vivo* even when given as a single dose as a monoagent, was orally active, and increased TRAIL protein and markers of TRAIL-mediated apoptosis in tumors. Stable knockdown of TRAIL inhibited the ability of TIC10 to induce the regression of tumor xenografts as well as TRAIL and markers of TRAIL-mediated apoptosis in tumors. In addition to demonstrating efficacy in several subcutaneous xenografts, we also found that TIC10 prolongs the survival of transgenic Eμ-myc mice that spontaneously develop lymphomas and mice harboring intracranial human glioblastoma xenografts.

3.2 Introduction

TRAIL has received considerable attention, primarily due to its apoptosis-inducing capability demonstrated in several human cancer cell lines (Walczak et al., 1997). The rapid apoptotic activity of rhTRAIL has been demonstrated in numerous solid and hematological malignant cell lines as a monotherapy (Ashkenazi et al., 1999b; Gazitt, 1999; Kelley et al., 2001; Marini et al., 2005; Pollack et al., 2001) and in combination with chemotherapy and radiotherapy (Chinnaiyan et al., 2000; Gliniak and Le, 1999; Keane et al., 1999a; Keane et al., 1999b; Mizutani et al., 1999; Nimmanapalli et al., 2001).

TRAIL initiates apoptotic signaling through the pro-apoptotic death receptor 4 (DR4; TRAIL-R1) (Pan et al., 1997c) and death receptor 5 (DR5; TRAIL-R2) (Pan et al., 1997b; Wu et al., 1997) at the cell surface through engagement of the extrinsic or intrinsic apoptotic pathways (Ashkenazi, 2002). Following ligand binding, the proapoptotic receptor death domains recruit Fas-associated death domain (FADD) and procaspase-8 to form the death inducing signaling complex (DISC). At the DISC, procaspase-8 is activated by autocatalytic cleavage to form caspase-8, which can cleave effector caspases-3, -6, and -7 to induce apoptosis by the intrinsic death pathway in type I cells. In type II cells, caspase-8 cleaves Bid to form tBid, which then interacts with Bax and Bak at the mitochondrial membrane to promote cytochrome c release (Li et al., 1998; Luo et al., 1998). Once released, cytochrome c binds to apoptotic peptidase activating factor 1 (Apaf-1) and caspase -9 to form the apoptosome, which initiates the caspase cascade.

Various forms of rhTRAIL have been engineered, including His tag (Pitti et al., 1996), Flag tag (Pascal, 2000), leucine zipper (Ganten et al., 2006; Walczak et al., 1999a), or isoleucine zipper versions of TRAIL. It has been reported that the leucine or isoleucine zipper rhTRAIL are effective and do not kill hepatocytes (Ganten et al., 2006). Several limitations of TRAIL as a therapeutic have been recognized and resulted in novel approaches to target the TRAIL pathway for the treatment of human cancer.

Recapitulating the efficacy of the natural ligand as a recombinant protein and enhancing its stability have been addressed by numerous studies describing the development of antibodies, peptide mimetics, and mutant versions of TRAIL (Abdulghani and El-Deiry, 2010; Bremer and Helfrich, 2010; van der Sloot et al., 2004; van der Sloot et al., 2006). The poor delivery of TRAIL, particularly to the brain, clearly limits its use in brain malignancies such as glioblastoma, which is an extremely lethal malignancy without any attractive therapy options. Recent efforts in the field aimed at overcoming limited biodelivery have utilized adenoviral expression of TRAIL on the surface of mesenchymal stem cells as a delivery vehicle, though its clinical feasibility is unclear. In conclusion, TRAIL is a potent cancer cell-specific inducer of apoptosis that has demonstrated some efficacy in clinical trials as a recombinant protein but may be therapeutically hindered by several molecular and practical limitations that include stability, half-life, biodistribution, expense,

and administration route. We therefore tested the ability of TIC10 to serve as an antitumor agent and to overcome efficacy-limiting properties of recombinant TRAIL that include poor thermal stability and the inability to cross the intact blood-brain barrier and treat brain tumors.

3.3 Materials and Methods

Reagents

zVAD-fmk (Promega) was used at a working concentration of 20 μM and was preincubated with cells for 15 minutes prior to addition of drug. The TRAIL-sequestering (RIK-2) antibody was used at a working concentration of 10 μg/mL (Santa Cruz).

Cell viability assay

Cells were plated into 96-well clear bottom, black-walled plates at 5,000 cells per well and allowed to adhere for 12 hours. Media was replaced the next day with complete containing the reagents as indicated at a volume of 100 μL per well. Cell viability was evaluated using the Cell TiterGlo (Promega) according to the manufacturer's protocol and analyzed using the IVIS imaging system (Xenogen). Dose-response curves were generated and IC50 values were calculated by a linear regression fit of the two treatment conditions flanking 50% viability.

Clonogenic assays

The indicated cell lines were plated at 500 cells per well and treated the following day after adherence as indicated. At 3 days post-treatment, the media was replaced with drug-free media and propagated for 10 days with fresh media given every 3 days. Cells were then washed in PBS, fixed and stained with Coomassie blue, rinsed, and air-dried for quantification.

Immunofluorescence by microscopy

Cells were grown in chambered slides and treated as indicated. At endpoint, cells were rinsed in PBS and incubated with CytoFix/CytoPerm (BD Laboratories) for 20 minutes and washed in CytoPerm/CytoWash. Primary antibodies were incubated overnight at 4°C or for 3 hours at room

temperature. The cleaved caspase-3 antibody was incubated at 1:200 (9664S, Cell Signaling). Cells were then rinsed twice and the appropriate secondary antibody was added at 1:250 for 1 hour at room temperature while protected from light. Cells were rinsed twice and mounted with a coverslip in fluorescent mounting media.

Western blot analysis

Western blot analysis was conducted as previously described (Wang et al., 2006) using NuPAGE 4–12% Bis-Tris and visualized using Supersignal West Femto (Thermo Scientific) and X-ray film. For all lysis buffers, fresh protease inhibitor (Roche) and 1 mM sodium orthovanadate was added immediately prior to use.

Retroviral infection

Phoenix-ampho cells or HEK293T (lentiviral) cells were seeded into a well of a 6 well plate at ~25% confluency and allowed to adhere for 24 hours. Cells were then transfected with 4 μg of the indicated plasmid using Lipofectamine 2000 by the manufacturer's protocol. Cells were then allowed to propagate in complete media for 48 hours. The supernatant was then harvested and centrifuged to clear cells. The cells to be infected were then trypsinized from log phase growth and placed into a well of a six well plate at ~40% confluency. 0.5mL of the phoenix-ampho supernatant and polybrene (20 μg/mL) was then added to the cell suspension. The well plate was then centrifuged at 1800 RPM for 2 hours. The media was then replaced by compete media and cells were allowed to propagate for 24 hours prior to selection with the appropriate. G418 selected was started at 40 μg/mL and puromycin selection was started at 0.5 ug/mL. A parallel "mock" infection with PBS was carried out as a positive control for selection. TRAIL shRNA was Mission shRNA (Sigma, SHGLY) and the vector was pLKO.1-pure (SHC002). For lentiviral infection, pCMV-dR8.2dvpr (plasmid #8455), and pCMV-VSVG were cotransfected with the indicated plasmid.

Subcutaneous xenografts in athymic nude mice

All animal experiments were conducted in accordance with the Institutional Animal Care and Use Committee (IACUC). For subcutaneous xenografts, 4-6 week old female, athymic nu/nu mice (Charles River Laboratories) were inoculated with $1X10^6$ cells ($2.5X10^6$ for T98G) of indicated cell lines in each rear flank as a 200 µL suspension of 1:1 Matrigel (BD):PBS. All intraperitoneal and intravenous injections were given at a total volume of 200 µL. Oral formulations of TIC10 were administered using an oral gavage and given as a 200 µL suspension containing 20% Cremophor EL (Sigma), 10% DMSO, and 70% PBS. Tumors were monitored using digital calipers at indicated time points. All subcutaneous tumors were allowed to establish for 1-4 weeks post-injection until reaching a volume of ~125 mm^3 before treatment initiation. Relief of tumor burden was monitored for 3 weeks following disappearance of the tumor and confirmed by necropsy after euthanasia. Bioluminescent imaging of tumors was carried out on an IVIS imaging system as previously described (Wang and El-Deiry, 2003). Near-infrared imaging of mice was carried out on the Pearl Impulse imaging system (LI-COR) following tail-vein injection of Angiosense 680 (VisEn Medical, Woburn, MA) according to the manufacturer's protocols. 6-week-old Eµ-myc mice were obtained from The Jackson Laboratory (B6.Cg-Tg(IghMyc)22Bri/J).

Immunohistochemistry and histology

Tissues were harvested and immediately fixed in 4% paraformaldehyde in PBS in microcentrifuge tubes for 48 hours at 4°C. Samples were then transferred to tissues cassettes in 70% ethanol and submitted to the Penn State Hershey Medical Center Tissue & Histology core facility for paraffin embedding and sectioning. Slides were dewaxed by an ethanol gradient (2 X 3' each of xylene, 95, 90, 80, and 70% ethanol. Slides were then immersed in 10 mM citric acid buffer (pH 6.0) and boiled for 6 minutes in the microwave. Slides were cooled in the solution for 15 minutes and rinsed in running water for 5 minutes. Tissues were circumscribed using a hydrophobic pen and blocked using FBS. The primary antibody was diluted in PBT (10% BSA, 10X Triton, in PBS) and incubated overnight at 4°C in a humidity chamber. The next day the samples were rinsed twice with PBS and incubated with the appropriate secondary antibody (Impress, Vector Lab).

Signal was developed using DAB (Vector Labs) deposition for 2-5 minutes and monitored by light microscopy. The slides were washes in dH_2O for 10 minutes, counterstained with hematoxylin (Daiko) for 5 minutes, rinsed PBS, rinsed in dH_2O, dehydrated with the reverse ethanol/xylene gradient, and mounted with a xylene-based medium and coverslip. For immunohistochemistry the following antibodies for used: cleaved caspase-8 (9496L, Cell Signaling), TRAIL (ab2435, Abcam). TUNEL staining was performed with the ApopTag Peroxidase In Situ Apoptosis Detection Kit (S7100, Millipore).

Primary glioblastoma tissue

All primary specimens were obtained in accordance with the Institutional Review Board at Penn State Hershey Medical Center using approved protocols. Samples were received immediately following resection, manually digested in complete DMEM with a scalpel and vortexing, filtered with a 100-µm nylon mesh, and plated at $2X10^5$ cells/mL in complete DMEM.

Intracranial xenografts

6-8 week old anesthetized athymic female nude mice were implanted with $2X10^5$ SF767 cells in a 25 µL suspension of serum- and antibiotic-free RPMI. The site of injection was a burr hole created 1mm lateral to the midline of the skull and 1mm anterior to the coronal suture to avoid ventricular deposition. The injection was administered over 5 minutes with a Hamilton syringe and the burr hole was sealed using bone wax. Tumor take was assessed by bioluminescent imaging 2 weeks following implantation. Bioluminescent imaging of tumors was carried out on an IVIS imaging system as previously described (Wang and El-Deiry, 2003). Near-infrared imaging of mice was carried out on a Pearl Impulse imaging system (LI-COR).

Statistical Analyses. For pair-wise comparisons, we analyzed data by the Student's two-tailed *t* test using Excel (Microsoft). Log-rank statistical analysis was performed using a web-based script that interfaces with the statistical package R (http://bioinf.wehi.edu.au/software/russell/logrank/).

3.4 Results

TIC10 has stable antiproliferative activity against cancer cells *in vitro*

With the observation that TIC10 induces TRAIL gene transcription in a manner that upregulates TRAIL on the surface of tumors cells in a temporally sustained manner, we next determined the activity profile of TIC10 *in vitro*. We found that TIC10 caused a dose-dependent decrease in the cell viability of HCT116 cells (Figure 3.1A). Furthermore, TIC10 decreased the clonogenic survival of DLD-1, SW480, and HCT116 human colon carcinoma cell lines (Figure 3.1B). We then determined if TIC10 could induce Sub-G1 DNA content, which can occur during apoptosis due to DNA fragmentation. TIC10 induced Sub-G1 content in the TRAIL-sensitive HCT116 cells at 5-10 μM doses in a p53-independent and Bax-dependent manner, as we previously reported for TRAIL-mediated apoptosis (Burns and El-Deiry, 2001) (Figure 3.1C).

One of the objectives of identifying TICs was to overcome limitations of rhTRAIL. We therefore compared the thermal stability of TIC10 and TRAIL using cell viability assays following a short-term incubation of a range of temperatures. We found that rhTRAIL rapidly loses activity following a 1 hour incubation at temperatures $\geq$40°C. This lack of thermal stability has been previously reported and was ascribed to protein denaturation (van der Sloot et al., 2004). In contrast, TIC10 maintained its activity at all tested incubation temperatures that reached as high as 100°C. This provides direct evidence of a superior drug property of TIC10 compared to rhTRAIL and bodes well for the stability of TIC10.

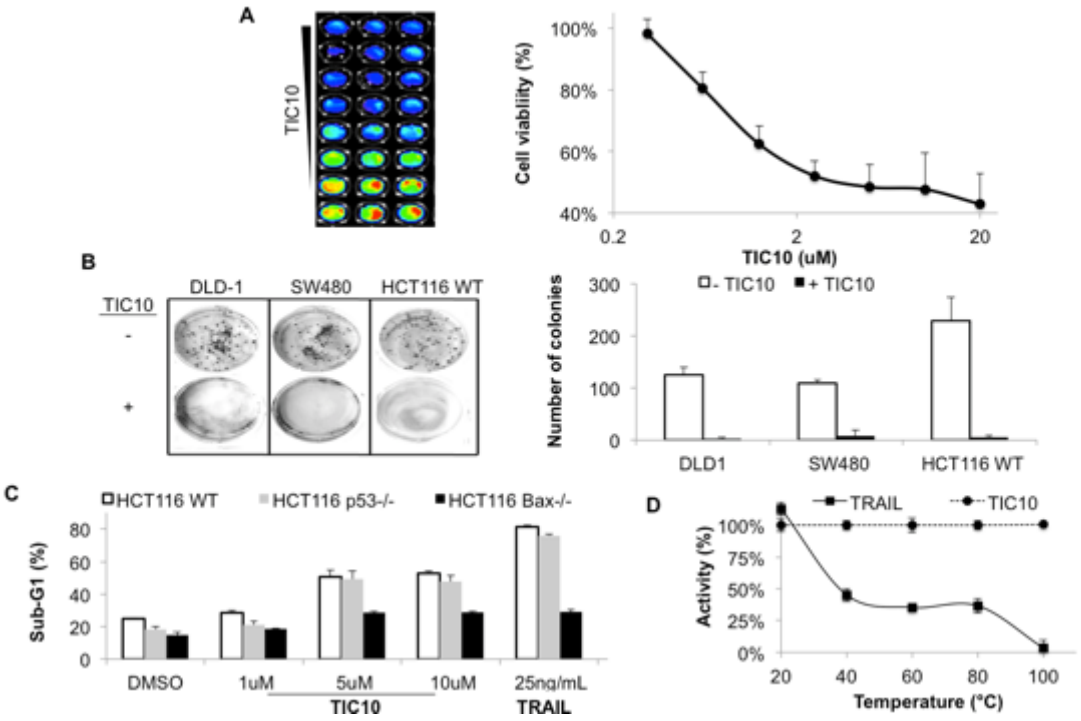

Figure 3.1. TIC10 has p53-independent anticancer activity *in vitro*. (A) Dose response of HCT116 cells to TIC10 treatment in cell viability assay (72 hr). Quantification shown in right panel (n=3). **(B)** Exemplary wells (left panel) and quantification (right panel) of colony formation assays of cancer cells treated with TIC10 (10 μM) for 72 hr followed by a 10 day proliferation period (n=3). (**C**) Sub-G1 analysis of HCT116 WT, $p53^{-/-}$, and $Bax^{-/-}$ cells following treatment with DMSO, TIC10 (1, 5, or 10 μM), or rhTRAIL (25 ng/mL) for 72 hr (n=3). **(D)** Ability of TIC10 or rhTRAIL to reduce cell viability in HCT116 cells following a 1 hr incubation at the indicated temperatures (n=3). Error bars indicate standard deviation (s.d.) of replicates.

TIC10 exhibits a broad-spectrum activity profile

As TIC10 is part of a library of NCI compounds, the growth inhibitory-50 (GI50) concentrations have been calculated for the molecule across the NCI panel of cancer cell lines. Mining this data revealed that TIC10 has broad-spectrum activity against all tested malignancies, which includes renal, prostate, ovarian, non small-cell lung cancer (NSCLC), melanoma, leukemia, colon, central nervous system (CNS), and breast cancers (Figure 3.2). The vast majority of these cancer cell lines possess a GI50 in the lower micromolar range, though there are a few that appear resistant as judged by a GI50 of $\geq$50 μM: RXF393, IGROV-1, KM12, and SF539. These cell line are of various tissues of origin and do not contain common oncogenic genetic alterations that have been previously reported (Ikediobi et al., 2006). The GI50 values reported by the NCI were in close agreement with IC50 values that we calculated for several cancer cell lines (Figure 3.3A). The broad-spectrum activity of TIC10 is attractive as a cancer therapeutic and is much more broad that that of rhTRAIL. Interestingly, the sensitivity of cancer cell lines to TIC10 does not correlate with sensitivity to rhTRAIL (Figure 3.3B). This suggests that the activity of TIC10 may involve changes that include but are not limited to TRAIL. This is not surprising given that the mechanism of TRAIL induction is transcriptional as demonstrated by RT-PCR data and therefore is highly likely to cause transcriptional changes in other genes. Furthermore, small molecules virtually always have pleiotropic effects that may or may not contribute to their activity and must be considered.

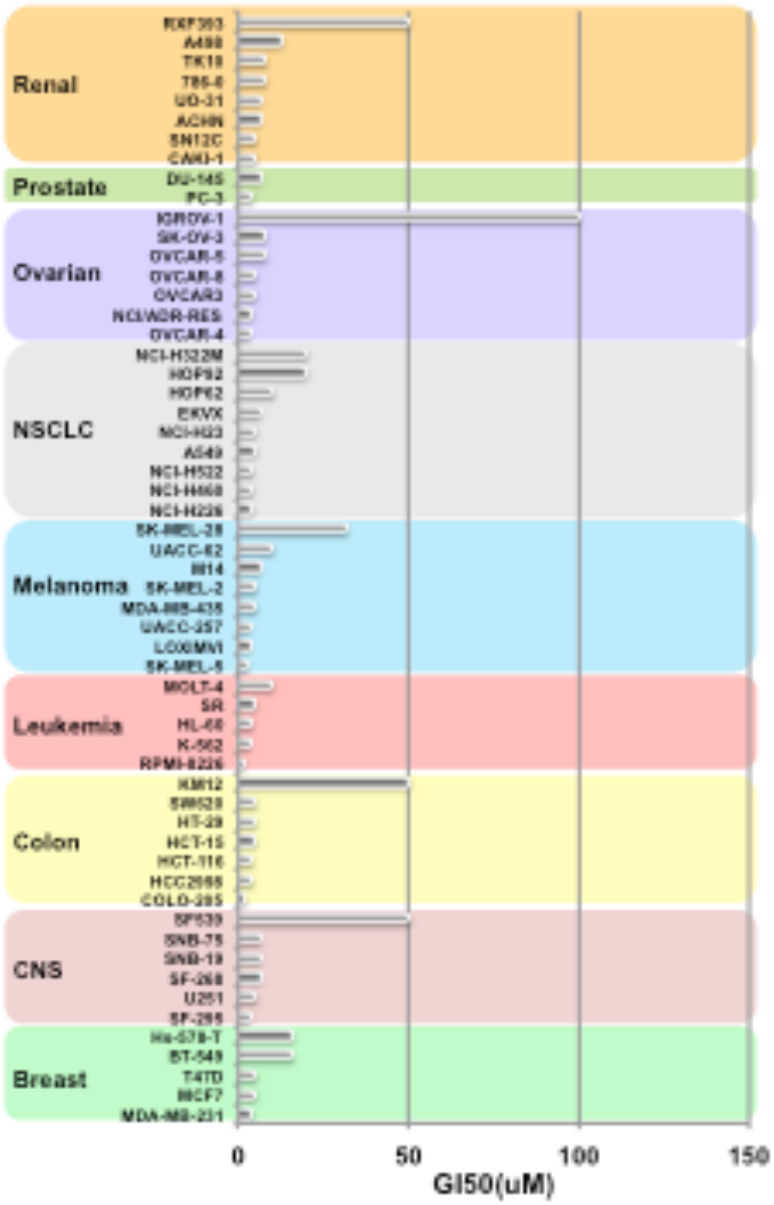

Figure 3.2. TIC10 exhibits broad-spectrum across the NCI60 *in vitro*. GI50 for TIC10 data from NCI database across the NCI60 panel of human cancer cell lines.

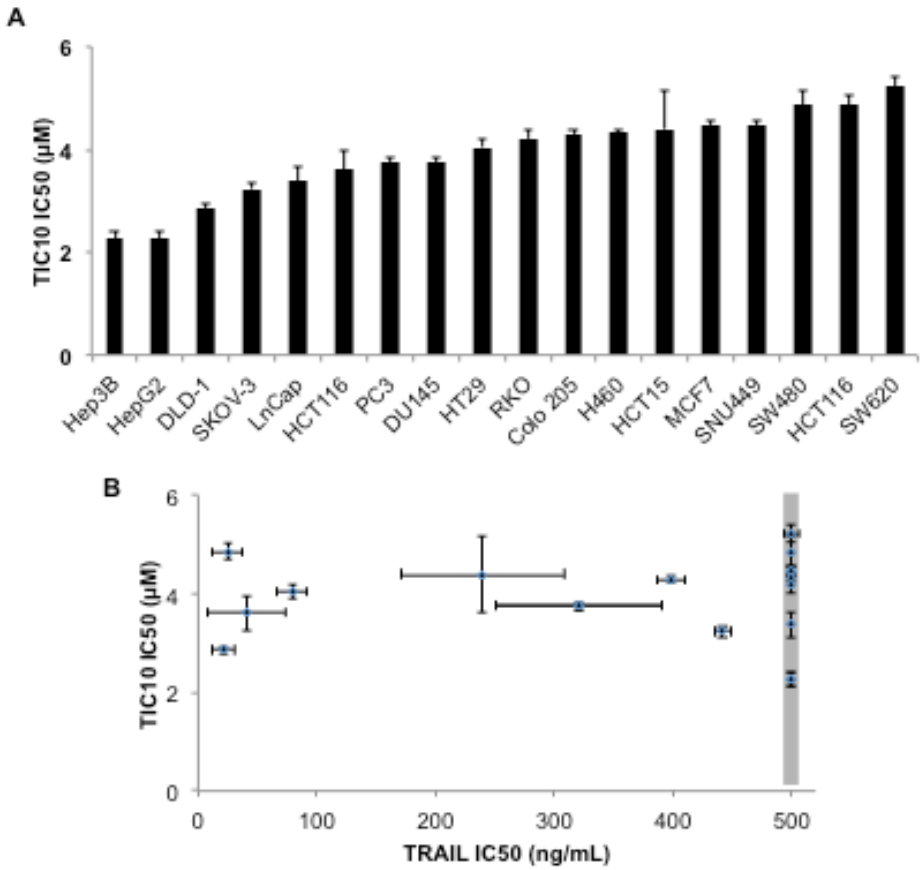

Figure 3.3 Activity profile of TIC10 and rhTRAIL. (A) IC50 for TIC10 in several human cancer cell lines extrapolated from cell viability assays conducted 72 hr post-treatment (n=2). **(B)** Lack of correlation between TIC10 and rhTRAIL sensitivity by IC50 values, IC50s for rhTRAIL determined as in (A) (n=2). Cell lines with a rhTRAIL IC50 greater than 500 ng/mL were not able to be accurately calculated and are displayed along the gray vertical line. Error bars indicate s.d. of replicates.

TIC10 causes TRAIL-mediated apoptosis

We next tested if the small molecule TIC10 induces apoptosis in cancer cells. We found that TIC10 treatment caused a large increase in the amount of Sub-G1 content in the cell cycle profile of HCT116 $p53^{-/-}$ cells (Figure 3.4A). TIC10 also increased protein levels of cleaved caspase-3, the active form of the effector caspase that is intimately involved in apoptosis, by Western blot analysis and immunofluorescence (Figure 3.4B). In accordance with apoptotic cell death, Sub-G1 content induced by TIC10 was significantly inhibited by co-incubation with zVAD-fmk in several cancer cell lines (Figure 3.4C). zVAD-fmk is a pan-caspase apoptosis inhibitor that functions by binding to the active site in caspases that carry out proteolysis by mimicking its substrate.

With the observations that TIC10 induces significant levels of TRAIL on the cell surface as well as apoptosis, we next tested whether TRAIL mediates apoptosis induced by TIC10 using a multitude of approaches. The first approach was to create a stable knockdown of TRAIL using short hairpin (shRNA) delivered by infection with lentiviral particles. TIC10-induced apoptosis was completely inhibited by shRNA-mediated stable knockdown of TRAIL (Figure 3.5A). Additional evidence for the requirement of TRAIL in TIC10-dependent tumor cell death was observed following abrogation of DR5 signaling (Figure 3.5B). We accomplished this by overexpressing a DR5 construct with its death-domain replaced by EGFP . The death domain is the region of the receptor that modulates proapoptotic TRAIL signaling by initiating the formation of the DISC, which activates caspase-8. Additionally, we inhibited TIC10-induced cell death with experimental sequestration of TRAIL by use of a blocking antibody (RIK-2) that has been previously characterized in the literature (Figure 3.5C) (Kayagaki et al., 1999). Taken together, these data demonstrate that TRAIL and TRAIL signaling plays a critical role in TIC10-mediated apoptosis.

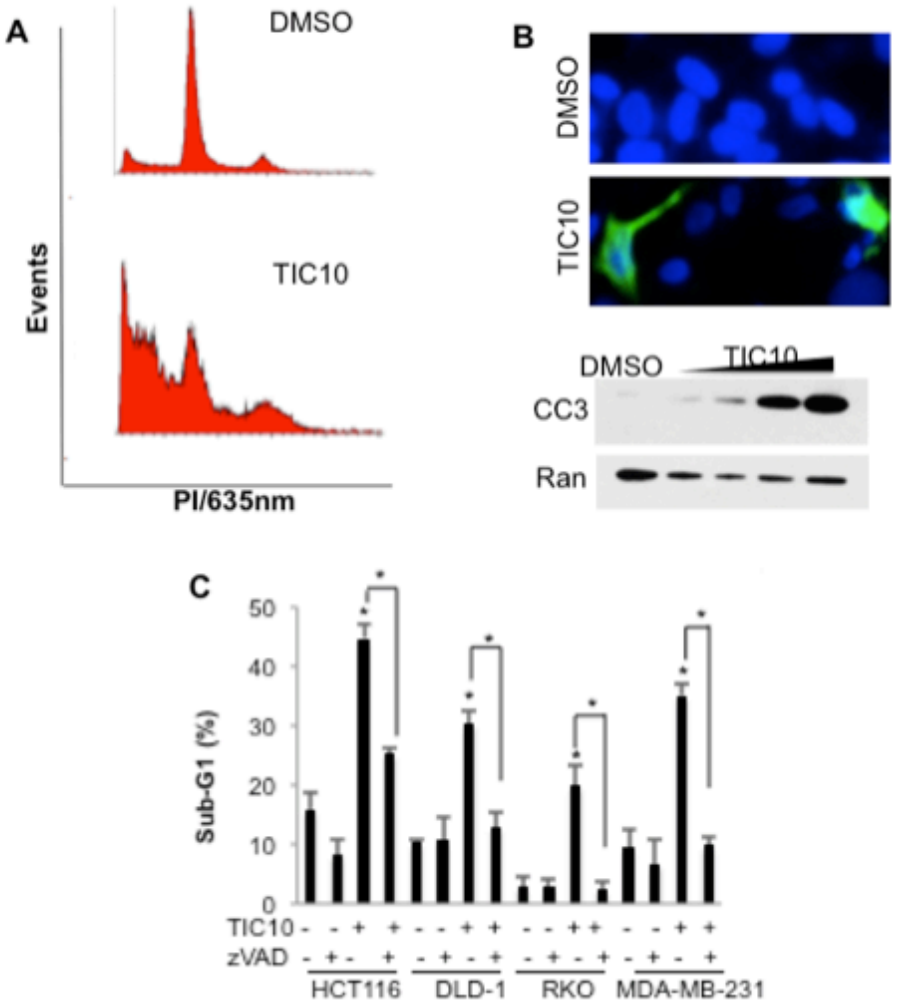

Figure 3.4. TIC10 induces caspase-mediated apoptosis. (A) Cell cycle profiles of HCT116 $p53^{-/-}$ cells treated with TIC10 (5 μM, 72 hr, n=3). **(B)** Active caspase-3 in HCT116 $p53^{-/-}$ cells assayed by immunofluorescence (top panel, 5 μM TIC10) or Western blot analysis (bottom panel) treated with TIC10 (0, 2.5, 5, 10 μM) for 72 hr. **(C)** Sub-G1 analysis of TIC10-treated cancer cells pre-incubated with or without zVAD-fmk (10 μM, 72 hr, n=3). Error bars indicate s.d. of replicates. *$P < 0.05$ between the indicated condition and controls unless indicated otherwise.

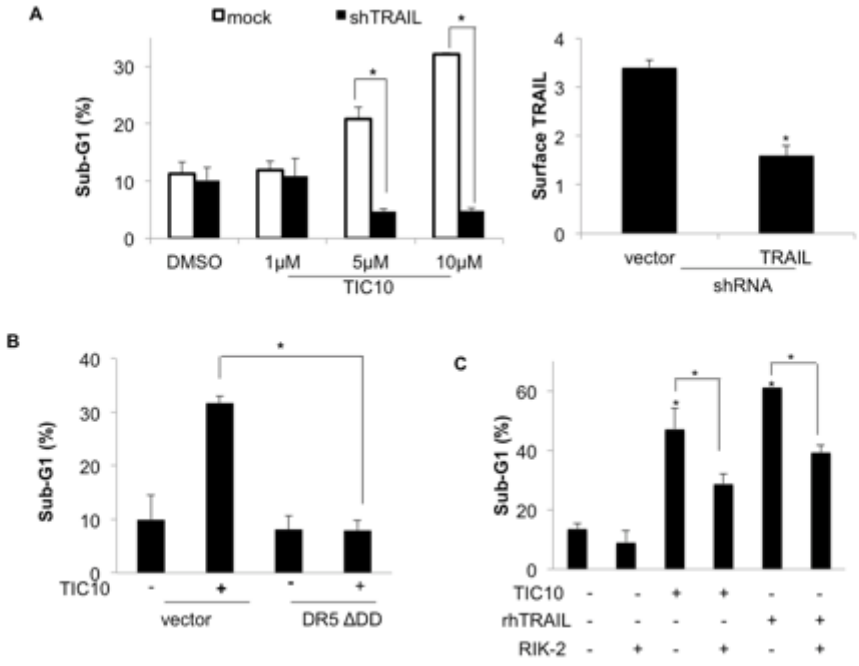

Figure 3.5. TIC10 induces TRAIL-mediated cell death *in vitro*. (A) Sub-G1 analysis of MDA-MB-231 cells with stable knockdown of TRAIL by short hairpin RNA (72 hr, n=3) (left panel). Verification of MDA-MB-231 shTRAIL knockdown by flow cytometry analysis of TIC10-treated cells (5 μM, 72 hr, n=3) (right panel). **(B)** Sub-G1 analysis of TIC10-induced cell death in H460 cells with endogenous DR5 or overexpression of a DR5 construct with its death domain replaced by EGFP (10 μM, 72 hr, n=3). **(C)** Sub-G1 analysis of HCT116 cells treated with DMSO, rhTRAIL (25 ng/mL), or TIC10 (10 μM) in the presence or absence of a TRAIL-sequestering antibody, RIK-2 (72 hr, n=3). Error bars indicate s.d. of replicates. *P < 0.05 between indicated condition and control unless otherwise indicated.

TIC10 is a potent antitumor agent in subcutaneous xenografts

We next tested the efficacy of TIC10 in several subcutaneous xenografts of several human cancer cell lines in athymic, nude mice. We found that TIC10 caused tumor regression in the HCT116 $p53^{-/-}$ xenograft to a comparable extent to that observed with TRAIL when both were administered as multiple doses (Figure 3.6A). Single intraperitoneal doses of TIC10 in HCT116 WT human colon cancer xenograft-bearing mice also exhibited a sustained response as monitored with bioluminescent imaging (Figure 3.6B). Single dose experiments comparing rhTRAIL and TIC10 in the RKO xenograft corroborated the potent anti-tumor activity of TIC10 and demonstrated clearly superior efficacy compared to rhTRAIL in this xenograft (Figure 3.6C). These effects were grossly apparent by measurements of tumor volume as well as near-infrared imaging of the tumors (Figure 3.6D).

One of the limitations of rhTRAIL is the requirement of intravenous administration, which is a practical barrier for patients that can limit therapeutic administration in the clinical setting. We therefore tested the activity of TIC10 upon oral administration. TIC10 caused a sustained regression of the SW480 xenograft as a single dose by intraperitoneal or oral delivery with a magnitude that was independent of delivery route. This result suggests that TIC10 has favorable bioavailability and/or that the dose of TIC10 administered (100 mg/kg) exceeds a threshold of efficacy saturation (Figure 3.6E). We next found that the formulation of TIC10 in 20% Cremophor EL and 80% PBS was a suitable solvent for oral administration by gavage to mice and that TIC10 was soluble in this mixture (data not shown). Titration of a single dose of orally administered TIC10 in the HCT116 xenograft model revealed sustained anti-tumor efficacy that plateaued at 25 mg/kg (Figure 3.6F). Based on these observations, TIC10 was given orally at 25 mg/kg for the subsequent *in vivo* experiments.

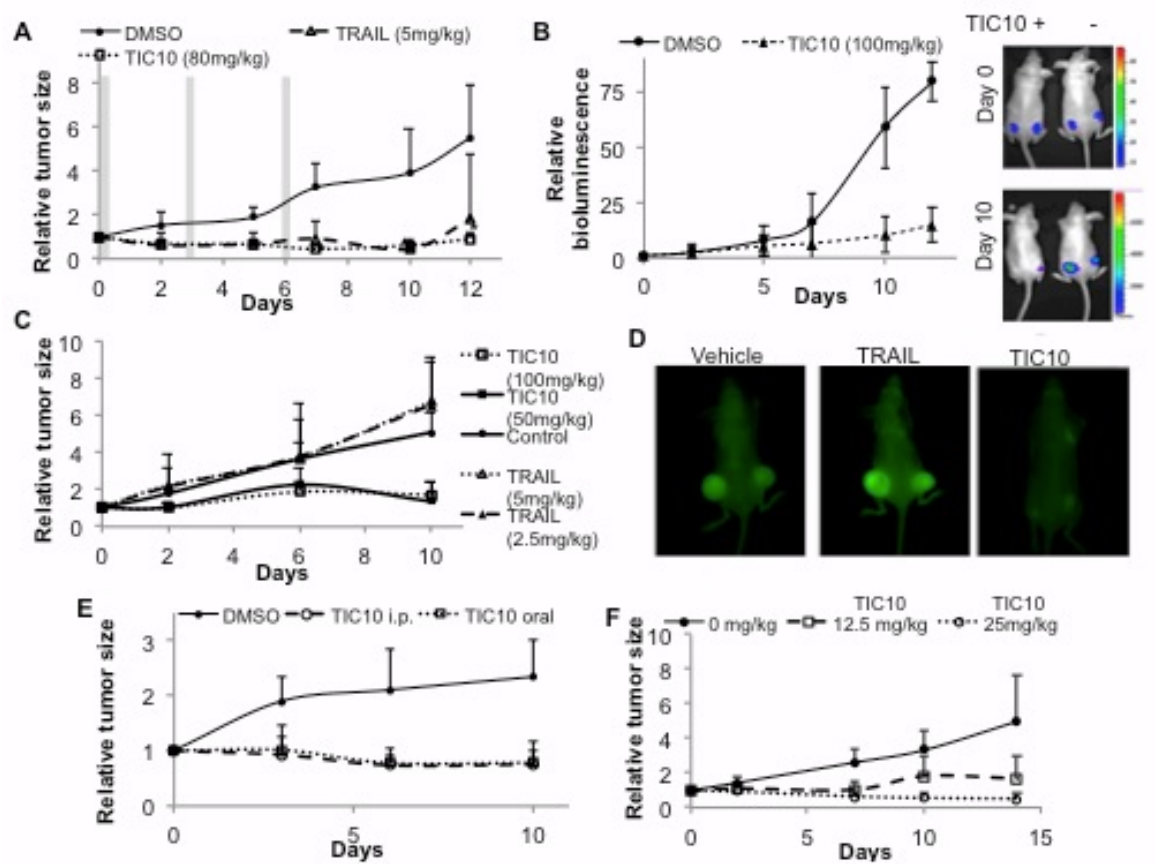

Figure 3.6. TIC10 exerts potent antitumor effects in subcutaneous xenografts of human cancer cell lines. (A) HCT116 $p53^{-/-}$ xenograft treated with 3 doses of TIC10 (i.p.), TRAIL (i.v.), or vehicle (i.p.) administered on day 0, 3, and 6 as indicated by gray vertical bars (n=10). **(B)** Bioluminescent imaging of luciferase-infected HCT116 $p53^{-/-}$ xenografts that received a single i.p. injection of TIC10 or vehicle (n=6). **(C)** RKO xenograft with a single dose of TIC10 (i.p.), TRAIL (i.v.), or vehicle (i.p., n=10). **(D)** Exemplary mice from RKO cohorts on day 13 post-treatment and 3-days post-injection with Angiosense 680. **(E)** Relative tumor volume of SW480 xenografts treated with TRAIL (i.v.), TIC10 (i.p.), or DMSO (i.p.) as a single dose at day 0 at 30 mg/kg (n=8). **(F)** Titration of TIC10 administered as a single oral dose in the HCT116 xenograft indicated concentrations (n=6). For all animal experiments, day 0 is defined as the day of treatment initiation. Error bars indicate s.d. among the cohort.

TIC10 induces TRAIL and hallmarks of TRAIL-mediated apoptosis in tumors

TIC10 clearly causes potent antitumor effects *in vivo*. We next assayed TIC10-treated tumors from the HCT116 $p53^{-/-}$ xenograft for evidence that TIC10 induces TRAIL and markers of TRAIL-mediated apoptosis as it does *in vitro*. Histological analysis using H&E staining revealed an obvious increase in fragmented nuclei in TIC10-treated tumors, which is a consequence of apoptosis-mediated DNA fragmentation. Immunohistochemical (IHC) analysis of TIC10-treated tumors revealed increased protein levels of TRAIL and cleaved caspase-8, which is the initiator caspase involved in triggering TRAIL-mediated apoptosis upon receptor-ligand binding (Figure 3.7). Also in support of apoptosis, there was a striking increase in the amount of TUNEL (TdT-mediated dUTP Nick-End Labeling) staining that labels DNA double stranded breaks that result from apoptosis. Interestingly, TRAIL induction was high 2 days following TIC10 treatment though it was still slightly elevated at 1 week post-treatment and other markers of TRAIL-mediated apoptosis were also persistent at this time point. This evidence suggests that TIC10 induces TRAIL and TRAIL-mediated apoptosis in tumor xenografts in a temporally sustained manner.

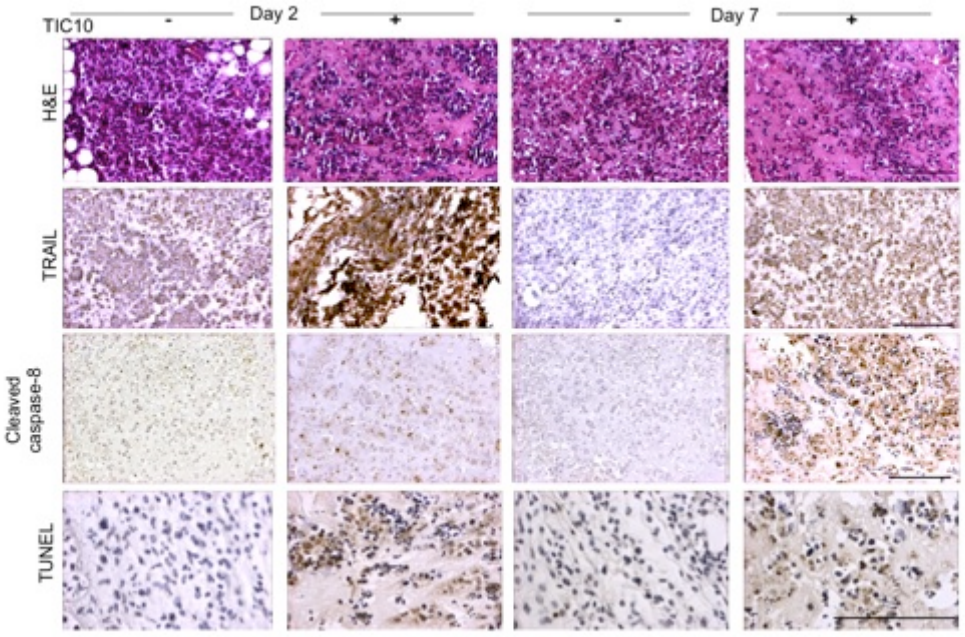

Figure 3.7. TIC10 induces TRAIL and TRAIL-mediated cell death in tumors. Histological and immunohistochemical analysis of HCT116 $p53^{-/-}$ tumors following a single dose of TIC10 (100 mg/kg, i.p.) on day 0.

TRAIL is required for the activity of TIC10

We then tested the requirement of TRAIL for TIC10 antitumor activity *in vivo* by shRNA-mediated stable TRAIL knockdown cells. A single dose of TIC10 induced regression of MDA-MB-231 human triple-negative breast cancer xenografts that was significantly inhibited by knockdown of TRAIL whereas TRAIL-treated tumors progressed in terms of tumor volume (Figure 3.8A). Additionally, the stable knockdown of TRAIL ablated the apoptosis induced in tumors as judged by TUNEL staining (Figure 3.8B), which labels free nucleotides at the end of double stranded DNA breaks that occur during apoptosis. This directly demonstrates that the anti-tumor activity of TIC10 is superior to that of TRAIL when administered as single doses in this xenograft and this activity is mediated at least in part by TRAIL produced by tumor cells.

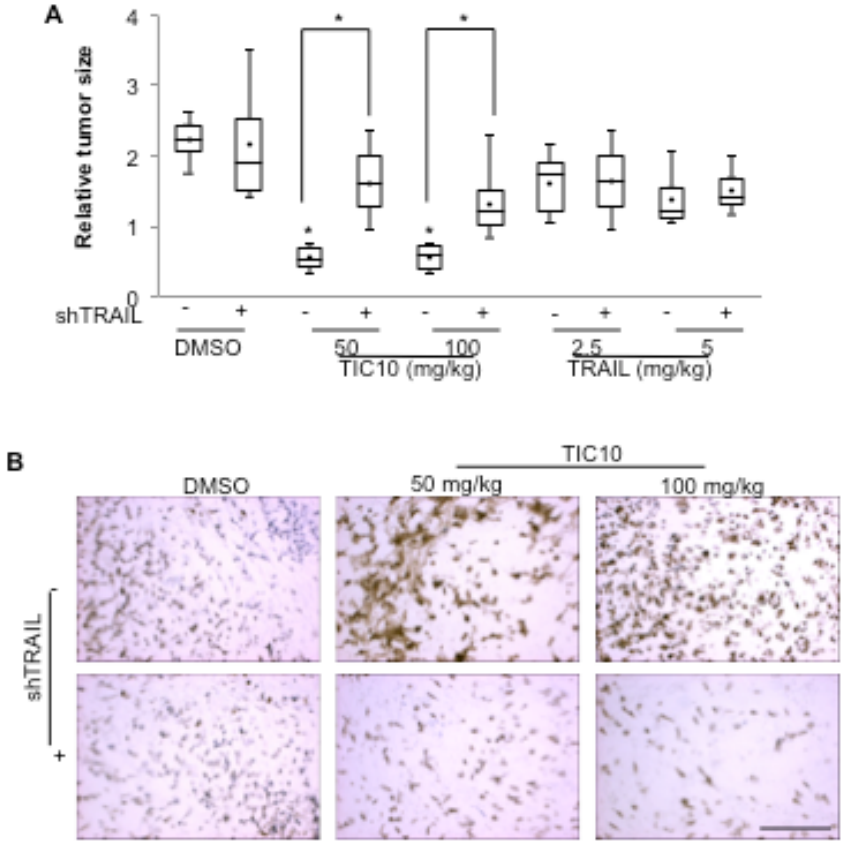

Figure 3.8. The antitumor effects of TIC10 are mediated by TRAIL. (A) Box and whisker plot of tumor volume on day 9 following treatment initiation in MDA-MB-231 vector or shTRAIL xenografts with single doses of TIC10 (i.p.), rhTRAIL (i.v.), or vehicle (DMSO, i.p.) (n=8). **(B)** TUNEL staining of tumors from the MDA-MB-231 vector and shTRAIL xenografts 2 days post-treatment. Error bars indicate s.d. among the cohort. *P < 0.05 between indicated condition and control unless otherwise indicated.

TIC10 prolongs the survival of transgenic mice with spontaneous lymphoma

Testing the efficacy of novel therapies in mouse models is considered essential in the translation process for cancer therapeutics, though specific models have pros and cons. For instance, subcutaneous xenografts of human cancer cell lines require immunocompromised mice to prevent immune rejection of the transplanted cells. This means that this model does not account for the immune system, which can be affected or even utilized by therapies. Transgenic mice offer an alternative model that allows for a wild-type immune system by introducing oncogenic alterations in the mouse genome to allow for spontaneous or inducible cancer. The disadvantage of transgenic mice as a model is that the cancer cells are of mouse origin, which means that they may respond differently to therapeutics due to differences in genetics. To test the efficacy of TIC10 in an immuno-competent preclinical cancer model, we utilized Eμ-Myc transgenic mice that spontaneously develop lymphoma. We treated these mice with oral TIC10 (25 mg/kg) or vehicle once a week from weeks 9-12 of age, which is when these mice develop lymphoma. TIC10 significantly prolonged the survival of these mice by 4 weeks (Figure 3.9). It should be noted that these mice are incurable due to their oncogenic transgene and that treatment was terminated at week 12 due to experimental design, though no signs of toxicity were evident.

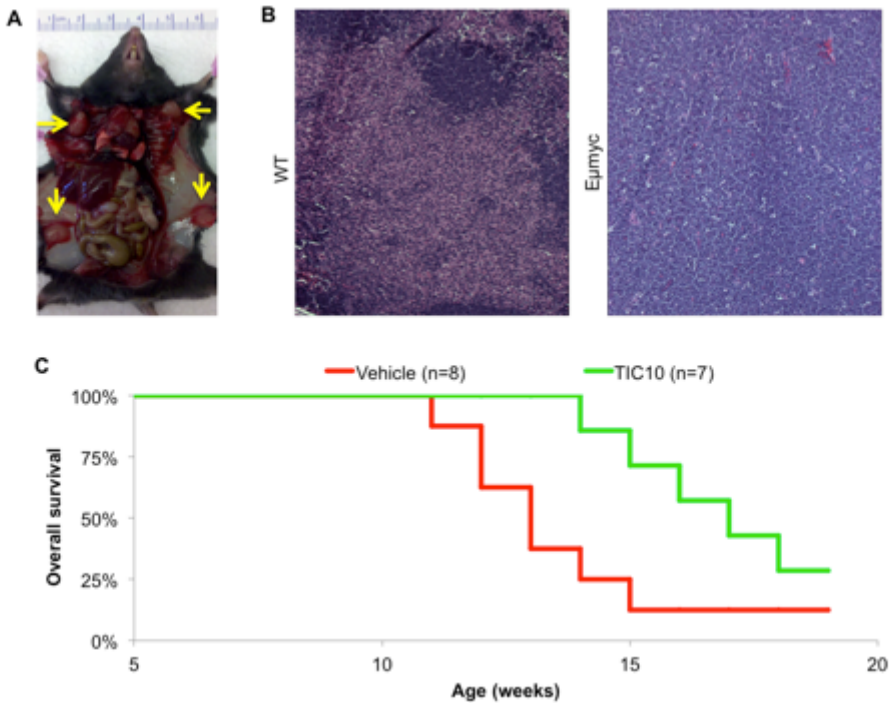

Figure 3.9. TIC10 prolongs the survival of transgenic mice with spontaneous lymphoma. **(A)** 14-week old Eμ-myc mouse with swollen axillary and inguinal lymph nodes. **(B)** H&E staining of Eμ-myc and WT C57/B6 axillary lymph nodes. **(C)** Overall survival of Eμ-myc treated during weeks 9-12 with TIC10 (PO, qwk). *P*=.00789 determined by log-rank test.

Clinical trials with novel cancer therapeutics with efficacy as an endpoint often involve the addition of the investigational drug to the standard-of-care treatment. It's therefore useful to identify approved therapeutics that synergize with the investigational agent to aid in future clinical trial design. We searched for synergistic combinations of TIC10 with approved chemotherapeutic agents using cell viability assays in HCT116 and HT29 human colon carcinoma cell lines (Figure 3.10). For these assays, we selected doses based on $IC_{12.5}$, IC_{25}, and $IC_{50.}$values reported in the literature, though disparities exist because of fundamental differences between assays and other experimental conditions.

Among the tested chemotherapies, we observed *in vitro* synergy between TIC10 and the taxanes paclitaxel and docetaxel. This synergy was subsequently confirmed in the SW620 metastatic human colon carcinoma cell line and the H460 NSCLC cell line (Figure 3.11). Taxanes are cancer therapeutics that inhibits mitosis by inhibiting the function of microtubules through targeting GDP-bound tubulin. Paclitaxel is approved by the FDA in the treatment of AIDS-related Kaposi sarcoma, breast cancer, NSCLC, and ovarian cancer. Docetaxel is approved for the treatment of breast cancer, advanced gastric cancer, NSCLC, prostate cancer, and squamous cell carcinoma of the head and neck.

We then tested the combination of TIC10 with paclitaxel or docetaxel as single doses in a subcutaneous xenograft of H460 NSCLC cells. Both TIC10 and the taxanes alone had a potent effect on the tumor growth, which limited the ability to conclude about the degree of cooperativity with the combination (Figure 3.12A-B). Nevertheless, the combination of TIC10 and either of these taxanes cooperated to yield several sustained cures in the H460 non-small cell lung cancer xenograft, unlike the monoagents (Figure 3.12C-D).

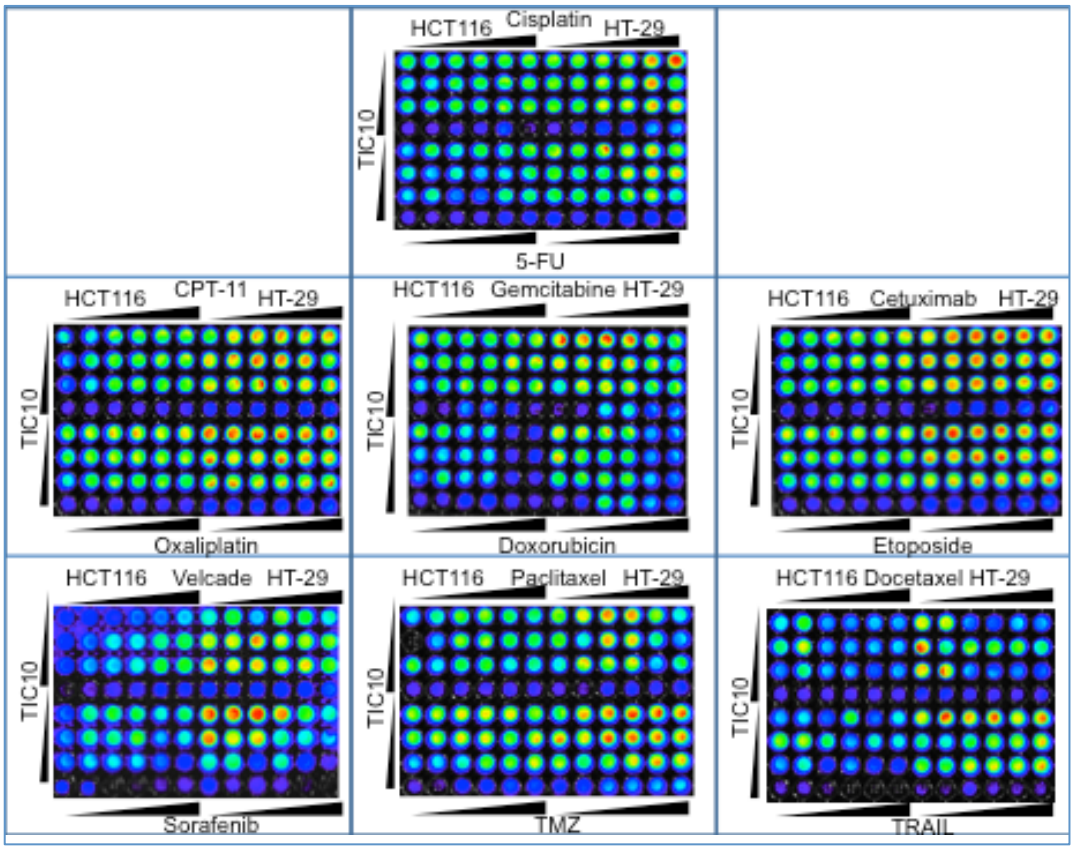

Figure 3.10. Combination of TIC10 with approved cancel therapeutics. Cell viability assays of HCT116 and HT-29 cell lines treated with the indicated drug at $IC_{12.5}$, IC_{25}, and IC_{50} doses reported in the literature (72 hr, n=3). 5-FU: 5-fluorouracil; TMZ: temozolomide.

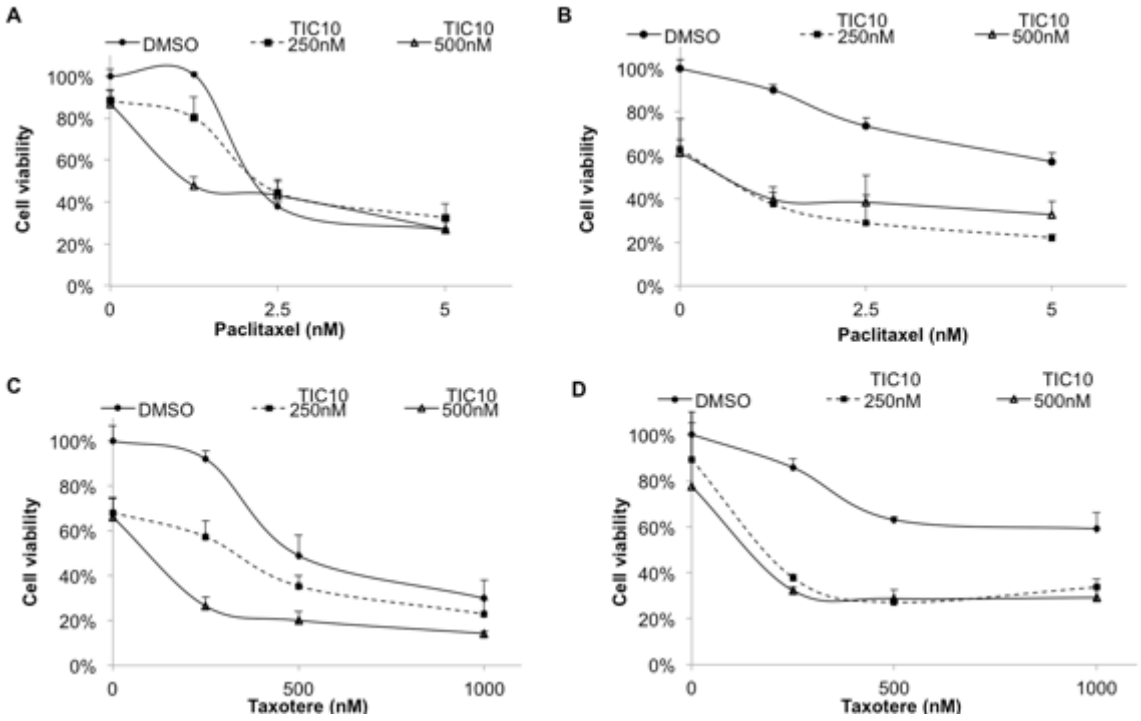

Figure 3.11. TIC10 synergizes with taxanes *in vitro*. Cell viability of **(A)** DLD-1 and **(B)** SW620 cells treated with TIC10 in combination with paclitaxel in at indicated conditions (72 hr, n=3). Cell viability of **(C)** DLD-1 and **(D)** SW620 cells treated with TIC10 in combination with taxotere in at indicated conditions (72 hr, n=3). Error bars indicate s.d. of replicates.

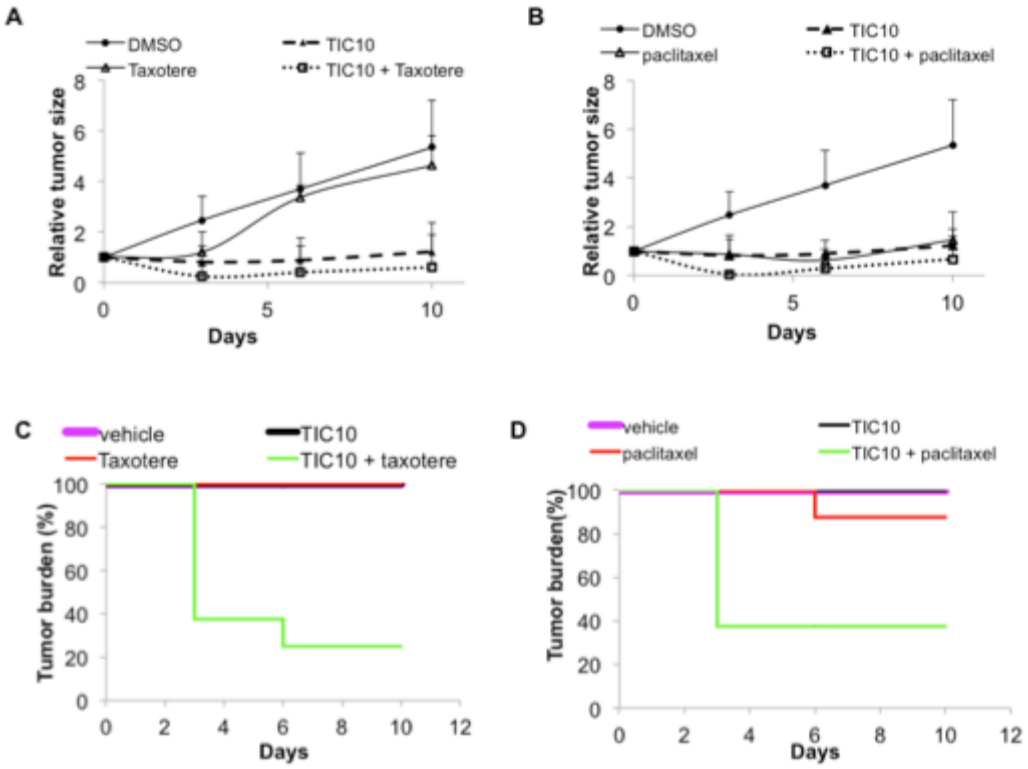

Figure 3.12. TIC10 cooperates with taxanes in vivo. (A) Relative tumor volume of H460 xenograft treated with TIC10 (30 mg/kg, i.p.) or taxotere (20 mg/kg, i.v.) alone, in combination, or with vehicle (DMSO, i.p.) (n=8). **(B)** Relative tumor volume of H460 xenograft treated with TIC10 (30 mg/kg, i.p.) or paclitaxel (20 mg/kg, i.v.) alone, in combination, or with vehicle (DMSO, i.p.) (n=8) as single doses. **(C)** and **(D)** are the tumor burden curves for the cohorts described in (A) and (B), respectively. Error bars indicate s.d. among the cohort.

TIC10 is effective against glioblastoma

The inability of rhTRAIL to cross the blood-brain barrier greatly limits its utility in cancers involving the central nervous system. Unlike the large proteins, many lipophilic small molecules are able to permeate the blood-brain barrier. We explored the possibility that TIC10 may serve as an anti-tumor agent against brain tumors. We selected glioblastoma multiforme (GBM) as it is the most common and most aggressive of the brain tumors. We first tested the activity of TIC10 in GBM cell lines and found that TIC10 induced TRAIL (Figure 3.13A) and had a p53-independent GI50 in the low micromolar range that is comparable with the GI50 values observed for TIC10 in other cancer cell lines (Figure 3.2). Importantly, this panel of GBM cell lines includes cells that are resistant to temozolomide such as T98G (Figure 3.13B) (Kanzawa et al., 2003).

In addition to cell lines, we also tested the cytotoxicity of TIC10 on freshly resected brain tumor cells from a 38 year-old female patient with grade IV glioblastoma with an oligodendroglial component that was previously resected and irradiated. TIC10 exerted a strong cytotoxic effect against these cells even at the lowest tested dose of 1.25 μM as opposed to temozolomide, which had no significant effect under these conditions (Figure 3.13C). We then tested TIC10 in GBM *in vivo* as a monoagent and in combination with bevacizumab, the antiangiogenic monoclonal antibody that targets VEGF and is approved for the treatment of recurrent gliomas. *In vitro* testing involving bevacizumab is not readily possible, as angiogenesis is not represented *in vitro*. TIC10 induced a sustained regression of subcutaneous temozolomide-resistant T98G xenografts to an extent similar to a clinical dose of bevacizumab when given as a single oral dose (Figure 3.13D).

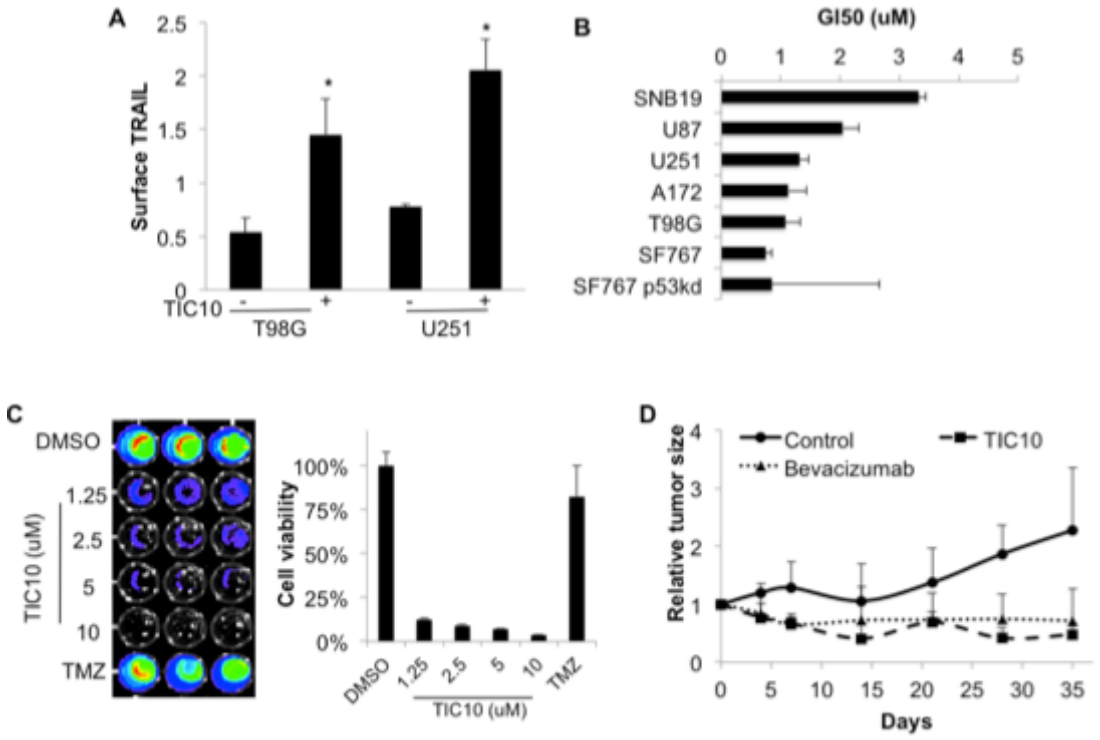

Figure 3.13. TIC10 is an effective antitumor agent against human glioblastoma. (A) Surface TRAIL in GBM cell lines following incubation with TIC10 (5 μM, 72 hr, n=3). (**B**) GI50 values extrapolated from cell viability assays of indicated GBM cell lines at 72 hr post-treatment with TIC10 or DMSO (n=3). (**C**) Cell viability assay of freshly resected glioblastoma tissue treated with DMSO, TIC10, or temozolomide (TMZ, 10 μM) (72 hr, n=3). Tissue was a grade IV glioblastoma with oligodendroglial component taken from a 38 year-old female patient that had undergone prior cytoreductive surgery and radiation. (**D**) Subcutaneous xenograft of T98G with mice receiving a single dose of vehicle, TIC10 (30 mg/kg, PO), or bevacizumab (10 mg/kg, i.v.) on day 0 (n=8). Error bars indicate s.d. of replicates. *P < 0.05 between indicated condition and control.

TIC10 prolongs the survival of mice harboring intracranial human GBM

Based on the potent activity of TIC10 in GBM including cells that are resistant to temozolomide, we tested the impact of TIC10 on the overall survival of mice with brain tumors. For this model, we utilized SF767 human GBM cells that we labeled with luciferase and EGFP to allow for *in vivo* imaging. Imaging is necessary for this model as the tumor grows inside on the skull and therefore does not allow for tumor volume measurements. We performed orthotopic implantation of these cells and evaluated successful tumor taken by verifying placement with pericranial imaging (Figure 3.12A) and tumor growth using quantitative bioluminescent imaging. Following verification of a viable and growing tumor, mice were randomized into 4 treatment cohorts that received single doses of vehicle, oral TIC10 (25mg/kg), bevacizumab (10mg/kg i.v.), or concomitant TIC10 and bevacizumab. Treatment was initiated 2 weeks following intracranial implantation of the tumor cells. TIC10 as a monoagent had strong effects in this model both in terms of tumor regression and survival (Figure 3.12B-C, Table 3.1) We found that a single dose of TIC10 significantly doubled the overall survival of mice as a monoagent this aggressive intracranial xenograft of human GBM using the SF767 cell line. Furthermore, TIC10 cooperated with bevacizumab to triple the duration of survival of such brain tumor-bearing mice.

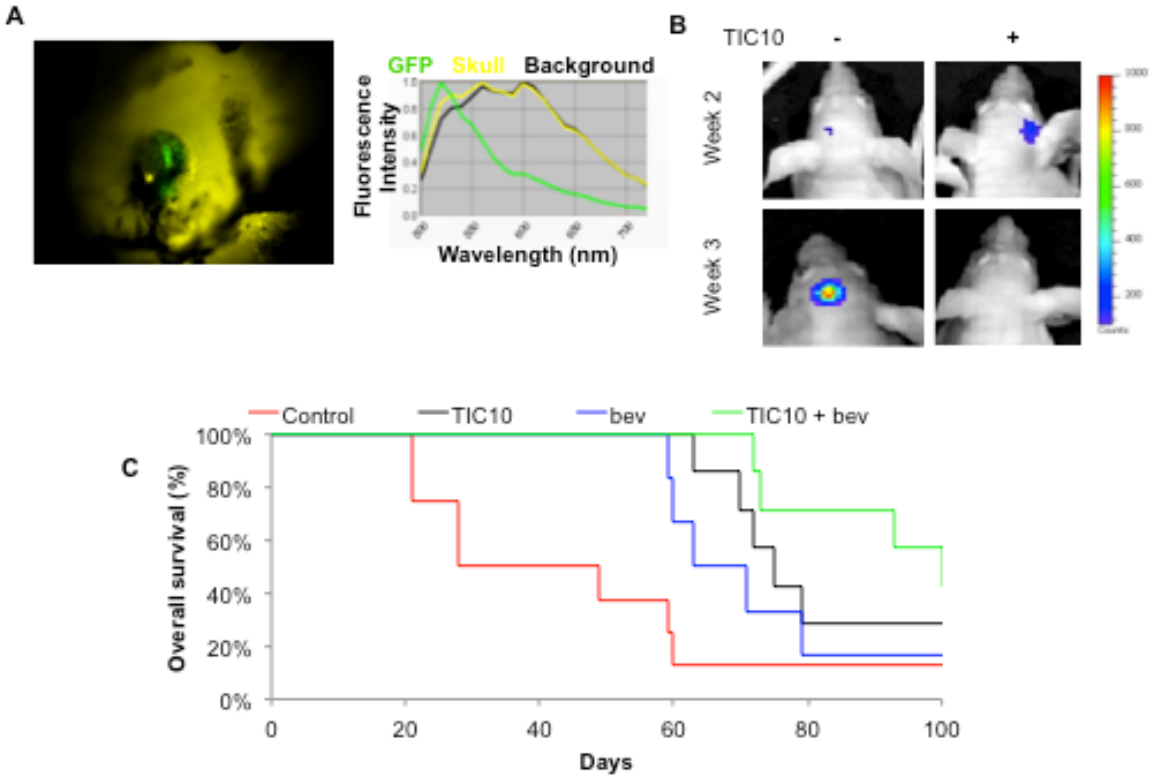

Figure 3.14. A single dose of TIC10 prolongs the survival of mice with intracranial human brain tumors. (A) Confirmation of GFP-labeled SF767 GBM intracranial implantation 1-week post-implantation using spectral unmixing. **(B)** Bioluminescent imaging of an exemplary control mouse and a TIC10-treated mouse showing a response. The luminescent scale bar on the right applies to all images in the panel. (**C**) Overall survival of mice harboring SF767 intracranial tumors treated with a single oral dose of vehicle (n=8), TIC10 (25 mg/kg, n=7), bevacizumab (10 mg/kg, i.v., n=6), or TIC10 and bevacizumab (n=7) at 2 weeks post-implantation.

Cohort	n	Median Survival (days)	ΔMedian Survival (days)	*P*
Control	8	28	-	-
TIC10	7	74	46	0.038
bev	6	70	42	0.119
TIC10 + bev	7	96.5	68.5	0.0308

Table 3.1. Change in overall survival of mouse treatment cohorts with SF767 intracranial tumors. Change in overall survival of mice from experiment in Figure 3.14.

3.5 Discussion

TIC10 exhibited broad activity amongst cancer cell lines with no obvious trend in resistant cell lines in terms of tumor type or common genetic aberrations. The cancer cell lines IGROV-1 (ovarian), SK-MEL-28 (melanoma), KM12 (colon), and SF539 (CNS) are relatively resistant to TIC10 and should be examined in future studies of resistance mechanisms. The activity of TIC10 appears cytotoxic as it reduces cell viability in a dose-dependent manner, ablates clonogenic survival, and causes caspase-mediated apoptosis. The cell death induced by TIC10 is p53-independent, which is in agreement with the previous observation that TIC10 induces TRAIL by a p53-independent mechanism. TIC10 fully maintains its cytotoxic potential at temperatures up to and perhaps beyond 100°C, which is in sharp contrast to the rapid loss of activity of recombinant TRAIL at higher temperatures as previously reported (van der Sloot et al., 2004). This results is encouraging given that the thermal stability of an agent is often related to its shelf life and sustained activity *in vivo.* This superior property of TIC10 is an example of the overall goal of this project, which was to improve drug properties of recombinant TRAIL that limit its efficacy.

The lack of correlation between cancer cell sensitivity to TRAIL and TIC10 has several implications. First, this suggests that the biological activity of TIC10 is clearly different than TRAIL. This could be due to several reasons: (1) TIC10 causes other effects other than TRAIL induction that alter sensitivity to TRAIL-induced cell death, (2) the activity of TIC10-induced TRAIL differs from recombinant TRAIL, and (3) the activity of TIC10 is unrelated to TRAIL-

mediated cell death. However, possibility (3) is unlikely given the demonstration of TRAIL-dependent cell death induced by TIC10 using gene silencing, disruption of death receptor-mediated proapoptotic signaling, and sequestration with a TRAIL-targeted antibody. Possibility (2) has precedent in the literature as different versions of recombinant TRAIL exhibited drastically different potency (Ganten et al., 2006; Pascal, 2000; Pitti et al., 1996; Walczak et al., 1999a) and membrane-bound TRAIL has been reported to have an enhanced potency and spectrum of activity compared to recombinant TRAIL (Armeanu et al., 2003; Mohr et al., 2004; Voelkel-Johnson et al., 2002). It is a reasonable possibility that TIC10 causes changes in other proteins involved in TRAIL sensitivity (1) through regulation of gene transcription or other effects resulting from changes in cell signaling given that TIC10 is a small molecule and that its mechanism of TRAIL induction is possibly transcriptional. The activity of TIC10 in TRAIL-resistant cell lines bodes well for the utility of TIC10 as an anticancer agent.

TIC10 is a potent antitumor agent *in vivo* even when administered as a single dose. This may be a result of a prolonged half-life, temporally sustained effects of the molecule as demonstrated *in vitro*, potent cell death induction in tumors, and/or effects on cancer stem cells. In support of this, analysis of TIC10-treated tumors revealed a sustained upregulation of TRAIL and cell death throughout the tumor several days following treatment with a single dose. As seen *in vitro*, the antitumor activity of TIC10 requires TRAIL *in vivo* though this does not exclude the possibility that other molecular changes cooperate with TRAIL to cause the antitumor effects of TIC10. TIC10 treatment caused a sustained reduction of tumor growth or regression in the MDA-MB-231 and RKO xenografts that was clearly superior to recombinant TRAIL under the given conditions and doses. The equivalent activity of TIC10 when administered as an intraperitoneal injection or oral dose suggests that TIC10 is bioavailable and represents an opportunity not possible with TRAIL, which requires intravenous administration. Dose titration revealed that TIC10 is highly active at an oral dose of 25 mg/kg, a dose that is achievable in patients. Weekly administration of oral TIC10 at this dose was sufficient to prolong the survival of transgenic mice harboring spontaneous myc-driven lymphoma by several weeks. The therapeutic effects of this

dosing schedule in such an aggressive model of cancer supports the use of this regimen in future studies.

The identification of synergy between TIC10 and taxanes provides a promising rationale for combining these agents in future clinical trials. Future studies should examine the mechanism of synergy between TIC10 and the approved agents. Both paclitaxel and docetaxel are approved for the treatment on NSCLC, among other malignancies, and synergize with TIC10 in NSCLC cell lines *in vitro* and cooperate to yield tumor cures *in vivo*. This makes NSCLC a promising disease target for TIC10 in future clinical trials. Future studies should also examine other potentially synergistic combinations with TIC10 such as sorafenib. Synergy has been reported with TRAIL combined with sorafenib (Ricci et al., 2007; Rosato et al., 2007), paclitaxel, and docetaxel.

The antitumor activity of TIC10 in GBM is promising as a monoagent and in cooperation with bevacizumab, which is an approved agent for the treatment of human GBM. The strong effect of TIC10 on overall survival in the intracranial tumor mouse model strongly suggests that TIC10 cross the intact blood-brain barrier and strongly argues for the clinical exploration of TIC10 as a new treatment for GBM. The activity of TIC10 in primary tumor specimens and cell lines that are resistant to temozolomide, the standard-of-care chemotherapy administered in GBM, also bodes well for utility of TIC10 in GBM as a malignancy with dismal outcomes and few treatment options. TIC10 represents a novel and promising opportunity for offering the antitumor activity of TRAIL to brain malignancies and may be more readily amenable to clinical trials than other experimental approaches that have been proposed in preclinical studies such as TRAIL delivery by mesenchymal stem cells (Kim et al., 2008; Sun et al., 2011).

CHAPTER 4

THE EFFECTS OF TIC10 ON NORMAL CELLS

4.1 Abstract

The ability to selectively kill cancer cells while sparing normal cells is a virtue of targeted cancer therapies and is one of the most attractive properties of TRAIL. We therefore tested the effects of TIC10 on normal cells and hypothesized that TIC10 could increase TRAIL production in normal cells without toxic effects on themselves. Unlike cancer cells, TIC10 did not induce cell death in normal cells or inhibit their long-term proliferation. TIC10 also exclusively ablated the tumor cell subpopulation in a coculture of normal fibroblasts and p53-deficient cancer cells. In agreement with this tumor-selective *in vitro* activity, TIC10 did not induce any significant toxicity in immuno-deficient or –competent mice by assays that included body weight, liver histology, and serum chemistry. We next tested the hypothesis that TIC10 causes normal cells to upregulate TRAIL. We found that TIC10 induces TRAIL in normal fibroblasts and stromal fibroblasts in addition to serum, the brain, kidney, and spleen tissue of mice lacking tumors. As TRAIL does not induce apoptosis in normal cells, we next tested the possibility that TIC10-induced TRAIL upregulation on the surface of normal cells could selectively kill tumor cells. Interestingly, normal fibroblasts pretreated with TIC10 were capable of inducing cancer-specific cell death in a coculture with p53-deficient cancer cells. We also showed that this cancer-specific cell death could be inhibited by sequestration of TRAIL by a monoclonal antibody. These observations suggest that TIC10 is not toxic to normal cells but does cause them to upregulate TRAIL *in vitro* and *in vivo*, which can result in an antitumor response through a TRAIL-mediated bystander effect.

4.2 Introduction

The original discovery reports of TRAIL showed its expression in a variety of human fetal and adult tissues including spleen, thymus, prostate, small intestine, and placenta (Pitti et al., 1996; Wiley et al., 1995). This was interpreted as promising for the safety of TRAIL by reasoning that wide expression throughout the body perhaps suggests tolerance of TRAIL by normal cells. While TRAIL is a very selective antitumor agent, there have been a few reports of potential toxicity issues. Despite a promising preclinical toxicity profile, one report found that recombinant His-tagged TRAIL at a dose of 200 ng/mL potentiated high levels of apoptosis in human hepatocytes

but not other species (Jo et al., 2000). This raised concern over the ability of the preclinical safety studies to predict safety. The El-Deiry lab confirmed the hepatotoxicity of His-tagged TRAIL and found that inhibition of caspase-9 was able to ablate hepatotoxicity while maintaing tumor cell cytotoxicity (Ozoren et al., 2000). Hepatocyte sensitivity to TRAIL was subsequently linked to bile acid-induced DR5 gene upregulation (Higuchi et al., 2002). However, a follow up study found that His-tagged rhTRAIL contains less zinc, which is important for structural integrity of the soluble trimer, and is less potent at inducing apoptosis than rhTRAIL that lacks the exogenous tag (Lawrence et al., 2001). Importantly, the untagged version of rhTRAIL did not induce human hepatocyte apoptosis, unlike its His-tagged counterpart, and similar observations were made with hepatotoxicity markers and histological analysis in cynomolgous monkeys.

Despite difficulties with delivery to the central nervous system (CNS), preclinical studies have suggested that TRAIL can eradicate intracranial human GBM tumors when administered intracerebrally (Roth et al., 1999). The selective apoptotic effects of rhTRAIL on glioma versus normal astrocytes have been directly demonstrated (Pollack et al., 2001). While human endothelial cells that comprise the blood-brain barrier are resistant to rhTRAIL (Wosik et al., 2007), other types of normal brain cells have been reported as sensitive though these studies used a FLAG-tagged version of rhTRAIL and dose of >200 ng/mL (de Vries et al., 2000; Nitsch et al., 2000). TRAIL-induced cell death of human oligodendrocytes in the adult human brain appears to require either protein synthesis inhibition or interferon-gamma (Matysiak et al., 2002). One report found that the analgesic flupirtine-maleate could act as a protectant from TRAIL-mediated neurotoxicity (Dorr et al., 2005). DR5 is more highly expressed than DR4 in GBM and expression levels of either DR4 or DR5 are independent prognostic factors in GBM (Kuijlen et al., 2006).

It is also worth noting that the cancer selective-activity and safety of adenoviral TRAIL has been reported, which causes a continuous production of TRAIL. This includes the demonstration of apoptotic selectively for cancer cells over normal cells in addition to a safety study in male baboons that found no clinical, serologic, or pathologic abnormalities with adenoviral TRAIL administration (Ni et al., 2005)(Cao et al., 2011). Due the intimate involvement of endogenous TRAIL in the mechanism of TIC10-induced cell death and our preliminary in vitro

data, we did not anticipate any significant toxicity. Nevertheless, we next directly determined the cancer-selective activity of TIC10 and assessed potential toxicity to normal cells *in vitro* and *in vivo* associated with TIC10 treatment at therapeutic doses.

4.3 Materials and Methods

Co-cultures

Co-cultures of HCT116 $p53^{-/-}$ and HFF cells were performed in a 1:1 mixture of complete DMEM and McCoy's 5A medium. For fluorescence images, the two cells were separately labeled using the Fluorescent Cell Linkers Kits for gene cell membrane labeling (Sigma) according to the manufacturer's protocols. Cells were counterstained with Hoechst 33342 (1 μg/mL) for 10 minutes. For flow cytometry analysis of cell death, the two populations of cells were determined by differential light scattering and analyzed as described for Sub-G1 analysis in the cell death assays section.

TRAIL ELISA

ELISA for TRAIL was carried out using the Quantikine TRAIL/TNFSF10 kit according to the manufacturer's protocol (DTRL00, R&D systems, Minneapolis, MN). Optical correction was performed as suggested by the manufacturer with absorbance at 540nm. Absorbance was measured with a DTX 880 plate reader (Beckman Coulter).

Serum Chemistry

1mL of blood was harvested from anesthetized mice by terminal cardiac puncture of the left ventricle. For serum chemistry, 500 μL of harvested blood was placed into a microfuge tube and allowed to clot for 30 minutes at room temperature followed by centrifugation. Serum was removed, centrifuged again to remove any further clots, and serum was submitted for analysis.

4.4 Results

TIC10 kills cancer but not normal cells

One of the attractive therapeutic properties of TRAIL is its ability to induce cancer-specific cell death with no appreciable effects on normal cells. A key selection criterion for selecting TIC10 over other TICs was its ability to kill cancer cells while sparing normal cells. However, these observations were made at lower doses that induced a modest amount of cancer cell death. We sought to test the effects of TIC10 on normal cells at more therapeutic doses. Our hypothesis was that TIC10 induces cancer-specific cell death due to the cancer-specific effects of TRAIL and the demonstrated involvement of TRAIL in the cytotoxic activity of TIC10. Treating normal fibroblasts and colon cancer cells with a dose of 5 μM clearly increased the Sub-G1 content in cell cycle profiles of cancer cells but not normal cells (Figure 4.1A). Furthermore, this dose of TIC10 had no affect on the ability of the normal cells to proliferate following incubation with TIC10 (Figure 4.1B). We next wished to directly prove that TIC10 killed tumor cells and not normal cells under identical conditions. To test this, we labeled normal fibroblasts and cancer cells with spectrally distinct amphipathic fluorescent dyes that insert into the membrane of cells. We found that TIC10 treatment eradicated the cancer cell population while sparing the normal cells (Figure 4.1C). The ability of TIC10 to induce cancer-specific cell death is an important characteristic as a therapeutic and is a virtue of targeted therapies.

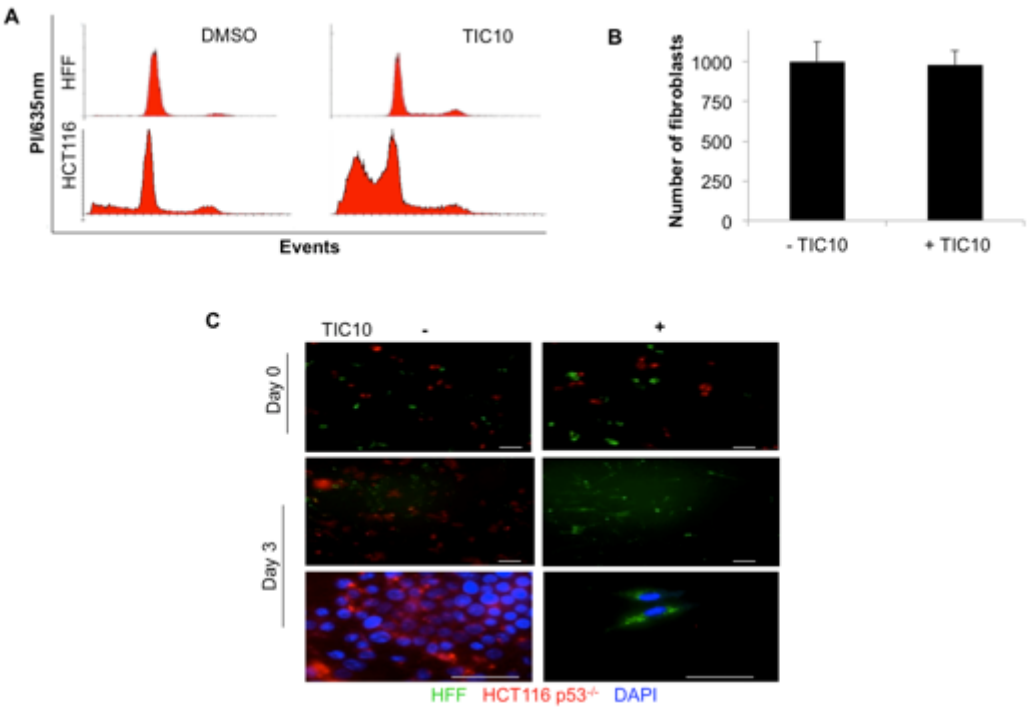

Figure 4.1 TIC10 induces cell death in tumor but not normal cells. (A) Cell cycle profiles of HFF untransformed fibroblasts and HCT116 cancer cells treated with TIC10 (5 μM, 72 hr, n=3). **(B)** Number of HFF cells at the end of a 10 day proliferation period preceded by TIC10 (10 μM) or DMSO treatment for 72 hr (n=3). **(C)** Co-culture of HCT116 $p53^{-/-}$ and HFF cells labeled as red and green, respectively. TIC10 (10 μM)- or DMSO-treated wells are shown immediately prior to treatment (day 0) or 3 days post-treatment. The bottom two panels were taken at the 3-day endpoint after being counterstained with Hoechst. Scale bar is 100 μm. Error bars indicate s.d. of replicates.

TIC10 has a favorable safety profile in vivo

To corroborate the *in vitro* data that indicated the tumor-specific cytotoxic activity of TIC10, we next evaluated the safety of TIC10 *in vivo*. A single intraperitoneal dose of TIC10 at 100 mg/kg caused no changes in body weight of athymic nude mice (Figure 4.2A). Histological analysis of liver tissue harvested from these mice revealed no changes in liver histology at 3 days post-treatment (Figure 4.2B). Chronic exposure to oral TIC10 at 25 mg/kg weekly for 4 weeks in immuno-competent C57/B6 female mice also did not cause any changes in body weight (Figure 4.2C). It is also important to evaluate toxicity profiles in combination with other approved therapies. TIC10 alone and in combination with bevacizumab was well tolerated and caused no significant changes in body weight when given once a week for 4 weeks (Figure 4.2D). The lack of apparent toxicity at multiple doses delivered at 4-fold above this therapeutic dose in a previous xenograft along with no adverse effects on body weight or liver histology bodes well for the safety profile of TIC10. We additionally evaluated a panel of serum chemistry markers of toxicity to identify potential toxicity of specific organs that could be monitored closely in early phase trials through molecular. Encouragingly, oral TIC10 at 25 mg/kg weekly for 4 weeks in immuno-competent C57/B6 female mice caused no alterations in the tested serum chemistry markers (Table 4.1).

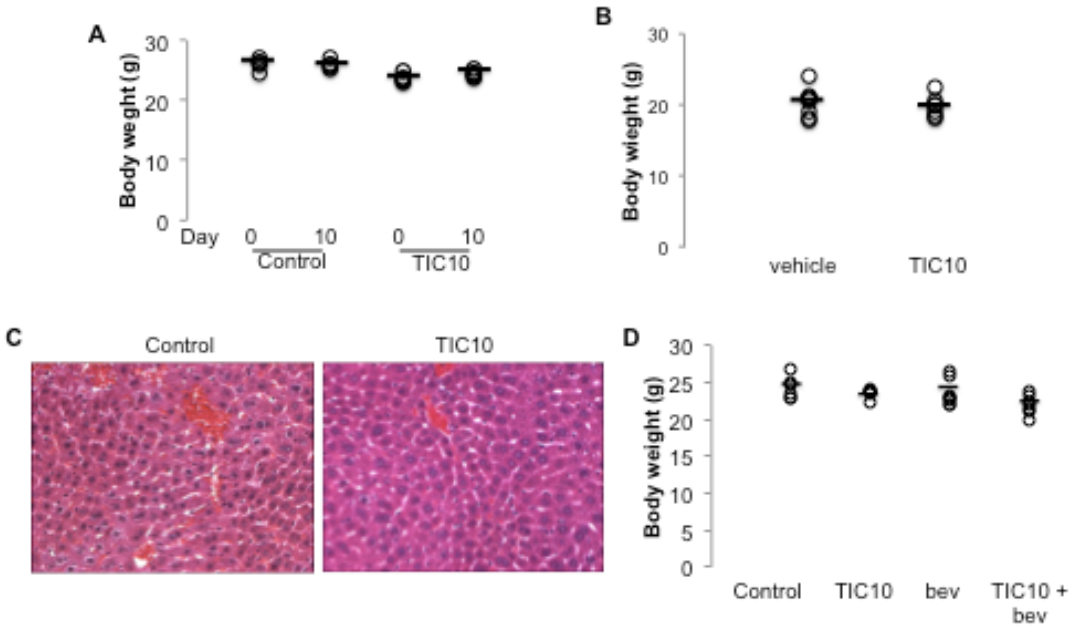

Figure 4.2 TIC10 does not alter mouse body weight, liver histology, or serum chemistry. **(A)** Body weight of athymic, female nude mice treated with TIC10 (100 mg/kg, i.p.). **(B)** Body weight of C57/B6 female mice at the end of week 4 of treatment with TIC10 (25 mg/kg, PO, qwk). **(C)** H&E staining of liver from athymic, female nude mice harvested 3 days post-treatment with TIC10 (100 mg/kg, i.p.). **(D)** Body weight of athymic, female nude mice at the end of treatment consisting of TIC10 (25mg/kg, PO), bevacizumab (bev, 10mg/kg, i.v.), or the combination of TIC10 and bevacizumab once a week for 4 weeks. Serum chemistry is shown in Table 4.1.

Cohort	Control	TIC10
Sodium (mM)	151.5±4.2	154.5±5.2
Potassium (mM)	9.025±2.2	7.325±3.2
Chloride (mM)	106.75±1.7	104
Total bilirubin (mg/dl)	3.075±1.6	2.725±2.4
Blood urea nitrogen (mg/dl)	26±1.6	33.75±7.3
Creatinine (mg/dl)	0.25±.06	0.15±.06
Total Protein (g/dl)	4.9±.36	4.97±.61
Albumin (g/dl)	3±.08	2.9
Alkaline phosphate (U/L)	104.5	112±12
Lactate dehydrogenase (U/L)	265	287.5±125

Table 4.1. Serum chemistry of C57/B6 female mice treated with oral vehicle or TIC10 (25 mg/kg) weekly for 4 weeks. Values are not significantly different between vehicle and TIC10 treatment groups.

Normal cells upregulate TRAIL in response to TIC10

While performing IHC analysis on TIC10-treated tumors, we found that TIC10 not only induced TRAIL in the tumor but also in stromal fibroblasts bordering the tumor (Figures 4.3A). Following this observation, we explored the possibly that normal cells could make TRAIL in response to TIC10. Assaying for soluble TRAIL using ELISA in the serum of TIC10-treated non-tumor-bearing mice revealed elevated serum levels of TRAIL for at least 72 hours following TIC10 treatment, which is far longer than the serum half-life of recombinant TRAIL (~30 minutes) (Avi Ashkenazi, 1999) (Figures 4.3B). This data suggests that normal cells produce TRAIL in response to TIC10 and that the effects of TIC10, i.e. TRAIL induction, are temporally sustained for days *in vivo* as seen *in vitro*.

IHC analysis of normal tissues in TIC10-treated non-tumor bearing mice revealed that TRAIL is upregulated at the protein level in the brain, kidney, and spleen of mice without apparent toxicity as determined by histology and TUNEL staining (Figure 4.3C). The sustained induction of TRAIL in brain tissue suggested that TIC10 could cross the intact blood-brain barrier, unlike a large trimeric protein such as recombinant TRAIL, as previously suggested in the orthotopic GBM xenograft (Chapter 3).

We also found that TIC10 induces a significant amount of TRAIL on the surface of normal fibroblasts (Figure 4.4A). Based on these observations, we tested the possibility that normal cells may contribute to the anti-tumor efficacy of TIC10 through a TRAIL-mediated bystander effect. We found that transplanting normal fibroblasts that were preincubated with TIC10 into a co-culture with p53-deficient colon cancer cells resulted in a modest but significant increase in cell death of the cancer cell sub-population (Figure 4.4B). Importantly, this increase in cancer-specific cell death was blocked with coincubation with the RIK-2 antibody that sequesters TRAIL (Kayagaki et al., 1999). Together, these data indicate that TIC10 has safe tumor-selective activity and induces TRAIL in tumor, stromal, and normal cells that may contribute to the anti-tumor efficacy of TIC10 through direct as well as bystander mechanisms.

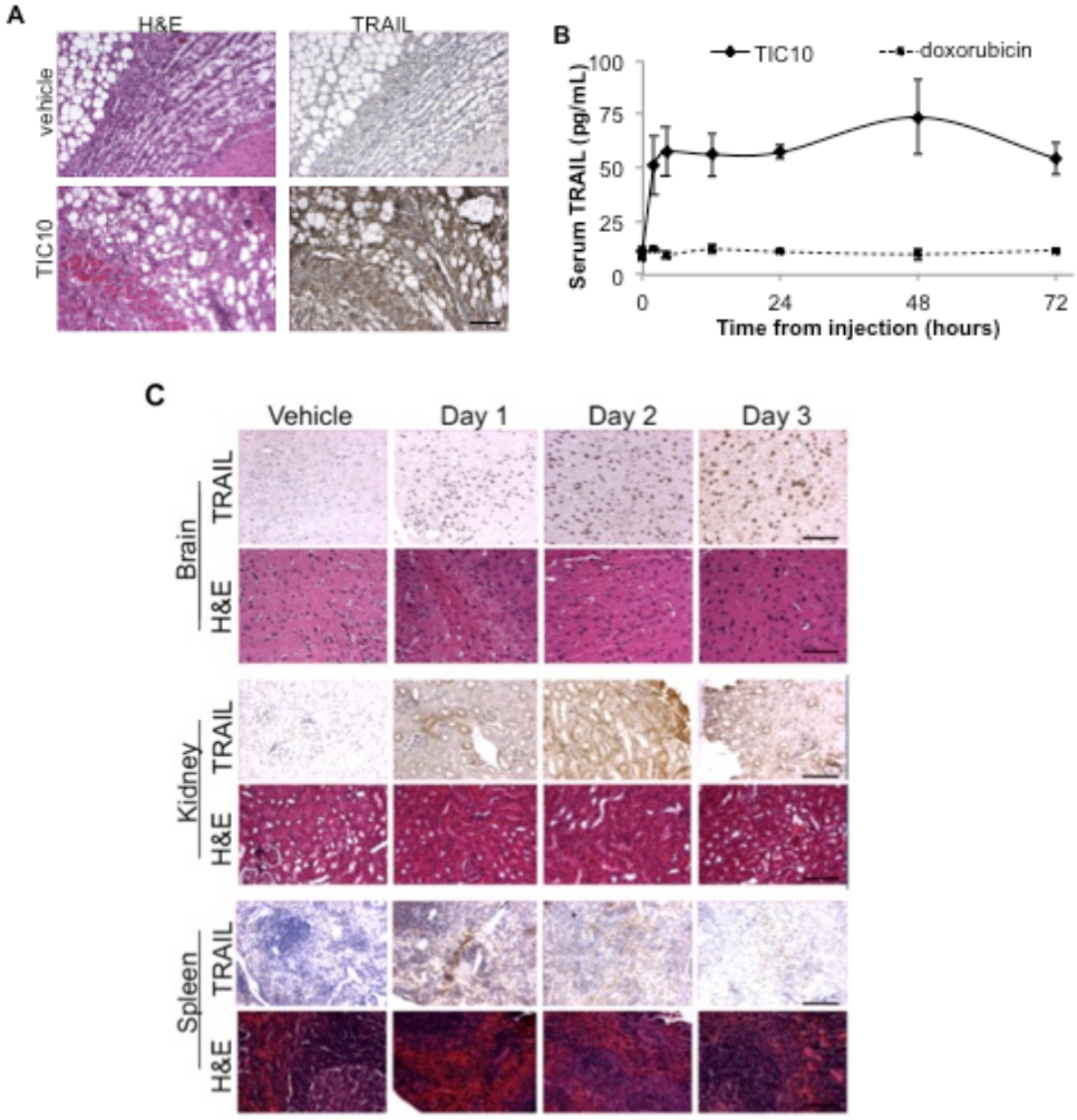

Figure 4.3 TIC10 induces TRAIL in normal tissues *in vivo*. (A) H&E and IHC analysis for TRAIL at the border of tumor and stromal fibroblasts from HCT116 $p53^{-/-}$ xenograft tumors following treatment with TIC10 (100 mg/kg, i.p.) or vehicle on day 2 post-treatment. **(B)** TRAIL serum levels in tumor-free mice following TIC10 (100 mg/kg, i.v.) or doxorubicin (30 mg/kg, i.p.)

(n=2). **(C)** Histological and TRAIL IHC analysis of normal tissue in athymic, nude mice following TIC10 administration on Day 0 (100 mg/kg, i.v.). Error bars indicate s.d. of replicates.

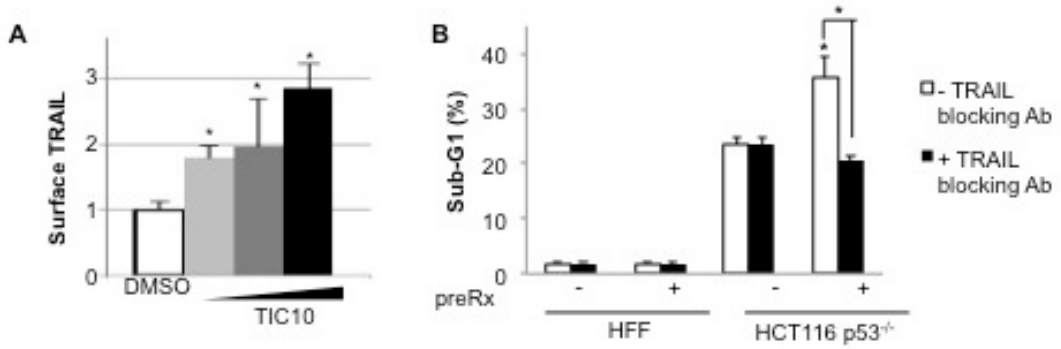

Figure 4.4. TIC10 can induce a TRAIL-mediated bystander effect involving normal cell-mediated cell death of tumor cells. (A) Surface TRAIL analysis of HFF cells following TIC10 treatment (0, 2.5, 5, or 10 μM from left to right) (72 hr, n=3). (**B**) Sub-G1 analysis of a coculture of HCT116 $p53^{-/-}$ cells and pretreated HFFs (24 hr, n=3). HFF pretreatment consisted of 72 hr incubation with TIC10 (10 μM) or DMSO. These experiments were performed in the presence or absence of a TRAIL sequestering antibody (RIK-2; TRAIL blocking Ab). Error bars indicate s.d. of replicates. *$P < 0.05$ between the indicated condition and control unless otherwise indicated.

4.5 Discussion

The ability of TIC10 to induce cancer-specific cell death is an attractive property underlying its selection as the lead TIC and is a property shared by recombinant TRAIL. The direct demonstration of TIC10 cytotoxic selectivity was demonstrated in a coculture experiment where TIC10 exclusively killed p53-deficient tumor cells but not normal cells. This *in vitro* demonstration of therapeutic index was corroborated by *in vivo* studies that showed no significant effects of TIC10 on the body weight, tissue histology, or serum chemistry profile of immuno-competent or –compromised mice.

Serum TRAIL levels were elevated for days and detectable as early as 8 hours following intravenous injection of TIC10, which has several important implications. First, this means that normal cells are capable of upregulating TRAIL in response to TIC10. Second, the kinetics of TRAIL induction is quicker in vivo than the kinetics of TIC10-induced TRAIL observed *in vitro*. This difference in kinetics could be because: (1) there are additional cofactors present *in vivo* that may contribute to the more rapid TRAIL induction, (2) TIC10 is metabolized into an active compound and this occurs more quickly *in vivo*, (3) cells respond at different rates in the physiological setting as opposed to cell culture, and/or (4) the normal cells, or specific types of normal cells, in mice respond more quickly to TIC10 than human cells tested in cell culture. Third, the ability of TIC10-induced TRAIL to be secreted *in vivo* represents an opportunity for distal normal cells to respond to TIC10 in a way that may result in a tumor response. The feasibility of normal cells to upregulate TRAIL and contribute to cancer-specific cell death by a TRAIL-dependent by stander effect was shown *in vitro* with coculture experiments using normal human fibroblasts.

The potential of TRAIL to induce cancer-specific cell death using normal cells has been recently recognized in the field. One such example has been the direct demonstration that mesenchymal stem cells overexpressing surface TRAIL can specifically kill tumors cells (Sun et al., 2011). This observation has also been seen with normal fibroblasts overexpressing TRAIL following adenoviral infection (Kagawa et al., 2001). Interestingly, the same group reported that these normal cell-mediated bystander effects with TRAIL require cell to cell contact and is

specifically mediated by surface rather than soluble TRAIL (Huang et al., 2003). TRAIL-mediated bystander effects have also been reported in response to radiation (Shareef et al., 2007; Unnithan and Macklis, 2004).

Utilizing small molecules to gain efficacy and biodistribution by inducing an endogenous gene in lieu of administering the recombinant protein is a promising notion. Limitations of the recombinant protein such as perfusion and pharmacokinetic properties can be effectively overcome by adjusting that of the small molecule. Furthermore, a secreted protein such as TRAIL may be a particularly well-suited target for such strategy as normal cells at distal sites relative to the tumor can produce soluble proteins that contribute to the therapeutic response via a bystander mechanism. This strategy has the potential to produce large quantities of TRAIL as the trillions of cells in the human body universally harbor the potential to produce endogenous proteins in a temporally sustained fashion. However, this bystander protein production strategy must be employed carefully as normal cells must maintain their normal function and the target protein must be nontoxic to the normal cells, as is the case for TRAIL.

CHAPTER 5

TIC10 REQUIRES FOXO3A FOR TRAIL UPREGULATION AND ANTITUMOR ACTIVITY

5.1 Abstract

TIC10 induces TRAIL in a p53-independent manner by a transcriptional mechanism. We performed expression profiling on TIC10-treated HCT116 $p53^{-/-}$ cells at 18 and 48 hours following TIC10 treatment. Network analysis of these changes in mRNA levels suggests that TIC10-induced changes were occurring in FOXO target genes. FOXO is a family of transcriptional factors that have been reported to regulate the TRAIL gene as well several other pro-apoptotic genes such as DR5. In accordance with this observation, we found that TIC10 induced DR5 upregulation in several cancer cell lines *in vitro* and in xenograft tumors. Immunofluorescence experiments indicated that Foxo3a rather than other family members was translocating to the nucleus following exposure to TIC10. Chromatin immunoprecipitation experiments revealed that Foxo3a binds to the TRAIL promoter in a dose-dependent manner. Using siRNA and shRNA, we found that knockdown Foxo3a was responsible for TIC10-induced TRAIL and the ensuing cell death *in vitro* and *in vivo*. These data directly demonstrate that Foxo3a is the transcription factor that drives TIC10-induced TRAIL.

5.2 Introduction

The TRAIL gene contains a ~1.6kB promoter region upstream of the start of transcription, which is 97 bp upstream of the start of translation (Wang et al., 2000) (reviewed in Chapter 1.3). This report identified several putative transcription factor binding sites in the TRAIL gene promoter: NHF3, GKLF, AP-1, CEBP, NFAT, GATA, and Inteferon-γ-activated sequence (GAS), GSP1, GSP2, and GSP4. Sequential deletion of various regions of the TRAIL promoter controlling luciferase reporters revealed that the regions between -1371 to -819 and -165 to -35 are responsible for basal TRAIL transcriptional activity. Since this initial report, several inducers of the TRAIL gene have been identified and transcription factor binding sites have been evaluated.

As TRAIL is conditionally expressed by a variety of immune cells, it is perhaps not surprising that the TRAIL gene is positively regulated by several transcription factors involved in modulating, activating, or attenuating immune cell responses such as interferons (Griffith et al., 1999) (Kim et al., 2002) (Tu et al., 2011) (Kayagaki et al., 1999) (Solis et al., 2006) (Yanase et al.,

2005), NFAT (Wang et al., 2000; Wang et al., 2011c), and NFκB (Baetu et al., 2001) (Matsuda et al., 2005) (Cippitelli et al., 2003) (Su et al., 2012). Some small molecules with other targets have been described to induce the TRAIL gene such as retinoids through an IRF-1-dependent mechanism (Clarke et al., 2004) (Kirshner et al., 2005), or HDACi through an SP-3-dependent mechanism (Nebbioso et al., 2005), and thalidomide (Yang et al., 2011).

The human TRAIL gene promoter contains two putative FOXO binding sites, one of which has been shown to play a role in FOXO-mediated TRAIL transcriptional activity by a luciferase reporter gene assay (Modur et al., 2002). FOXO contains four human family members: Foxo1, Foxo3a, Foxo4, and Foxo6. While differential regulation by these family members has not been completely elucidated, it is clear that they have unique actives and play different roles in development and diseases. In the context of TRAIL gene regulation, Foxo1 and particularly Foxo3a have been identified as transcriptional regulators but the differential affinity and biological consequences have not been defined.

Some oncogenic mechanisms routinely involved in transformation have been linked to TRAIL gene regulation in its promoter region such as mutant Ras-induced TRAIL expression silencing (Lund et al., 2011) and the TRAIL gene is also under positive regulation by the p53 tumor suppressor protein (Kuribayashi et al., 2008). Among FOXO family members, Foxo3a has been shown to induce TRAIL gene expression in prostate cancer cells (Modur et al., 2002) via a consensus binding site between -121 and -138 in the TRAIL gene promoter. There are several other putative transcription factor-binding sites within the TRAIL gene promoter that have not been tested and may play a role in particular physiological settings or could be usurped by small molecules to regulate TRAIL expression.

5.3 Materials and Methods

Gene expression analysis. HCT116 $p53^{-/-}$ cells were grown in log-phase and treated with DMSO or TIC10 (10μM). At 48 hr post-treatment, RNA was isolated using the RNeasy Mini Kit (Qiagen). Microarray analysis was performed using the Illumina HT-12 Beadchip (Illumina) in the PSU-COM Genome Sciences Facility. RNA quality and concentration was assessed using an

Agilent 2100 Bioanalyzer with RNA Nano LabChip (Agilent). cRNA was synthesized by TotalPrep Amplification (Ambion) from 500 ng of RNA according to manufacturer's instructions. T7 oligo (dT) primed reverse transcription was used to produce first strand cDNA. cDNA then underwent second strand synthesis and RNA degradation by DNA Polymerase and RNase H, followed by filtration clean up. *In vitro* transcription (IVT) was employed to generate multiple copies of biotinylated cRNA. The labeled cRNA was purified using filtration, quantified by NanoDrop, and volume-adjusted for a total of 750 ng/sample. Samples were fragmented, and denatured before hybridization for 18 hr at 58°C. Following hybridization, beadchips were washed and fluorescently labeled. Beadchips were scanned with a BeadArray Reader (Illumina). A project was created with the resultant scan data imported into GenomeStudio 1.0 (Illumina). Results were exported to GeneSpring Gx11 (Agilent Technologies). Measurements less than 0.01 were then set to 0.01, arrays normalized to the 50th percentile, and individual genes normalized to the median of controls. For network analysis of transcriptional changes induced by TIC10, the dataset was analyzed using the Ingenuity Pathway Analysis software (Ingenuity Systems). Microarray data is included in Appendix 1 and the raw data has been deposited to GEO (http://www.ncbi.nlm.nih.gov/geo/query/acc.cgi?token=ppihbcummescwji&acc=GSE34194).

Surface DR5 analysis

Cells were harvested by brief trypsinization and fixed in 4% paraformaldehyde in PBS for 20 minutes at room temperature. After washing with PBS, cells were then incubated with the anti-DR5 primary antibody (IMG-120A, Imgenex) for 1 hr at 1:200 followed by a secondary antibody incubation and flow cytometry analysis as with surface TRAIL assays described in Chapter 2.

Immunofluorescence

Immunofluorescence was performed as described in Chapter 3 with the following antibodies: Foxo1A (ab39670, abcam), Foxo3a (ab47409, abcam), Foxo4 (ab63254, abcam).

Western blot analysis

Western blot analysis was performed as described in Chapter 3. Nuclear and cytoplasmic extracts were prepared using a cytoplasmic lysis buffer (10 mM HEPES, 10 mM KCl, and 2 mM $MgCl_2$, 1 mM DTT) followed by a nuclear lysis buffer (20 mM HEPES, 420 mM NaCl, 1.5 mM $MgCl_2$, 250 μM EDTA, 25% glycerol). The following antibodies used were at 1:500 or 1:1000: pIκB (9241S, Cell Signaling), pS294 Foxo3a (5538S, Cell Signaling), pS253 Foxo3a (9466S, Cell Signaling), Foxo3a (9467S, Cell Signaling), pGSK3-β (9323S, Cell Signaling), ERK (9102S, Cell Signaling), pERK (4377S, Cell Signaling), pT308 Akt (9275S, Cell Signaling), pT473 Akt (92755S, Cell Signaling), Caspase-3 (9662S, Cell Signaling), Caspase-8 (9746S, Cell Signaling), DR5 (3696S, Cell Signaling), Akt (4685S, Cell Signaling), actin (sc-10731, Santa Cruz), Lamin B1 (ab16048, Abcam). Ran (610341, BD Transduction) was used at 1:10,000.

Stable knockdown of Foxo3a

The construct containing the Foxo3a shRNA was obtained from Sigma. Lentiviral infection was performed as described in Chapter 3.

Chromatin Immunoprecipitation Assay

Cells were grown under indicated conditions in one T75 flask per condition. Adherent cells were harvested by trypsinization and rinsed twice with PBS at room temperature. Cells were resuspended at $5X10^5$ cells per mL in PBS. Formaldehyde was added to a final concentration of 1% and incubated for 10 minutes on ice. Glycine (2.5 M stock) was added to a working concentration of 0.125 M and incubated at room temperature for 5 minutes. Cells were pelleted at 1100 RPM for 5 minutes, washed with ice cold PBS, and resuspended in 6 mL of Lysis Buffers (5 mM PIPES, pH 8.0, 85 mM KCl, .5% NP-40, protease inhibitors (Roche). Cells were centrifuged for 5 minutes at 1100 RPM, rinsed in PBS, and the supernatant was removed to leave the pellet (nuclear fraction). The pellet was lysed in high salt Lysis buffer (1X PBS, 1% NP-40, .5% sodium deoxycholate, 0.1% SDS, protease inhibitors) and placed into 1.5 mL centrifuge tubes in 300 μL

aliquots. Aliquots were sonicated to shear DNA and centrifuged for 15 minutes at 10,000 RPM at 4°C. The protein concentration was determined using the BioRad protein assay according to the manufacturer's protocol and bovine serum albumin (BSA) as a standard. 500 µg of protein was aliquoted into a new microcentrifuge tube and diluted to 1 mL in high salt lysis buffer. Each aliquot was then precleared with 30 µL of Protein A-G Plus beads (Santa Cruz) for 30 minutes at 4°C. Suspension was then centrifuged at full speed for 5 minutes at 4°C and aliquoted between 2 tubes per sample in addition to 100 µL for an input control. The primary antibody was added overnight at 1 µg per sample and incubated overnight at 4°C rotating. The following day, 30 µL of Protein A-G Plus beads were added to each tube and tubes were rotated for 2 hours at 4°C. Suspension was then centrifuged, washed twice with high salt Lysis buffer, and 4 times with wash buffer (100 mM Tris, pH 8.0, 500 mM LiCl, 1% NP-40, 1% sodium deoxycholate). 100 µL of Chelex (10% in dH_2O) was added, vortexed, boiled for 10 minutes, and cooled to room temperature. The mixture was then vortexed, pelleted, and 75 µL of supernatant was removed to a new microcentrifuge tube. 100 µL of solution was added to the beads, vortexed, pelleted, and 100 µL was extracted and added to the other 75 µL of extract. PCR was then conducted by standard protocol using primers against the appropriate genomic region as previously described (Nebbioso et al., 2005). Electrophoresis and visualization was performed as described for the RT-PCR standard protocol.

Transient knockdown by siRNA

siRNA stocks were made by diluting the siRNA to a stock concentration of 10 µM using nuclease free H_2O. 100 µL of Optimem was mixed with 8 µL of siRNA in a sterile transfection tube for 5 minutes under sterile conditions. 100 µL of Optimem was mixed with 8 µL Lipofectamine RNAiMax in a separate sterile transfection tube for 5 minutes. Mixtures were then combined into one tube and incubated for 30 minutes. The mixture was then added to a 2 mL suspension of cells (500,000 cells in a 35mm dish) with media containing serum without antibiotics. Cells were incubated overnight under standard conditions and complete media was provided the following

day. The following siRNA were used: Foxo1A (L-003006-00, Dharmacon), Foxo3A (M-003007-02, Dharmacon).

5.4 Results

TIC10 causes changes in FOXO target genes

TIC10 causes the transcriptional upregulation of TRAIL via a mechanism that leads to potent antitumor effects. To identify the molecular events driving TIC10-induced upregulation of TRAIL, we investigated gene expression profiles in TIC10-treated HCT116 $p53^{-/-}$ cells at 18 and 48 hours following treatment. These experiments revealed numerous changes in mRNA levels with the majority of events occurring at 48 hours post-treatment rather than 18 hours (Figure 5.1, Appendix 1). Next we performed a network analysis of these transcriptional changes to identify transcription factors that could potentially mediate these events. We found that target genes of the FOXO family of transcription factors were changing at 48 hours post-treatment (Figure 5.2), which have been previously shown to regulate the TRAIL gene promoter that harbors a consensus binding sequence (Modur et al., 2002).

Among the identified TIC10-induced changes in FOXO target genes was the upregulation of DR5, one of the proapoptotic TRAIL receptors. We found that DR5 was upregulated by TIC10 in a dose-dependent manner (Figure 5.3A). This induction of DR5 was also seen at the surface of several cancer cell lines and to a much lesser extent in normal cells (Figure 5.3B). Furthermore, IHC analysis of TIC10-treated tumors revealed an induction of DR5 at the protein level (Figure 5.3C).

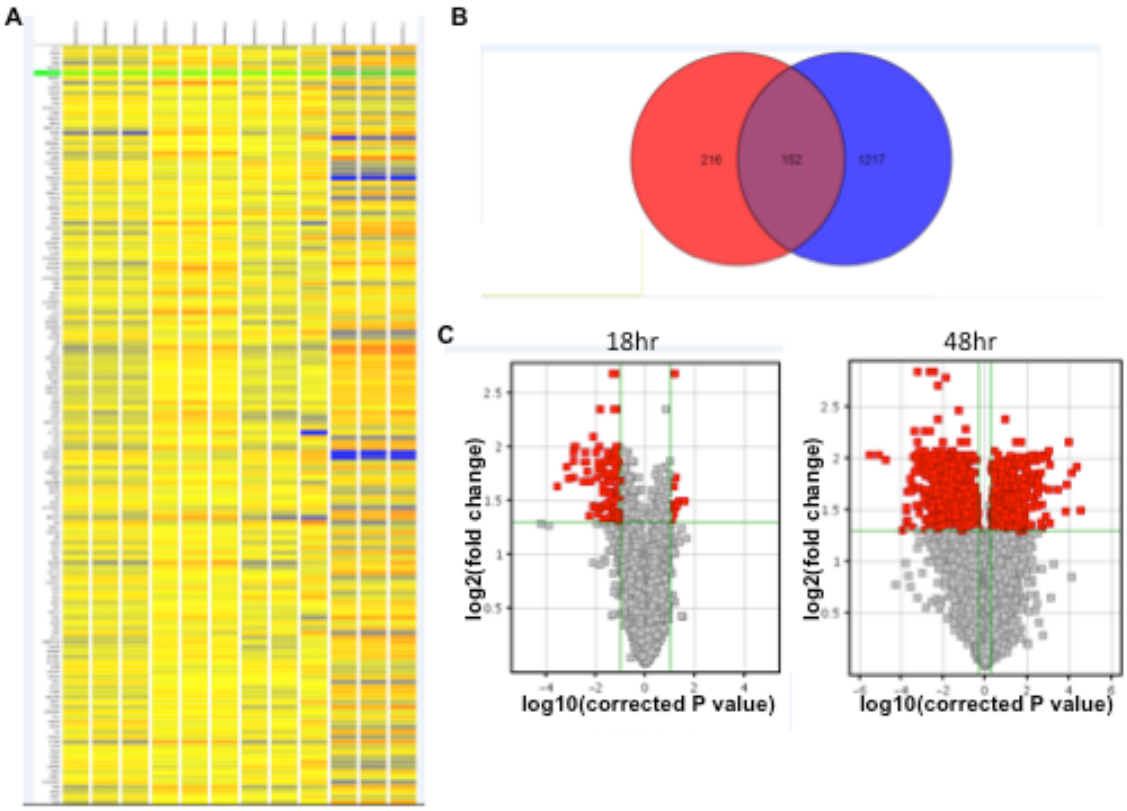

Figure 5.1. Expression profiling of TIC10-induced changes. (A) Heat map of significant changes in mRNA levels between DMSO- versus TIC10 (10 uM)-treated HCT116 $p53^{-/-}$ cells at 18 and 48 h post-treatment (n=3). **(B)** Venn diagram of significant TIC10-induced changes at 18 hr (red) and 48 hr (blue). **(C)** Volcano plots of TIC10-induced changes at 18 or 48 hr.

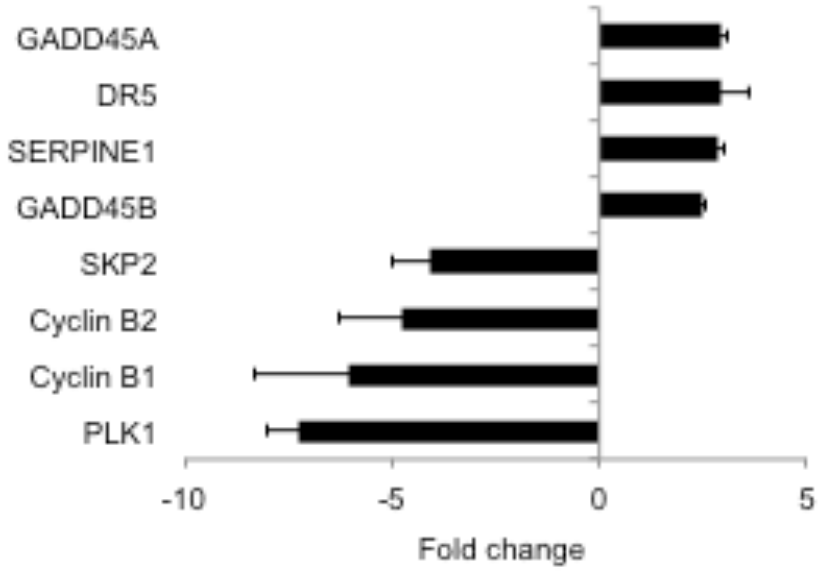

Figure 5.2. TIC10 induces transcriptional changes in FOXO target genes. Transcriptional changes associated with FOXO signaling from expression profiling of HCT116 $p53^{-/-}$ cells at 48 hr following DMSO or TIC10 treatment (10 μM) treatment (n=3). All transcriptional changes were *P*<.05 between control and TIC10 treatment groups.

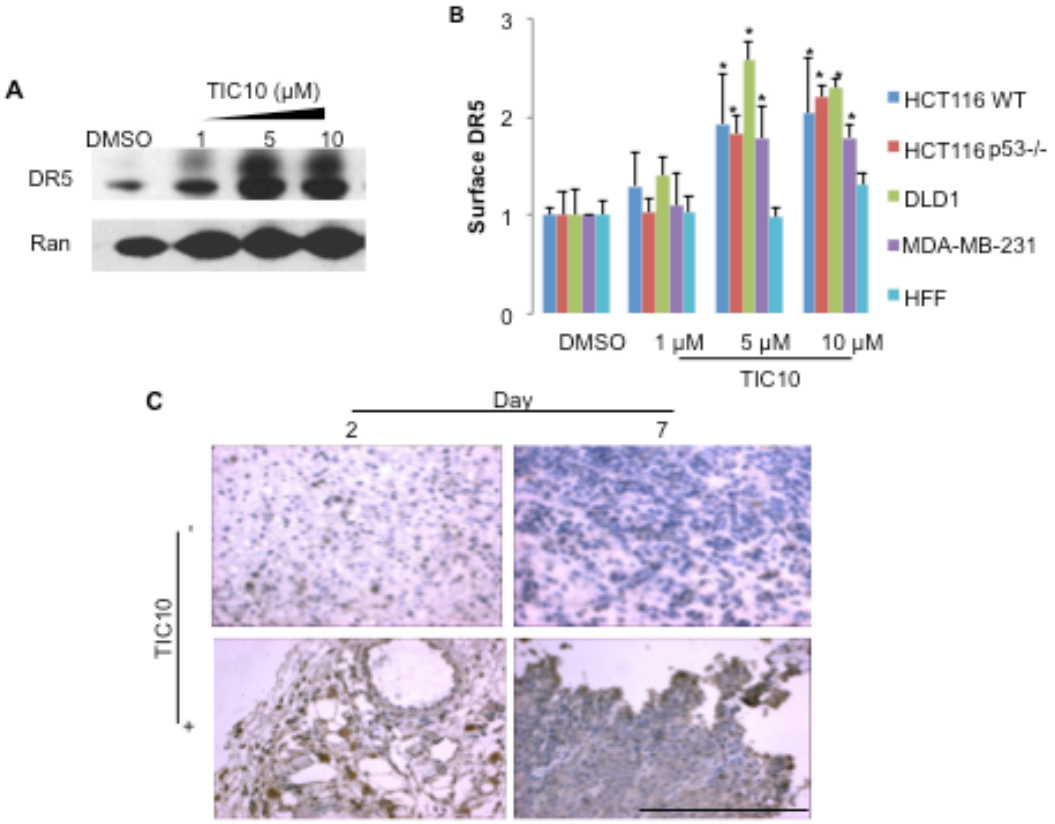

Figure 5.3. DR5 is induced by TIC10 *in vitro* and *in vivo*. (A) Western blot analysis of DR5 in HCT116 cells treated with TIC10 or DMSO at indicated concentrations for 72 hr. Ran shown as a loading control. **(B)** Flow cytometry analysis of surface DR5 levels in cancer and normal cells treated with TIC10 for 72 hr (n=3). **(C)** IHC analysis of DR5 in HCT116 xenograft tumors treated with vehicle (i.p.) or TIC10 (100 mg/kg, i.p.) on day 0. Error bars indicate s.d. of replicates. *P < 0.05 between indicated conditions.

TIC10 induces the nuclear translocation of Foxo3a

The regulation of FOXO family members is often achieved by modifications that change their sub-cellular localization, i.e. transcriptional activity is positively correlated with nuclear localization. Therefore we performed immunofluorescence analysis of FOXO family members to identify which of the family members were potentially responding to TIC10. We found that among FOXO family members, Foxo3a underwent a nuclear translocation in response to TIC10 at 48 hours post-treatment with TIC10 (Figures 5.4). To gain additional evidence that Foxo3a was translocating to the nucleus in response to TIC10, we performed Western blot analysis on subcellular fractions. These subcellular fractionation experiments corroborated the immunofluorescence experiments that indicated a TIC10-induced nuclear translocation (Figure 5.5A). Furthermore, this translocation was also noted in other cell lines that included H460 NSCLC and SW480 colon cancer cells (Figure 5.5B-C).

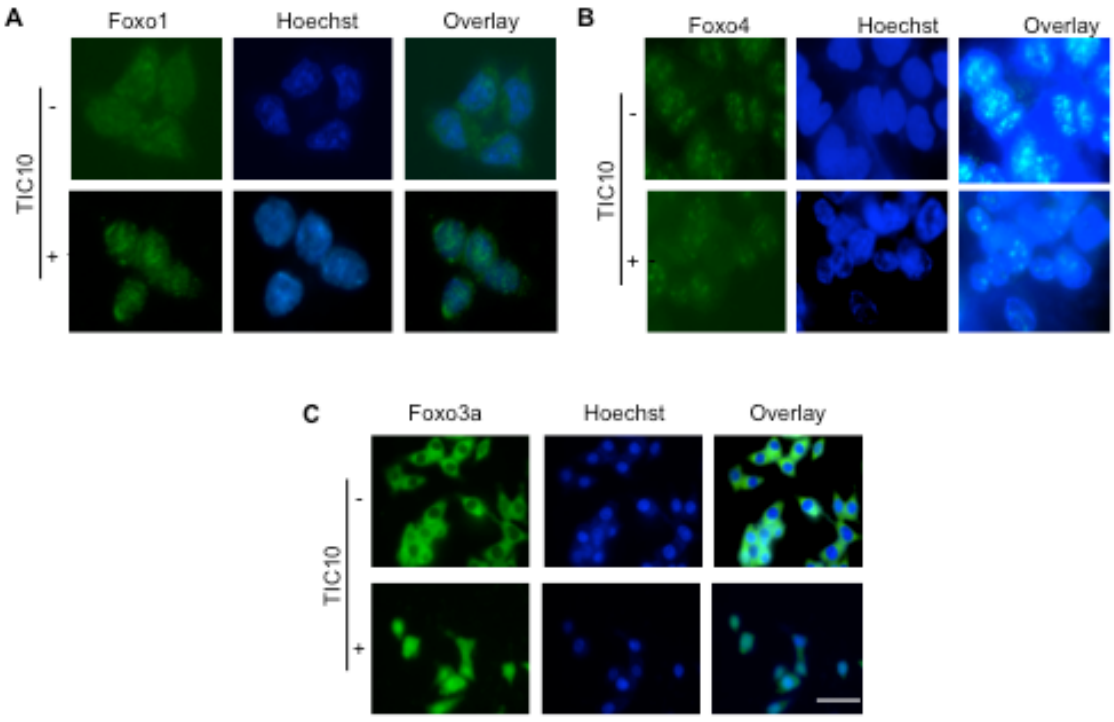

Figure 5.4. Foxo3a but not other FOXO family members translocate to the nucleus in response to TIC10. Immunofluorescence of **(A)** Foxo1, **(B)** Foxo4, and **(C)** Foxo3a in HCT116 $p53^{-/-}$ cells at 48 hr post treatment with DMSO or TIC10 (10 μM). FOXOs are shown in green and Hoechst 33342 is shown in blue as a nuclear counterstain.

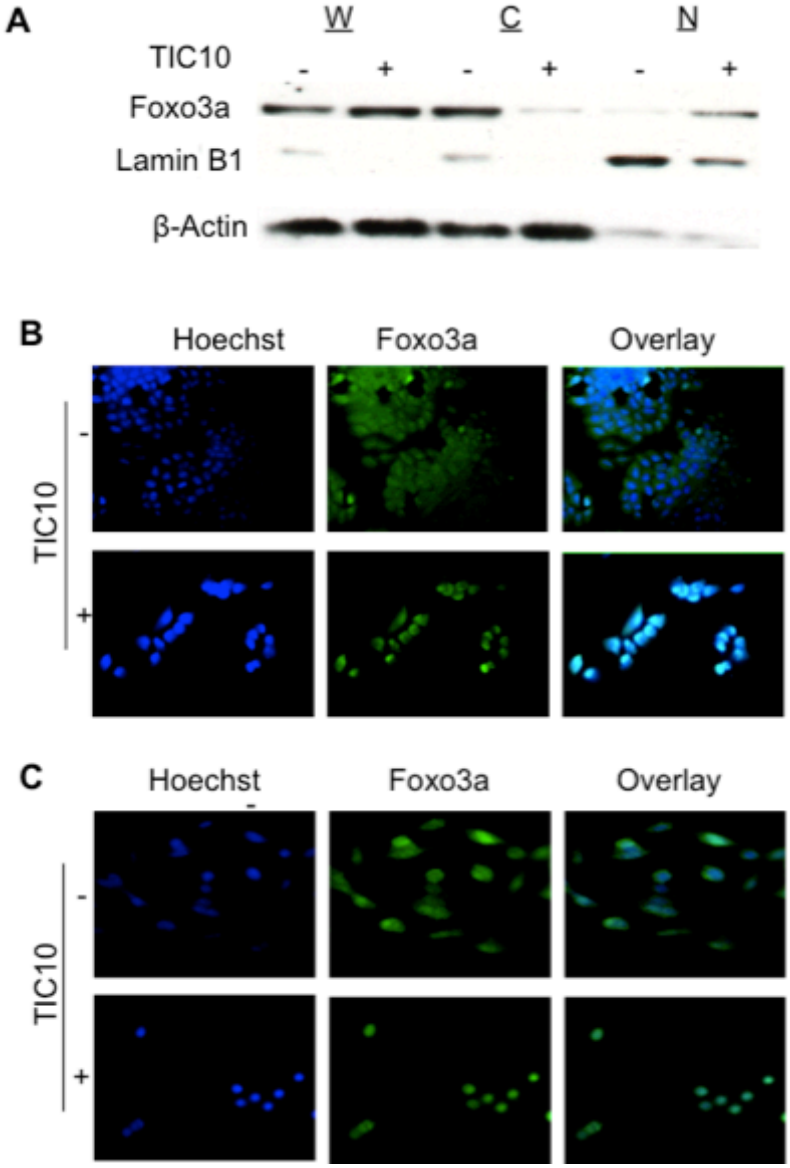

Figure 5.5. TIC10 induces the nuclear translocation of Foxo3a. (A) Western blot analysis of whole cell lysates (W) and cytoplasmic (C) and nuclear (N) extracts from HCT116 cells treated with DMSO or TIC10 (48 hr, 10 μM). β-actin and lamin B1 are shown as cytoplasmic and nuclear loading controls, respectively. Immunofluorescence of Foxo3a in **(B)** H460 and **(C)** SW480 cells at 48 hr post treatment with DMSO or TIC10 (10 μM). Foxo3a is shown in green and Hoechst 33342 is shown in blue as a nuclear counterstain.

Foxo3a mediates TIC10-induced TRAIL in vitro

With the observation that TIC10 was causing the nuclear translocation of Foxo3a, we predicted that this would result in an increase in Foxo3a binding to the TRAIL promoter. We conducted a chromatin immunoprecipitation assay that revealed a dose-dependent increase in the amount of Foxo3a localized to the TRAIL promoter (Figure 5.6). Next, we tested if the TIC10-induced effects on Foxo3a were responsible for the upregulation of TRAIL by TIC10. Using siRNA, we found that Foxo3a specifically mediates TIC10-induced TRAIL upregulation (Figure 5.7A). For further mechanistic studies, we created a cell line with stable knockdown of Foxo3a using shRNA delivered by lentiviral infection. Stable knockdown of Foxo3a significantly inhibited TIC10-induced upregulation of TRAIL as well as cell death (Figure 5.7B-C). Importantly, stable knockdown of Foxo3a was also sufficient to strongly inhibit the antitumor effects and hallmarks of TRAIL-mediated apoptosis resulting from TIC10 *in vivo* (Figures 5.8). Together, these data clearly indicate that Foxo3a is critical for TRAIL upregulation in response to TIC10 and the ensuing antitumor activity.

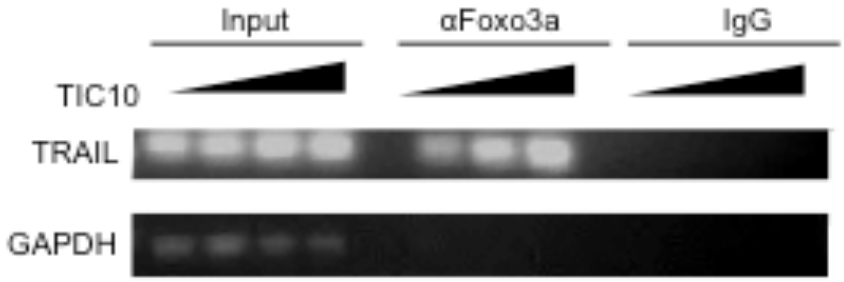

Figure 5.6. Foxo3a binds to the TRAIL promoter in response to TIC10. Chromatin immunoprecipitation assay for TIC10-induced translocation of Foxo3a to the TRAIL promoter at 48 hr post-TIC10 treatment in HCT116 $p53^{-/-}$ cells (0, 2.5, 5, or 10 μM from left to right).

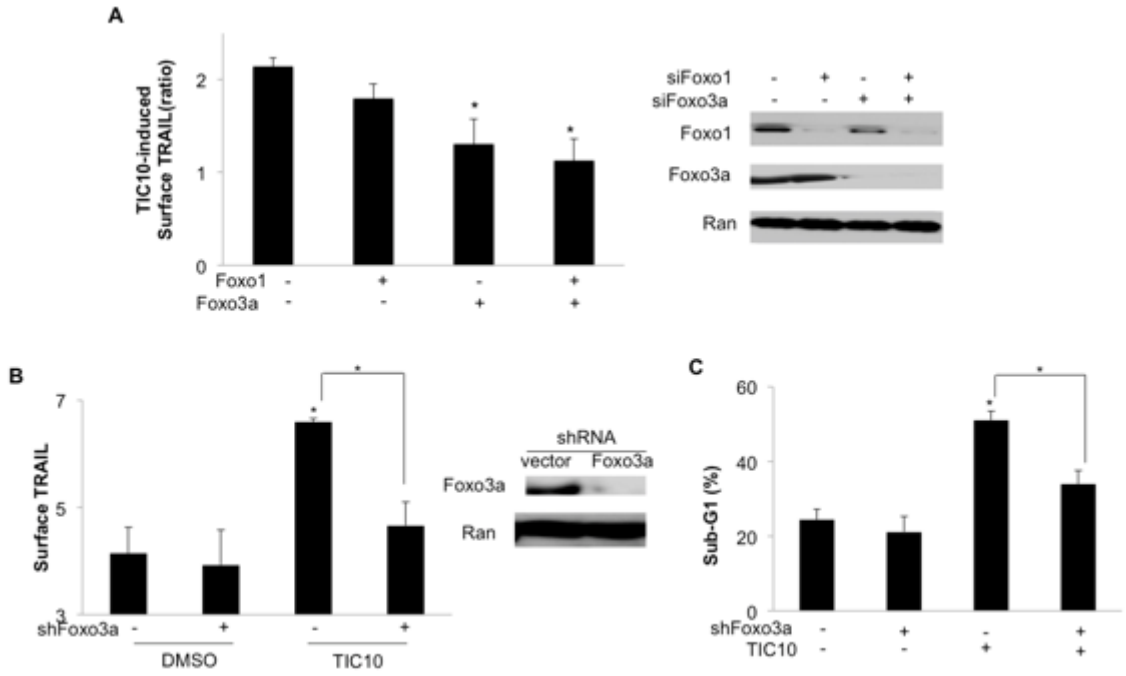

Figure 5.7. Foxo3a mediates TIC10-induced TRAIL and cell death *in vitro*. (A) Flow cytometry analysis of cell surface TRAIL levels induced by TIC10 (10 μM) with or without transient knockdown of Foxo1 and/or Foxo3a in HCT116 $p53^{-/-}$ cells using siRNA (72 hr, n=3). Confirmation of knockdown is shown by Western blot analysis (right). **(B)** Flow cytometry analysis of cell surface TRAIL levels induced by TIC10 with or without stable knockdown of Foxo3a in HCT116 WT p53 cells (10 μM, 72 hr, n=3). **(C)** Sub-G1 analysis of TIC10-induced cell death with or without stable knockdown of Foxo3a in HCT116 cells (10 μM, 72 hr, n=3). Error bars indicate s.d. of replicates. *$P < 0.05$ between indicated conditions.

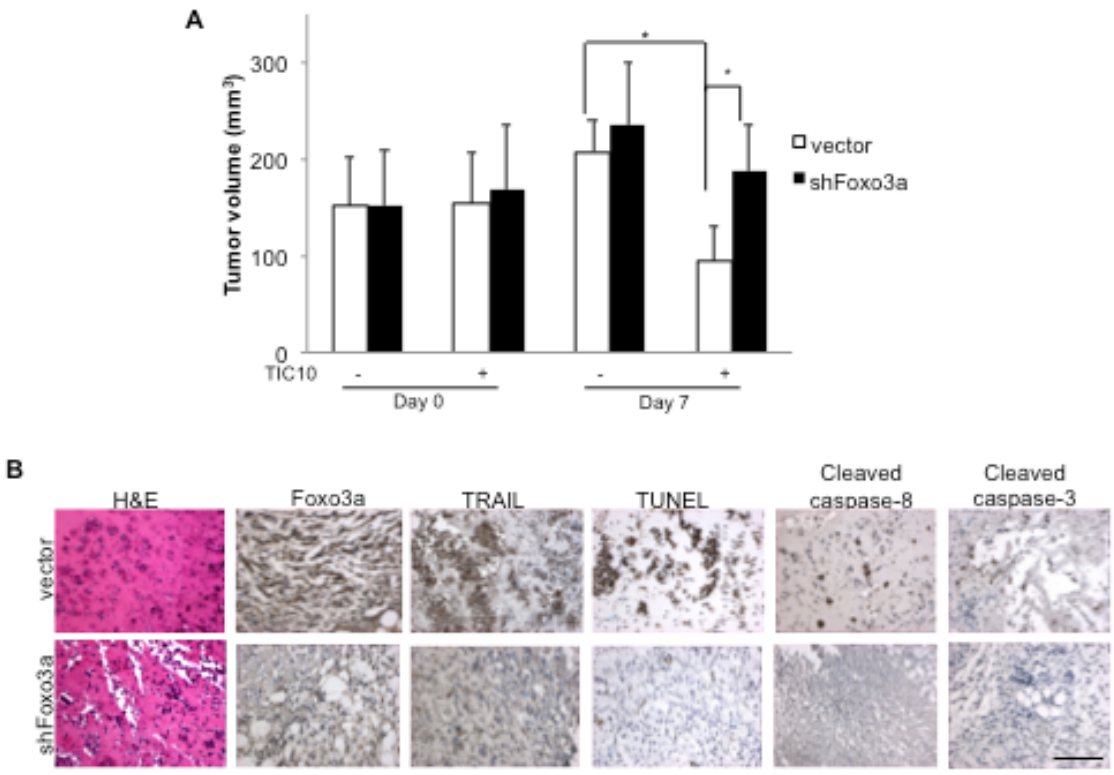

Figure 5.8. Foxo3a mediates TIC10-induced TRAIL and cell death *in vivo*. (A) Tumor volume of HCT116 xenograft with or without stable knockdown of Foxo3a following a single oral dose of vehicle or TIC10 (25 mg/kg) on day 0 (n=10). **(B)** TRAIL IHC analysis and TUNEL staining of HCT116 tumors with or without stable knockdown of Foxo3a 3 days after a single dose of TIC10 (25 mg/kg, oral). Scale bars are 100 μm. Error bars indicate s.d. of replicates. *$P < 0.05$ between the indicated condition and control unless otherwise indicated.

5.5 Discussion

We utilized expression profiling to identify transcriptional changes that occur in response to TIC10 in an effort to identify the mechanism of TIC10-induced TRAIL gene upregulation. We found that TIC10-induced changes in Foxo3a target genes were occurring at 48 hours post-treatment, which is in accordance with the kinetics of TRAIL induction by TIC10. Foxo3a has been previously described to regulate the TRAIL gene promoter via a canonical binding site proven to be essential for positive regulation using luciferase reporter gene assays (Modur et al., 2002). We had previously noted that TIC10 induces TRAIL-mediated apoptosis in some cancer cell lines that were moderately resistant to recombinant TRAIL. In an effort to explain this difference in activity, we explored the possibility that TIC10 caused changes in proteins that impact on TRAIL sensitivity. Among these factors, we found that DR5 is upregulated in TIC10-treated cancer cells and xenograft tumors. This observation is in accordance with activation of Foxo3a by TIC10 as DR5 is also a Foxo3a target.

The unique effects of TIC10 on Foxo3a among the FOXO family imply that this member has potentially unique modes of regulation and perhaps activity. This exclusive effect may be due to the potent effects of TIC10 on pERK, as ERK appears to be a unique regulator of Foxo3a (Yang et al., 2008a; Yang et al., 2008b). Another noteworthy observation is the critical involvement of TRAIL rather than other proapoptotic FOXO targets such as FasL and Bim. As described in detail in Chapter 1, the activity of FOXO is governed by multiple factors including post-translational modifications and transcription cofactors that are thought to give rise to a "FOXO code" (Calnan and Brunet, 2008). FOXOs have been reported to induce different subsets of FOXO target genes such as the recent report of Foxo3a-mediated TRAIL gene induction but not DR4 or DR5 (van Grevenynghe et al., 2011).

It is clear that TIC10 causes a dose-dependent increase in the amount of Foxo3a localized to the TRAIL promoter in a very similar manner to the dose-dependent increase of TIC10-induced surface TRAIL. This suggests a linear positive relationship between Foxo3 and TRAIL gene transcription. Future studies should examine if this dose-dependent effect is absent for certain FOXO target genes such as FasL, which we did not see in expression profiling of

TIC10-induced changes. The role of transcription cofactors in TIC10-induced Foxo3a activation should also be examined as these proteins can critically regulate its activity and specificity for certain target genes, which may explain the preference of Foxo3a for certain target genes such as TRAIL following TIC10 exposure.

The identification of Foxo3a as the critical transcription factor responsible for TIC10-induced effects has implications that extend beyond the molecule itself. Firstly, our observations strongly argue that TRAIL plays an essential role in the apoptotic response induced by Foxo3a and positions Foxo3a as a promising drug target for inducing the TRAIL gene. The conservation of the Foxo3a-dependent mechanism of TIC10 in the presence of upstream oncogenic alterations such as mutant KRAS or PTEN deletions holds promising therapeutic potential. The observation that Foxo3a rather than Foxo1, which has been previously targeted by small molecules (Kau et al., 2003), specifically regulates the TIC10-induced response lends credence to the notion that different members of the FOXO family of transcription factors play distinct roles.

CHAPTER 6

THE DUAL INHIBITION OF AKT AND ERK COOPERATIVELY INDUCES TRAIL

6.1 Abstract

The regulation of Foxo3a is primarily by post-translational modifications that affect its subcellular localization. Therefore, we explored changes in the activity of kinases that regulate Foxo3a following TIC10 treatment. We found that both Akt and ERK were being inactivated by TIC10 and this inactivation concomitantly decreased the phosphorylation of Foxo3a at their respective binding sites. Importantly, these events started at later time points following TIC10 treatment, as did the upregulation of TRAIL, which supports these observations as a plausible mechanism for TRAIL upregulation by TIC10. Also in support of this mechanism, we found that overactivation of Akt could induce TIC10 resistance and that TIC10 sensitivity determinants appear to involve the PI3K/Akt and MAPK pathways. This putative mechanism led us to the hypothesis that Akt and ERK are critical regulators of Foxo3a and that dual inhibition of these kinases is sufficient to induce Foxo3a-dependent TRAIL and cytotoxicity. In support of this hypothesis, we found that dual inactivation of Akt and ERK using commercially available compounds cooperatively increased TRAIL and cancer cell death in a Foxo3a-dependent manner. These observations support that the mechanism of TIC10 involves inactivation of Akt and ERK, which is sufficient to upregulate Foxo3a-dependent TRAIL and cause cancer cell death.

6.2 Introduction

FOXO is a family of transcription factors comprised of 4 mammalian members (Foxo1, Foxo3a, Foxo4, and Foxo6) that regulate genes involved in numerous cellular processes that include metabolism, longevity, tumor suppression, and development (Calnan and Brunet, 2008). Foxo3a has been previously described as a direct regulator of the TRAIL through a FOXO binding site in the TRAIL gene promoter (Modur et al., 2002). The regulation of Foxo3a can be through post-translational modifications (PTMs) that currently include phosphorylation, acetylation, and ubiquitination. These modifications often affect FOXO subcellular localization through the changing the accessibility of nuclear localization and nuclear export sequences that is conserved among FOXOs.

Akt is a particularly strong regulator of FOXOs that phosphorylates 3 conserved residues (Biggs et al., 1999; Brunet et al., 1999; Kops et al., 1999; Nakae et al., 1999). Upon phosphorylation, the Akt phosphorylation sites allow 14-3-3 proteins to bind to FOXOs, expose their nuclear export sequences, and affects the accessibility of their nuclear localization sequences (Brunet et al., 2002; Obsilova et al., 2005). Serum glucocorticoid kinase (SGK) can functionally substitute for Akt-mediated phosphorylation events on FOXOs. Several other FOXO residues are phosphorylated to facilitate its interaction with the nuclear export proteins Ran and Crm1 that shuttle FOXOs between the nucleus and cytoplasm (Rena et al., 2002; Zhao et al., 2004). The stress-activated kinases JNK and MST1 cause activating phosphorylation events on Foxo3a (Lehtinen et al., 2006) and Foxo4 (Essers et al., 2004; Oh et al., 2005), respectively, which results in their nuclear translocation. These activating phosphorylation events antagonize the Akt-mediated inhibitory phosphorylation events. AMPK phosphorylates Foxo3a at two sites and results in a distinct response that activates transcription of FOXO target genes specifically involved in energy metabolism and stress resistance (Greer et al., 2007).

FOXO proteins can also be regulated by ubiquitin-mediated proteasomal degradation. FOXO degradation has been reported following phosphorylation by Akt (Matsuzaki et al., 2003; Plas and Thompson, 2003). Foxo1 degradation has been linked to polyubiquitination by the SCF^{skp2} complex (Huang et al., 2005). Skp2 has been recently shown to also polyubiquitinate Foxo3a (Wang et al., 2011a),. Interestingly, there may be a negative feedback mechanism in place as Foxo3a negatively regulates Skp2 gene transcription (Wu et al., 2012). Foxo3a is also degraded following phosphorylation by IkappaB kinase (Hu et al., 2004a).

Activation of cytoplasmic FOXO may be accomplished through inactivation of the phosphorylating kinases that antagonize FOXO activity and/or activation of phosphatases such as PP2A (Singh et al., 2010). FOXO is also controlled and fine-tuned by numerous transcription cofactors in response to various stimuli in a highly context-dependent manner. Thus, FOXO regulation is quite multi-modal and FOXO may be activated through a number of mechanisms that include post-translational modifications mediated by kinases and phosphatases, acetylation mediated by acetylases and deacetylases, degradation mediated by Skp2, and differential

association between transcription cofactors. With these previously defined mechanism of FOXO regulation, we began to search for TIC10-induced changes in regulators of Foxo3a.

6.3 Materials and Methods

Reagents

U-126 monoethanolate (Sigma) and A6730 were suspended at 20mM in DMSO and stored at -20°C.

Western blot analysis

Western blot analysis was performed as described in Chapter 3. The following antibodies were used: Ran (610341, BD Transduction), pIκB (9241S, Cell Signaling), pS294 Foxo3a (5538S, Cell Signaling), pS253 Foxo3a (9466S, Cell Signaling), Foxo3a (9467S, Cell Signaling), pGSK3-β (9323S, Cell Signaling), GSK3β (Cell Signaling 9315), ERK (9102S, Cell Signaling), pERK (4377S, Cell Signaling), pT308 Akt (9275S, Cell Signaling), pT473 Akt (92755S, Cell Signaling), Akt (4685S, Cell Signaling), actin (sc-10731, Santa Cruz). Densitometry was performed using NIH ImageJ software.

Gene set enrichment analysis

Gene set enrichment analysis was performed with default settings using GSEA software (http://www.broadinstitute.org/gsea/index.jsp) (Subramanian et al., 2005).

Transient knockdown of Akt and ERK

siRNA-mediated knockdown was performed as described in Chapter 5. siRNA used was: Akt (6211S, Cell Signaling) and ERK (6560S, Cell Signaling).

6.4 Results

TIC10 inhibits Akt and ERK-mediated phosphorylation of Foxo3a

We explored TIC10-induced changes in previously described regulators of Foxo3a starting with the prosurvival kinases IKK (Finnberg and El-Deiry, 2004; Hu et al., 2004b), Akt (Wang and El-Deiry, 2004), and ERK (Yang et al., 2008a; Yang et al., 2008b). We selected these kinases as a starting point due to their well-defined signaling mechanisms, availability of antibodies for substrates as a readout of activity, and their previously described potent regulation of FOXO activity. We found that both pAkt and pERK were abolished with TIC10 treatment in a dose-dependent manner that was accompanied by decreased phosphorylation at their respective sites on Foxo3a (Figure 6.1A). These TIC10-induced effects on Foxo3a were evident in several cancer cell lines of different tumor types, which include human cancer cell lines with diverse genetic backgrounds that harbor heterogeneous oncogenic alterations in p53, KRAS, PTEN, and others (Figure 6.1B).

We then tested if the identified effects of TIC10 involving Akt, ERK, and Foxo3a coincided with the induction of TRAIL in terms of kinetics. A time course analysis revealed that TIC10-induced inactivation of Akt and ERK occurred after 48 hours - kinetics that were concerted with the dephosphorylation of Foxo3a and TRAIL upregulation (Figures 6.2). It appears that TIC10-induced effects on Akt, ERK, Foxo3a, and TRAIL begin at 48 hours and increase at 60 and 72 hours post-treatment.

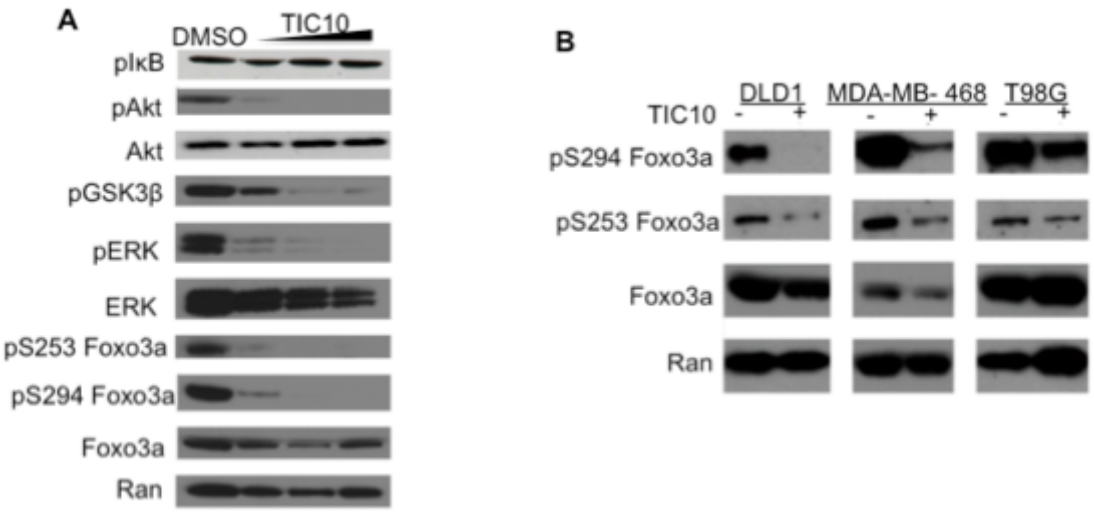

Figure 6.1. TIC10 inactivates Akt and ERK. (A) Western blot analysis of HCT116 $p53^{-/-}$ cells treated with DMSO or TIC10 (2.5, 5, 10 μM) for 72 hr. **(B)** Western blot analysis of TIC10-induced effects on Foxo3a phosphorylation in DLD1 human colon cancer cells, MDA-MB-468 human breast cancer cells, and T98G human glioblastoma multiforme cell lines (10 μM, 72 hr).

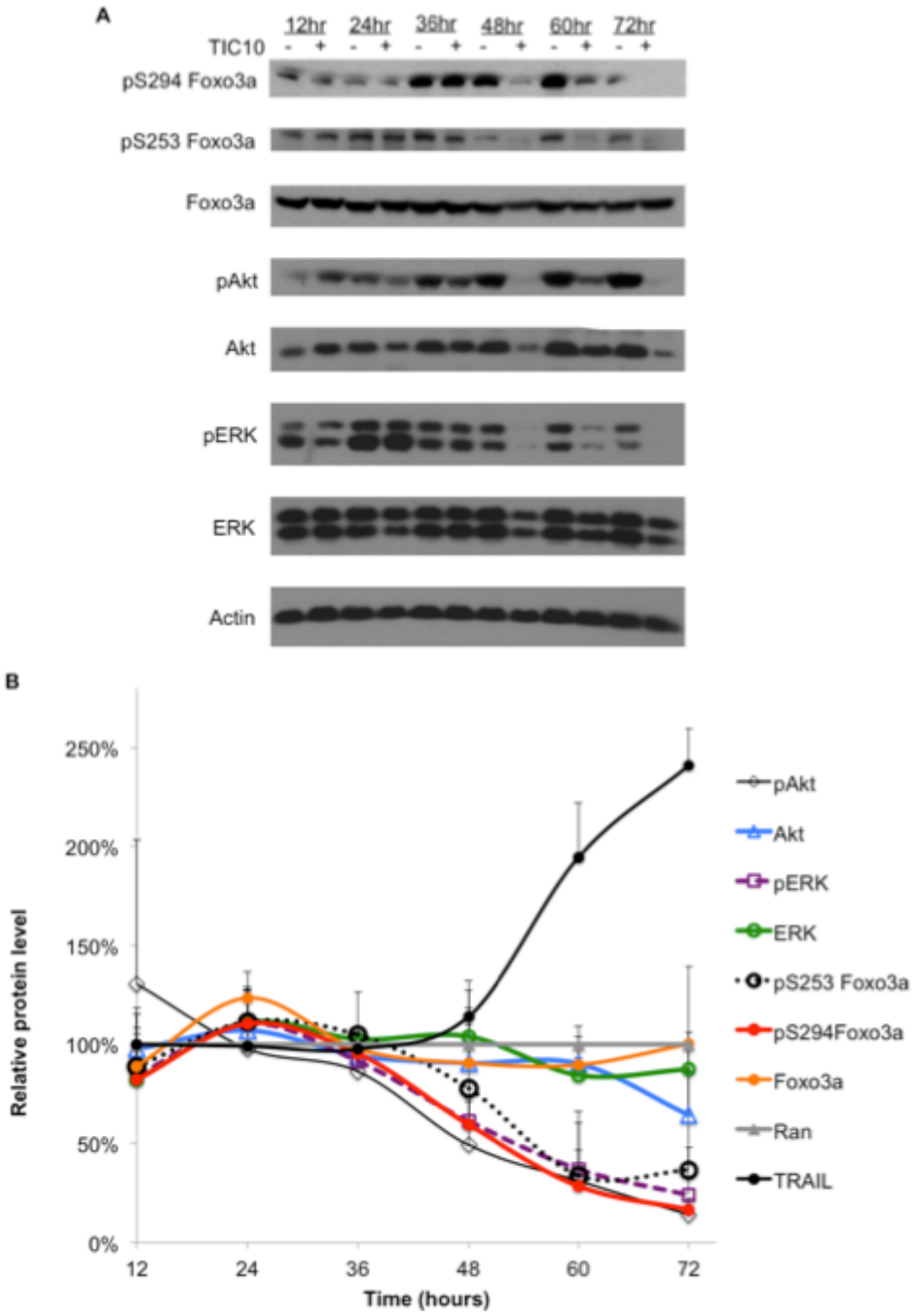

Figure 6.2. TIC10-induced effects on Foxo3a and TRAIL upregulation occur with similar kinetics. (A) Western blot analysis of HCT116 $p53^{-/-}$ cells treated with TIC10 (10 μM) for indicated time periods. **(B)** Time course of protein expression levels of TIC10-induced effects determined by densitometry of blots from (A) (n=3). TRAIL was quantified by flow cytometry as a parallel experiment (n=3).

Overactivation of Akt confers resistance to TIC10

Our observations indicate that TIC10 inhibits Akt activation and requires Foxo3a for TIC10-induced TRAIL and cancer cell death. We found that Akt is an important determinant of cytotoxic sensitivity to TIC10 as overexpression of myristoylated Akt was sufficient to reverse the TIC10-induced nuclear translocation of Foxo3a (Figure 6.3A). In accordance with this observation, overexpression of myristoylated Akt also inhibited TIC10i-nduced TRAIL and cancer cell death (Figure 6.3B-C).

We previously noted that the cancer cell lines RXF393, IGROV-1, KM12, and SF539 are resistant to TIC10 compared to other cancer cell lines in the NCI 60 panel. We then performed an *in silico* analysis on expression profiles of TIC10-resistant versus –sensitive cancer cell lines from the NCI60. Interestingly, TIC10-resistant cell lines were enriched for transcriptional events associated with G-protein coupled receptor signaling (Figure 6.4), which involves the PI3K/Akt pathways as well as the MAPK pathway. The results of this analysis are in agreement with the observations that the mechanism of TIC10 involves PI3K/Akt and the MAPK pathway and that Akt overactivation of Akt can potentiate TIC10 resistance. Together, these data indicated that TIC10 inactivates Akt and ERK, which subsequently inhibits their phosphorylation of Foxo3a that normally sequesters Foxo3a to the cytoplasm (Figure 6.5).

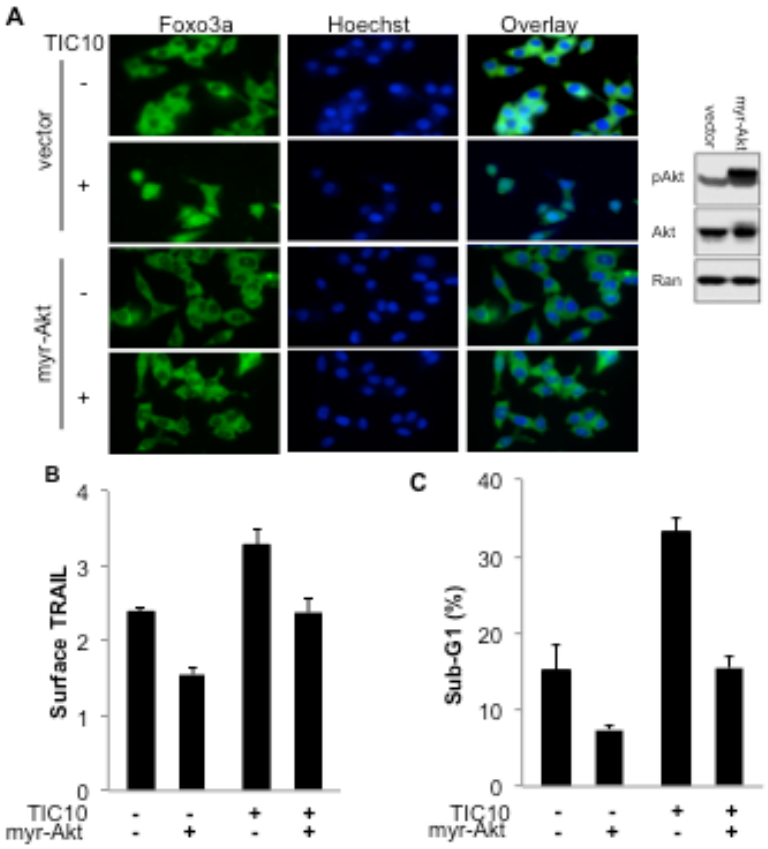

Figure 6.3. Overactivation of Akt contributes to cancer cell resistance to TIC10-induced TRAIL and cell death. (A) Immunofluorescence of Foxo3a in HCT116 cells overexpressing an empty vector or myristoylated Akt (myr-Akt) with TIC10 treatment (10 μM, 48 hr). Confirmation of overexpression of myr-Akt by Western blot analysis shown in right panel. **(B)** Flow cytometry analysis of surface TRAIL and **(C)** Sub-G1 content of HCT116 cells overexpressing an empty vector or myr-Akt with TIC10 treatment (10 μM, 72 hr, n=3).

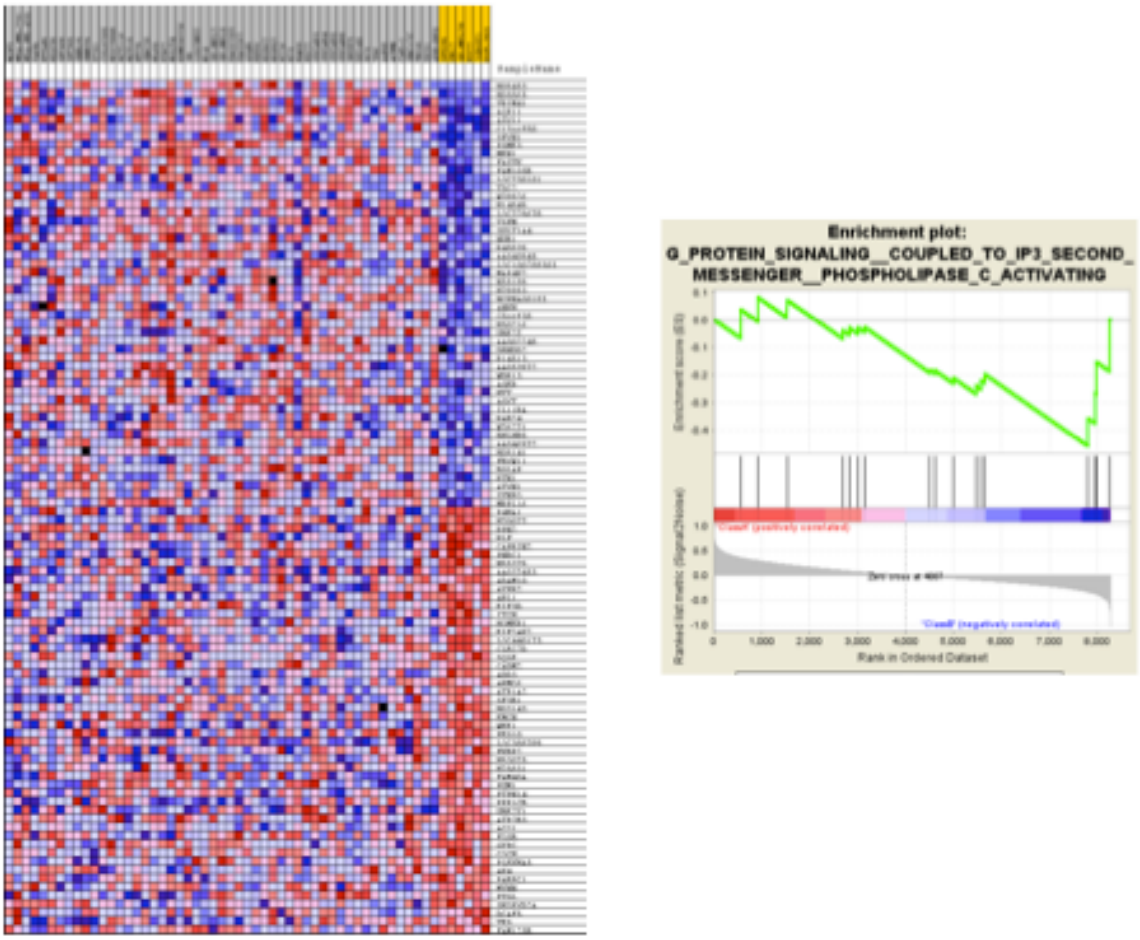

Figure 6.4. Gene set enrichment analysis of TIC10-sensitive versus –resistant cancer cell lines from the NCI60. TIC10-resistant cells are highlighted in yellow. Genes that are upregulated are indicated in blue whereas downregulated genes are indicated in red. Right panel shows enrichment plot for GPCR signaling genes in TIC10-resistant cell lines.

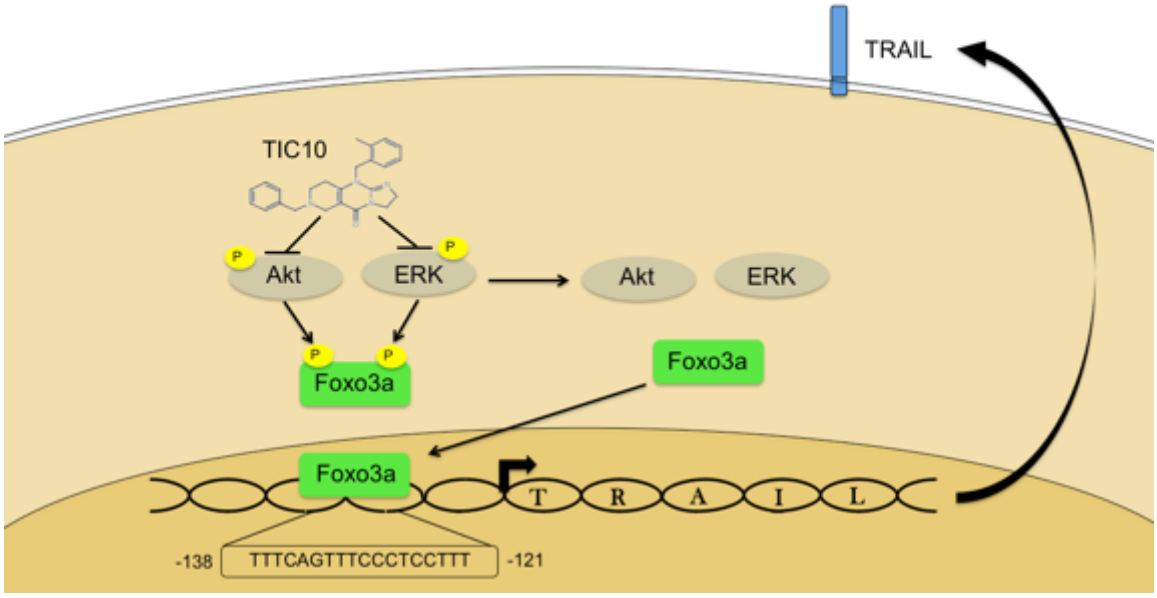

Figure 6.5. Model of TIC10-induced signaling effects that upregulate TRAIL. TIC10 causes dual inactivation of the prosurvival kinases Akt and ERK, which normally phosphorylate Foxo3a at S253 and S294, respectively. These phosphorylation events create docking sites for 14-3-3 proteins that bind Foxo3a and sequester it to the cytoplasm, thereby inhibiting its activity as a transcription factor. TIC10 inhibits Foxo3a phosphorylation, which also allows it to translocate to the nucleus where it binds to the TRAIL promoter at a previously reported FOXO binding site (Modur et al., 2002). This binding results in upregulated TRAIL gene transcription and translation that yields an elevated presence of TRAIL on the cell surface.

The dual inactivation of Akt and ERK

Based on the proposed model for TIC10, we hypothesized that dual inhibition of the Akt and the MAPK pathways would cooperatively lead to the nuclear translocation of Foxo3a and TRAIL upregulation. To test this, we utilized A6730 and U0126 monoethanolate that are commercially available and previously described inhibitors of Akt1/2 (Desplat et al., 2008) and MEK (Favata et al., 1998), respectively (Figure 6.6A). We found that the combination of MEK and Akt inhibitors synergistically induced TRAIL at the mRNA and surface protein level (Figure 6.6B-C). Furthermore, the dual inactivation of Akt and ERK was sufficient to cooperatively induce Foxo3a-dependent TRAIL upregulation as well as TRAIL-mediated cell death (Figure 6.6D-E). These novel observations were corroborated by siRNA experiments, revealing that ERK and Akt can be inhibited to cooperatively upregulate TRAIL gene transcription and protein (Figure 6.7). Together, these data indicate that TIC10 causes a dual inactivation of Akt and ERK, which leads to the nuclear translocation of Foxo3a that transcriptionally induces the TRAIL gene to potentiate cell death and potent anti-tumor effects in vivo.

Due to the involvement of Akt- and ERK-mediated phosphorylation of Foxo3a in the mechanism of TIC10, we next tested if other TICs affected Foxo3a in a similar manner to TIC10. Interestingly, TIC9 and TIC10 were the only TICs that affected both pAkt and pERK levels, which were accompanied by decreased levels of pS253 and pS294 Foxo3a (Fig. 6.8). TIC5 also decreased pAkt levels but this did not correlate with a decreased amount of pS253 Foxo3a, which is unexpected. The exclusive ability of TIC9 and TIC10 to affect Akt and ERK activity among TICs, particularly with respect to Foxo3a, is noteworthy given that these two TICs also exclusively induced cell death and surface TRAIL (Chapter 2). Together, these observations argue that Foxo3a is an attractive mechanism for inducing the TRAIL gene as it may result in increased TRAIL protein on the cell surface and cancer cell death.

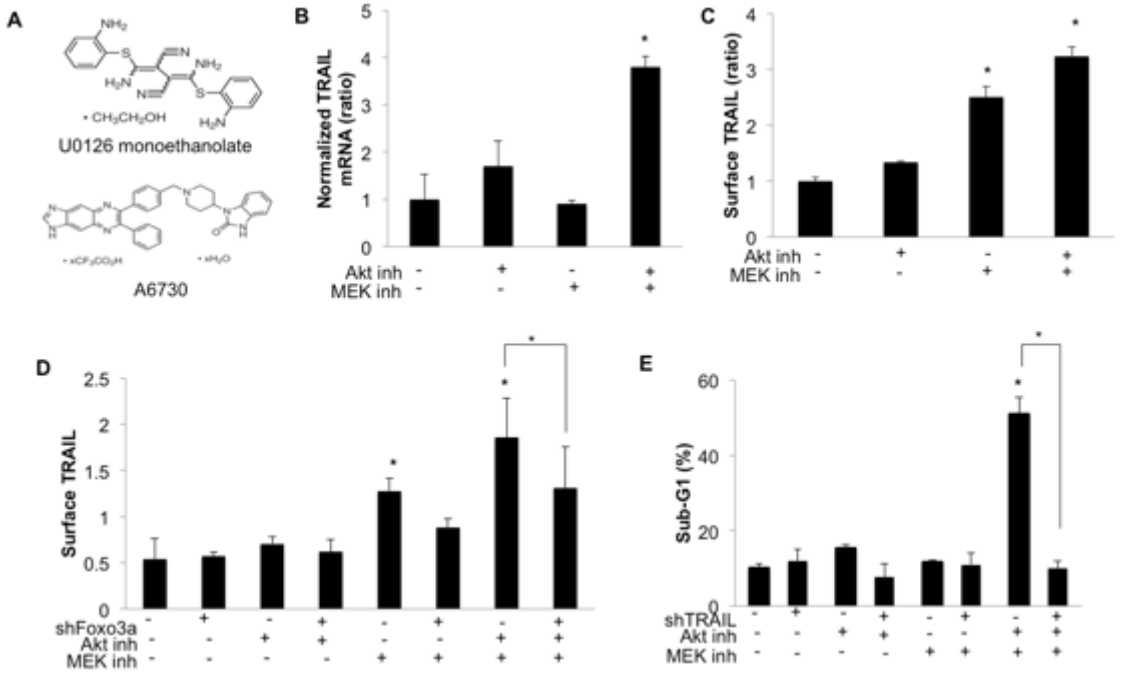

Figure 6.6. Dual inhibition of Akt and ERK cooperatively induces TRAIL. (A) Structure of the utilized Akt inhibitor (U0126 monoethanolate, top panel) and the MEK inhibitor (A6730, bottom panel). **(B)** RT-qPCR and **(C)** Surface TRAIL induction in HCT116 $p53^{-/-}$ cells following incubation with 10 μM A6730 (Akt inh), U0126 monoethanolate (MEK inh), or both (48 hr, n=3). For Akt + MEK inh, P<.05 compared to all other conditions. **(D)** Surface TRAIL induction as in (C) with or without stable knockdown of Foxo3a (n=3). **(E)** Sub-G1 analysis of MDA-MB-231 with or without TRAIL knockdown by shRNA following incubation with 10 μM Akt inh, MEK inh, or both for 48 hr (n=3). Error bars indicate s.d. of replicates. *P < 0.05 between the indicated condition and control unless otherwise indicated.

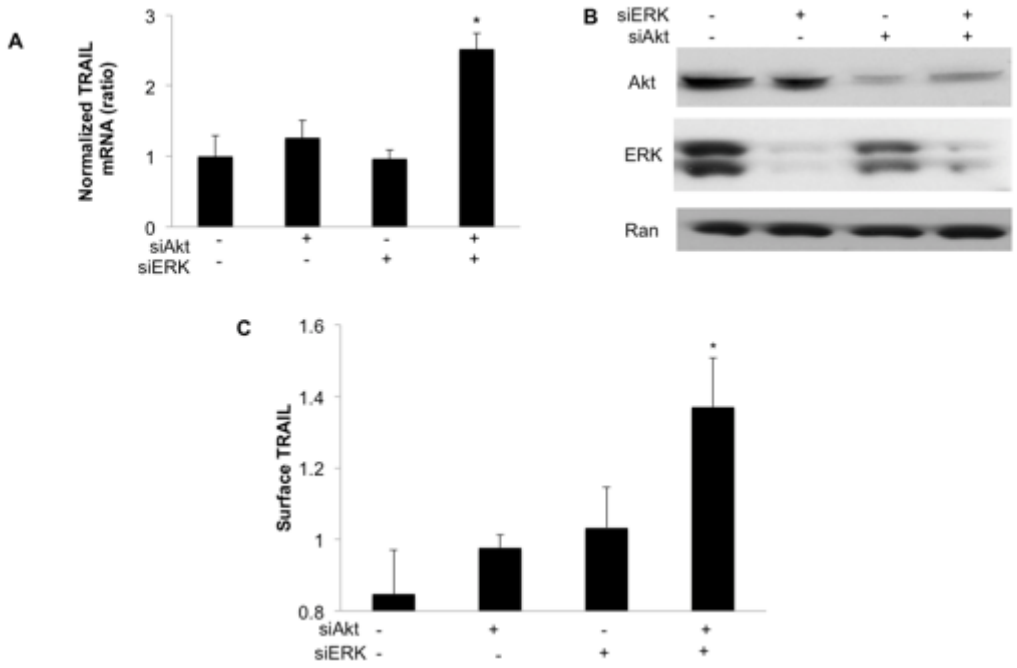

Figure 6.7. Dual knockdown of Akt and ERK cooperatively induces TRAIL. (**A**) RT-qPCR analysis of TRAIL mRNA levels following ERK or Akt knockdown by siRNA in HCT116 p53$^{-/-}$ cells (48 hr, n=3). (**B**) Confirmation of Akt and ERK knockdown by Western blot analysis. **(C)** Surface TRAIL induction following transient knockdown of Akt and/or ERK in HCT116 cells at 48 hr post-knockdown (n=3). For siERK and siAkt condition, P<.05 compared to all other conditions. *P < 0.05 between the indicated condition and control.

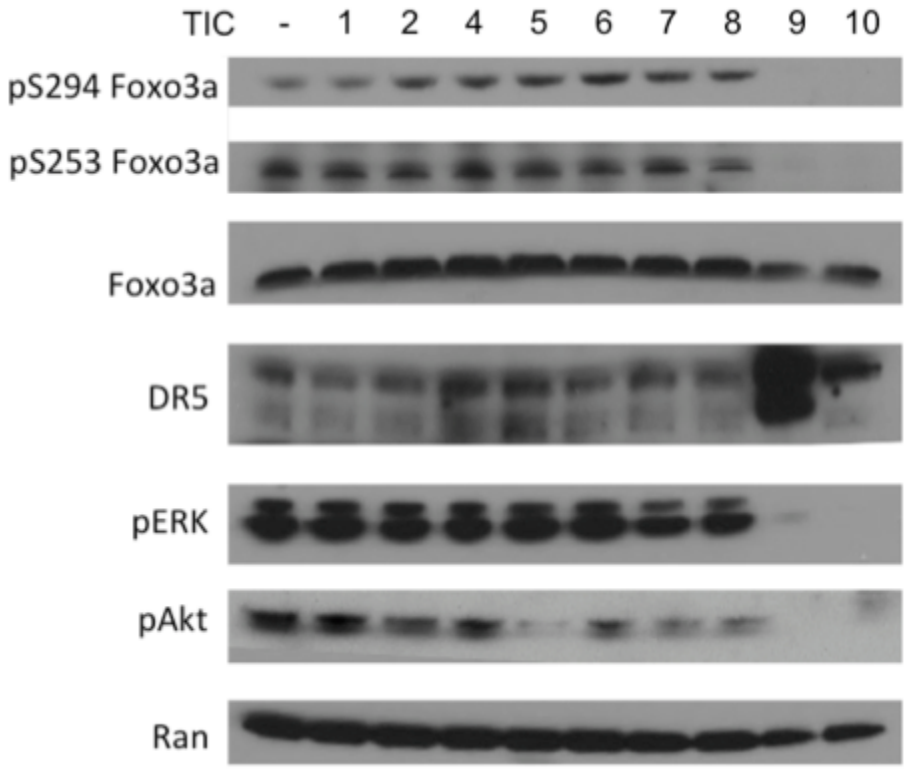

Figure 6.8. TIC9 and TIC10 decrease Akt- and ERK-mediated phosphorylation of Foxo3a.

Western blot analysis of HCT116 $p53^{-/-}$ cells treated with TICs (5 μM, 60 hr).

6.5 Discussion

The effects of TIC10 specifically on Foxo3a rather than other family members suggested that TIC10 was likely affecting a unique regulator of Foxo3a. We first tested the possibility that TIC10 was affecting IKK, as Foxo3a contains a IKK phosphorylation site at serine 644, which is not possessed by anything other FOXO family member (Hu et al., 2004b). However, we did not find any changes in IKK activity following TIC10 treatment as measured by phosphorylation of its substrate IκB and subsequent NFκB subcellular localization, which is sequestered to the cytoplasm when IKK is active (Hoffmann et al., 2002). Next, we tested the possibility of ERK involvement since ERK has been described to specifically regulate Foxo3a (Yang et al., 2008a; Yang et al., 2008b), which was indeed involved. Interestingly, we observed a striking decrease in pERK levels and phosphorylation levels of Foxo3a at a previously described phosphorylation site but did not observe any striking changes in total Foxo3a protein levels. However, a slightly lower level of total Foxo3a was noted in the MDA-MB-468 human breast cancer cell line. The possibility of TIC10-induced degradation of Foxo3a should be explored in future studies as ERK has been reported to causes ubiquitin-dependent degradation of Foxo3a through E3 ligases that involve Skp2 (Yang et al., 2008a; Yang et al., 2008b). The lack of degradation could be a result of negative regulation of Skp2 expression by Foxo3a that has been previously reported (Wu et al., 2012) and was evident in the TIC10-induced changes determined during expression profiling.

Akt is a potent regulator of Foxo3a and contains 3 conserved phosphorylation sites among FOXOs that are critical for 14-3-3-mediated shuttling between the cytoplasm and the nucleus (Biggs et al., 1999; Brunet et al., 1999; Kops et al., 1999; Nakae et al., 1999). We therefore tested the affect of TIC10 on Akt activity due to its intimate regulation of FOXOs. We found that TIC10 indeed reduced Akt phosphorylation along with its activity as judged by pGSK3B and pS294 Foxo3a. It has been suggested that the inhibition of Akt is completely required for the nuclear translocation of FOXOs. For TIC10, it is possible that Akt inhibition functions as a necessary but not sufficient aspect of activating Foxo3a and that concomitant ERK inhibition surpasses the threshold necessary to drive the nuclear translocation of Foxo3a and could be responsible for Foxo3a specificity over other family members.

We found that the kinetics of TIC10-induced Akt, ERK, and Foxo3a activation coincided with the effects of TIC10 beginning at 48 hours. While these events are congruous with each other, the kinetics of TIC10-induced TRAIL seems to differ *in vivo*. As opposed to 48 hours *in vitro*, our previous experiments with serum TRAIL induced by intravenous TIC10 in mice demonstrated TRAIL elevation as soon as 8 hours following treatment. One consideration is that these biological systems are very different: the in vitro setting is human cancer cells in cell culture whereas the in vivo setting is normal mouse cells from virtually any tissue origin in a physiological setting. Nevertheless, it is very likely that there are factors present *in vivo* but not *in vitro* that expedite the response to TIC10. The possibility that TIC10 requires metabolism into an active compound is a possible explanation and is being explored in future studies.

Due to the involvement of Akt in the mechanism of TIC10 and its well-described regulation of Foxo3a, we determined the effect of Akt overactivation on TIC10 activity. We found that Akt overactivation through overexpression of myristoylated Akt was sufficient to reverse the TIC10-driven Foxo3a nuclear translocation and subsequent TRAIL-induction and tumor cell death. The identification of this pathway as a marker of sensitivity has implications for its use in future clinical trials with TIC10. This observation is in accordance with our *in silico* analysis that revealed elevated GPCR signaling in TIC10-resistant cell lines, as GPCR signaling intimately involves the MAPK and Akt signaling pathways. Future studies are exploring the prevalence of Akt overactivation in evolved TIC10-resistant clones in addition to the MAPK signaling pathway among others.

Based on the affects of TIC10 on both Akt and ERK, we tested the ability of Akt and MAPK pathway inhibitors to regulate Foxo3a and TRAIL expression alone and in combination. Interestingly, the combination of Akt and MEK inhibitors cooperatively induced Foxo3a-dependent TRAIL and synergistically induced TRAIL-mediated cell death. With both the siRNA and pharmacological inhibitors, the combination of Akt and ERK inhibition cooperatively upregulated TRAIL. These data suggest that TRAIL is an essential proapoptotic effector of Foxo3a, which is uniquely and cooperatively regulated by Akt and ERK. These observations provide a novel molecular explanation for recent reports of synergistic activity with dual inhibition of the PI3K/Akt

and MAPK (Ebi et al., 2011) and is also in line with a recent clinical observation that highlighted Foxo3a-dependent TRAIL as the critical axis mediating chronic HIV infection-induced cell death of memory B cells (van Grevenynghe et al., 2011). These data also argue for the combination of approved antitumor agents that target these two pathways indirectly may recruit Foxo3a/TRAIL-dependent activity in addition to monoagent efficacy.

The observations that TIC9 and TIC10 uniquely affect Akt- and ERK-mediated phosphorylation of Foxo3a is particularly interesting, given their unique ability to induce TRAIL localized to the cell surface and their potent ability to induce cancer cell death. While the two molecules are very diverse in structure and likely differ in other effects on cell signaling, this common effect suggests that Foxo3a may be an attractive transcriptional mechanism for inducing the TRAIL gene as an antitumor strategy and also that perhaps Foxo3a induces a unique isoform of TRAIL that remains localization to the cell surface. Since breflate is the prodrug of a canonical ER stressor, future studies should examine the role of TRAIL as well as Foxo3a activation in the proapoptotic response to ER stress.

CHAPTER 7

CONCLUSIONS

7.1 Summary of Results

TIC10 is a small molecule that was identified in a high throughput screen with the NCI Diversity Set II library of compounds to identify p53-independent inducers of the human TRAIL gene using a luciferase reporter gene under transcriptional control of part of the TRAIL gene promoter, which excludes the p53 binding site that we previously identified (Kuribayashi et al., 2008). TIC10 induces TRAIL gene transcription in a p53-independent manner and TRAIL-mediated apoptosis. In addition to impressive efficacy in numerous xenografts, this therapeutic strategy results in improved drug properties compared to recombinant TRAIL such as delivery to the brain, greatly superior stability, temporally sustained induction of TRAIL for days beyond its normal half-life of <30 minutes, and no evidence of toxicity by numerous studies in various mouse models. TIC10 also prolongs the survival of transgenic mice that spontaneously develop myc-driven lymphoma or mice harboring intracranial human glioblastoma tumors by weeks.

TIC10 induces the TRAIL gene through Foxo3a by inactivating the prosurvival kinases Akt and ERK that are previously described upstream regulators that directly phosphorylate Foxo3a at Ser 253 and Ser 294, respectively. As Foxo3a is no longer phosphorylated, it translocates to the nucleus where it binds directly to the TRAIL promoter and upregulates its transcription. We assayed for other FOXO family members and found that TIC10 is affecting only Foxo3a and not other family members such as Foxo1, which has been targeted by small molecules (Kau et al., 2003). Accordingly, the dual inhibition of the Akt and MAPK pathways by the combination of other small molecules targeting Akt and MEK cooperatively induced Foxo3a-dependent TRAIL upregulation and TRAIL-mediated cell death. These findings were corroborated by siRNA experiments and highlight Akt and ERK as key regulators of Foxo3a that may be utilized as a potent apoptosis-inducing strategy.

These findings also suggest that the combination of MAPK and PI3K/Akt pathway targeted agents may be therapeutically advantageous by uniquely inducing the potent TRAIL-mediated cell death pathway involved in innate tumor suppression. These are very novel insights demonstrating the convergence of key kinases to regulate a transcription factor, Foxo3a and not Foxo1, leading to critical induction of a pro-apoptotic and tumor suppressing secreted factor,

TRAIL, which is required for the observed anti-tumor effects of TIC10. Our observations suggest that TRAIL is a unique effector target gene of Foxo3a that confers its proapoptotic effects in response to TIC10, which is reminiscent of $p21^{WAF1}$ being a unique effector target of p53 that confers cell cycle arrest in response to DNA damage (El-Deiry et al., 1993).

It is important to note that neither the specific pharmacological induction of the TRAIL gene by Foxo3a nor the nuclear translocation of Foxo3a has been specifically targeted as a therapeutic strategy to combat cancer. Additionally, this mechanism has novel implications that extend beyond TIC10, i.e. underscoring the cooperative regulation of Foxo3a by Akt and ERK and supporting the combination of Akt and ERK inhibitors to gain Foxo3a- and TRAIL-mediated therapeutic effects. However TIC10 provides these properties in a single small molecule along with safety in preclinical models. The delivery of TRAIL-based therapies to the brain is a problem that is widely recognized as a limitation by the field and has resulted in several preclinical efforts to deliver TRAIL by adenovirus or mesenchymal stems cells overexpressing TRAIL on their cell surface (Jeong et al., 2009; Kim et al., 2008). We find that serum TRAIL is elevated over a period of days following a single dose of TIC10, which is in stark contrast to the poor pharmacokinetics of recombinant TRAIL. We also found that TIC10 exhibits thermal stability unlike TRAIL, which is important for shelf-life and activity *in vivo*. In summary, TIC10 is a potent antitumor agent that requires Foxo3a and TRAIL and improves the properties of recombinant TRAIL to yield superior efficacy and spectrum of activity.

Our data shows that the antitumor effects of TIC10 are mediated through TRAIL and Foxo3a as indicated by stable knockdown in vitro and xenograft experiments. TIC10 is a first-in-class anti-cancer therapy that provides an excellent opportunity for modulation of host anti-tumor responses and the pharmacokinetic properties of an endogenous antitumor protein. Moreover, the pharmacological induction of TRAIL in the brain demonstrates a novel therapeutic approach in brain malignancies otherwise refractory to current therapies. This provides an alternative solution for the general limitation of protein delivery by stimulating TRAIL production within the tumor microenvironment. TIC10 demonstrates a novel and effective cancer therapeutic strategy that utilizes both normal and tumor cells to produce an anti-tumor agent via conserved signaling

pathways that results in a therapeutic response. The modulation of pharmacokinetic properties of endogenous TRAIL as a tumor suppressive agent by a small molecule such as TIC10 suggests that exploration of pharmacological induction/pharmacokinetic tuning of other endogenous anti-tumor proteins is feasible and warranted. The molecular mechanism of TIC10 suggests that the anti-tumor effects of Foxo3a and TRAIL gene can be harnessed through the dual inhibition of Akt and ERK, which should be explored with such targeted agents in clinical development.

TIC10 possesses an excellent broad-spectrum activity profile that does not rely exclusively on commonly altered molecules in cancer such as EGFR, Her2, KRAS, p53, or PTEN. This is in agreement with a previous study describing the utility of Foxo3a activation as an anticancer mechanism for targeting cancer cells resistant to therapies that inhibit upstream regulators of MAPK signaling (Yang et al., 2010). The elucidation of the mechanism of TIC10 yields important information for the clinical translation of this molecule as it allows for the identification of potential resistance mechanisms such as over-activated Akt, which we demonstrate directly, and offers phospho-ERK, phospho-Akt, Foxo3a localization, and surface and serum TRAIL as correlative biomarkers in early phase clinical trials.

Together, these findings demonstrate that TIC10 is a safe and orally active anti-tumor agent that has potent cancer-specific cytotoxicity that results from sustained stimulation of the endogenous TRAIL tumor suppressor in normal and tumor tissues, including the brain. TIC10-induced TRAIL is dependent on Foxo3a, which also upregulates TRAIL death receptor DR5 among other targets, allowing for sensitization of some TRAIL-resistant tumor cells. Our observations support that harnessing Foxo3a is a powerful antitumor strategy that is mediated by TRAIL and may be achieved by dual inhibition of Akt and ERK as exemplified by the small molecule TIC10. Interestingly, the induction of TRAIL caused by TIC10 is sustained in tumor, stromal, and host cells and in vitro evidence suggests that these normal host cells may contribute to TIC10-induced cancer cell death. Due to the promising preclinical safety and efficacy profile of TIC10 demonstrated herein, an early phase clinical trial has been planned to evaluate the safety and efficacy of TIC10 in patients with lymphoma, brain, breast, or lung cancer. The molecular

mechanisms and clinical exploitation of the synergistic combination of TIC10 with taxanes will also be examined in future clinical development.

7.2 Future Directions

Overview

TIC10 is an extremely potent antitumor agent that requires Foxo3a and TRAIL upregulation for its activity. Clinical translation of the molecule is being pursued due to the highly promising efficacy and safety profile of the molecule. Complete elucidation of the mechanism of action of TIC10 will greatly facilitate the translation of this molecule, more clearly delineate a potent antitumor strategy, and potentially yield novel drug targets. Our preliminary data suggest that TIC10 inhibits the PI3K/Akt and MAPK pathways and that these pathways cooperatively regulate the TRAIL gene through Akt- and ERK-mediated phosphorylation of Foxo3a. However, future studies should explicitly evaluate their individual and cooperative contribution to the overall antitumor effects of TIC10 and determine if any additional modifications to Foxo3a occur in response to TIC10. Lastly, the mechanism and target of TIC10 should be validated *in vivo* as part of the translation of TIC10. These future studies will facilitate the clinical translation of the first-in-class molecule TIC10 by defining its mechanism of action and providing a better understanding of FOXO regulation of the TRAIL gene.

Understanding the regulation and activity of Foxo3a

As previously outlined, the activity of FOXO family members can be controlled by a number of events with some events being unique to particular members. Future studies should define differential regulation of the TRAIL gene by FOXO family members to better understand FOXO biology and the relative suitability of Foxo3a as a drug target compared to other FOXOs. TRAIL is a potent and selective tumor suppressor gene that serves as an attractive drug target for cancer treatment as exemplified by TIC10. It is important that we understand if certain FOXO family members may more prominently regulate the TRAIL gene promoter so that the family member can be preferentially targeted. Additionally, the coregulation of FOXO binding sites by different

FOXO family members is unclear. For instance, does upregulating Foxo1 and Foxo3a simultaneously result in a cooperative, antagonistic, or similar effect compared to upregulating just one? Do cofactors influence these relationships? Can these relationships be explained by in vitro binding or does the genomic context influence the relationship? The answers to these questions should be obtained in future studies as this will yield essential information regarding how FOXO family members regulate the TRAIL gene in comparison or in concert and provide information on how to best therapeutically harness the TRAIL gene using FOXO.

The localization of Foxo3a has been linked to prognosis in select malignancies. High expression levels of Foxo3a has been linked to a better prognosis in hepatocellular carcinoma and ovarian cancer (Fei et al., 2009; Lu et al., 2009). High phospho-Foxo3a has been linked to a poorer outcome in AML and ovarian cancer (Kornblau et al., 2010; Lu et al., 2011). However, none of these studies have examined Foxo3a expression levels, phosphorylation levels, or localization in colon cancer disease progression. Furthermore, most of the previous studies only noted the localization of Foxo3a rather than its activity. Simultaneously evaluating the post-translational modifications, localization, and expression of Foxo3a in primary colon cancer specimens will have important implications for the biology of Foxo3a in disease progression and identify prevalent Foxo3a modifications in patient tumors that should be evaluated for there effects on therapeutic sensitivity.

TRAIL and Late Effects of Gamma Radiation

The majority of cancer patients receive radiation therapy (Chua et al., 2004; Ringborg et al., 2003) such as gamma radiation (GR), as it is noninvasive and controlled in temporal and spatial dimensions. GR is dose-limited by toxicity issues that manifests as early effects such as skin irritation, and mucositis. However, late effects also surface including fibrosis, atrophy, vascular damage, and neural damage which persist indefinitely and intensify (Bentzen et al., 1989). While still under investigation, radiation-induced fibrogenesis has generally been attributed to cytokines, endothelial cell damage, and reactive oxygen species (ROS) (Bentzen, 2006). One such cytokine is TGFβ, which possesses roles in wound healing (Leask and Abraham, 2004), tumor

suppression and progression (Dumont and Arteaga, 2003; Siegel and Massague, 2003), inhibition of endothelial cell proliferation (Reiss, 1997), and promotion of invasion and metastasis in breast cancer (Reiss, 1997; Siegel et al., 2003). GR causes immediate activation and secretion of TGFβ from damaged endothelial cells (Ehrhart et al., 1997; Ewan et al., 2002). Activation of TGFβ triggers the SMAD-pathway signaling, resulting in transcription of target genes which direct fibroblast differentiation and tissue remodeling (Bayreuther et al., 1988; Feng and Derynck, 2005; Herskind et al., 1998; Herskind and Rodemann, 2000; Martin et al., 1974; Rodemann et al., 1991). In direct support, $SMAD3^{-/-}$ mice have reduced fibrogenesis and epithelial-mesenchymal transitions (EMT) (Roberts et al.), a process involved in fibrogenesis (Kalluri and Neilson, 2003).

Genetic correlations of SNPs with radio-responsiveness have failed (Andreassen, 2005), nevertheless there have been attempts to combat these late effects. Amifostine is a cytoprotective compound used in head and neck cancer (Brizel et al., 2000) but itself has severe side effects (Rades et al., 2004) and preclinical data suggests that it possesses tumor-protective effects (Lindegaard and Grau, 2000). Small-molecule TGFβ inhibitors such as SM305 (Ishida et al., 2006) and halofuginone (Xavier et al., 2004) are in preclinical development but TGFβ is a risky target due to its suppressor and promoter dual role in cancer (Iyer et al., 2005; Reiss, 1997; Wakefield and Roberts, 2002). Clearly, a molecular understanding of the late effects of GR is necessary for development of more effective therapies.

Novel findings from our lab suggest a role for the TRAIL pathway in these late effects as $TRAIL\text{-}R^{-/-}$ mice develop chronic inflammation and fibrosis sooner and more severe than wild type littermates (Finnberg et al., 2008). Based on these findings, we hypothesize that late effects of GR are due, at least in part due to diminished TRAIL-signaling and administration of small molecule upregulators of TRAIL will ameliorate the late effects of GR. Future studies should test this hypothesis with both TRAIL and TIC10, which causes a sustained elevation of TRAI levels for days.

Identifying the direct binding target of TIC10

While the mechanism of TRAIL gene induction by the small molecule TIC10 has been elucidated, the direct binding target of TIC10 has not been identified. We are undertaking several approaches as future directions to identify the binding target for TIC10: (1) deductive reasoning from upstream cell signaling changes, (2) gene expression profiling of TIC10 response in wild-type versus TIC10-resistant isogenic cell lines, (3) in vitro kinase activity assays against the kinome, and (4) mass spectrometry-mediated identification of proteins bound to bead-conjugated TIC10. The mechanism of TRAIL gene induction by TIC10 involves the dual inactivation of Akt and ERK that cooperatively activate Foxo3a, which translocates to the nucleus where it upregulates TRAIL gene transcription. We looked further upstream of ERK in the MAPK pathway, which is compromised of the Ras/Raf/MEK/ERK axis, and found that phospho-MEK expression was also being ablated in response to TIC10 to a similar extent seen with phospho-ERK (Figure 7.1A). This phosphorylation event on MEK is mediated by Raf, suggesting that Raf activity was being inhibited by TIC10.

The activity spectrum of TIC10 is very broad and TIC10-induced cytotoxicity and TRAIL production has been demonstrated in cells that lack EGFR (SW620) and HER2 (MDA-MB-231). Furthermore, TIC10 did not affect total- or phospho-Her-2 expression levels (Figure 7.1A). This suggests that EGFR and HER2 may not be involved in the mechanism of action of TIC10 or at least, do not exclusively mediate the effects of TIC10. Next, we tested Ras activation following TIC10 treatment using a functional assay that precipitates active Ras protein using Raf-1-conjugated beads followed by immunoblotting for Ras. A time course experiment found no significant differences in active Ras levels between TIC10- and DMSO-treated cancer cells (Figure 7.1B). Together, these data suggest that TIC10 decreases Raf activity to inhibit the MAPK pathway.

Current studies are focusing on the mechanism of Raf inhibition that may involve decreased Raf protein expression, increased Raf protein degradation, or negative regulation by RKIP. RKIP activation is a promising candidate effector mechanism for TIC10 as this protein inhibits both the MAPK and PI3K/Akt pathways (Lin et al., 2010). In any case, Raf inactivation by

TIC10 is still a late event and further upstream effects must be elucidated for TIC10 target identification. As a parallel and unbiased approach, we have evolved RKO human cancer cell lines that are completely resistant to the cytotoxic effects of TIC10 even after withdrawal of the drug (Figure 7.2A). Interestingly, these cells have completely silenced TRAIL expression on their cell surface and no longer respond to TIC10 in terms of TRAIL production, Akt or ERK inhibition, or Foxo3a activation (Figure 7.2B-C). As an approach to target identification, we will perform gene expression profiling at early time points (~8 hours) in response to TIC10 and compare the wild-type versus TIC10-resistant isogenic cancer cells. Genes with TIC10-induced changes that are significantly different between the wild-type and TIC10-resistant cell lines will be identified. Ingenuity Pathway Analysis will be employed to determine common signaling networks and generate potential binding target candidates. RNAi and/or overexpression experiments will evaluate candidate binding targets of TIC10. Promising candidates will be evaluated for direct binding using NMR chemical shift perturbation and/or HPLC assays as appropriate.

Should these two approaches fail, we will explore two other approaches as alternatives. The in vitro kinase activity approach is expensive and assumes that the direct binding target is a kinase and that the molecule does not require modifications inside the cell for activity. Conjugation of small molecules to beads requires chemical moieties that are amenable to chemistry with a given chemical linker attached to the bead. While this is available on TIC10, this process will require chemistry expertise and will alter the chemical structure of the molecule, change its enthalpic and entropic energies, and may change its ability to interact with natural binding targets. While these approaches have significant limitations, they have proven useful in target identification for some small molecules and will be employed if necessary.

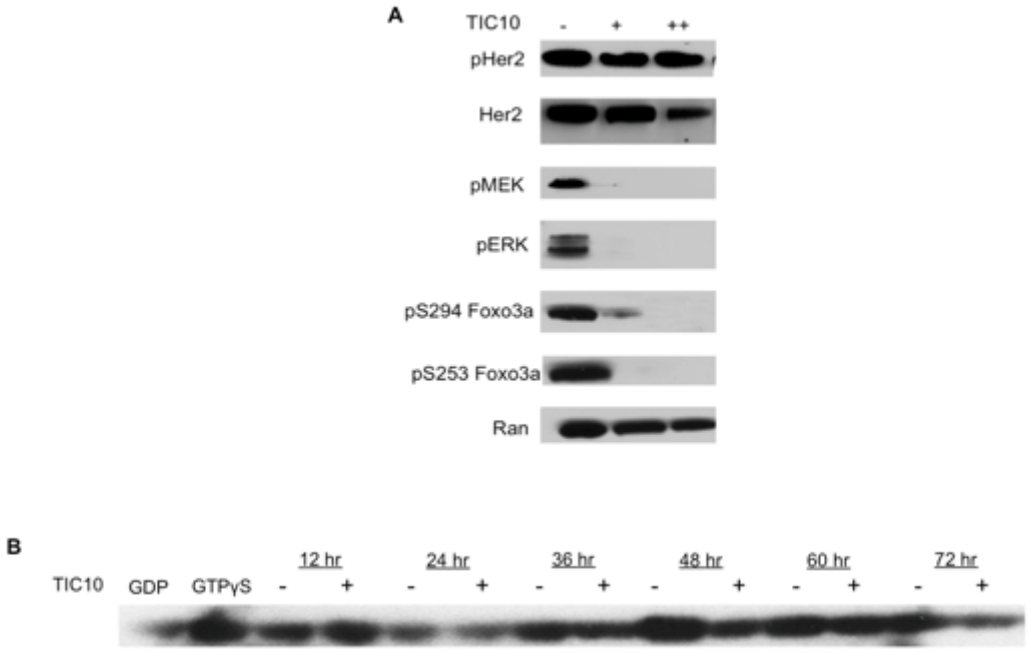

Figure 7.1. TIC10 does not affect Her2 or Ras activation. (A) Western blot analysis of HCT116 $p53^{-/-}$ cells treated with TIC10 (0, 2.5, or 5μM) for 72 hrs. (**B**) Immunoblot for Ras following precipitation with Raf-1-conjugated beads. HCT116 $p53^{-/-}$ cells were treated with TIC10 (5 uM) or DMSO for the indicated time period and processed according to the manufacturer's protocols (STA-400-K, Cell Biolabs, Inc.). GDP and GTPγS are included as negative and positive controls, respectively.

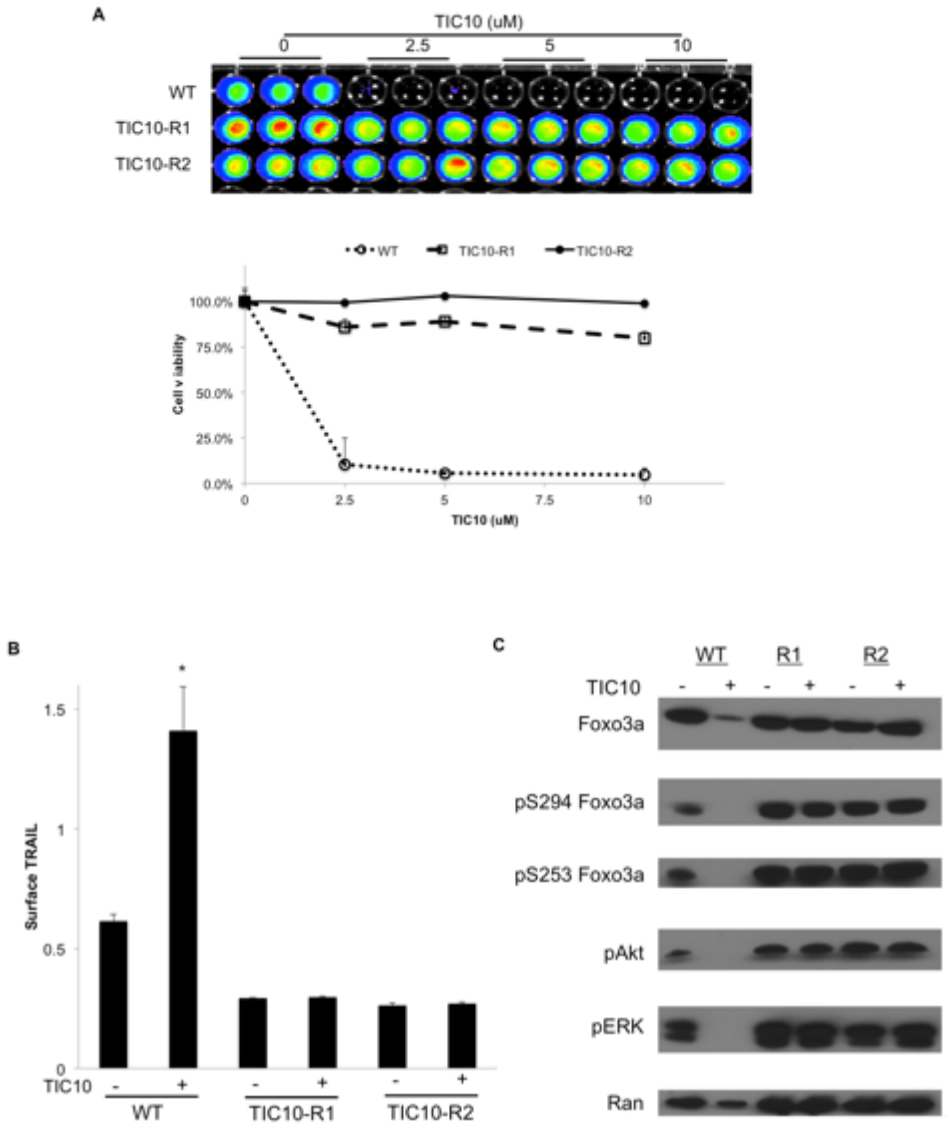

Figure 7.2. TIC10-resistant clones have silenced TRAIL expression and do not inhibit Akt or ERK in response to TIC10. (**A**) Cell TiterGlo analysis on RKO cells at 72 hr post-treatment with TIC10 at indicated doses (n=3). Assay was performed 3 weeks following removal of TIC10 selection for resistant cell lines. For evolution of TIC10-resistant clonal cell lines (TIC10-R1 and TIC10-R2), RKO cell were treated with 500 nM TIC10 for 1 week and the dose was doubled weekly until 16 uM. (**B**) Surface TRAIL analysis following a 72 hr treatment with TIC10 (10 uM) or DMSO (n=3). (**C**) Western blot analysis of RKO cells treated with TIC10 (10 uM) for 72 hrs. *P < 0.05 between the indicated condition and control.

Translating TIC10 to the clinic

Our studies with TIC10 reported herein have provided the foundation for rationalizing and designing a human clinical trial testing a new cancer treatment through preclinical studies that established efficacious and safe dosing schedules, efficacy profiling to identify target malignancies, identify correlative assay markers, and elucidated the mechanism of action for the potentially first-in-class small molecule. A phase I/II study with TIC10 in cancer patients has been planned. Based on our preclinical data, the patient population will include glioblastoma, NSCLC, breast cancer, lymphoma, head and neck, and colorectal cancer. The primary objectives of this study will be to determine safety, optimal dose, pharmacokinetics, pharmacodynamics, and efficacy of TIC10. Secondary endpoints will be analyzed by Kaplan Meier methods and include overall survival, objective response, disease control, time to response, duration of response, and statistically significant responses in correlative assays.

Our mechanistic studies have revealed several proteins that are intimately involved in the mechanism of TIC10. Our data strongly suggest that phospho–ERK, phospho–Akt, Foxo3a localization, phospho-Foxo3a, DR5, surface TRAIL, and serum TRAIL protein levels may serve as molecular markers of response in TIC10-treated cancer patients and will be incorporated in correlative assays in future clinical trials. Enrolled patients will include colorectal and breast cancer, have been approved by the FDA for prognostication based on circulating tumor cell (CTC) enumeration (Appendix 3). Pharmacodynamic response will be defined as a 20% elevation in serum TRAIL, 20% increase in lymphocyte DR5 or TRAIL expression, or a 20% decrease in phospho-ERK levels in CTCs. Disease will be monitored by CT or MRI scan/PET scans and efficacy will be evaluated by time to progression (TTP) and response rate according to Response Evaluation Criteria in Solid Tumors (RECIST). Based on preclinical data, we expect to achieve pharmacodynamic endpoints below the maximum tolerated dose.

Appendix 1 – Expression profiling of TIC10-induced changes

Table A1.1 TIC10-induced changes that occur at 18 but not 48 hours.

Symbol	Fold change	Direction of change	Corrected p-value
SLFN5	5.2536516	up	0.013630901
C1orf24	4.767111	up	0.020882903
LOC729779	4.317111	up	0.007861736
ULBP1	3.863834	up	0.01914735
FAM129A	3.8311636	up	0.015890285
NRP1	3.7627487	up	0.0415099
PSAT1	3.7295916	up	0.009730678
LAMP3	3.5428753	up	0.015890285
CARS	3.4032776	up	0.035969965
SERPINB8	3.3323784	up	0.015136981
LCN2	3.2839663	up	0.022725973
BEX2	3.1873887	up	0.01736496
SYTL1	3.028134	up	0.035387393
ATF4	2.9628785	up	0.03377527
SLC3A2	2.9154215	up	0.033348393
GPR56	2.828719	up	0.032397754
SMOX	2.7758727	up	0.035969965
MAP1B	2.7032073	up	0.03377527
ZCCHC12	2.5327935	down	0.031600256
CARS	2.4839833	up	0.031037325
SLC3A2	2.4613535	up	0.012894535
LOC285216	2.419268	up	0.013630901
SARS	2.4026952	up	0.004370419
CYP4F3	2.3913798	up	0.046903133
SLC7A1	2.372022	up	0.035969965
CXorf45	2.3611965	up	0.0424862
OR51B5	2.3410978	up	0.017769916
OR51B5	2.3251212	up	0.03832007
C9orf91	2.323258	up	0.03754234
GPT2	2.322226	up	0.01914735
WARS	2.3204963	up	0.015136981
MTHFD2	2.3183424	up	0.018310567
LOC650215	2.3182306	up	0.045011252
MTHFD2	2.2629762	up	0.009730678

FTHL16	2.2629623	up	0.030300215
IFI35	2.2365541	up	0.03377527
C2orf18	2.2235944	up	0.023232972
GADD45A	2.2223954	up	0.03377527
AARS	2.203837	up	0.035969965
KLHL29	2.2029133	up	0.0424862
LETMD1	2.194489	up	0.04149641
TACSTD2	2.1636503	up	0.047248807
CCNB1IP1	2.1506143	up	0.02516231
LOC644100	2.1153002	up	0.040577903
TRIM25	2.1108935	up	0.046464972
NCRNA00219	2.1059155	up	0.013630901
AHNAK2	2.084259	up	0.04166845
TIGA1	2.0792367	up	0.028295735
GOT1	2.0616658	up	0.030248642
WARS	2.035528	up	0.027487637
YARS	2.025761	up	0.015890285
NFE2L1	2.023078	up	0.04794338
STK40	2.0103016	up	0.02055652
CDC25A	2.0061474	down	0.04143007
ANKRD41	1.9957383	down	0.013276912
ABCC3	1.9893185	up	0.034122363
TES	1.9855434	up	0.045349706
CLIC4	1.9744818	up	0.04219793
SMOX	1.9712912	up	0.010293334
CLDN7	1.9673108	up	0.038438715
LOC644877	1.9475921	down	0.017769916
PRSS3	1.9405015	up	0.024025438
SNHG8	1.933677	up	0.03295909
PYCR1	1.9311128	up	0.043904882
HMOX1	1.9302819	up	0.01736496
CCNB1IP1	1.9219142	up	0.048921436
ATF4	1.9183371	up	0.02516231
TUFT1	1.9114358	up	0.0424862
PGAM1	1.8919657	down	0.02516231
MT1G	1.8550231	up	0.033348393
PPM1M	1.853048	up	0.025818529

TP53I3	1.8434186	up	0.04794338
CLIP4	1.8357545	up	0.02516231
LARS	1.8327401	up	0.015136981
LAMC2	1.8307914	up	0.02516231
C6orf48	1.8263745	up	0.02516231
SNORD30	1.8227549	down	0.03522341
CALCOCO2	1.8179024	up	0.035969965
LOC728188	1.8174123	down	0.02516231
KCTD15	1.8155324	up	0.023033692
ETV5	1.7755473	up	0.035969965
LETMD1	1.7748973	up	0.023033692
LRP3	1.7607368	down	0.03832007
ATF5	1.7407991	up	0.015890285
SLC16A5	1.7315388	up	0.035387393
IDH1	1.7256097	up	0.046762653
GRB10	1.7219803	up	0.03754234
IARS	1.7086833	up	0.042942364
ALDH2	1.7025706	up	0.04166845
PITX1	1.7019013	down	0.047705967
VPS28	1.6996351	up	0.045349706
FLNB	1.6966534	up	0.011017979
PSME3	1.694756	down	0.042370286
C20orf127	1.690119	up	0.035387393
TXNRD1	1.6883202	up	0.040577903
TFRC	1.6775392	up	0.033348393
SFRS2	1.6736805	down	0.031570848
JOSD1	1.670766	up	0.018388763
ETV5	1.6706791	up	0.023232972
JAG2	1.6562698	down	0.04998421
FLJ10986	1.654353	up	0.048788186
MTO1	1.6475526	up	0.011017979
YWHAE	1.6474224	down	0.03851196
P2RX4	1.6406866	up	0.023232972
NAP1L4	1.6232096	down	0.03377527
LOC387825	1.6173114	up	0.03186376
TACC2	1.6127528	up	0.043904882
LOC100133163	1.5947231	down	0.02516231

RAG1AP1	1.5885754	up	0.039074127
ZNF25	1.5853447	up	0.013276912
ECGF1	1.5740145	up	0.03377527
NCAPD3	1.573892	down	0.035969965
HLA-G	1.5714598	up	0.01914735
ZNF473	1.5704359	up	0.04852033
C1orf41	1.5127012	down	0.039863512
TOMM40	1.5104885	down	0.043260563
FAM107B	1.5074275	up	0.04998421
AHSA1	1.50516	down	0.035969965
MT1A	1.4974539	up	0.018310567
EIF2B1	1.493862	down	0.042965356
HAX1	1.4836705	up	0.03377527
MT2A	1.4782473	up	0.03832007
C13orf15	1.4750918	down	0.0424862
KIAA1324L	1.4750146	up	0.035969965
EHBP1	1.47026	up	0.030091554
KIAA0430	1.466113	up	0.02516231
SNORA61	1.4616472	down	0.035969965
PRPF38A	1.4600328	down	0.032736808
HMBS	1.4593867	down	0.035387393
RPA1	1.45915	down	0.048921436
NOL12	1.458158	down	0.043904882
MT1E	1.4551145	up	0.032736808
AP1S1	1.4540619	down	0.03754234
LOC100130561	1.4518129	down	0.038431063
PARD6G	1.4499322	down	0.025818529
TUBB6	1.4494025	down	0.046364475
SFRS4	1.449192	down	0.040804602
ZSWIM7	1.4460802	up	0.036312204
TPD52L1	1.4301215	up	0.029162576
ATP9A	1.4247177	up	0.02516231
CIR1	1.4222693	up	0.0480779
VDAC3	1.4192182	down	0.034097776
DCTPP1	1.4172494	down	0.02055652
NIT2	1.4153856	up	0.04622574
C12orf76	1.413956	up	0.039074127

TIMM44	1.4129331	up	0.02516231
HIATL1	1.4115709	down	0.042370286
LOC653505	1.4115399	down	0.025818529
LOC729086	1.4102656	down	0.045709208
HEATR2	1.4101177	down	0.036609683
SERINC3	1.4095489	up	0.04806973
PGS1	1.4080536	down	0.03377527
RABAC1	1.40511	up	0.02516231
EDEM2	1.4044122	up	0.04143007
LOC729500	1.4039483	up	0.035969965
RFXANK	1.4008156	up	0.04852033
CCNE1	1.3986037	down	0.03978613
KIAA0355	1.3940547	up	0.03377527
TMEM167B	1.3928344	up	0.044718616
OCRL	1.390933	up	0.013630901
FLJ12684	1.3903908	down	0.03377527
LOC643949	1.3869902	up	0.04714453
CCT7	1.3847481	down	0.046364475
ZDHHC8	1.3839697	down	0.035969965
CCDC84	1.379626	down	0.03691505
C9orf6	1.378823	up	0.036143113
LOC391019	1.3775201	up	0.029162576
SLBP	1.3741986	down	0.02516231
C1orf122	1.3701819	up	0.04166845
HLA-E	1.3694867	up	0.0415099
FKBP9L	1.368465	up	0.039863512
CAMK2G	1.3684158	down	0.043904882
NUP85	1.3650339	down	0.027487637
BLVRB	1.3619043	up	0.035969965
LOC647349	1.356989	up	0.02554246
SLC25A42	1.355689	down	0.039582886
MLH1	1.3553423	up	0.046464972
RPL29	1.3552064	down	0.045110192
CTNNA1	1.3544421	up	0.025818529
BRE	1.3544145	up	0.043260563
ZFP90	1.3539084	up	0.02516231
C20orf111	1.350331	up	0.035969965
KRT18P13	1.3498448	up	0.040804602

LOC652864	1.348653	down	0.046364475
LOC642282	1.3457245	up	0.046903133
PDCD4	1.3455595	up	0.042370286
DBNDD1	1.3407319	down	0.04582269
GARNL4	1.3327382	up	0.02516231
ACN9	1.326853	down	0.046364475
ITGB1	1.3260574	up	0.049887963
C14orf173	1.3255491	down	0.047705967
ERN1	1.3244102	up	0.0424862
CHD1L	1.3195786	up	0.039863512
CSE1L	1.3186004	down	0.040804602
PIAS1	1.3145103	down	0.017720023
GEMIN6	1.2970588	down	0.04714453
SERPINE2	1.2951967	up	0.04219793
C1orf149	1.2934092	up	0.02516231
BSPRY	1.2891803	up	0.04166845
TNRC6B	1.287398	down	0.02516231
FBXL20	1.2782476	up	0.043904882
CNN2	1.2772377	down	0.045620862
TMEM131	1.2741445	up	0.034981884
NDUFS3	1.2740364	down	0.049490392
F12	1.2736617	down	0.043904882
UBAP1	1.2734244	up	0.039582886
KRT18	1.2674093	up	0.01914735
C16orf72	1.2638713	up	0.04705363
FOXRED1	1.2572327	down	0.040804602
MKI67IP	1.247975	up	0.035969965
SS18L2	1.2477217	down	0.043904882
C10orf116	1.2438484	up	0.04143007
STMN1	1.2424924	down	0.04166845
CCNH	1.2417604	up	0.040577903
CALHM2	1.2293093	up	0.01914735
C8orf33	1.2162672	up	0.01914735

Table A1.2 TIC10-induced changes that occur at 18 and 48 hours.

Symbol	Fold change (18 hr)	Direction of change (18 hr)	Corrected p-value (18 hr)	Fold change (48 hr)	Direction of change (48 hr)	Corrected p-value (48 hr)
SESN2	11.819792	up	0.023033692	5.85784	up	0.019069718
PCK2	9.12146	up	0.015136981	4.832417	up	0.014007526
BEGAIN	8.528189	up	0.019491911	6.289588	up	0.0437373
IL20RB	7.5523267	up	0.013276912	7.994223	up	0.008422944
DDIT3	7.410269	up	0.011017979	6.3575916	up	0.046669953
UPP1	7.4030914	up	0.019147335	15.519281	up	0.006875412
PCK2	7.2715816	up	0.009730678	3.3627062	up	0.024277335
MIR1974	6.9898806	up	0.009730678	14.479351	up	0.017613085
TRIB3	5.6356206	up	0.020556552	5.0162215	up	0.009082349
TSC22D3	5.4871993	up	0.013630901	1.7840397	up	0.04959872
SLC6A9	5.3645306	up	0.011017979	6.124898	up	0.013490164
ASNS	5.0690565	up	0.016703121	5.9591856	up	0.010108237
ASNS	4.8894877	up	0.043260563	6.38537	up	0.02737664
OR2A9P	4.389211	up	0.034763664	6.166382	up	0.009282365
TSC22D3	4.1785417	up	0.035969965	2.2149007	up	0.03343619
SUNC1	4.0198045	up	0.011017979	7.436066	up	0.009637909
GDF15	3.8177516	up	0.015890285	2.7162862	up	0.006875412
ATF3	3.7389376	up	0.013630901	4.5627646	up	0.016343728
SERPINE1	3.5904937	up	0.037542334	4.3190026	up	0.046277195
DDIT4	3.556292	up	0.004370419	5.3310637	up	0.010494264
RBCK1	3.3280146	up	0.013766917	4.5174375	up	0.009637909
ADM2	3.3132143	up	0.046225774	3.2425497	up	0.006875412
FGF19	3.296934	up	0.034806404	4.52479	up	0.029269956
SLC3A2	3.296031	up	0.0258185	2.1448486	up	0.02245333

			29			
LAMB3	2.96298	up	0.0191473 5	6.7913866	up	0.009082349
SERPINB 8	2.9558315	up	0.0132769 12	3.1991768	up	0.048220243
MYB	2.954644	down	0.0312813 4	9.934199	down	0.028245559
MOCOS	2.8860984	up	0.0110179 79	2.904689	up	0.017037364
LAT2	2.8307748	up	0.0453497 06	5.394362	up	0.019069718
TNFRSF 10B	2.8061705	up	0.0337752 7	2.9231594	up	0.04085896
GPR56	2.7960327	up	0.0173649 6	1.6894411	up	0.012055384
MAP1LC 3B	2.7872233	up	0.0256566 48	2.5377803	up	0.010975787
PPP1R15 A	2.7776794	up	0.0124213 62	3.3632076	up	0.02000229
LOC6441 00	2.7344277	up	0.0208829 03	1.5932164	up	0.04671367
MXD1	2.7020228	up	0.0268950 31	6.237349	up	0.041504502
STC2	2.6722522	up	0.0260177 85	3.8782978	up	0.019293752
BTG1	2.5891666	up	0.0415099	3.2664702	up	0.031236254
IFFO1	2.5648751	up	0.0136309 01	5.4991302	up	0.028620897
GADD45 A	2.521268	up	0.0020158 49	2.915081	up	0.009637909
CEBPG	2.4901845	up	0.0181588 75	2.8173778	up	0.039217066
IRF2BP2	2.387892	up	0.0458226 9	2.7528107	up	0.028689677
LOC3898 16	2.3747094	down	0.0340977 76	7.4285874	down	0.008422944
MGC399 00	2.3426023	down	0.0359699 65	46.10521	down	0.009082349
WDR45	2.334724	up	0.0020158 49	3.0526786	up	0.037460446
HERPUD 1	2.3304486	up	0.0151369 81	2.8943672	up	0.021350387
MGC399 00	2.3293552	down	0.0191473 5	27.370665	down	0.010320948
KCNG1	2.3217037	up	0.0183105 67	2.192606	up	0.021902733
GADD45 B	2.3041892	up	0.0167395 96	2.4565637	up	0.013956664
DUSP5	2.3010147	up	0.0110179 79	5.689019	up	0.02172359
HERPUD 1	2.2780652	up	0.0353873 93	3.3228686	up	0.029931428

MCM4	2.2435672	down	0.002015849	4.560677	down	0.009082349
CYP4F11	2.2395053	up	0.004370419	2.5944374	up	0.013018658
TMSB15A	2.2045834	down	0.023033692	33.989494	down	0.009082349
HBEGF	2.1940482	up	0.0427416	3.5346715	up	0.031252235
GARS	2.1923409	up	0.040804427	2.1795294	up	0.037335012
FEN1	2.1898549	down	0.0415099	7.0433836	down	0.01970352
SRXN1	2.1729677	up	0.012894535	2.9000022	up	0.04029018
AXIN2	2.171488	down	0.01914735	5.7443695	down	0.010494264
ARHGEF2	2.1660032	up	0.009730678	3.0829825	up	0.021209413
GINS2	2.153951	down	0.03377527	9.536368	down	0.011621549
JUN	2.1348608	up	0.02516231	2.9465241	up	0.03648406
FTH1	2.0999665	up	0.015890285	2.205528	up	0.045399822
PABPC1L	2.0856695	up	0.035969965	4.142922	up	0.017658098
TUBA4A	2.0830116	down	0.046364475	2.4606605	down	0.049851265
AXL	2.076982	up	0.047943338	3.9583647	up	0.012673016
SERPINB1	2.0723882	up	0.03377527	2.8195195	up	0.018760737
PLAU	2.0501742	up	0.020149391	3.6245394	up	0.02330884
CACYBP	2.0180218	down	0.035969965	4.067813	down	0.008422944
CDCP1	2.0178082	up	0.020556552	2.5135884	up	0.020999888
C6orf48	1.9998101	up	0.018362569	3.0774543	up	0.044947993
DDX46	1.9714651	down	0.042370286	5.5628347	down	0.020818258
HSPA1B	1.9080081	down	0.043260563	4.0661254	down	0.009082349
KCNS3	1.9051995	down	0.042197973	4.533024	down	0.01739141
FHL2	1.9047492	up	0.030091554	3.5383282	up	0.015292713
CHRNA5	1.8925257	down	0.026895031	5.2328634	down	0.010320948
SHPK	1.8831948	down	0.020556552	4.5155196	down	0.018237824
JPH2	1.87579	up	0.041335218	3.1295772	up	0.035261743

SDF2L1	1.8671106	down	0.02516231	1.9737438	down	0.043860547
NFIL3	1.8632436	up	0.04531118	2.9946795	up	0.023780325
DHCR24	1.8471593	down	0.02516231	3.794173	down	0.01739141
ELL2	1.8428729	up	0.047991898	2.0854042	up	0.02484479
GOLT1A	1.8420486	up	0.011017979	3.6333747	up	0.011907834
LETMD1	1.8409784	up	0.029162576	3.0706787	up	0.044628672
BRI3BP	1.8380828	down	0.035969965	2.954526	down	0.03469577
LOC644877	1.8343229	down	0.044718616	5.3968477	down	0.013536799
MTE	1.8257971	up	0.03372931	2.5802236	up	0.029269956
WIPI1	1.8093309	up	0.02055652	2.1866047	up	0.019069718
PTPRM	1.7988014	up	0.03426985	2.959382	up	0.022564188
SH3KBP1	1.7915754	up	0.029345037	2.2837772	up	0.049368307
FOXRED2	1.7697657	down	0.004370419	4.7976832	down	0.023234107
RBM35A	1.7588271	up	0.025818529	2.2318382	up	0.028689677
KRT15	1.7535143	up	0.015890285	2.9456031	up	0.027835343
LHX2	1.7372339	down	0.03377527	6.1057386	down	0.01979206
RGMA	1.7255824	down	0.035969965	2.7792342	down	0.02483875
WNT3A	1.7084576	down	0.015136981	3.7459834	down	0.010494264
EXOSC9	1.6995902	down	0.035969965	2.3549697	down	0.018415125
MLKL	1.6928365	down	0.034011453	2.6070924	down	0.034152403
SKP2	1.6798143	down	0.046364475	6.201134	down	0.011175673
MCM6	1.6751058	down	0.036976308	4.515005	down	0.0293418
HSPA14	1.6679413	down	0.020397097	2.4655054	down	0.03239546
C16orf57	1.6609529	down	0.043904882	2.3285222	down	0.013623286
DENND5B	1.6467699	down	0.043260563	3.0113428	down	0.025281847
ISCU	1.6310554	up	0.03377527	2.0759463	up	0.019925347
MCM3	1.5997593	down	0.015890285	4.7376986	down	0.036083378

MAPK1	1.5989597	down	0.0385724	1.6372826	down	0.033621464
C19orf33	1.5845016	up	0.039582886	2.9641342	up	0.009637909
KPNA2	1.5718057	down	0.02055652	5.1316524	down	0.009637909
VEGFB	1.5688016	down	0.02516231	1.6781598	down	0.040961143
HBE1	1.5623577	up	0.020882903	1.7742529	up	0.04189587
CAPRIN2	1.5605733	up	0.048921436	3.5148416	up	0.027339572
AGPAT9	1.5551192	up	0.0385724	2.5523818	up	0.02000229
IRF2BP2	1.5423459	up	0.04166845	2.382568	up	0.023199093
SOX18	1.5361217	down	0.046364475	3.5983922	down	0.014546686
PDK3	1.5346462	down	0.039582886	4.000597	down	0.006875412
FTHL12	1.5322818	up	0.043904882	1.6962612	up	0.028919566
CXXC5	1.5229149	down	0.0415099	2.1759	down	0.023516852
PALM	1.5123409	down	0.034122363	1.8638031	down	0.019069718
HNRPR	1.5016694	down	0.03592511	2.3435025	down	0.03302884
MNX1	1.5010701	down	0.039582886	3.2384956	down	0.010320948
EBP	1.4891913	down	0.037232377	3.0118616	down	0.03704989
SESTD1	1.4801818	down	0.043260563	1.8491256	down	0.037892688
OR51B4	1.4797486	up	0.013276912	2.2153027	up	0.042767514
ZFAND2B	1.4774361	up	0.04166845	2.6522803	up	0.035803158
HOXB5	1.4752026	down	0.03832007	1.4037037	down	0.034659225
TIMP1	1.4701642	up	0.040804602	1.7006038	up	0.019676114
PLK4	1.4559085	down	0.019147335	2.9407966	down	0.035803158
RFC5	1.4477861	down	0.029864009	3.5814073	down	0.030800033
FBXL6	1.4369808	down	0.043904882	1.5586385	down	0.03550055
EIF1	1.4366524	up	0.035969965	1.9157197	up	0.035803158
THOC4	1.4345134	down	0.035969965	2.03639	down	0.027054867
POLE3	1.4310231	down	0.03754234	1.8999945	down	0.04700748
HINT3	1.4115971	up	0.0416684	2.188101	up	0.04526477

			5			
CHAF1B	1.4074318	down	0.03754234	5.3974214	down	0.034900032
ATP6V0E2	1.4064207	down	0.03372931	1.6914942	down	0.038681243
FKBP11	1.3944719	down	0.03377527	2.1215975	down	0.02172359
SLC30A3	1.3893262	down	0.015890285	1.8657	down	0.031863093
HSPE1	1.3826358	down	0.040804602	2.1072977	down	0.048814435
ZBED1	1.3727813	down	0.039074127	3.144089	down	0.036608156
SBK1	1.3684316	down	0.047705967	1.9522434	down	0.040106535
AP1B1	1.3552212	down	0.048921436	1.9763128	down	0.02149589
FSD1	1.3415892	down	0.035969965	11.134916	down	0.04572148
AURKA	1.3264245	down	0.03377527	6.139144	down	0.009637909
LQK1	1.3059943	down	0.046903133	2.4335284	down	0.034964904
PXMP2	1.3001416	down	0.047991898	2.7315168	down	0.01220171
LOC401115	1.295779	down	0.04681878	1.8712622	down	0.03828878
LOC283953	1.2954808	up	0.046364475	1.6647888	up	0.026660295
AOF2	1.2897426	down	0.039074127	2.2657194	down	0.04863222
LOC285074	1.2809885	up	0.02516231	1.9150605	up	0.04572148
RPLP0	1.2571274	up	0.043904882	1.8747282	up	0.010948853
C15orf23	1.2525215	down	0.046364475	3.4935677	down	0.02172359

Table A1.3 TIC10-induced changes that occur at 48 but not 18 hours.

Symbol	Fold change (48 hr)	Direction of change (48 hr)	Corrected p-value (48 hr)
KRT81	22.87212	up	0.031330235
SPRR2D	20.364887	up	0.011803946
LOC644350	17.00929	up	0.013623286
PDE4B	15.559404	down	0.04863222
CHAC1	13.896631	up	0.032282915
KITLG	13.712438	down	0.040961143
DUT	13.518569	down	0.03166666
WNT16	13.495952	down	0.029269956
NASP	13.279105	down	0.020884402
KITLG	13.210174	down	0.039560787
EPN3	12.114876	down	0.020786807
SYTL2	12.064288	down	0.015676063
OAS3	11.712095	down	0.017849304
E2F2	10.880897	down	0.019979259
LOC728285	10.840668	up	0.019676114
CCNE2	10.770494	down	0.009637909
SCARA3	10.474275	down	0.013284133
KIF20A	10.363674	down	0.005355649
MUM1L1	9.766091	down	0.009082349
GLDC	9.538173	down	0.010494264
CENPI	9.49716	down	0.006875412
LMNB1	9.3915205	down	0.001415815
ASF1B	9.102031	down	0.02845703
OVOL2	9.011101	down	0.033800293
SPC25	8.890372	down	0.011175673
ERCC6L	8.85409	down	0.019112604
TRIOBP	8.815069	down	0.008422944
LOC643031	8.438131	up	0.042351622
FAM83D	8.312255	down	0.013383459
SLC22A15	8.255252	up	0.011299649
ACBD7	8.246232	down	0.009082349
FGD6	8.156124	up	0.019676114
FAM64A	7.8254695	down	0.012055384
HMGB3	7.775924	down	0.02084703

CDC25C	7.6466446	down	0.020786807
KIF11	7.63171	down	0.011175673
DPYSL4	7.557704	down	0.024277335
BIRC5	7.555325	down	0.009637909
LRRC26	7.466722	down	0.005355649
PSRC1	7.404295	down	0.014698844
FAM110C	7.3803325	up	0.035745442
MCM10	7.3715243	down	0.048089013
PSRC1	7.304031	down	0.026639156
C14orf106	7.25503	down	0.038681243
PLK1	7.2176604	down	0.02015493
GMNN	7.176904	down	0.02172359
FEN1	7.1521206	down	0.010108237
KIF11	7.0250816	down	0.01403898
STMN1	6.7894835	down	0.012480085
CDCA1	6.7659674	down	0.038666554
DLGAP5	6.6393757	down	0.011155665
EXO1	6.628085	down	0.028030183
ELOVL3	6.559566	down	0.011401887
TMPO	6.5349975	down	0.02149589
AURKA	6.5040994	down	0.009082349
GPR162	6.5033436	down	0.009082349
GAS2L3	6.4982243	down	0.040173456
SPC25	6.4783406	down	0.021489922
ETS1	6.475164	up	0.018952347
CENPM	6.433197	down	0.037676003
ZWINT	6.31953	down	0.009637909
EXO1	6.3011165	down	0.013018658
NUDT1	6.2899933	down	0.03735992
KCNMB4	6.2493415	down	0.029155023
CDC25C	6.2168417	down	0.001415815
DLGAP5	6.1732335	down	0.011621549
CENPA	6.1197023	down	0.005355649
SHMT1	6.0678115	down	0.011859206
TNFAIP8L1	6.0572195	down	0.038865466
NEIL3	6.0508375	down	0.011175673
CCNB1	6.0448055	down	0.015017457
RRM2	6.004174	down	0.009282365

RDM1	6.0035253	down	0.013623286
CCNF	5.9901285	down	0.010494264
DLEU2	5.9863257	down	0.01539818
NDRG4	5.904548	down	0.011153566
POLA1	5.892396	down	0.032528717
RACGAP1	5.841873	down	0.029243037
AURKB	5.8355775	down	0.022848561
KIFC1	5.7849426	down	0.001415815
TK1	5.7416725	down	0.022310423
KIF23	5.7285833	down	0.02084703
KIF18A	5.632663	down	0.037592698
LAT2	5.626406	up	0.01634601
BUB3	5.55705	down	0.046907336
CDCA8	5.5439386	down	0.015017457
PBK	5.5204873	down	0.027295636
CRABP2	5.4847765	down	0.048815902
ERCC6L	5.469881	down	0.026067587
NMU	5.427126	down	0.009637909
CDC45L	5.4190116	down	0.030849408
CTSL2	5.4095516	down	0.001415815
CDCA2	5.3990536	down	0.01739141
NUDT6	5.3896294	down	0.009637909
CDCA3	5.347088	down	0.011175673
C6orf173	5.337447	down	0.02124337
REEP1	5.336049	down	0.009082349
HELLS	5.3230834	down	0.037041813
ZWINT	5.317235	down	0.01539818
CCNA2	5.29894	down	0.009637909
RHBDL3	5.2750874	down	0.009082349
UHRF1	5.139834	down	0.037676003
KIAA0101	5.1377764	down	0.02094271
CENPF	5.0995736	down	0.019069718
RAB26	5.092979	down	0.027581686
IRX3	5.0789595	down	0.008422944
KIF4A	5.0721436	down	0.048220243
SGOL2	5.0188484	down	0.02172359
DEPDC1B	4.9824233	down	0.016343728
HES2	4.9699864	down	0.04393202

CENPM	4.940828	down	0.03343619
C9orf116	4.919287	down	0.037592698
MYD88	4.9079204	down	0.019118873
CENPE	4.906756	down	0.013199668
GTSE1	4.899883	down	0.009082349
C6orf48	4.8808703	up	0.025907174
KIF20B	4.8604856	down	0.009082349
FAM111A	4.8383613	down	0.001946386
KIF2C	4.812601	down	0.014965564
LOC100132715	4.8096275	down	0.02483875
LOC642458	4.80832	down	0.015017457
SPC24	4.7974977	down	0.010320948
UBE2T	4.7957363	down	0.019502776
HNRNPA1	4.78581	down	0.01888759
BUB1	4.7817197	down	0.010494264
MCM10	4.771218	down	0.048815902
CCNB2	4.770637	down	0.004092405
TYMS	4.748552	down	0.026067587
RAD54B	4.7445145	down	0.02315677
CBR4	4.7408314	down	0.021557467
CCDC18	4.664032	down	0.020105906
HJURP	4.663956	down	0.028689677
UBE2L6	4.6557636	down	0.019676114
MATN2	4.646336	down	0.0256847
RACGAP1	4.6359878	down	0.018049316
SLC2A6	4.633281	down	0.015232953
CENPO	4.621668	down	0.039560787
CDC2	4.591013	down	0.03507711
CEP78	4.5884104	down	0.02219234
PLEC1	4.580634	up	0.010494264
TACC3	4.5760083	down	0.03729315
ACAT2	4.5652003	down	0.020616097
RAD51AP1	4.533677	down	0.02000229
NEURL1B	4.5141263	down	0.019069718
GCA	4.513552	down	0.009637909
LOC400750	4.511523	up	0.043520328
AGPAT4	4.5046287	up	0.01765344
HMMR	4.5022225	down	0.011459867

RBCK1	4.497043	up	0.009282365
PARP12	4.4935718	down	0.03648406
LOC100128007	4.47767	down	0.01970352
MARCKSL1	4.468236	down	0.04703808
H3F3B	4.4668083	down	0.028689677
PARM1	4.465968	down	0.039991904
MCM7	4.4410844	down	0.020818258
ENPP1	4.438927	down	0.03475651
DNAJB9	4.4387183	up	0.013845812
C1orf112	4.4327664	down	0.012480085
GINS3	4.42987	down	0.03704989
RBMS2	4.3906484	up	0.022892712
KIF14	4.3718767	down	0.030929556
PITX2	4.3705945	down	0.03510957
MXD3	4.3543115	down	0.029269956
STX1A	4.3463745	up	0.042888787
CD47	4.3413696	down	0.027504178
PACSIN1	4.3391404	down	0.014711096
CBX2	4.3391232	down	0.023166766
POLE2	4.3360443	down	0.046907336
CDC2	4.3216915	down	0.028785033
MT1X	4.3185945	up	0.015757278
FANCL	4.3055544	down	0.031866338
ORC6L	4.3038898	down	0.01739141
SGOL1	4.3006773	down	0.019069718
CDCA5	4.2843122	down	0.019594423
CCDC34	4.2837777	down	0.046669953
FBXO5	4.2822437	down	0.010494264
CKAP2	4.238105	down	0.011299649
NCAPG	4.2282734	down	0.028197957
ANLN	4.1818213	down	0.018512405
BRCA1	4.1777787	down	0.04029018
HYLS1	4.1775956	down	0.013623286
NEK2	4.1753235	down	0.010494264
WDR54	4.170082	down	0.01855878
HNRPDL	4.162792	down	0.03686227
CDCA7	4.1429157	down	0.046559807
SGOL1	4.1425056	down	0.015017457

FAM111A	4.141056	down	0.009637909
HNRNPM	4.140647	down	0.028785033
DEPDC1	4.1376324	down	0.04648964
RFC3	4.1326513	down	0.048089013
PTTG3P	4.0963674	down	0.012480085
ALDOC	4.0802355	down	0.021112772
CA2	4.077626	down	0.04201881
SKP2	4.047142	down	0.034872416
MGC40489	4.0452466	down	0.02483875
CD24	4.017256	down	0.043520328
SNN	4.0092673	down	0.009637909
PCNA	4.0073233	down	0.0332967
PRC1	4.0032325	down	0.012673016
HERC6	3.997227	down	0.025628919
CYB5B	3.9949327	down	0.018563876
C17orf97	3.9880593	down	0.019069718
NUSAP1	3.9862816	down	0.022564188
MELK	3.9852543	down	0.009082349
POLR3H	3.980437	down	0.02488853
RBM14	3.971714	down	0.04572148
HMMR	3.963014	down	0.017037364
PHLDA1	3.9527283	down	0.018850883
NDC80	3.9501443	down	0.026832432
HSPA13	3.9345326	up	0.020781957
ASRGL1	3.9328437	down	0.015468261
FZD4	3.9322994	down	0.024964584
FGFR3	3.9094398	down	0.014711096
CCDC99	3.9052114	down	0.019069718
IFI30	3.9048216	down	0.023196464
DEPDC1B	3.9041016	down	0.032282915
RBBP9	3.9000237	down	0.04755203
CDCA4	3.887337	down	0.04526477
CENPE	3.887026	down	0.013490164
SH3PXD2A	3.8855195	down	0.04648964
CPA4	3.8793988	up	0.009637909
RFC3	3.8566208	down	0.014711096
LOC100134134	3.8513467	down	0.01539818
LOC645726	3.8433201	down	0.032760013

PTTG1	3.8410702	down	0.011808776
HSH2D	3.8332627	down	0.01739141
DPYSL2	3.8260615	down	0.048866253
STIL	3.8210115	down	0.013276903
EME1	3.8202705	down	0.043860547
UNC5A	3.8127027	down	0.010494264
EFCAB4A	3.8048882	up	0.010108237
ISL1	3.8047178	down	0.009082349
FAM54A	3.8043194	down	0.029269956
LOC644124	3.7998812	down	0.035803158
MYBL1	3.7910256	down	0.033783652
RP2	3.7896633	down	0.03236323
KLHDC8B	3.7868638	down	0.02149589
C4orf33	3.7797513	down	0.048089013
PTTG1	3.7756996	down	0.009282365
LOC644150	3.7662976	up	0.014307831
LRRCC1	3.7488236	down	0.015445222
C16orf75	3.740168	down	0.049701784
CDT1	3.7399356	down	0.022848561
CKAP2L	3.7398145	down	0.00971984
KREMEN2	3.739478	down	0.029269956
RBBP4	3.7386875	down	0.04122609
SRI	3.7375934	down	0.044783186
TUBB2C	3.7355642	down	0.024964584
LOC728037	3.7274244	down	0.045280136
CENPA	3.7237263	down	0.001634129
HAUS8	3.7235696	down	0.037634652
SPAG5	3.7217443	down	0.035745442
MCM4	3.7176435	down	0.04915255
LOC729816	3.7057064	down	0.009082349
C15orf23	3.7038693	down	0.013536799
HNRPM	3.6866455	down	0.025281847
RNASE4	3.6794984	down	0.015232953
NUSAP1	3.676112	down	0.009282365
SDC4	3.6619465	up	0.015757278
NUDT18	3.661188	down	0.024277335
TMEM158	3.652971	up	0.041504502
CD68	3.642541	up	0.03354969

POLQ	3.6384122	down	0.024277335
CDKN3	3.6350853	down	0.015445222
SUV39H1	3.6176925	down	0.011175673
FAM72A	3.613847	down	0.031774323
C13orf34	3.6107843	down	0.028689677
BARD1	3.6092045	down	0.047984716
LOC653874	3.607259	down	0.030849408
ANKRD32	3.6036756	down	0.045905516
PAQR4	3.6035013	down	0.009637909
PCNXL2	3.600421	up	0.027041782
PYROXD1	3.5899117	up	0.049825776
CEP55	3.579297	down	0.014711096
TMEM14A	3.5748649	down	0.010108237
MICB	3.5682986	down	0.015017457
C13orf3	3.5656912	down	0.037944797
PGK1	3.562374	down	0.021018256
NEK2	3.5611677	down	0.011933
SPRY4	3.5595887	up	0.037335012
ZNF207	3.5574408	down	0.03239546
NDRG2	3.5564778	down	0.009082349
TCF7L2	3.5501168	down	0.045280136
UCA1	3.5494118	down	0.009082349
SORT1	3.5491068	down	0.024277335
CALM1	3.5483825	down	0.015017457
ACYP1	3.54442	down	0.011188068
TTK	3.543055	down	0.013623286
INCENP	3.5400562	down	0.04189587
TOP2A	3.5302217	down	0.028689677
TMEM19	3.5301304	down	0.04122609
CCDC34	3.512553	down	0.009637909
HIBCH	3.5112617	down	0.028532717
MIPEP	3.5091436	down	0.03497738
PSMC3IP	3.504071	down	0.039536465
GNA12	3.4916215	down	0.030929556
ATAD2	3.4891775	down	0.029155023
HPCAL4	3.4840522	down	0.045905516
LOC728069	3.4818	down	0.03893217
C10orf6	3.4797213	down	0.04122609

RILPL2	3.476999	down	0.020818258
RAD54L	3.4714081	down	0.048719645
PKMYT1	3.4531517	down	0.039217066
FHL2	3.4501648	up	0.018237824
HELLS	3.4411922	down	0.048075076
MASTL	3.439919	down	0.015065883
CD55	3.439779	up	0.026923697
SFRS7	3.4309611	down	0.0389214
KIF5C	3.429676	down	0.029269956
OIP5	3.4275894	down	0.036367454
TCEB2	3.4249864	down	0.033800293
DSCC1	3.4217265	down	0.032754973
OIP5	3.4169834	down	0.013536799
MGST2	3.4129136	down	0.025863012
NCAPG2	3.4111958	down	0.048909087
HIRIP3	3.4090297	down	0.03984006
WDR76	3.4080312	down	0.033621464
FBXO5	3.3992612	down	0.04189587
ASPM	3.3934994	down	0.04317722
CDC20	3.3808331	down	0.021350387
XPOT	3.3783824	up	0.04150014
HNRNPM	3.3716192	down	0.02124337
LOC100134530	3.35707	up	0.011046462
ECT2	3.3529403	down	0.03367808
CAPRIN2	3.352481	up	0.01828428
FAM195B	3.344682	up	0.011153566
LOC100133489	3.3443143	down	0.033800293
FAT1	3.3363414	down	0.014711096
STS-1	3.3298702	down	0.026706144
DLK2	3.3275895	down	0.024277335
CELSR2	3.318977	down	0.04360168
ID2	3.313955	down	0.026923697
EHHADH	3.3133967	down	0.043520328
CRYZ	3.3112588	down	0.047384284
C12orf48	3.3108082	down	0.023635108
LOC442727	3.3098009	down	0.019069718
MKX	3.3055725	up	0.04393202
SCD5	3.3049436	down	0.03984006

RAD51	3.3023434	down	0.04029018
CACNA2D2	3.2997856	down	0.021618756
C16orf59	3.2955656	down	0.017037364
HPSE	3.2883108	down	0.028689677
TMEM98	3.2862358	down	0.015676063
TUBB4Q	3.2766209	down	0.02149589
TUBA1A	3.2555857	down	0.013536799
ID2	3.2357852	down	0.009637909
SLC27A3	3.2256792	down	0.01539818
LOC649679	3.2232687	down	0.02626058
RHOF	3.2223847	up	0.04863814
CCND3	3.2148898	down	0.027339572
CEP78	3.2146413	down	0.04199974
HSPBL2	3.2138243	down	0.03239546
SMC2	3.2035306	down	0.022496616
PGAM4	3.2032897	down	0.01539818
SLC25A37	3.2009163	up	0.04172988
DPY19L1	3.2007232	down	0.023712968
CKS2	3.2002091	down	0.019069718
HNRNPC	3.1915262	down	0.040688314
MELK	3.1901002	down	0.028050097
APITD1	3.1822155	down	0.010494264
C14orf143	3.1799107	down	0.013383459
KNTC1	3.1770813	down	0.034067824
TRIM5	3.1683927	down	0.023166766
CENPL	3.163046	down	0.027728345
HMGB2	3.1623216	down	0.028689677
C9orf140	3.1615777	down	0.04534044
MCM7	3.1593392	down	0.033800293
C16orf33	3.1516464	down	0.030929556
SLC37A4	3.13561	down	0.021712786
SLC31A2	3.1221423	down	0.020105906
PFKFB4	3.1210818	down	0.035803158
ZNF480	3.119704	down	0.009082349
LOC100133012	3.109374	down	0.037676003
KIAA1524	3.1090415	down	0.031794265
SMC4	3.109021	down	0.04890672
C3orf31	3.1079314	down	0.042214286

BNIP1	3.1028907	up	0.047412697
FANCI	3.100701	down	0.03477001
HNRNPH2	3.1000047	down	0.037041813
LOC727848	3.0923474	up	0.01539818
LOC729298	3.0883057	down	0.027339572
LOC286016	3.0872667	down	0.02124337
CRISPLD2	3.0848513	down	0.016971381
SEPX1	3.073966	down	0.008422944
TUBGCP5	3.0710745	down	0.018850883
B3GNT1	3.0690162	down	0.03327353
CCDC77	3.0682442	down	0.011299649
CDAN1	3.0673432	down	0.019293752
FAM178A	3.0498574	down	0.037460446
BCAP29	3.048951	down	0.017393887
DPYSL3	3.0364485	down	0.035004396
YWHAB	3.035052	down	0.017927684
LIN54	3.0324829	down	0.03166666
SMC2	3.0317595	down	0.031863093
P704P	3.0305374	up	0.011859206
LOC100132112	3.0297573	up	0.011175673
MYOM2	3.0195127	down	0.045986656
METTL13	3.0168867	down	0.037892688
TTLL3	3.0134888	up	0.034964904
FTHL3	3.0121117	up	0.02993696
C11orf82	3.009817	down	0.030572256
COMMD4	3.007248	down	0.032760013
C5orf34	3.0067594	down	0.028689677
CCDC136	2.995271	down	0.042351622
PSMC3IP	2.9945176	down	0.03239546
IL11RA	2.9911304	down	0.025628919
FZD2	2.989978	down	0.020818258
LOC441019	2.9842482	up	0.030621788
DYNLL1	2.9824443	down	0.029931428
C9orf40	2.9782815	down	0.035698585
ANG	2.975779	down	0.016343728
SFRS6	2.9749725	down	0.04410758
C14orf80	2.9690497	down	0.028614627
CRIP1	2.9618313	down	0.037460446

CDK5	2.9599915	down	0.028689677
ENO2	2.9534712	down	0.011046462
LOC645430	2.9495406	up	0.02172359
DNAJA1	2.9494371	down	0.019069718
PIM2	2.9444952	down	0.02172359
TOPBP1	2.9427814	down	0.019069718
LOC653820	2.9413242	down	0.042351622
CHEK1	2.9242191	down	0.040106535
HSBP1	2.9192536	down	0.036083378
LAMC2	2.9175026	up	0.046559807
TNFRSF10B	2.9140403	up	0.034964904
TRA2A	2.9135418	down	0.029155023
TPM4	2.909412	up	0.049701784
TST	2.908785	down	0.031863093
CHSY3	2.9025369	down	0.008422944
HSPH1	2.8990865	down	0.04572148
NCAPD2	2.8966422	down	0.04661127
OR7E156P	2.8924937	up	0.035803158
VASH1	2.891771	down	0.038008302
LOC732007	2.8914173	down	0.011299649
LOC100134304	2.8889635	down	0.044505358
ST3GAL5	2.8851223	down	0.013284133
CLCC1	2.8849442	down	0.025361717
ID3	2.884441	down	0.022213638
SUOX	2.8810081	down	0.013956664
WDR51A	2.871488	down	0.023618625
TTLL3	2.8569467	up	0.024226021
PDGFRL	2.8559062	down	0.027256878
MSX1	2.8526742	down	0.025628919
LOC730284	2.8526366	up	0.027728345
C18orf54	2.8478231	down	0.019069718
SYTL4	2.8365095	down	0.016327243
TMEM50B	2.834119	down	0.015232953
NSBP1	2.8321507	down	0.036434762
LOC440043	2.8321135	down	0.01739141
TUBB	2.8316617	down	0.02149589
ZC3H4	2.8316422	down	0.028785033
RFWD3	2.8303266	down	0.015232953

LOC727848	2.8263502	up	0.037041813
VPS36	2.8247864	down	0.03735992
PHF19	2.823849	down	0.04201881
BRI3BP	2.8203974	down	0.0332967
PRDX2	2.8191094	down	0.009637909
MSH6	2.8175948	down	0.03704989
MYH10	2.8165193	down	0.024277335
PGAM1	2.8051245	down	0.012765218
DNAJC22	2.8043616	down	0.025412573
LOC728554	2.7910333	down	0.048075076
MAGEE1	2.7875392	down	0.02154171
MAP6D1	2.7852998	down	0.031774323
GPSM2	2.7820997	down	0.010948853
LOC653071	2.7796497	down	0.03648406
UBL5	2.7731595	down	0.030113384
RAB11A	2.7723866	down	0.01855878
TIMELESS	2.7712085	down	0.04552708
SPIN4	2.7642436	down	0.048075076
TRIM9	2.7621667	up	0.03787446
NMB	2.7555475	down	0.019889398
C17orf53	2.7549064	down	0.025662778
FASTKD5	2.7514584	down	0.02484479
SRGAP2	2.7477193	down	0.010494264
ACYP1	2.7377877	down	0.03704989
SSH2	2.7345333	down	0.009082349
CASP7	2.730084	down	0.02483875
LOC728975	2.7291954	up	0.026206655
LUZP1	2.7287505	down	0.018049316
CAMK2N1	2.7215588	up	0.04709403
DCUN1D3	2.7183058	down	0.025856461
ANKFY1	2.7167091	down	0.027835343
SNORD3A	2.7075815	up	0.0470869
RPA3	2.7063687	down	0.036434762
BCAR3	2.6989	up	0.03147083
HOXA5	2.6988916	down	0.038435854
ECE2	2.6945715	up	0.02149589
HRIHFB2122	2.6875632	down	0.036741998
ELK3	2.6833365	up	0.028689677

MTERF	2.6815927	down	0.048837963
CLDN23	2.6786895	down	0.017037364
ETS1	2.6785412	up	0.030572256
CPT2	2.6757777	down	0.009082349
SFRS5	2.671986	down	0.011621549
WDR79	2.670065	down	0.03704989
C11orf67	2.6698403	down	0.009637909
HMGCR	2.6664257	down	0.04057321
TROAP	2.6657176	down	0.014852929
AKAP12	2.6646588	up	0.046907336
HMGA2	2.6634648	down	0.046217654
AXL	2.6633112	up	0.037944123
ARAP2	2.6585877	up	0.019983377
TTC26	2.6565683	down	0.009637909
CRELD2	2.6538162	down	0.009282365
ST7	2.6474783	up	0.018512405
NDUFB6	2.6462922	down	0.027041782
RFC2	2.637395	down	0.031002449
HMGB2	2.635687	down	0.040984523
LOC93622	2.6325326	down	0.048508342
LMAN2L	2.6308708	down	0.027289473
FBXL2	2.6288323	down	0.030849408
C3orf21	2.627443	down	0.03562497
BCOR	2.6259348	down	0.020818258
SIVA	2.6202457	down	0.048089013
OR7E156P	2.6156414	up	0.019069718
LOC729101	2.6134353	down	0.032760013
WDR67	2.6101182	down	0.010108237
LOC728873	2.6089678	down	0.009637909
UBE2C	2.6023574	down	0.037892688
PPM1H	2.5987866	down	0.018563876
TMEM44	2.5980058	down	0.024756262
ARID5B	2.5951836	down	0.04863222
GALK1	2.5937145	down	0.011175673
NUP107	2.5934649	down	0.04526477
ENTPD3	2.592584	up	0.010494264
CSNK2A1P	2.5919604	up	0.028689677
HNRNPR	2.5899053	down	0.014307831

CARHSP1	2.5885742	down	0.014032008
COL7A1	2.587748	up	0.038873874
C1orf85	2.5834363	down	0.014308982
LARP6	2.5814035	up	0.027457168
PGAM4	2.5789425	down	0.011859206
GLIPR2	2.5762346	down	0.021712786
LOC727761	2.5727322	down	0.04234465
RNASE4	2.570997	down	0.023780325
DSN1	2.5704174	down	0.034064546
FXYD5	2.5702758	up	0.024277335
DCAF6	2.5689318	down	0.024277335
LOC653884	2.568462	down	0.019112604
SIVA	2.5632894	down	0.018389799
THOC3	2.5627053	down	0.033800293
LOC646993	2.5625517	down	0.037892688
PIM1	2.5610344	up	0.033128947
SRA1	2.5581427	down	0.034964904
SLC2A1	2.554747	down	0.023367506
ZWILCH	2.553166	down	0.037676003
TFAP2C	2.5512326	down	0.028007232
SLC9A3R1	2.550676	down	0.0262167
MCM8	2.5501223	down	0.03239546
EIF4EBP2	2.5500455	down	0.038022514
LRRC20	2.5414517	down	0.027835343
TRIM8	2.536754	up	0.013536799
VCP	2.5337343	down	0.04572148
FANCG	2.5332866	down	0.019069718
TMEM30A	2.5316613	down	0.009082349
UBE2C	2.52912	down	0.021112772
VAMP1	2.5271137	down	0.010320948
FAT1	2.526669	down	0.043520328
RAN	2.5225947	down	0.036815345
FRMD8	2.518517	down	0.019069718
FN3KRP	2.517292	down	0.009637909
PREI3	2.5134122	down	0.039287504
MOBKL3	2.506754	down	0.04080518
C3orf37	2.5035908	down	0.02615731
ALPK1	2.4971986	up	0.04986984

RRM1	2.4968355	down	0.02483875
IFRD1	2.4946222	up	0.04572148
IRX1	2.4937544	up	0.013311975
VASN	2.4917755	down	0.010494264
PAFAH1B1	2.4912255	down	0.009637909
EML1	2.490393	down	0.013623286
ARL6IP6	2.4828806	down	0.048075076
PRDX2	2.4787025	down	0.013956664
MALL	2.4761944	down	0.01337127
LOC387882	2.4715059	down	0.04168716
SLC25A14	2.469494	down	0.021350387
ZRANB2	2.4693487	down	0.04671367
SLC7A5	2.4658372	up	0.02483875
KIF15	2.4657977	down	0.045133196
CASP6	2.4634297	down	0.0291741
DNAJC9	2.4630656	down	0.01539818
ANG	2.460756	down	0.028425978
LOC646135	2.4578223	up	0.032420322
LOC100133600	2.4566765	up	0.028050097
GGH	2.4523826	down	0.0332967
LOC389386	2.4495063	down	0.010108237
FSTL1	2.4486938	down	0.009637909
PECR	2.4478743	down	0.029084174
TSGA14	2.4470835	down	0.033642087
PPIA	2.4447687	down	0.04307706
PDCL	2.444215	down	0.029166568
LLGL1	2.442108	down	0.04312602
ZDHHC13	2.4322915	down	0.034900032
DGCR11	2.4246979	up	0.028007232
KIAA1128	2.422853	up	0.029948562
PTP4A2	2.42155	down	0.04172988
TTC8	2.421174	down	0.042888787
HPS6	2.41799	down	0.01539818
THAP11	2.41664	down	0.038887545
DNMT1	2.4160693	down	0.035698585
GAMT	2.41501	down	0.03510957
HEYL	2.4148042	down	0.029319767
GOLGA6B	2.4116368	up	0.042340405

C3orf75	2.410935	down	0.043304022
REEP5	2.4082963	down	0.022525989
BCL2L12	2.4080884	down	0.013535026
TSPAN3	2.4078395	down	0.023755241
NSL1	2.4075866	down	0.04700748
CSTF3	2.4055622	down	0.033800293
CKS2	2.4050071	down	0.038199354
TFAP2C	2.4033628	down	0.015676063
LOC729708	2.4030635	down	0.035004396
LOC100128771	2.3971407	up	0.01539818
FAM46A	2.3959749	down	0.003363579
TUBB6	2.3948221	down	0.042351622
SKP1	2.391439	down	0.031863093
MID1	2.3876643	down	0.01473459
CTPS2	2.3843188	down	0.048815902
ZNF544	2.3842068	down	0.02149589
C17orf48	2.383193	up	0.026206655
NUP62CL	2.3821442	down	0.010494264
NEBL	2.380658	down	0.033128947
KDELR3	2.3790455	down	0.036434762
ARL6IP1	2.3755505	down	0.035803158
GEM	2.3753128	up	0.0359933
KATNAL1	2.3736618	down	0.040961143
SLC44A3	2.3729758	down	0.027041782
RNU1A3	2.37189	up	0.03302884
DEF8	2.3700402	down	0.027603064
LOC653226	2.367699	down	0.014307831
ISCA2	2.3659983	down	0.03343619
TRAPPC3	2.3624034	down	0.036434762
ARID3B	2.359981	up	0.020105906
ATP6V1E2	2.3594182	down	0.03239546
PPIL5	2.3585556	down	0.028050097
KIAA1618	2.357438	down	0.046277195
DNCL1	2.3574347	down	0.03735992
VGF	2.3571107	up	0.028197957
RHBDD1	2.3515217	up	0.04869699
NCRNA00094	2.3509653	down	0.021112772
LOC645609	2.3427892	up	0.014720959

PSMD5	2.342009	down	0.014965564
LOC654161	2.3415682	up	0.037592698
DIAPH3	2.338686	down	0.01855878
DHX9	2.3385954	down	0.025628919
LOC728969	2.3345785	down	0.011401887
PRKAB2	2.332961	up	0.045311127
ZDHHC13	2.330754	down	0.009282365
PLAUR	2.3292725	up	0.02483875
LRIG2	2.3249514	up	0.02488853
C2orf7	2.3207424	down	0.03735992
LMNA	2.3159363	down	0.023354659
HNRPA2B1	2.3140907	down	0.037892688
FAM190B	2.3138266	up	0.04572148
SIVA1	2.312023	down	0.029448941
RAB23	2.3080893	down	0.010297052
RTN4R	2.304563	down	0.022213638
LOC100132863	2.302821	down	0.035536382
LOC644422	2.298969	down	0.027835343
RPA1	2.2988896	down	0.04757001
LOC100134634	2.2967913	up	0.032038588
HSPB1	2.294966	down	0.013538596
PFDN2	2.2945962	up	0.03548969
LOC644101	2.2922812	down	0.035487957
UBE2N	2.2898746	down	0.044768553
LOC729021	2.2842572	up	0.04572148
GSDMD	2.2827885	down	0.048075076
SH3KBP1	2.279302	up	0.009282365
HSPA4	2.2782433	down	0.020980466
PABPC5	2.2767103	up	0.040888242
SFRS5	2.267842	down	0.009637909
KLHDC5	2.2668524	down	0.04862383
ALAD	2.2652564	down	0.02172359
TSPAN3	2.2639294	down	0.027314134
TUBG1	2.2618132	down	0.038681243
PHTF1	2.261665	down	0.045311127
MRPL35	2.2536952	down	0.04514841
ZSCAN12L1	2.2515748	up	0.04112573
FAM36A	2.249075	down	0.035803158

PKIB	2.2448933	down	0.035803158
PGK1	2.2426114	down	0.009082349
ANKRD19	2.2421842	up	0.028689677
ANGPTL4	2.235869	up	0.02483875
TMEM50A	2.234504	down	0.042351622
TUBG1	2.2343614	down	0.006875412
LOC731049	2.2339597	down	0.009082349
ZNF277	2.2335758	up	0.021031635
BUB3	2.231718	down	0.032432362
PCF11	2.2307165	down	0.04490722
HN1	2.2256875	down	0.03548492
RIOK3	2.222921	up	0.038666554
CASP2	2.220837	down	0.01539818
GLA	2.2199676	down	0.010494264
HLA-DRB4	2.2194254	down	0.03787446
DKK1	2.2190561	down	0.045311127
TMEM44	2.2175806	down	0.045100342
ZW10	2.2161803	down	0.03916896
XRCC6	2.2144647	down	0.04572148
C14orf145	2.211147	down	0.014434496
SGK3	2.2002015	down	0.034964904
CHEK2	2.198004	down	0.038062993
CASP6	2.1969285	down	0.035803158
BCL2L12	2.1960955	down	0.010667075
FARP1	2.1941738	down	0.04572148
NKX3-1	2.1937046	down	0.037676003
WWC3	2.191947	up	0.042468995
EXOSC9	2.190376	down	0.045371383
TMC4	2.1902497	up	0.011046462
ZFAND3	2.1838598	up	0.011498103
DBNL	2.1774035	down	0.04314927
ETV6	2.177263	down	0.019594423
PSME2	2.1763046	down	0.022892712
SFRS13A	2.1752353	down	0.04085896
RAB23	2.17381	down	0.03704989
SLC44A2	2.1724863	down	0.02172359
ATP5G1	2.1699808	down	0.03327353
UBE2G1	2.1683578	down	0.035698585

MAPKAP1	2.1665704	up	0.035803158
ADAM19	2.1661768	down	0.0262167
DEF8	2.1642501	down	0.048205905
C6orf211	2.161218	down	0.035004396
CSNK2A1P	2.1612003	up	0.022564188
FNTB	2.159334	down	0.035539363
TAF15	2.1502001	down	0.036608156
TMEM118	2.1499128	down	0.009082349
NDUFB6	2.1470752	down	0.025628919
ARS2	2.143208	down	0.040173456
PACSIN2	2.1422448	down	0.04085896
STRN	2.1399987	up	0.019069718
SLC19A2	2.1347253	up	0.019069718
RHOD	2.131293	up	0.01970352
NAPEPLD	2.1312628	down	0.043520328
OCEL1	2.13092	down	0.013536799
ZDHHC16	2.126818	down	0.018563876
OAT	2.1267176	down	0.029269956
CDC42EP1	2.1246893	up	0.047412697
REPS2	2.1233356	up	0.033783652
HES6	2.1211483	down	0.01220171
SNX22	2.1201005	up	0.022727408
PDXK	2.118017	down	0.018389799
TIMM22	2.1122322	down	0.038435854
C5orf37	2.1121442	down	0.048089013
BAG3	2.1117723	down	0.023386316
TPI1	2.111044	down	0.01403898
BBC3	2.1042447	up	0.023780325
ITGA3	2.1027858	up	0.027041782
PLAUR	2.1024036	up	0.011175673
SNRPB	2.1012537	down	0.010494264
ATP6V1H	2.1004486	down	0.043520328
TPI1	2.1002083	down	0.02172359
IFITM3	2.0987191	down	0.03628379
ZMYM5	2.0978823	up	0.013536799
SNIP1	2.0973802	down	0.04862383
TUBB3	2.0958116	down	0.038008302
MLPH	2.0948637	up	0.04648964

ENTPD4	2.0944068	up	0.010216381
TCEA1	2.0921814	up	0.030929556
ZFYVE26	2.087797	down	0.020377327
TSR2	2.0832922	down	0.009637909
DHRS7B	2.0823681	down	0.018072816
LOC728312	2.0762994	up	0.035803158
SKA2	2.073603	down	0.04258914
ITPRIP	2.0707595	up	0.04558073
FBXO32	2.0692408	up	0.015676063
LPAR5	2.0682282	down	0.033506017
LOC651149	2.0681663	up	0.03507711
ZNF35	2.0676754	down	0.04192966
MAT2B	2.0664136	down	0.038417604
CYB5D2	2.0642722	down	0.02087893
CBX5	2.0594923	down	0.01855878
KLHDC3	2.0590522	down	0.02294802
IFITM2	2.0587075	down	0.04890672
C22orf13	2.0554903	down	0.02149589
DBI	2.0521846	down	0.041504502
MGST3	2.0516443	down	0.014307831
SASH1	2.0434108	down	0.038681243
EDC4	2.040717	down	0.028050097
MFSD3	2.0400789	down	0.04460674
DYNLL2	2.0376124	down	0.018453302
SGK	2.0367715	down	0.04572148
FTHL2	2.032172	up	0.027835343
BAIAP2L1	2.0290031	up	0.041504502
CHRNB1	2.0283635	up	0.03302884
ATP1B3	2.025569	down	0.045623463
BLMH	2.0253823	down	0.04572148
PSMD10	2.0248005	down	0.013816972
TNIK	2.0239892	down	0.04189587
TAP2	2.0234947	down	0.048075076
SEMA6A	2.0221891	down	0.024458047
LOC440093	2.0218225	down	0.011175673
LOC644931	2.021412	up	0.029319767
UNC84B	2.019348	down	0.04172988
MDH1	2.0135365	down	0.04890672

ZSCAN2	2.013515	down	0.030118773
MRPL22	2.0129333	down	0.04572148
NUDT9	2.0094955	down	0.034736086
LOC729009	2.0079455	up	0.01220171
SLC2A4RG	2.0078657	down	0.013623286
PPHLN1	2.0073416	down	0.028689677
ALDH7A1	2.002995	down	0.036083378
PGRMC1	1.9963276	down	0.04149974
LOC148915	1.9961442	down	0.04234465
EFNA4	1.99493	down	0.019096363
PSME1	1.9928318	down	0.01177688
NCLN	1.99048	down	0.019676114
CHST7	1.9864012	down	0.029516006
LOC652481	1.9851632	down	0.046232376
HRK	1.9851315	up	0.01855878
TRIM68	1.9847863	down	0.010494264
IGSF3	1.983644	down	0.049429696
ATP5J2	1.9833268	down	0.046232376
ABCC5	1.9822242	down	0.047412697
PEX11A	1.9792893	down	0.023196464
DDX19A	1.9766625	down	0.04149974
SMAP2	1.9763136	down	0.034900032
LOC100133478	1.97512	up	0.035803158
CASP3	1.9748405	down	0.043922964
ASAP2	1.9712756	up	0.031774323
EML2	1.967289	up	0.019069718
SCPEP1	1.9661797	down	0.019069718
ELF1	1.9656851	down	0.019293752
RNF34	1.9648895	down	0.048220243
LOC729926	1.9643978	up	0.048075076
GEM	1.9630088	up	0.032760013
SC5DL	1.9610842	up	0.039613925
CLEC16A	1.9603151	down	0.024277335
LOC643387	1.9598637	down	0.039572667
DIAPH3	1.9592938	down	0.019237109
DERA	1.9589968	down	0.042767514
ADAR	1.9565771	down	0.032076553
KATNB1	1.9565588	down	0.039991904

H3F3A	1.9549757	down	0.024098575
CCDC85B	1.9528179	up	0.02484479
SGK1	1.9523624	down	0.038199354
ZNF185	1.950274	up	0.004092405
PSMC3	1.9475496	down	0.032282915
TSEN34	1.9454978	down	0.037592698
TUBA1C	1.944842	down	0.019069718
HDAC1	1.9447743	down	0.03608366
RNU1-5	1.9445789	up	0.028689677
RNU1-3	1.9426543	up	0.029448941
RPS6KA2	1.9369316	down	0.019069718
HMGCS1	1.9368217	down	0.034964904
ELL3	1.9361682	down	0.033621464
ADAR	1.9314932	down	0.030351898
SLC25A44	1.9303552	down	0.045399822
HSP90AA1	1.9300863	down	0.031863093
DPM2	1.9272642	up	0.04703808
PLOD1	1.9257163	down	0.01855878
RUSC1	1.9256564	down	0.042912345
SOD1	1.9251478	down	0.024163518
IFI27L1	1.9247444	down	0.037676003
PRDX4	1.9223267	down	0.045280136
GLCE	1.9220053	down	0.026637582
PSMA4	1.9218047	down	0.042421788
TECR	1.920321	down	0.02483875
CAST	1.9202244	up	0.03648406
CLDN15	1.9196409	up	0.031236254
GPR161	1.9190731	down	0.01855878
FLOT2	1.9178506	down	0.020818258
XYLT2	1.9157287	down	0.035803158
ABHD14A	1.9103876	down	0.033800293
EGLN2	1.9102005	down	0.03828878
KIAA0586	1.9100363	down	0.045886032
PHC2	1.9088957	up	0.018453302
HIATL1	1.9074413	down	0.014711096
SPA17	1.9050996	down	0.01739141
G3BP1	1.902162	down	0.0296058
VKORC1	1.8999367	down	0.009637909

C1orf25	1.8990179	down	0.034964904
PDE6D	1.897796	down	0.013284133
ATPIF1	1.8932486	down	0.005179285
MKNK2	1.8894386	up	0.04559176
UBE2L3	1.8875589	down	0.029084174
IDH3A	1.8839631	down	0.035487957
SLC25A4	1.8838784	down	0.041509036
CISD2	1.8836389	down	0.036608156
RIPK1	1.8824623	down	0.019049704
BMPR2	1.8790548	down	0.04890672
LOC440926	1.8740941	down	0.020055518
PREP	1.8737358	down	0.04700748
LOC653496	1.8737037	up	0.025082106
FXYD5	1.8714827	up	0.019069718
MEPCE	1.8698133	down	0.038724948
H3F3A	1.8637253	down	0.030929556
TEX264	1.8621624	down	0.028007232
WDR23	1.8592465	down	0.042351622
NAPRT1	1.8582858	down	0.045399822
CGGBP1	1.8579247	up	0.04572148
AMD1	1.8568666	down	0.036434762
ATP6V0D1	1.8539879	down	0.041891284
CNFN	1.8539863	down	0.04138328
ZYX	1.852298	up	0.031902928
SRP14	1.8513546	down	0.037190944
ISCU	1.8497925	up	0.03475651
PIN1	1.8469632	down	0.021618756
CACNB3	1.8456475	down	0.025628919
LOC100129086	1.8453916	down	0.03648406
CALM3	1.8416986	down	0.011175673
RAC2	1.8410966	up	0.02366577
CENPB	1.8409839	down	0.030929556
TOB1	1.8382611	down	0.018850883
LOC730455	1.837833	down	0.026923697
QDPR	1.8351489	down	0.040758733
OPLAH	1.8348721	up	0.019069718
FLJ22795	1.8317157	up	0.02580871
NDUFA2	1.8295574	down	0.04172988

RNU1G2	1.8288412	up	0.024277335
SLC16A3	1.8285453	down	0.006875412
GLIS3	1.8258412	up	0.019069718
CYB5A	1.824672	down	0.033363737
POLR2F	1.8236839	down	0.046669953
COL13A1	1.8227136	up	0.03916896
GBA	1.822089	down	0.032528717
KIAA1949	1.8189731	up	0.035803158
TMEM2	1.8182248	down	0.012765218
CCDC50	1.81404	up	0.04964428
UROS	1.8129905	down	0.03641784
POLR2A	1.8110342	down	0.025628919
MAP3K6	1.8083137	down	0.02617137
CTNS	1.8071579	down	0.045905516
SUV420H1	1.7995939	up	0.043520328
DCTN3	1.7970397	down	0.009637909
OCIAD2	1.7968637	up	0.013018658
PREI3	1.7961609	down	0.024277335
GNPTG	1.7946063	down	0.010320948
P2RY11	1.7942638	up	0.034964904
LOC650152	1.7932342	down	0.020055518
TRADD	1.7924784	down	0.027589478
NSMCE2	1.7917875	down	0.041504502
MDP1	1.7848517	down	0.04122609
ZNF280D	1.7847052	up	0.048089013
C1orf216	1.7832832	down	0.014965564
HMOX2	1.7829376	down	0.039649706
SIRPA	1.7759986	down	0.025361717
RWDD3	1.773068	down	0.025856461
LOC729082	1.7726059	down	0.014711096
WBP5	1.7724512	down	0.038824502
EFTUD1	1.7709858	up	0.046907336
STRADB	1.7709445	down	0.019293752
PMP22	1.7686049	down	0.04112573
TMEM185A	1.7674834	down	0.019069718
WFS1	1.765298	down	0.03953686
NIPSNAP3A	1.760197	down	0.041504502
ATG4A	1.7597799	down	0.02172359

LOC728640	1.7593037	down	0.033800293
LOC729774	1.7577783	up	0.012480085
PCNX	1.7560498	up	0.02172359
HPCAL1	1.7557108	up	0.02149589
LOC100133836	1.7540352	down	0.038008302
UBFD1	1.7535197	up	0.018279748
EEF1D	1.7474966	up	0.043665167
LDHA	1.7449604	down	0.031863093
LMNA	1.7432162	down	0.04149974
C7orf49	1.7429291	down	0.046559807
ATG4A	1.7429218	down	0.033800293
LOC390530	1.7423959	up	0.016408468
HIATL1	1.7405473	down	0.01739141
IMPDH1	1.7402518	down	0.044806257
C21orf70	1.7365458	up	0.013816972
PACSIN2	1.7362001	down	0.045399822
KIAA1715	1.7315495	down	0.04572148
PHYH	1.7300463	down	0.045311127
GSTM1	1.722758	down	0.028444633
SEC22C	1.717465	down	0.009282365
TNK2	1.7157543	up	0.02626058
FAM32A	1.7148389	down	0.02149589
C2orf44	1.7141751	down	0.028050097
LOC389386	1.7067255	down	0.04280589
FTSJD2	1.7043935	down	0.019069718
DIAPH3	1.7025119	down	0.04558073
C6orf85	1.7024462	down	0.04258914
NAAA	1.698816	down	0.037892688
BRMS1	1.6955105	down	0.034998596
NEDD8	1.692254	down	0.034964904
GTF2B	1.691369	down	0.0256847
TMEM159	1.6909148	up	0.04234465
ACTB	1.685421	up	0.046559807
FAM3A	1.6838074	up	0.038724948
TUBA1B	1.6823925	down	0.035803158
METTL14	1.6821189	down	0.02315677
LAMP2	1.6757674	down	0.028087284
KHDRBS3	1.6752328	up	0.034964904

CMTM6	1.6746193	down	0.03543404
GABARAPL1	1.673321	up	0.010494264
ECHS1	1.6726921	down	0.038681243
LYPD6B	1.6712608	up	0.042351622
LMO2	1.6712217	down	0.033363737
ETFB	1.6695048	down	0.02149589
UBE2G1	1.6693809	down	0.046907336
TMEM189	1.6670496	down	0.02483875
ZNF252	1.6632276	down	0.034964904
TAX1BP3	1.6610056	down	0.04700748
ABCB9	1.6587981	down	0.034073226
MXRA7	1.658485	down	0.02845703
BCAS4	1.6581538	down	0.04890672
LOC388564	1.658051	up	0.030849408
SNORA64	1.6577507	up	0.043304022
MAD2L1BP	1.6552869	down	0.026308447
ATP1B1	1.6541446	down	0.044947993
GAD1	1.6539686	down	0.02094271
PNRC2	1.6527961	down	0.018237824
VEZT	1.6502063	up	0.041891284
MSRA	1.646211	up	0.02124337
RQCD1	1.6448789	down	0.03681862
DECR2	1.6445986	down	0.04890672
NDUFB8	1.6441631	down	0.04757121
HMGN2	1.6437201	down	0.049524475
PPP1R14C	1.6436099	down	0.03327353
RPRC1	1.6432465	down	0.019983377
SLC25A4	1.6422108	down	0.04741928
NLRX1	1.641721	down	0.010494264
TGFA	1.6409804	up	0.038617827
LOC100130886	1.6376448	down	0.013623286
DDX19B	1.6360087	up	0.041422
MEF2D	1.624607	up	0.045311127
PAF1	1.6240042	down	0.04426554
CCDC24	1.6222067	down	0.048940428
MUL1	1.6185335	down	0.01539818
TBC1D7	1.6142925	down	0.039536465
CD83	1.6109163	down	0.019069718

TPRG1L	1.608728	down	0.010494264
LOC642741	1.6081612	up	0.048075076
ZNF689	1.6079979	down	0.016471576
ELP4	1.6074173	down	0.045280136
C1orf115	1.6056024	down	0.04189587
BMS1	1.6043997	down	0.022892712
CFL1	1.6040475	down	0.036571972
TMEM62	1.6038047	down	0.037892688
CASK	1.6011963	up	0.038008302
GNPTAB	1.5999289	down	0.041739967
PLEKHA9	1.5981113	down	0.036083378
FTHL8	1.5955532	up	0.020449188
CENTA1	1.5942328	up	0.034964904
COMMD5	1.5939044	down	0.042165942
GOLGA2	1.5899768	up	0.021618756
LOC100132795	1.5886334	up	0.04572148
CCDC102A	1.5863236	down	0.04122609
PDHB	1.5831347	down	0.033128947
LOC645683	1.581841	up	0.042892084
ATP6V1E1	1.5796431	down	0.029319767
TBC1D16	1.5787191	down	0.035261743
PPP1R11	1.5751987	up	0.013018658
LGMN	1.574408	down	0.023780325
FSCN1	1.5721909	down	0.019069718
RAB35	1.569938	down	0.009082349
LOC648390	1.5693458	down	0.01855878
VPS45	1.5667963	down	0.03079516
TUBA1C	1.5666658	down	0.021565048
RPS13	1.5656661	up	0.031863093
ALKBH5	1.5653794	down	0.037460446
HNRPK	1.565194	down	0.04062007
DHRS11	1.5639763	down	0.040106535
P4HA2	1.5597963	down	0.032420322
ARL5A	1.5580226	down	0.04558073
PABPC1	1.5570418	up	0.025980588
ZNF787	1.5561702	up	0.030113384
HEXB	1.5561432	down	0.02483875
C16orf61	1.5559562	down	0.048075076

H2AFZ	1.5531687	down	0.046158504
CDC42EP4	1.5473899	down	0.020003647
PKNOX1	1.5436722	down	0.021712786
EPDR1	1.5429212	down	0.04360388
KLF9	1.542067	up	0.04410758
ACADVL	1.5412841	up	0.019069718
RHBDD2	1.5397365	down	0.047412697
ACAA1	1.5385607	down	0.009282365
GPRC5C	1.5385214	down	0.013383459
SDHAF2	1.5351368	down	0.028689677
SLC20A2	1.5345851	up	0.026221393
LOC646463	1.5342712	up	0.010494264
INPP1	1.5339279	up	0.038762942
LAMP1	1.5339043	down	0.009637909
PHGDH	1.5303309	up	0.048814435
ERGIC1	1.5293468	down	0.023386316
UBIAD1	1.5237821	up	0.048220243
TPT1	1.5236621	up	0.009082349
PHRF1	1.5231704	down	0.048495024
PROS1	1.5167624	down	0.049254738
SEMA4F	1.5162967	down	0.046504095
LOC347544	1.5162748	up	0.04890672
PANX2	1.5139613	up	0.04779945
CSDA	1.508813	up	0.049368307
LDHA	1.5085973	down	0.02015493
RPL30	1.5084274	up	0.018674165
UPRT	1.5080874	down	0.034152403
H3F3A	1.5027332	down	0.027339572
PRPH	1.5022211	up	0.02172359
C20orf52	1.4999593	down	0.042351622
GBA2	1.4979966	up	0.029516006
TUBA1A	1.4933972	down	0.031565446
RPL17	1.4923319	up	0.041313168
ZGPAT	1.4895499	down	0.042912345
HSD17B4	1.4895364	down	0.043722387
ELOVL1	1.4836608	up	0.020105906
ALG9	1.4830817	down	0.04863814
PKP4	1.4825488	down	0.02766136

COBL	1.4820364	down	0.039610695
ECD	1.4788536	down	0.02253104
MORN2	1.4764404	down	0.04890672
LOC255783	1.476252	up	0.03704989
ASPSCR1	1.4718401	up	0.03477001
LOC643863	1.4677135	up	0.029516006
STX16	1.4670261	up	0.03475651
LOC441073	1.465301	up	0.030929556
GUSB	1.4643276	down	0.04149974
ELF4	1.4624544	up	0.023234107
CTGLF7	1.4564838	down	0.0470869
TAX1BP1	1.4522345	up	0.032282915
TAX1BP1	1.4510216	up	0.034872416
RANGAP1	1.4508991	down	0.033774253
LOC92755	1.4492096	down	0.04180456
BTBD6	1.4482794	down	0.037521012
PRNP	1.4452238	up	0.04572148
GANAB	1.4389031	down	0.036608156
MAP4K2	1.4388651	down	0.046504095
CXCL16	1.4374852	down	0.04572148
RNF121	1.4357687	down	0.025281847
PSAP	1.435669	up	0.03648406
LGMN	1.4257519	down	0.045986656
COMT	1.4231652	down	0.035803158
DGCR6	1.4203942	down	0.028689677
LRWD1	1.4167193	down	0.035803158
SLC29A4	1.4151039	down	0.013536799
GALT	1.41286	down	0.035425775
SH3GLB1	1.4049065	up	0.043520328
LOC92755	1.4047092	down	0.024277335
LOC284821	1.4040616	up	0.04572148
LOC649548	1.4038401	up	0.04741928
ARFGAP2	1.4032774	down	0.02172359
RALY	1.4016869	down	0.04360388
LOC653314	1.3994539	up	0.03885861
BCDIN3D	1.3974133	down	0.03641784
PSMC2	1.3968891	down	0.047412697
AVPI1	1.3893579	down	0.028050097

RPS5	1.3850408	up	0.026583182
LOC644039	1.3844177	up	0.046907336
LOC647276	1.3819826	up	0.029269956
DUSP22	1.3775834	down	0.046669953
LOC642250	1.3760663	up	0.046232376
ID1	1.3729534	down	0.018453302
NPC2	1.3708401	down	0.036627322
MPDU1	1.3695003	up	0.035698585
LOC648000	1.3685265	up	0.028572276
RPL3	1.3684282	up	0.034964904
TSPAN9	1.3628871	down	0.04481828
TCP11L1	1.3611637	up	0.028342376
INSIG2	1.3609029	down	0.048909087
LOC644464	1.3593427	up	0.046907336
LOC284230	1.3557851	up	0.025687447
RPL18A	1.3552552	up	0.028689677
RPL19	1.3542988	up	0.031330235
LOC728576	1.3495469	up	0.03302884
ZMAT2	1.348114	down	0.010320948
LOC100129141	1.3460437	up	0.008422944
RPS11	1.3447782	up	0.030929556
LOC389141	1.3445668	up	0.024631007
LOC728244	1.3414055	up	0.011299649
RPL24	1.3391696	up	0.01406658
RPS3A	1.3343464	up	0.015757278
FTHL7	1.3310994	up	0.016343728
RPS6	1.3301564	up	0.019983377
RPL9	1.3291724	up	0.020003647
LOC653162	1.3236942	up	0.027314134
LOC646294	1.3235198	up	0.013906971
LOC100133931	1.3197521	up	0.035487957
EEF1AL7	1.3143861	up	0.048075076
LOC374395	1.3142676	down	0.038008302
RPS15A	1.3134183	up	0.035261743
RPS27	1.312983	up	0.037460446
UBN1	1.3111799	down	0.02483875
LOC653888	1.3096539	down	0.03408292
CD63	1.3094215	down	0.03239546

CAP2	1.3072184	down	0.04479318
STAMBP	1.3066535	up	0.04757001
LOC391777	1.3058945	up	0.01970352
LOC286444	1.305658	up	0.012055384
RPL12	1.3037874	up	0.039560787
LOC648729	1.301176	up	0.037892688
LOC728517	1.2995949	up	0.020763682
RPSA	1.2981296	up	0.04572148
ELMO2	1.2964569	down	0.023234107
EEF1A1	1.2954857	up	0.02154171
IKBKG	1.2939274	down	0.029448941
NUP50	1.2894573	down	0.04699871
RPL11	1.2881604	up	0.033621464
LOC646294	1.2842408	up	0.045311127
PTPN1	1.2823339	down	0.02484479
SKAP2	1.2796323	down	0.035803158
LOC728553	1.2735767	up	0.02483875
RPLP1	1.2705739	up	0.011175673
LOC730754	1.2668962	up	0.035803158
LOC642755	1.2655188	down	0.046504095
DHX40	1.2649869	down	0.03354969
UBA52	1.2643192	up	0.028532717
LOC729402	1.2621671	up	0.040961143
LOC728937	1.2617986	up	0.04430744
SENP5	1.2579005	up	0.048089013
LOC100129553	1.2569504	up	0.024166062
RPS24	1.253881	up	0.042673428
RPL18A	1.2423534	up	0.031541027
RPL11	1.2410629	up	0.024631007
LOC645899	1.2372204	up	0.013383459
RNASEK	1.2300932	up	0.03426691
LOC644464	1.2106695	up	0.012480085
LOC100129158	1.2082447	up	0.04768977

Appendix 2 – Visualization and enrichment of live putative cancer stem cell populations following p53 inactivation or Bax deletion using non-toxic fluorescent dyes

RESEARCH PAPER

Cancer Biology & Therapy 8:22, 101-112; November 15, 2009; © 2009 Landes Bioscience

Visualization and enrichment of live putative cancer stem cell populations following p53 inactivation or Bax deletion using non-toxic fluorescent dyes

Joshua E. Allen,[1,2] Lori S. Hart,[1] David T. Dicker,[1] Wenge Wang[1] and Wafik S. El-Deiry[1,2,*]

[1]Laboratory of Molecular Oncology and Cell Cycle Regulation; Departments of Medicine (Hematology/Oncology), Genetics and Pharmacology; the Institute for Translational Medicine and Therapeutics; and the Abramson Comprehensive Cancer Center; University of Pennsylvania School of Medicine; Philadelphia, PA USA; [2]Biochemistry and Molecular Biophysics Graduate Group; University of Pennsylvania School of Medicine; Philadelphia, PA USA

Key words: cancer stem cells, p53, Hoechst 33342, Calcein AM, Bax, colon cancer, microscopy, flow cytometry, side population, calcein low population

Abbreviations: CSC, cancer stem cell; SP, side population; $C^{lo}P$, calcein low population; AML, acute myeloid leukemia; ALDH, aldehyde dehydrogenase; ABC, ATP binding cassette; MDR, multidrug resistance; FS, forward scatter; SS, side scatter; WT, wild-type; P-gp, P-glycoprotein

Putative cancer stem cell (CSC) populations efflux dyes such as Hoechst 33342 giving rise to side populations (SP) that can be analyzed or isolated by flow cytometry. However, Hoechst 33342 is highly toxic, more so to non-SP cells, and thus presents difficulties in interpreting in vivo studies where non-SP cells appear less tumorigenic than SP cells in immunodeficient mice. We searched for non-toxic dyes to circumvent this problem as well as to image these putative CSCs. We found that the fluorescent dye calcein, a product of intracellular Calcein AM cleavage, is effluxed by a small subpopulation, calcein low population ($C^{lo}P$). This population overlaps with SP and demonstrated long term cell viability, lack of cell stress and proliferation in several cancer cell lines when stained whereas Hoechst 33342 staining caused substantial apoptosis and ablated proliferation. We also found that the effluxed dye D-luciferin exhibits strong UV-fluorescence that can be imaged at cellular resolution and spatially overlaps with Calcein AM. In order to evaluate the hypothesis that p53 loss promotes enrichment of putative CSC populations we used Calcein AM, D-luciferin and Mitotracker Red FM as a counterstain to visualize dye-effluxing cells. Using fluorescence microscopy and flow cytometry we observed increased dye-effluxing populations in DLD-1 colon tumor cells with mutant p53 versus wild-type (WT) p53-expressing HCT116 cells. Deletion of the wild-type p53 or pro-apoptotic Bax genes induced the putative CSC populations in the HCT116 background to significant levels. Restoration of WT p53 in HCT116 $p53^{-/-}$ cells by an adenovirus vector eliminated the putative CSC populations whereas a control adenovirus vector, Ad-LacZ, maintained the putative CSC population. Our results suggest it is possible to image and quantitatively analyze putative CSC populations within the tumor microenvironment and that loss of pro-apoptotic and tumor suppressing genes such as Bax or p53 enrich such tumor-prone populations.

Introduction

The notion that cancer emanates from a small subpopulation of cells which possess the ability to self renew as well as differentiate was first suggested over 150 years ago.[1] Since then, empirical evidence has amassed to buttress this theory including the identification of a small subset of cells isolated from tumor tissues which contained a pronounced capacity to proliferate under in vivo conditions.[2,3] To explore the alternative explanation that all cancer cells simply have a low probability of clonogenicity, one study isolated cancer cells from acute myeloid leukemia (AML) tissue samples and sorted for populations expressing $CD34^+/CD38^-$, mammalian cell surface glycoproteins which are putative CSC markers found in AML.[4,5] The subpopulation possessing the aforementioned marker properties indeed possessed an exclusive and potent potential to transfer AML from humans to NOD/SCID mice.[6] Corroboration of the CSC theory has expanded to include animal models and other CSC markers such as CD133 (PROM1)[7] and $CD44^+/CD24^-$,[8] in brain and breast solid tumors, respectively. These attributions of self renewal and differentiation potential in conjunction with the manipulation of normal cellular regulatory processes give rise to a cogent putative mechanism of the unique tumorigenicity of CSC and its suggested role in metastasis. Functional properties of putative CSC populations have also been noted such as increased aldehyde dehydrogenase (ALDH) activity[9] and dye-efflux which gives rise to side populations (SP).[10]

SP cells are a small subset of a cellular population initially identified in murine bone marrow by flow cytometry due to their efflux of the fluorescent dye Hoechst 33342.[11] This efflux property has

*Correspondence to: Wafik S. El-Deiry; Email: wafik@mail.med.upenn.edu
Submitted: 10/27/09; Accepted: 10/27/09
Previously published online: www.landesbioscience.com/journals/cbt/10450

been ascribed to the ATP binding cassette (ABC) transporters,[12] including P-glycoprotein (P-gp) as well as ABCG2, and identification of these subpopulations is qualified by inhibiting the SP efflux via ABC transporter inhibitors such as verapamil. P-gp is encoded by the MDR1 gene which has been shown to be transcriptionally regulated by Ras and p53.[13] This regulation has been found to be disrupted upon p53 mutation in vivo and has been extended to MRP1 as well.[14-16] Further studies have also revealed a relationship of inactivating pro-apoptotic genes p53 or INK4a in addition to overexpressing the anti-apoptotic Bcl-2 with increased resistance to chemotherapy in vivo.[17-19] The substrates of ABC transporters include small molecule chemotherapeutic agents such as topotecan,[20] methotrexate,[21] paclitaxel[22] and Imatinib mesylate[23] thus implicating SP cells in multidrug resistance (MDR).[24] SP cells have been characterized in several cancer cell lines and in primary tumor samples of mesenchymal neoplasms,[25] neuroblastomas,[12] as well as ascites of ovarian cancers.[26] Continuing research on the identification of SP cell properties has yielded an imperfect but clearly recognizable overlap with that of various stem cell markers. Such overlapping properties have been found in murine tissues including the majority of isolated SP cells expressing CD45 in bone marrow,[27] CD34 in skin tissue,[28] Sca-1 in bone marrow,[29] skeletal tissue,[30] mammary gland,[31] testis[32] and skin tissue,[33] as well as c-kit in brain tissue[34] and bone marrow.[29]

Disparities between properties identified from putative CSCs and SP cells are inherent for a few reasons. First of all, SP cells have been shown to be sensitive to variables such as method of preparation, confluency, hypoxia and serum levels which sensitizes isolation to inconsistency across samples.[35] Additionally, SP cells as well as putative CSCs are identified based on an operational definition, e.g., cell surface markers, which may contribute to the phenotype but not exclusively confer it. For instance, SP cells are identified by their efflux property which has been attributed to ABC transporters such as ABCG2 and have been shown to be tumorigenic in nude mice.[36] However, ABCG2$^+$ and ABCG2$^-$ SP cells, while both are more tumorigenic than non-SP cells, have been shown to have similar tumorigenicity.[37]

Hoechst 33342 is known to inhibit DNA topoisomerase I in addition to increasing levels of ATM, Chk2 and p53 phosphorylation.[38,39] A change in γH2AX is also noted and is thought to occur as a result of Hoechst 33342 binding to the minor groove of DNA which alters chromatin structure.[40] Importantly, despite the significant efflux of the dye in stem cells, it has been shown that stem cells still retain 10–80% of Hoechst 33342 relative to non stem cells.[11,41] At exposures of 18 hours to Hoechst 33342 (1 μM), cells arrest in G_2 and exhibit significantly increased levels of activated ATM, activated Chk2, and phosphorylated p53(Ser15).[39] It should also be noted that these observations were made at a concentration 10-fold less than the prototypical staining concentration recommended for SP analysis by flow cytometry (5 μg/mL).[11] As Hoechst 33342 clearly alters protein expression levels, cellular properties are likely to be differentially affected throughout the population. Using Hoechst 33342 staining as a sorting method for tumorigenicity studies is also confounded by the toxicity of Hoechst 33342 which strongly influences proliferation. Therefore an alternative method of identifying subpopulations with this putative CSC efflux property in a non-toxic manner is warranted and would potentially allow for longitudinal and/or in vivo studies without altering cell properties. Such studies have the potential to dispel the small but persistent empirical disparities between CSC and SP cells.

Visualizing live CSCs in cell culture and in vivo holds great value for understanding cancer pathogenesis, metastasis, resistance to therapy, and the development of novel therapies targeting CSCs within the tumor microenvironment. Current methods for identifying CSCs typically involve sorting by flow cytometry or immunohistochemical staining for putative CSC marker properties. A significant limitation of these approaches is that they cannot be performed in vivo as they require the removal of cells from their natural environment for analysis and in some cases fixation of the cells so that they are no longer viable. Visualizing live CSCs via a noninvasive, non-toxic stain would provide a window to observe CSCs in a more biologically and clinically relevant environment, possibly in vivo. Several studies have employed dyes to differentiate between SP cells and non-SP cells including luciferin assays for determining ABCG2 inhibitors.[42] Interpretation of such experiments is subject to caution due to the possibility of displaying altered properties due to dye-retention and not physiological properties. The ensuing method allows for visualization of putative CSCs and extends as a tool for clarification of these ambiguities.

To address these concerns, we propose calcein as an alternative fluorescent dye to Hoechst 33342 due to its similar ability to be effluxed and its absence of cellular toxicity exhibited by Hoechst 33342 as an identifier for dye efflux associated with putative CSCs. Calcein AM is a cell permeable, non-fluorescent compound which is cleaved by intracellular esterases to produce calcein which fluoresces and is retained in the cytosol.[43] We have identified cells capable of effluxing calcein (calcein low population, C^{L}P) in several human cancer cell lines. C^{L}P cells are a small subpopulation, though larger than SP, which exhibit significant overlap with SP which has the potential to identify a larger population of putative CSCs. Visualization of cells by fluorescence microscopy using Calcein AM and/or D-luciferin, efflux substrates, in concurrence with Mitotracker Red FM, a mitochondrial dye which is not effluxed, was carried out to identify live cells which possess efflux capability. A novel relationship with p53 inactivation or Bax deletion yielded an enrichment of putative CSCs by our visualization method and was corroborated by flow cytometry. This yields important mechanistic insight into how putative CSCs gain their efflux property which confers MDR.

Results

C^{L}P overlaps with SP as an identifier of putative CSCs. Hoechst 33342 has been used to identify dye-effluxing SP cells that have been proposed to be CSCs due to their apparently greater tumorigenic potential in vivo.[36] Due to the toxicity of Hoechst 33342 at low concentrations and on short time scales,[39] an alternative means of isolating putative CSC's based on dye efflux is desired. To evaluate the feasibility of Calcein AM staining as a way of determining dye effluxing cells, the DLD-1 colon carcinoma cell line which has a well described SP was stained with Calcein AM,

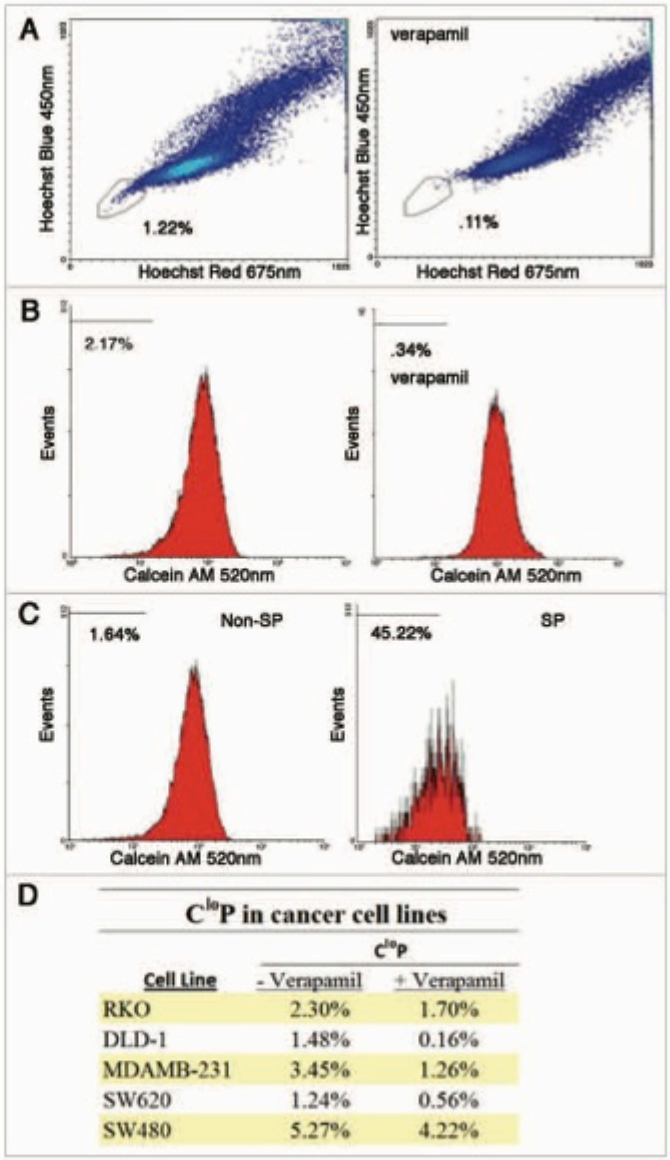

$C^{lo}P$ in cancer cell lines

Cell Line	$C^{lo}P$ - Verapamil	$C^{lo}P$ + Verapamil
RKO	2.30%	1.70%
DLD-1	1.48%	0.16%
MDAMB-231	3.45%	1.26%
SW620	1.24%	0.56%
SW480	5.27%	4.22%

Figure 1. Analysis of SP and $C^{lo}P$ by flow cytometry in cell lines treated with Calcein AM and Hoechst 33342. Dead cells were first gated out based on FS and SS as well as PI staining. SP cells were identified by its low Hoechst 33342 fluorescence and its efflux inhibition by verapamil treatment (A). After gating out dead cells, the $C^{lo}P$ was also quantified in the total population based on its low calcein fluorescence and its efflux inhibition by verapamil treatment (B). To determine the overlap of SP and $C^{lo}P$, the $C^{lo}P$ was quantified for non-SP and SP (C) as determined by the gate for SP shown in (A). A significant $C^{lo}P$ was identified in a number of human cancer cell lines (D).

Hoechst 33342 and PI. Cells were gated for viability based on PI exclusion as well as light scatter (FS and SS). Cells which were viable and considered SP by low Hoechst 33342 fluorescence were quantified as 1.22% and their low fluorescence was inhibited by verapamil, an ABC transporter inhibitor (Fig. 1A). Analyzing fluorescence of calcein yielded a $C^{lo}P$ of 2.17% which was significantly larger than that identified by SP and inhibited by verapamil (Fig. 1B). To assess the overlap of the SP and $C^{lo}P$, SP and non-SP cells were independently analyzed for their $C^{lo}P$ based on the same gating used earlier to determine these subpopulations (Fig. 1C). The SP was determined to have a $C^{lo}P$ of 45.22% and has a strong overall shift to lower calcein fluorescence intensity throughout the population compared to that of the non-SP which contained a $C^{lo}P$ of 1.64%. A number of human cancer cell lines including RKO, DLD-1, MDA-MB-231, SW620 and SW480 were found to contain a $C^{lo}P$ (Fig. 1D). The imperfect but significant overlap of $C^{lo}P$ and SP is likely due to irreversible Hoechst 33342 binding to the minor grove of DNA while the fluorescence of calcein does not require binding.[14,40] Thus putative CSCs which do not efflux Hoechst 33342 before it binds irreversibly are not identified via the SP identification method but would be contained in the $C^{lo}P$ as calcein is not bound. The identification of a larger $C^{lo}P$ relative to SP while exhibiting significant overlap suggests that the $C^{lo}P$ could potentially serve as a better identifier for the putative CSC dye effluxing subpopulations due to their unique respective dye properties.

Calcein AM is non-toxic to cells in contrast to Hoechst 33342. With the observation of a $C^{lo}P$, the toxicities of the dyes were evaluated. To evaluate levels of p53, a transcription factor which regulates many cellular processes such as cell cycle progression

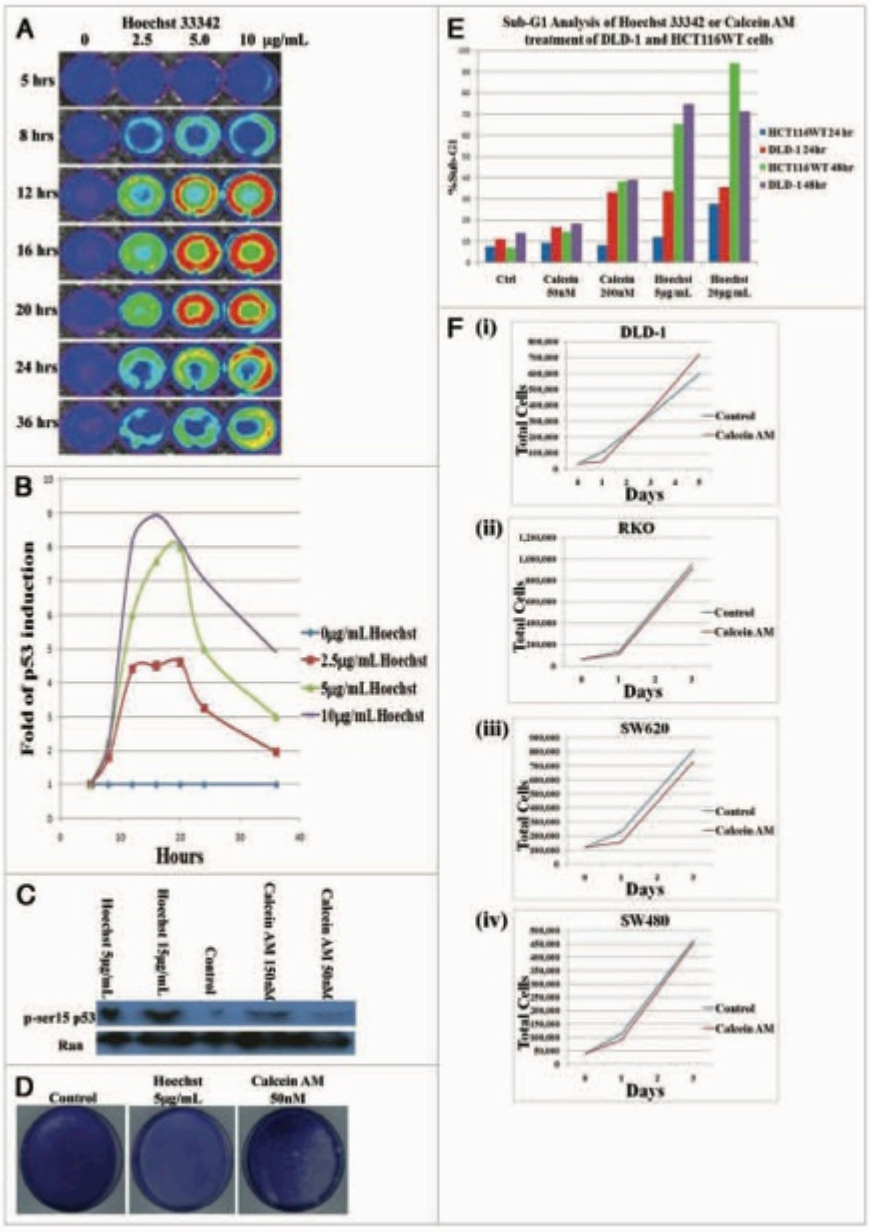

Figure 2. For legend, see p. 5.

Figure 2. Hoechst 33342 induces cell stress and death while Calcein AM does not. HCT116 cells containing a p53 luciferase reporter shows an induction of p53 mediated transcriptional activity in a dose and time dependent manner with Hoechst 33342 treatment (A and B). H460 cells were treated with Hoechst 33342 for 1.5 hr or Calcein AM for 2 hr at indicated concentrations and protein expression level of phospho-p53 (ser15) were determined by western blot (C). Coomassie stain after 10 days following plating at 70,000 cells/mL and treatment with Hoechst 33342 for 1.5 hr or Calcein AM for 2 hr at indicated concentrations (D). Sub-G_1 analysis by flow cytometry following incubation of DLD-1 or HCT116 cells with Hoechst33342 or Calcein AM at indicated concentrations after 24 or 48 hr incubation (E). Proliferation of DLD-1 (i), RKO (ii), SW620 (iii) or SW480 (iv) cell lines following Calcein AM staining (F).

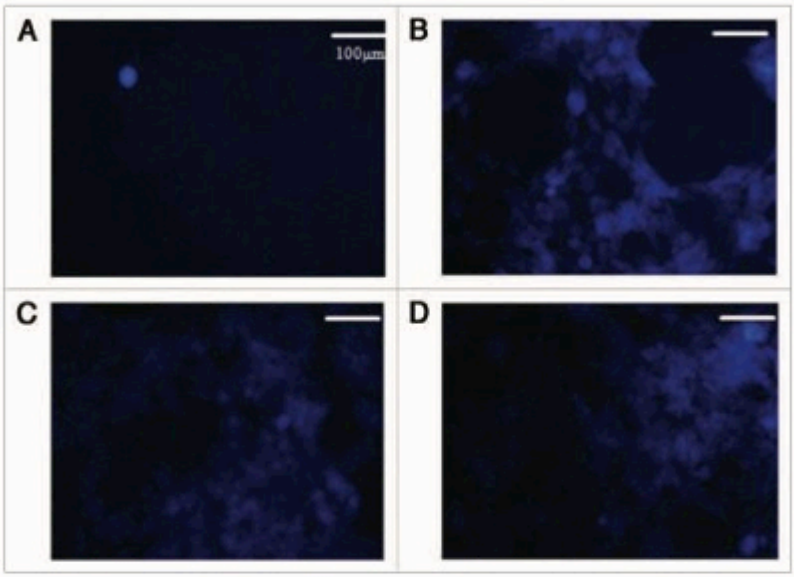

Figure 3. Fluorescence imaging of D-luciferin in the DLD-1 cell line at various concentrations of D-luciferin. Concentrations of D-luciferin were imaged at 50 μg/mL (A), 250 μg/mL (B), 500 μg/mL (C) and 750 μg/mL (D). The optimal concentration was determined to be 250 μg/mL which provided cellular resolution after washing with PBS.

after DNA damage, transcriptional activity was determined by a luciferase reporter assay in HCT116 cells treated with varying concentrations of Hoechst 33342 (0–10 μg/mL) at several time points (0–36 hr) (Fig. 2A and B). It is clear that Hoechst 33342 increases levels of p53-mediated transcription in a time and dose dependent manner. The decrease in activity at 24 and 36 hours is due to apoptosis. To assess the effects of Calcein AM staining as well as Hoechst 33342 staining on cell stress, levels of phosphorylated p53 (serine15) were determined by western blot in the H460 cell line which also expresses WT p53 (Fig. 2C). At both concentrations, Hoechst 33342 staining induced significant levels of phosphorylated p53 (serine 15) whereas Calcein AM staining demonstrated levels close to the control. We then investigated the ability of cells to proliferate following prototypical staining with Hoechst 33342 and Calcein AM. DLD-1 cells were plated at a concentration of 70,000 cells/mL and treated with Hoechst 33342 or Calcein AM at a working concentration of 5 μg/mL for 1.5 hours or 50 nM for 2 hours, respectively, as defined by their protocols. The stained populations were allowed to proliferate for 10 days and were then fixed and stained with Coomassie blue to visualize cell colonies (Fig. 2D). Markedly, Hoechst 33342 staining yielded no viable cells whereas Calcein AM staining yielded a population close to that of the control. Furthermore, levels of apoptosis were determined by flow cytometry analysis of sub-G_1 content following incubation with Hoechst 33342 or Calcein AM at the noted time points and concentrations in HCT116 and DLD-1 cell lines (Fig. 2E). Calcein AM at a 50 nM working concentration displayed levels of apoptosis similar to control cells that were maintained under identical conditions in the absence of fluorescent dye. At 200 nM, Calcein AM produced a modest increase in levels of apoptosis; however it should be remarked that these levels are still less than those of Hoechst 33342 staining under any conditions tested. At both concentrations (5 μg/mL and 20 μg/mL) of Hoechst 33342, levels of apoptosis were clearly elevated at all time points and in all cell lines tested relative to the control as well as Calcein AM. Lastly, the effects of Calcein AM staining

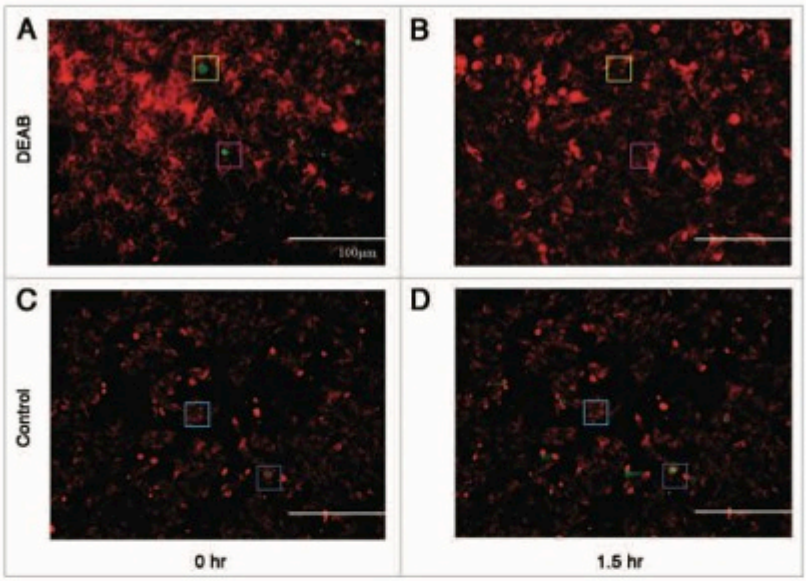

Figure 4. Visualization by fluorescence microscopy of an ALDH$^+$ population and its inhibition. DLD-1 cells were stained with Aldefluor and imaged in the same field of view before (A) and 1.5 hr after the addition of DEAB (B). DLD-1 cells were stained with Aldefluor and imaged in the same field of view before (C) and 1.5 hr after staining as a control for fluorescence quenching or photobleaching (D). Boxes of the same color show identical locations in the field of view as reference point for locating ALDH$^+$ cells. To emphasize putative CSCs expressing high ALDH activity, a threshold level was set so that only cells expressing higher than average Aldefluor fluorescence are shown in green. Mitotracker Red FM was used as a counterstain before Aldefluor staining and is shown in red.

on proliferation was quantitatively determined over several days in DLD-1, SW260, RKO and SW480 cell lines (Fig. 2F). It appears there is a slight lag phase during the first day but overall proliferation is similar to control levels. Taking this evidence together with previous observations, Calcein AM appears suitable as a non-toxic alternative fluorescent dye that is effluxed by and therefore a potential indicator of putative CSCs.

Luciferin exhibits strong UV-excited fluorescence that can be imaged at a cellular resolution and spatially overlaps with calcein. D-luciferin is a known substrate of ABC transporters[47] which have been associated with SP cells[48] and subsequently implicated in putative CSCs. Due to its strong fluorescence signal and availability, it is employed in a variety of both in vitro and in vivo assays.[47,48] Such studies include screening for ABC transporter inhibitors by means of determining efficacy based on luciferin retention. These studies assume the properties of the sorted populations to be dye-independent. Considering this, conclusions drawn from these studies about subpopulations based on dye-efflux must be taken with caution as differences may be caused by dye-induced alterations of cell cycling, differential toxicity and protein levels/status such as p53, ATM or Chk2.[19] For these reasons, we carried out image analysis of D-luciferin in DLD-1 cells that yielded visualization at cellular resolution not previously achieved. The cells were incubated with D-luciferin for 1 hour followed by washing twice with PBS and imaged in PBS + 2 mM $MgCl_2/CaCl_2$ to maintain cell adhesion. These procedures along with a minimal concentration of 250 μg/mL of D-luciferin allowed cell visualization of dye-containing cells (Fig. 3B) while higher concentrations yielded diminishing margins in image contrast improvement (Fig. 3C and D). Concentrations below this did not provide a desirable cellular resolution (Fig. 3A). Previous efforts employing D-luciferin lack cellular resolution and rely on bulk signal and fall subject to the previously outlined problems. The demonstrated capability of such resolution could be used in combination with viability stains and other fluorescent probes to visualize the level of dye-retention as well as other important cell properties in a simultaneous, noninvasive and dynamic fashion unparalleled by bulk-signal methods.

Visualization of ALDH$^+$ population and inhibition by DEAB. To further expand our efforts to provide an alternative and improved method for studying putative CSCs under relatively physiological conditions, we explored the use of ALDH activity within putative CSCs as a means to visualize such cells. In addition to dye efflux, ALDH activity has been positively correlated with tumorigenicity[50] and therefore has been suggested as a property of putative CSCs. Thus, we attempted to visualize ALDH activity

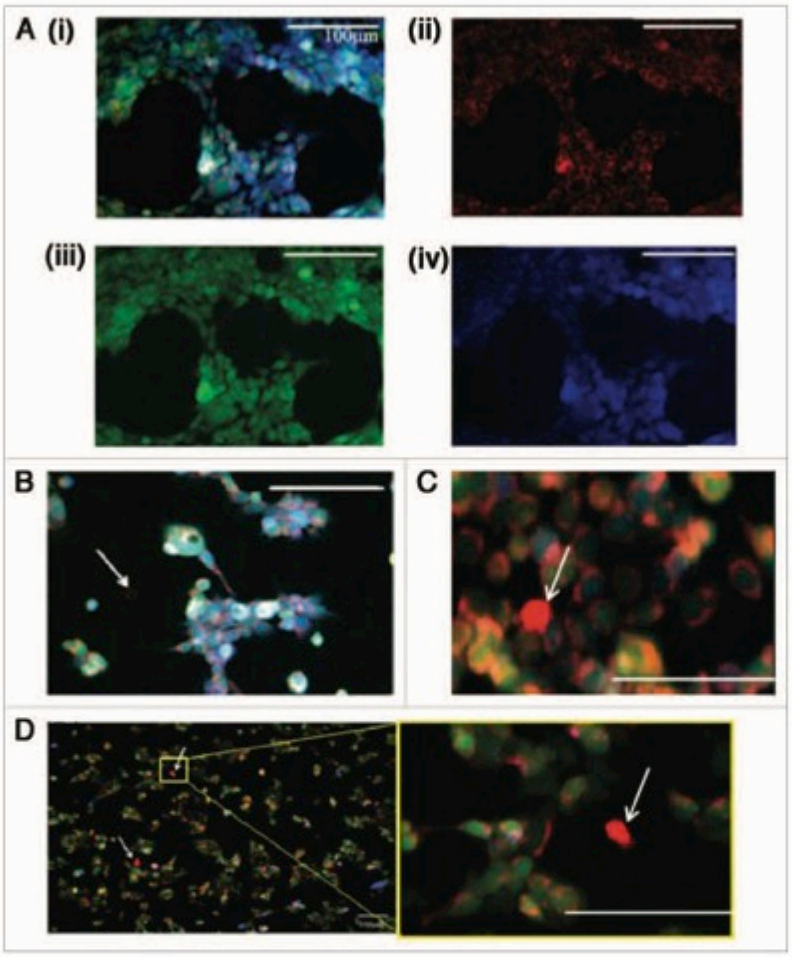

Figure 5. Visualization of dye effluxing population. Visualization of fluorescence in viable WT HCT116 cells (A) showing Mitotracker Red FM (red) (ii), calcein (green) (iii), D-luciferin (blue) (iv) and an overlay (i). The same staining was carried out in (B) $Bax^{-/-}$ HCT116, (C) $p53^{-/-}$ HCT116, and (D) DLD-1 cell lines. Dye-effluxing cells are indicated by white arrows. All scales bars are 100 μm.

in DLD-1 human colon carcinoma cells. Cells were stained with Mitotracker Red FM and Aldefluor, a fluorescent probe of ALDH activity, in the described manner and imaged (Fig. 4A). As all cells exhibited significant levels ALDH activity, a threshold was set for visualization of Aldefluor fluorescence so that only cells with higher than average ALDH activity display fluorescence in the image for clarity. DEAB, an inhibitor of ALDH, was added to the media and incubated at 37°C in 5% CO_2 for 1.5 hours and imaged in the same field of view (Fig. 4B). It is evident in Figure 4B that ALDH activity is inhibited by DEAB. Images were taken in an identical manner without addition of DEAB to demonstrate Aldefluor fluorescence is not being quenched by photobleaching (Fig. 4C and D). This capability demonstrated in this observation underscores the ability to capture dynamic information concerning cellular properties of putative CSCs. This method can be extended to time lapse studies that observe putative CSCs in real time; however caution is warranted with regards to exposure time and photobleaching.

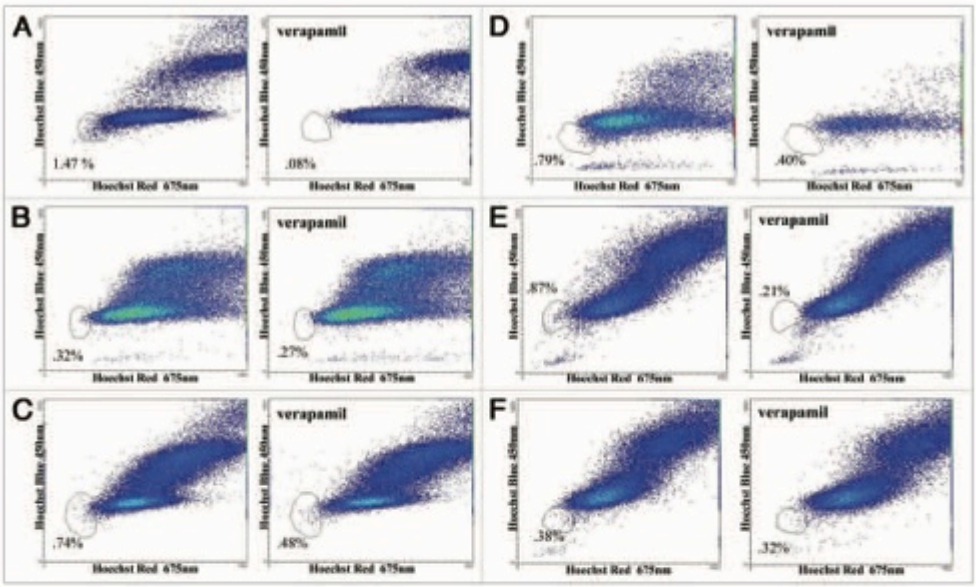

Figure 6. Quantification of SP using Hoechst 33342 staining by flow cytometry in colon carcinoma cell lines with different p53 and/or Bax gene status. SP were determined in (A) DLD-1 (mutant p53), (B) HCT116 (WT p53), (C) HCT116 Bax$^{-/-}$ and (D) HCT116 p53$^{-/-}$ cell lines. Noting the induction of SP upon Bax deletion or p53 inactivation, SP were then determined following the overexpression of p53 using (E) Ad-LacZ as a control and (F) Ad-p53 in HCT116 p53$^{-/-}$ to confirm the relationship between p53 and dye-effluxing properties.

Visualization of putative CSC populations induced upon p53 inactivation or Bax deletion using fluorescence microscopy and non-toxic dyes. We hypothesized that loss of the p53 tumor suppressor or the pro-apoptotic Bax gene may allow for enrichment of putative CSCs as these genes are often affected in cancer and thus may be involved in the CSC phenotype. Evidence for the transcriptional regulation of some MDR genes by p53 in addition to disease prognosis dependency on the status of these apoptotic genes in different models also led us to this hypothesis.[13-15,22,51-55] With the demonstrated visualization methods we then searched for putative CSCs in cell lines harboring these genetic aberrancies. The colon carcinoma cell lines mutant p53-expressing DLD-1, WT p53-expressing HCT116, p53$^{-/-}$ HCT116 and Bax$^{-/-}$ HCT116 were analyzed for potential CSC populations via the described putative CSC staining and visualization methods. As demonstrated in WT HCT116 by Figure 5A, cells were stained with Mitotracker Red FM (Fig. 5A, ii), Calcein AM (Fig. 5A, iii) and D-luciferin (Fig. 5A, iv). Cells were imaged, assigned pseudo-color and overlayed (Fig. 5A, i) for analysis. Visual analysis revealed a small dye-effluxing population in DLD-1 cells (Fig. 5D) which was absent in WT HCT116 cells. This observation is in full agreement with published data regarding the SP of these two cell lines.[35] It should also be noted that these putative CSCs have a smaller size than the rest of the population which is a property that has been linked to stem cells.[56] Scrutinizing these images for Bax$^{-/-}$ (Fig. 5B) and p53$^{-/-}$ (Fig. 5C) HCT116 cell lines, a rare dye-effluxing population was noted. In accordance with our hypothesis, these observations suggest a novel relationship between the putative CSC property of dye-efflux and p53 as well as the pro-apoptotic gene Bax. DLD-1, which has an established SP and herein demonstrated C^{bP}, harbors mutant p53 while WT HCT116 has WT p53. Thus it appears p53 inactivation, by mutation or gene deletion, gives rise to the putative CSC property of small molecule efflux. This is consistent with the notion that p53 represses MDR genes that provide detoxifying activity to enhance survival of stem cell populations, and that loss of p53 promotes the CSC phenotype in part at the level of small molecule efflux. The observation that Bax$^{-/-}$ HCT116 appears to have an SP as opposed to WT HCT116 provides evidence for a dependency of the CSC phenotype of dye-efflux on Bax as well. In summary, our method of visualizing CSC properties has suggested a novel relationship of p53 inactivation as well as Bax deletion with the induction of putative CSCs.

Putative CSC populations induced upon p53 inactivation or Bax deletion in colon cancer cell lines. The observation that dye-effluxing capabilities can be induced with inactivation of p53 or through Bax gene deletion is of mechanistic importance to CSCs and merits quantitative validation. To corroborate this assertion we performed SP analysis on DLD-1, WT HCT116, p53$^{-/-}$ HCT116

and Bax$^{-/-}$ HCT116 cells. Cells were prepared for analysis by the procedure outlined in the methods section and analyzed by flow cytometry for SP as determined by low Hoechst 33342 fluorescence in viable cells and efflux inhibition by verapamil. In agreement with our previous observations, DLD-1 yielded a significant SP population of 1.47% (**Fig. 6A**) while WT HCT116 had a negligible SP (**Fig. 6B**). Moreover, Bax$^{-/-}$ HCT116 had a SP of 0.74% (**Fig. 6C**) and p53$^{-/-}$ HCT116 had a SP of 0.79% (**Fig. 6D**) in agreement with qualitative observations by our visualization methods. Infection by an adenovirus vector, Ad-LacZ, in HCT116 p53$^{-/-}$ caused no appreciable change in SP (**Fig. 6E**) but expression of WT p53 via the adenovirus vector Ad-p53 returned the SP to background levels (**Fig. 6F**). It should be noted that SP populations are sensitive to their environment[35] and so while the quantification varies in the literature, to our knowledge a relationship of SP induction within a non-SP cell line by gene-deletion has not been previously reported.

Discussion

The relationship of p53 mutations or deletion as well as Bax deletion with putative CSCs provides mechanistic insight for understanding the aberrancies that differentiate CSCs from other cells. Previous studies have been confounded by isolation methods that utilize markers which are not exclusive qualifiers and/or employ toxic dyes to purify these putative CSC populations. The latter in the case of Hoechst 33342 has been shown to be toxic to all subpopulations at low concentrations relative to established protocols. The evidence that Calcein AM stains subpopulations in a non-toxic manner which allows for subsequent proliferation presents a viable possibility to surmount this impediment. The novel C^{lo}P identified in several cancer cell lines using this method also potentially presents a more accurate identification of dye-effluxing putative CSCs because calcein is localized in the cytosol[43] whereas Hoechst 33342 binds to the minor groove of DNA.[40] Using the staining method as a paradigm, other putative CSC properties could potentially be assayed with the ability to visualize cells in culture and in vivo. This concept is exemplified within this study by fluorescently probing ALDH activity. High ALDH activity has been posited as putative marker for tumorigenicity and has been extended to CSCs[7] and can now be visualized as exhibited by this study. Visualization of D-luciferin at a cellular resolution is unprecedented and has the potential to further elucidate diffidence pertaining to criticism of in vivo studies regarding subpopulation properties being induced by dye-toxicity effects in dye-retaining cells.

It should be noted that due to the limited availability of cell lines with gene knockouts which allows for isogenic comparisons, the enrichment of putative CSCs in this study has been observed exclusively in the colon carcinoma cell line HCT116. Establishing the presented putative CSC enrichment relationship should be extended to other cell lines to corroborate this relationship and/or expose a deeper understanding of the dependency. For the same purposes, visualization of properties such as calcein efflux and ALDH$^+$ activity visualization should be carried out on other cell lines. Recent evidence has emerged regarding the effects of fluorescent probes on gene expression profiles.[39] Therefore, future studies on identification of putative CSC properties should examine effects on protein expression profiles and cell cycle to limit induced alterations in cellular properties due to the method.

The impact of this work is in providing novel methods for visualization, isolation and tracking of dye-effluxing putative CSC populations in culture and could be extended to in vivo. This has not previously been possible in live cell populations and allows for dynamic monitoring. A range of options is provided by our studies for use of Calcein AM, D-luciferin and ALDH as markers for putative CSC visualization. Such methods can certainly be combined with analysis of cell surface markers by live cell immunofluorescence for further understanding the relationships between various CSC markers and phenotypes associated with cancer development and progression. Future studies can analyze the tumorigenicity of the C^{lo}P, herein identified in cancer cell lines possessing dye-effluxing properties associated with putative CSCs in a wide range of human tumor types. The described identification method allows for non-toxic sorting of cancer cell lines based on this property and subsequent evaluation of tumorigenicity in vivo.

An important aspect of our work is the demonstration that loss of the p53 tumor suppressor or the pro-apoptotic Bax genes results in enrichment of putative CSC populations by our analytical methods. In agreement with this novel p53 relationship, reintroduction of WT p53 eliminated these putative CSC populations which concurs with the previously noted p53 regulation of MDR genes such as MDR1 and MRP1.[13,15,53-55] While this work was being conducted, a number of studies were published which identified the loss of p53 as a promoter of more efficient reprogramming of differentiated cells into pluripotent cells, or induced pluripotent stem cells (iPS).[57-61] This along with our finding regarding loss of p53 as a promoter of MDR properties highlights the importance of p53 loss of function in conferring putative CSC phenotypic properties. The ability to visualize and track putative CSC populations should facilitate a host of cell culture and in vivo studies regarding cancer progression as well as novel therapy development, including the discovery and testing of agents that may directly target putative CSC populations. Such visualization of putative CSC populations in vivo may be coupled with cell death visualization, e.g., using fluorescently labeled Annexin V, to assess at cellular resolution the effects of specific therapies on CSC and non-CSC in the context of the tumor microenvironment.

Materials and Methods

Cell culture. All tumor cell lines were obtained from the American Type Culture Corporation (ATCC) except Bax$^{-/-}$ HCT116 and p53$^{-/-}$ cell lines which were provided by B. Vogelstein (Johns Hopkins University, Baltimore) and H460 which was from S.B. Baylin (Johns Hopkins University, Baltimore, MD). WT HCT116, Bax$^{-/-}$ HCT116 and p53$^{-/-}$ HCT116 cell lines were grown in McCoy's 5A medium with 10% FBS and 1% Penicillin/Streptomycin at 37°C in 5% CO_2. DLD-1, RKO, SW480, SW620 and DMAMB-231 cell lines were grown in DMEM (Gibco) with 10% FBS and 1% Penicillin/Streptomycin at 37°C in 5% CO_2. The H460 cell line

was grown in RPMI (Gibco) with 10% FBS and 1% Penicillin/Streptomycin at 37°C in 5% CO_2.

Fluorescent dyes. The following fluorescent dyes were used in flow cytometry and/or fluorescence microscopy experiments and the wavelength of light used for excitation (Ex) as well as the wavelength of light collected (Em) is noted parenthetically. Propidium iodide (PI) (488 nm Ex, 675 nm Em) was used exclusively in flow cytometry and was obtained from Sigma-Aldrich (St. Louis, MO). D-Luciferin (Ex 365 nm, Em 450) was obtained from Gold Biotechnology (St. Louis, MO). The fluorescent dyes Mitotracker Red FM (Ex 540 nm, Em 605 nm), Hoechst 33342 (Ex 365 nm, Em 450 nm) and Calcein AM (Ex 480 nm, Em 535 nm) were obtained from Invitrogen (Carlsbad, CA). Mitotracker Red FM was used for staining at a working concentration of 400 nM in all experiments unless otherwise indicated. Calcein AM was used at a working concentration of 50 nM in all experiments unless otherwise indicated. Aldefluor (Ex 480 nm, Em 535 nm) and DEAB were obtained from the ALDEFLUOR Kit from Stem Cell Technologies (Vancouver, BC, Canada), and used at concentrations described by the ALDEFLUOR kit protocol.

Luciferase reporter assay. HCT116 cells previously engineered to express a firefly luciferase gene under the control of 13 p53-response elements were treated with Hoechst 33342 at indicated concentrations.[44] Intensities of firefly luciferase activity were imaged and measured as previously described at indicated time points.

Adenovirus preparation and infection. We prepared replication-deficient adenovirus recombinants expressing wild-type p53 (Adp53) and β-galactosidase (AdLacZ) as previously described.[45] Determination of viral titers and multiplicity of infection (MOI) for the infected cell line has been described.[46] HCT116 $p53^{-/-}$ cells were infected at a MOI of 50.

Western blot analysis. Western blotting was carried out according to standard procedures, using horseradish peroxidase-conjugated secondary antibodies (Santa Cruz Biotechnology, Santa Cruz, CA) and the ECL+ detection system (Amersham, Arlington Heights, IL). The following antibodies were used: rabbit polyclonal antibodies against phosphorylated serine 15 of p53 at a dilution of 1:1,000 from Cell Signaling Technology (Beverly, MA); mouse monoclonal antibodies against Ran at a dilution of 1:10,000 from BD Technologies (Franklin Lakes, NJ).

Coomassie stain and growth assay. To visualize proliferation after dye staining, cells were plated at a density of 70,000 cells/mL in 3–100 mm x 20 mm cell culture dishes and stained with Hoechst 33342 for 1.5 hours at 5 μg/mL working concentration, Calcein AM at a 50 nM working concentration, or only media as a control. After staining, the dye-containing media was aspirated and replaced with fresh media containing no dye. Cells were incubated at 37°C in 5% CO_2 for 10 days, replacing with fresh media once every 3 days. At the end of this 10 day period, cells were washed in PBS and fixed in a solution of 10% methanol and 10% acetate for 5 minutes. Cells were then stained with Coomassie blue for 5 minutes and imaged. To quantitatively determine the effect of Calcein AM staining on cell proliferation a growth assay was performed. Cultured cells were treated with Calcein AM (50 nM in growth media) for 30 min at 37°C and 5% CO_2. The cells were washed and incubated with fresh complete medium for the indicated number of days. Cell counts were taken just prior to treatment and at the indicated times after treatment by trypan blue exclusion assay for living cells. Results are expressed as total cell number over time.

SP and $C^{\flat}P$ assays by flow cytometry. Flow cytometry was performed using an Elite ESP flow cytometer (Beckman-Coulter, Miami, FL). To analyze the SP, a solid state 355 nm UV laser (Lightwave Electronics, Mt. View, CA) was used to excite the Hoechst 33342 and the dual emission was captured with a 450 nm band pass filter (Hoechst Blue) and a 675 nm band pass filter (Hoechst Red) separated with a 550LP dichroic. Forward scatter (FS) and PI (675/40BP) were captured from a 488 nm argon laser 40 μsec upstream of the UV laser. For quantification of SP by flow cytometry, cells were grown to ~70% confluency and were harvested using trypsin (Gibco). Cells were washed and resuspended in cold HBSS (Gibco) at a concentration of 1 x 10^6 cells/mL containing Hoechst 33342 (5 μg/mL) (Invitrogen) for 1.5 hours at 37°C, vortexing gently every 30 min. A negative control sample was treated with verapamil (Sigma) (50 μM) for 15 min at room temperature prior to the addition of Hoechst 33342. After the incubation with Hoechst 33342, cells were centrifuged, washed, and resuspended in ~300 μL HBSS containing PI (2 μg/mL). Dead cells were gated out based on PI fluorescence at 675 nm as well as FS and side scatter (SS). $C^{\flat}P$ cells were analyzed in the same manner but instead of Hoechst 33342 fluorescence, calcein fluorescence was collected at 520 nm.

Sub-G_1 analysis. PI staining and analysis by flow cytometry were used to quantify the levels of apoptosis induced by Hoechst 33342 and Calcein AM in the indicated cell lines, dye concentrations and time points. Cells were grown to ~70% confluency in 6-well plates, washed with PBS, and digested by 1 mL trypsin at 37°C for 5 min. Cells were washed with 2 mL PBS/1% FBS, resuspended in 0.5 mL PBS. Resuspended cells were added dropwise into 5 mL cold 70% ethanol with gentle vortexing, then kept on ice for 30 min. Fixed cells were spun down to remove ethanol, washed with 2 ml PBS/1% FBS, and resuspended in 1.0 mL PBS. 0.5 mL of phosphate-citrate buffer (pH 7.8) was then added and the solution was incubated for 5 minutes. Cells were spun down, resuspended in 300 μL PI/RNase staining solution, and stored for 30 min at room temperature in the dark and subsequently analyzed by flow cytometry. Staining with Calcein AM was carried out by the described methods.

Fluorescence microscopy and images. Fluorescence microscopy images were recorded by a QImaging 2000R Camera on an Axiovert 100 inverted microscope. Images were collected and processed using iVision-Mac (BioVision Technologies, Exton, PA). During imaging, cells were maintained by the LiveCell™ system (Pathology Devices, Westminster, MD) at 37°C and 5% CO_2.

Acknowledgements

This work was supported in part by NIH Grant U54 CA105008 and by the Littlefield-AACR Grant in Metastatic Colon Cancer Research. W.S.E.-D. is an American Cancer Society Research Professor.

References

1. Sell S. Stem cell origin of cancer and differentiation therapy. Crit Rev Oncol/Hematol 2004; 51:1-28.
2. Bergsagel DE, Valleriote FA. Growth Characteristics of a Mouse Plasma Cell Tumor. Cancer Res 1968; 28:2187-96.
3. Bruce WR, Van Der Gaag H. A Quantitative Assay for the Number of Murine Lymphoma Cells capable of Proliferation in vivo. Nature 1963; 199:79-80.
4. Hasse D, Feuring-Buske M, Konemann S, Fonatsch C, Wolf C, Verbeek W, et al. Evidence for malignant transformation in acute myeloid leukemia at the level of early hematopoietic stem cells by cytogenetic analysis of CD34+ subpopulations. Blood 1995; 86:2906-12.
5. Mehotra B, George TI, Kavuma K, Avet-Loiseau H, Moore D, 2nd, Willman CL, et al. Cytogenetically aberrant cells in the stem cell compartment (CD34+/in') in acute myeloid leukemia. Blood 1995; 86:1139-47.
6. Dick DBJE. Human acute myeloid leukemia is organized as a hierarchy that originates from a primitive hematopoietic cell. Nature Med 1997; 3:730-7.
7. Singh SK, Hawkins C, Clarke ID, Squire JA, Bayani J, Hide T, et al. Identification of human brain tumour initiating cells. Nature 2004; 432:396-401.
8. Al-Hajj M, Wicha MS, Benito-Hernandez A, Morrison SJ, Clarke MF. Prospective identification of tumorigenic breast cancer cells. Proc Natl Acad Sci USA 2003; 100:3983-8.
9. Huang EH, Hynes MJ, Zhang T, Ginestier C, Dontu G, Appelman H, et al. Aldehyde Dehydrogenase 1 Is a Marker for Normal and Malignant Human Colonic Stem Cells (SC) and Tracks SC Overpopulation during Colon Tumorigenesis. Cancer Res 2009; 69:3382-9.
10. Hadnagy A, Gaboury L, Beaulieu R, Balicki D. SP analysis may be used to identify cancer stem cell populations. Exp Cell Res 2006; 312:3701-10.
11. Goodell MA, Katja Brose, Glenn Paradis A, Stewart Conner, Richard C. Mulligan. Isolation and Functional Properties of Murine Hematopoietic Stem Cells that are Replicating In Vivo. J Exp Med 1996; 183:1797-806.
12. Hirschmann-Jax C, Foster AE, Wulf GG, Nuchtern JG, Jax TW, Gobel U, et al. A distinct "side population" of cells with high drug efflux capacity in human tumor cells. Proc Natl Acad Sci USA 2004; 101:14228-33.
13. Chin KV, Ueda K, Pastan I, Gottesman MM. Modulation of activity of the promoter of the human MDR1 gene by Ras and p53. Science 1992; 255:459-62.
14. Angelis PD, Stokke L, Smedshammer B, Lothe A, Lehne G, Chen Y, Clausen OP. P-glycoprotein is not expressed in a majority of colorectal carcinomas and is not regulated by mutant p53 in vivo. Br J Cancer 1995; 72:307-11.
15. Sullivan GF, Yang J-M, Vassil A, Yang J, Bush-Bubula J, Hait WN. Regulation of expression of the multidrug resistance protein MRP1 by p53 in human prostate cancer cells. J Clin Invest 2000; 105:1261-7.
16. Bahr O, Wick W, Weller M. Modulation of MDR/MRP by wild-type and mutant p53. J Clin Invest 2001; 107:643-5.
17. Schmitt CA, Fridman JS, Yang M, Lee S, Baranov E, Hoffman RM, Lowe SW. A Senescence Program Controlled by p53 and p16INK4a Contributes to the Outcome of Cancer Therapy. Cell 2002; 109:335-46.
18. Schmitt CA, Rosenthal CT, Lowe SW. Genetic analysis of chemoresistance in primary murine lymphomas. Nature Med 2000; 6:1029-35.
19. Schmitt CA, Fridman JS, Yang M, Baranov E, Hoffman RM, Lowe SW. Dissecting p53 tumor suppressor functions in vivo. Cancer Cell 2002; 1:289-98.
20. Sparreboom A, Walter J. Loos, Herman Burger, Thirtan M. Sissung, Jaap Verweij, Willisen D. Figg, et al. Effect of ABCG2 Genotype on the Oral Viowailability of Topotecan. Cancer Biol Ther 2005; 4:650-3.
21. Chen Z-S, Robey RW, Belinsky MG, Shchaveleva I, Ren X-Q, Sugimoto Y, et al. Transport of Methotrexate, Methotrexate Polyglutamates and 17β-Estradiol 17-(β-D-glucuronide) by ABCG2: Effects of Acquired Mutations at R482 on Methotrexate Transport. Cancer Res 2003; 63:4048-54.
22. Green H, Peter Soderkvist, Per Rosenberg, Gyorgy Horvath, Curt Peterson. mdr-1 Single Nucleotide Polymorphisms in Ovarian Cancer Tissue: G2677T/A Correlates with Response to Paclitaxel Chemotherapy. Clin Cancer Res 2006; 12:854-9.
23. Burger H, van Tol H, Boersma AWM, Brok M, Wiemer EAC, Stoter G, Nooter K. Imatinib mesylate (STI571) is a substrate for the breast cancer resistance protein (BCRP)/ABCG2 drug pump. Blood 2004; 104:2940-2.
24. Juliano RL, Ling V. A surface glycoprotein modulating drug permeability in Chinese hamster ovary cell mutants. Biochimica et Biophysica Acta (BBA)—Biomembranes 1976; 455:152-62.
25. Wu C, Wei Q, Utomo V, Nadesan P, Whetstone H, Kandel R, et al. Side Population Cells Isolated from Mesenchymal Neoplasms Have Tumor Initiating Potential. Cancer Res 2007; 67:8216-22.
26. Szotek PP, Pieretti-Vanmarcke R, Masiakos PT, Dinulescu DM, Connolly D, Foster R, et al. Ovarian cancer side population defines cells with stem cell-like characteristics and Mullerian Inhibiting Substance responsiveness. Proc Natl Acad Sci USA 2006; 103:11154-9.
27. Wulf GG, Luo KL, Jackson KA, Brenner MK, Goodell MA. Cells of the hepatic side population contribute to liver regeneration and can be replenished with bone marrow stem cells. Haematologica 2003; 88:368-78.
28. Montanaro F, Liadaki K, Volinski J, Flint A, Kunkel LM. Skeletal muscle engraftment potential of adult mouse skin side population cells. Proc Natl Acad Sci USA 2003; 100:9336-41.
29. Pearce DJ, Bidler CM, Simpson C, Bonnet D. Multiparameter analysis of murine bone marrow side population cells. Blood 2004; 103:2541-6.
30. Asakura A, Seale P, Girgis-Gabardo A, Rudnicki MA. Myogenic specification of side population cells in skeletal muscle. J Cell Biol 2002; 159:123-34.
31. Welm BE, Tepera SB, Venezia T, Graubert TA, Rosen JM, Goodell MA. Sca-1pos Cells in the Mouse Mammary Gland Represent an Enriched Progenitor Cell Population. Devel Biol 2002; 245:42-56.
32. Falcinoti I, Bonsellino G, Haliassos N, Boinai C, Corallini S, Bartesini L, et al. Identification and enrichment of spermatogonial stem cells displaying side-population phenotype in immature mouse testis. FASEB J 2004; 18:376-8.
33. Yano S, Ito Y, Fujimoto M, Hamazaki TS, Tamaki K, Okochi H. Characterization and Localization of Side Population Cells in Mouse Skin. Stem Cells 2005; 23:834-41.
34. Ayuko M, Yumi M, Ayano K, Takuya S, Hideyuki O. Flow cytometric analysis of neural stem cells in the developing and adult mouse brain. Journal of Neuroscience Research 2002; 69:83747.
35. Tiwalso RT, Hart LS, Dicker DT, El-Deiry WS. Effects of low confluency, serum starvation and hypoxia on the side population of cancer cell lines. Cell Cycle 2007; 6:2554-62.
36. Kondo T, Setoguchi T, Taga T. Persistence of a small subpopulation of cancer stem-like cells in the C6 glioma cell line. Proc Natl Acad Sci USA 2004; 101:781-6.
37. Patrawala L, Calhoun T, Schneider-Broussard R, Zhou J, Claypool K, Tang DG. Side Population Is Enriched in Tumorigenic, Stem-Like Cancer Cells, whereas ABCG2+ and ABCG2- Cancer Cells Are Similarly Tumorigenic. Cancer Res 2005; 65:6207-19.
38. Chen AY, Yu C, Bodley A, Peng LF, Liu LF. A New Mammalian DNA Topoisomerase I Poison Hoechst 33342: Cytotoxicity and Drug Resistance in Human Cell Cultures. Cancer Res 1993; 53:1332-7.
39. Hong Z, Frank T, Jurek D, Donald W, Zbigniew D. Induction of DNA damage response by the supravital probes of nucleic acids. Cytometry Part A 2009; 75:510-9.
40. Chen AY, Yu C, Gatto B, Liu LF. DNA minor groove-binding ligands: a different class of mammalian DNA topoisomerase I inhibitors. Proc Natl Acad Sci USA 1993; 90:8131-5.
41. Leemhuis T, Yoder MC, Grigsby S, Agüero B, Eder P, Srour EF. Isolation of primitive human bone marrow hematopoietic progenitor cells using Hoechst 33342 and Rhodamine 123. Exp Hematol 1996; 24:1215-24.
42. Zhou S, John D. Schuetz, Kevin D. Bunting, Anne-Marie Colapietro, Janardhan Sampath, John J. Morris, et al. The ABC transporter Bcrp1/ABCG2 is expressed in a wide variety of stem cells and is a molecular determinant of the side-population phenotype. Nature Med 2001; 7:1028-34.
43. Bruot-Boucher F, Pichon J, Rat P, Adolphe M, Aubery M, Pont J. A non-isotopic, highly sensitive, fluorimetric, cell-cell adhesion microplate assay using calcein AM-labeled lymphocytes. J Immunol Meth 1995; 178:41-51.
44. Wang W, El-Deiry WS. Bioluminescent Molecular Imaging of Endogenous and Exogenous p53-Mediated Transcription In Vitro and In Vivo Using an HCT116 Human Colon Carcinoma Xenograft Model. Cancer Biol Ther 2003; 2:196-202.
45. El-Deiry WS, Tokino T, Velculescu VE, Levy DB, Parsons R, Trent JM, et al. WAF1, a potential mediator of p53 tumor suppression. Cell 1993; 75:817-25.
46. Sur JK, Dash BC, Hong R, Dicker DT, El-Deiry WS. The Cyclin-Dependent Kinase Inhibitor Butyrolactone Is a Potent Inhibitor of p21WAF1/CIP1 Expression. Cell Cycle 2002; 1:87-93.
47. Zhang Y, Bressler JP, Neal J, Lal B, Bhang H-EC, Laterra J, Pomper MG. ABCG2/BCRP Expression Modulates D-Luciferin Based Bioluminescence Imaging. Cancer Res 2007; 67:9389-97.
48. Summer R, Kotton DN, Sun X, Ma B, Fitzsimmons K, Fine A. Side population cells and Bcrp1 expression in lung. Am J Physiol Lung Cell Mol Physiol 2003; 285:97-104.
49. Zhang Y, Byun Y, Ren YR, Liu JO, Laterra J, Pomper MG. Identification of Inhibitors of ABCG2 by a Bioluminescence Imaging-Based High-Throughput Assay. Cancer Res 2009; 69:5867-75.
50. Christ O, Lucke K, Imren S, Leung K, Hamilton M, Eaves A, et al. Improved purification of hematopoietic stem cells based on their elevated aldehyde dehydrogenase activity. Haematologica 2007; 92:1165-72.
51. Park YB, Kim HS, Oh JH, Lee SH. The co-expression of p53 protein and P-glycoprotein is correlated to a poor prognosis in osteosarcoma. Int Orthopaedics 2001; 24:307-10.
52. van der Zee AG, Hollema H, Suurmeijer AJ, Krans M, Sluiter WJ, Willemse PH, et al. Value of P-glycoprotein, glutathione S-transferase pi, c-erbB-2 and p53 as prognostic factors in ovarian carcinomas. J Clin Oncol 1995; 13:70-8.
53. Vilgelm A, Wei JX, Pianetto MB, Washington MK, Prassolov V, El-Rifai W, Zaika A. [Delta]Np73[alpha] regulates MDR1 expression by inhibiting p53 function. Oncogene 2007; 27:2170-6.
54. Bush JA, Li G. Regulation of the Mdr1 isoforms in a p53-deficient mouse model. Carcinogenesis 2002; 23:1603-7.
55. Johnson RA, Inoe TA, Scoon KW. Transcriptional Repression by p53 through Direct Binding to a Novel DNA Element. J Biol Chem 2001; 276:27716-20.
56. Cintia SDB, Stephen CP, De-Quan L. Cell Size Correlates with Phenotype and Proliferative Capacity in Human Corneal Epithelial Cells. Stem Cells 2006; 24:368-75.

57. Marion RM, Strati K, Li H, Murga M, Blanco R, Ortega S, et al. A p53-mediated DNA damage response limits reprogramming to ensure iPS cell genomic integrity. Nature 2009; 460:1149-53.
58. Utikal J, Polo JM, Stadtfeld M, Maherali N, Kulalert W, Walsh RM, et al. Immortalization eliminates a roadblock during cellular reprogramming into iPS cells. Nature 2009; 460:1145-8.
59. Kawamura T, Suzuki J, Wang YV, Menendez S, Morera LB, Raya A, et al. Linking the p53 tumour suppressor pathway to somatic cell reprogramming. Nature 2009; 460:1140-4.
60. Hong H, Takahashi K, Ichisaka T, Aoi T, Kanagawa O, Nakagawa M, et al. Suppression of induced pluripotent stem cell generation by the p53-p21 pathway. Nature 2009; 460:1132-5.
61. Li H, Collado M, Villasante A, Strati K, Ortega S, Canamero M, et al. The Ink4/Arf locus is a barrier for iPS cell reprogramming. Nature 2009; 460:1136-9.

Appendix 3 - Circulating Tumor Cells and Colorectal Cancer

Joshua E. Allen[1] and Wafik S. El-Deiry[2]

(1) Penn State Hershey Cancer Institute, 500 University Drive, T3315, Hershey, PA 17033, USA

(2) Hematology/Oncology Division, Penn State Hershey Medical Center and Cancer Institute, 500 University Drive, Room T4423, Hershey, PA 17033, USA

Abstract

The significance of circulating tumor cells (CTCs) has been discussed for more than a century. The advent of modern technology has allowed for more reliable detection of CTCs, and recent studies have provided compelling evidence that CTCs predict clinical response in metastatic colorectal cancer (mCRC). Combination of CTC analysis with independent prognostic factors has demonstrated powerful synergy in some studies. The ability of CTCs to predict metastasis and therapy-specific response has high potential clinical utility, with early studies showing promising results in colorectal cancer (CRC). Reliable CTC detection has also allowed for examination of tumor cell dissemination during surgery, and there appears to be a heavy dependence on the approach chosen. This review discusses the evidence for CTC significance, with particular focus on detection methods, novel markers, and clinical outcomes in CRC. Numerous opportunities exist for preclinical, clinical, and translational studies to explore molecular determinants within CTCs, as well as the value of CTCs in directing targeted therapeutics.

Keywords Circulating tumor cells - Colorectal cancer - CRC - Colon cancer - Rectal cancer - CTC detection - CTC enrichment - Stratification - Prognosis - Overall survival - Progression-free survival - Clinical response - Hepatic resection - Liver resection - Hepatic ablation - Hepatic metastasis - Liver metastasis - Cytokeratin - Tumor cell dissemination - Epithelial cell adhesion molecule - EpCAM - Survivin - Cetuximab - *KRAS*

Introduction

Colorectal cancer (CRC) remains the third most common cancer in the United States, with an overall 5-year survival rate of 64%, which has risen significantly in the past several decades [*1*]. The stage of diagnosis is the chief variable dictating this statistic. Nineteen percent of patients with CRC are diagnosed with an advanced stage, decreasing their 5-year survival rate to 11% [*1*]. This highlights the need for improved accessibility and reliability for diagnosis of CRC at earlier stages. Currently, reliable diagnostic techniques include colonoscopy, sigmoidoscopy, and CT, as well as the more costly CT virtual colonoscopy. Development of reliable diagnostic methods that are relatively inexpensive and less invasive may allow for earlier-stage diagnosis and significantly raise survival rates. Furthermore, identification of subgroups of patients who would benefit from adjuvant therapy is a high priority. This has been underscored within the past decade in CRC by patient response to cetuximab being determined by *KRAS* mutational status of the tumor [*2*]. In advanced-stage disease, the availability of circulating tumor cells (CTCs) may allow for better disease monitoring, especially in patients with metastatic CRC (mCRC) who do not have any measurable increase in carcinoembryonic antigen (CEA) or other markers.

The first clinical suggestion that metastasis might arise from primary tumor cells by intravasation has been traced to postmortem clinical observations by Ashworth [*3*] in 1869. This idea regained attention almost a century later when Engell [*4*] found evidence of CTCs in live cancer patients. However, follow-up studies by Engell [*5*] and others [*6*] found no correlation between survival and the number of tumor cells in the blood, likely because of poor cytologic criterion largely founded on cell morphology and size. Technological advances in subsequent years have increased the ability to accurately and reliably detect CTCs. Detection technology now includes reverse transcriptase polymerase chain reaction (RT-PCR), immunomagnetic separation, microchips, and several others that have been reviewed recently [*7* •].

The CellSearch System (Veridex LLC, Raritan, NJ) gained approval from the US Food and Drug Administration (FDA) in 2004 for metastatic breast cancer and is now also approved for

metastatic prostate and colorectal cancer. This remains the only CTC detection method to have received FDA approval. Under this detection method, CTCs must possess the following properties: a round to oval shape by light scatter, an evident nucleus by 4′,6-diamidino-2-phenylindole (DAPI) staining, epithelial cell adhesion molecule positivity ($EpCAM^+$), and cytokeratin (CK)-8^+, -18^+, -19^+, and $CD45^-$ by immunofluorescence. This method is more efficient in sample size and processing time than other CTC enrichment methods, except for the CTC chip. However, it is limited by its requirement of EpCAM expression and therefore potentiates false-negative results. Nevertheless, this technology has allowed for reliable detection of CTCs (approximately 80–85% recovery of spiked samples) [*8*, *9*]. Studies using this technology have established CTCs as an independent prognostic indicator in metastatic breast cancer [*9*, *10*], castration-resistant prostate cancer [*11*], and mCRC [*12*••]. This review summarizes recent findings regarding CTCs in the clinic as a prognostic factor, novel efforts to improve CTC identification and enumeration, and the effect of resection on CTCs in the context of CRC. Figure 1 outlines CTC detection techniques and identification markers along with a putative CTC schematic for CRC. In the realm of preclinical and translational research, CTCs offer an exciting opportunity to explore new technologies for the recovery of live metastasis-initiating cells. The introduction of molecular characterization is expected to lead to important advances of relevance to prognostication and personalized therapy.

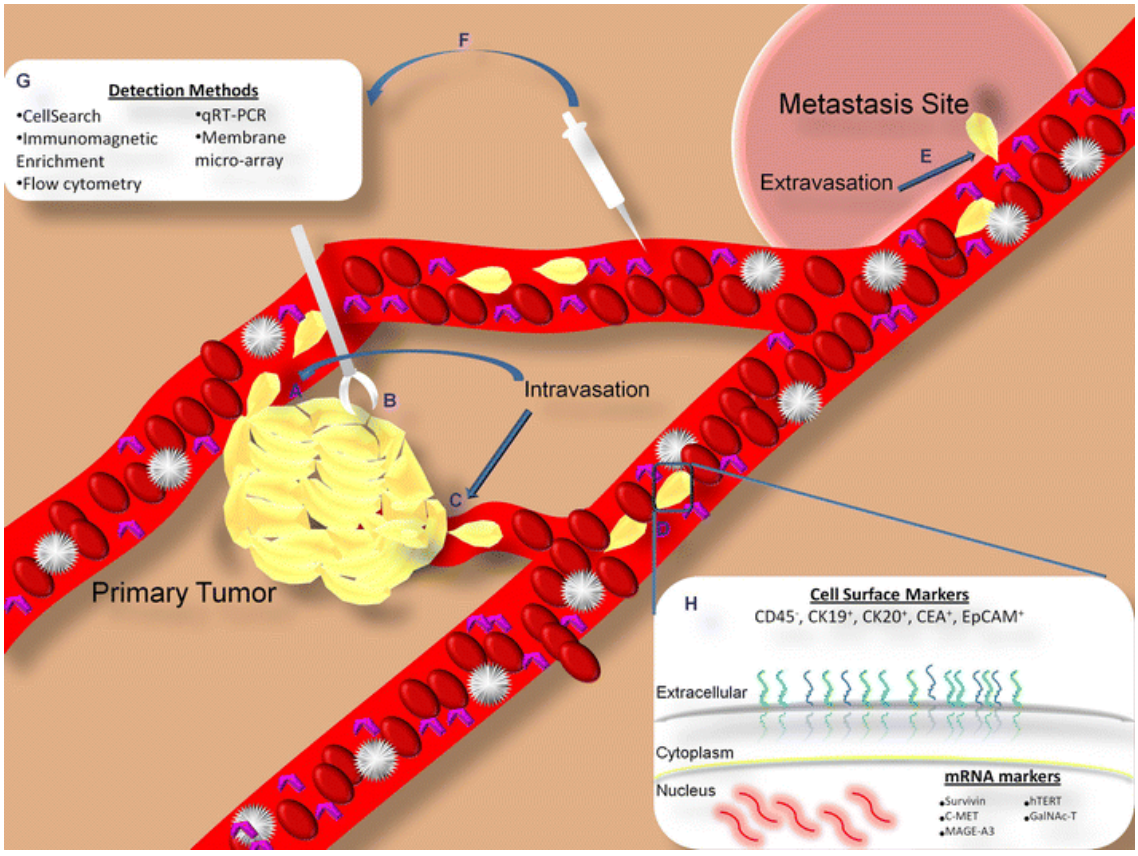

Fig. 1 Circulating tumor cell (CTC) generation, identification, and detection. CTCs are shed from the primary tumor and intravasate by several possible mechanisms: direct shedding into existing blood vessels*(A)*, mechanical disruption (eg, resection; *[B]*), or shedding into angiogenic capillaries *(C)*. CTCs then travel through the bloodstream *(D)* and later extravasate at a potential site of metastasis *(E)*. CTCs can be detected in peripheral blood by collection *(F)* using a variety of methods *(G)*. Published markers for CTCs in colorectal cancer are listed *(H)*. CellSearch is a registered trademark of Veridex LLC, Raritan, NJ. qRT-PCR, quantitative reverse transcriptase polymerase chain reaction

---

Prognostic Value in the Clinic

An early study by Sastre et al. [*13*] found the CellSearch system could identify CTCs in CRC patients and that CTC positivity correlated with disease stage ($P = 0.005$). No significant

correlation was found between tumor location, grade of differentiation, CEA levels, or lactate dehydrogenase (LDH) levels. A meta-analysis of nine studies conducted between 1998 and 2006 showed that CTC-positive patients, as detected by RT-PCR methods in blood samples collected from the tumor's draining vein, correlated with lymph node (LN)-positive patients (50%) versus LN-negative patients (21%) [*14*]. Furthermore, hepatic metastasis was found more often in CTC-positive patients (21%) than in CTC-negative patients (8%). These early reports demonstrated the feasibility and potential prognostic value of CTCs in CRC, allowing for larger-scale studies (Table 1).

Table 1 Clinical studies evaluating circulating tumor cells as a prognostic tool

Study	Inclusion criteria	Patients, *n*	CTC enumeration method	CTC positive threshold	Parameters examined	Main conclusion
Cohen et al. [*12*••]	mCRC initiating first-, second-, or third-line therapy with an EGFR inhibitor	430	CellSearch[a]	≥3/7.5 mL	Line of therapy, tumor type, ECOG PS, site of metastasis, CTC evaluation time point, PFS, OS	CTC number is an independent predictor of PFS and OS in mCRC
Cohen et al. [*15*••]	mCRC initiating first-, second-, or third-line therapy with an EGFR inhibitor	430	CellSearch	≥3/7.5 mL	Line of therapy, therapy choice, age, ECOG PS, PFS, OS	CTC prediction of PFS and OS is stronger in some treatment groups and subtypes
Garrigós et al. [*17*•]	Stage II or III CRC undergoing curative resection	16	Immunomagnetic beads or centrifugation enrichment followed by RT-PCR or FC	–	Detection method, relapse	Immunomagnetic enrichment and FC are the most efficient CTC detection methods; relapse in CRC may be correlated with CTC level
Katsuno et al. [*14*]	Curative surgery for CRC, blood collection from venous	646	RT-PCR	–	LN, disease stage, hepatic metastasis	CTC levels correlate to LN positivity and disease stage

Study	Inclusion criteria	Patients, *n*	CTC enumeration method	CTC positive threshold	Parameters examined	Main conclusion
	drainage of tumor at time of surgery					
Papavasiliou et al. [*33*]•]	CRC with hepatic metastases treatable with liver resection or tumor ablation, intact primary tumor	20	CellSearch	≥3/7.5 mL	Fong score, disease status, liver procedure, PFS, OS	Postoperative CTC may predict prognosis
Sastre et al. [*13*]	CRC, no preoperative chemo- or radiotherapy	127	CellSearch	≥3/7.5 mL	Disease stage, tumor location, differentiation, CEA and LDH levels	Reproducible CTC levels but correlated only with disease stage
Schmidt et al. [*23*]	>18 years old, eligible for hepatic resection by conventional and anterior approaches, no extrahepatic disease, liver cirrhosis, or positive LN	150	CK20 RT-PCR	–	Resection approach, OS, other parameters related to the surgery	Ongoing; primary aim is to conclude on tumor cell dissemination by conventional vs anterior hepatic resection
Tol et al. [*16*]	CRC with irresectable distant metastasis, ≥1 measurable disease parameter, WHO PS of 0 or 1, adequate organ functions	467	CellSearch	≥3/7.5 mL	CTC time point, CT imaging, PFS, OS	CTC number is an independent predictor of PFS and OS in mCRC; combination with CT imaging predicts OS more strongly
Tralhão et al. [*34*]	CRC	40	FC ($CD45^{-}$,CK^{+})	–	CTC levels influenced by surgery	No significant difference in CTC by surgical intervention

CEA carcinoembryonic antigen, *CK* cytokine, *CRC* colorectal cancer, *CTC* circulating tumor cell, *ECOG PS* Eastern Cooperative Oncology Group performance status, *EGFR* epidermal growth factor receptor,*FC* flow cytometry, *mCRC* metastatic CRC, *EGFR* epidermal growth factor receptor, *LDH* lactate dehydrogenase, *LN* lymph node, *OS* overall survival, *PFS* progression-free survival, *RT-PCR* reverse transcriptase polymerase chain reaction, *WHO PS* World Health Organization performance status

[a]Registered trademark of Veridex LLC, Raritan, NJ

Cohen et al. [*15*••] published one of the largest clinical studies of CTCs in mCRC involving 430 mCRC patients at 55 clinical centers in the United Kingdom, the Netherlands, and the United States. Patients were qualified for the study if initiating a new first-, second-, or third-line (with an epidermal growth factor receptor inhibitor) systemic therapy. Patients had peripheral blood collected before treatment initiation and at four time points after treatment initiation. For analysis, patients were grouped into favorable (<3 CTCs/7.5 mL blood) or unfavorable (≥3 CTCs/7.5 mL blood).

The study showed that median progression-free survival (PFS) and overall survival (OS) rates were approximately twice as high for patients in the favorable group based on low CTCs (PFS, 7.9 mo; OS, 18.5 mo) relative to the unfavorable group with elevated CTCs (PFS, 4.5 mo; OS, 9.4 mo) as determined at baseline. Importantly, this significance held to a similar extent when grouping was assigned by CTC count at any evaluated time point. Regardless of change to favorable or unfavorable, patients who switched their group classification 3 to 5 weeks after treatment initiation had a median OS between those of the baseline unfavorable and favorable groups. However, these patients maintained a PFS very close to the favorable group. A multivariate analysis of several significant factors (eg, CTC count, age, line of therapy) found that CTC number was a strong independent predictor of PFS and OS ($P \leq 0.001$) regardless of assessment time point. Interestingly, the study found a significant prognostic synergy between patient grouping by imaging response and CTCs. If patients continued to have elevated CTC counts for prolonged periods after therapy, this was associated with a worse prognosis.

Slightly more than a year later, Cohen et al. [*15*••] published a follow-up study with extended follow-up time points and expanded analyses using the same grouping described earlier [*12* ••]. The difference in PFS and OS between favorable and unfavorable groups was more pronounced in patients receiving first-line therapy than in second- and third-line therapy patients. OS was prolonged in the favorable group relative to the unfavorable group regardless of whether they were receiving oxaliplatin, bevacizumab, or irinotecan, but PFS was increased only in the latter. The change in OS with baseline CTCs seems independent of age, and the change in PFS is not statistically different between CTC groups with patients older or younger than 65 years old. Eastern Cooperative Oncology Group performance status (ECOG PS) had no large effect on the significant difference of OS in the favorable and unfavorable CTC groups. However, the difference in PFS between favorable and unfavorable CTC groups was insignificant in patients with an ECOG PS of 1 or 2. An updated multivariate analysis reconfirmed baseline CTC number as an independent factor in PFS and even more so in OS.

Together, the two analyses of these mCRC patients by Cohen et al. [*12*••, *15*••] demonstrate that CTCs correlate significantly with PFS, and even more so OS, after treatment or at baseline, regardless of age, previous treatment, or disease stage. These data strongly argue for the use of CTCs as an independent prognostic factor in mCRC that may be combined with other factors to improve assessment, as demonstrated with radiographic imaging in the earlier publication.

The largest published mCRC CTC study to date involved 467 patients who received capecitabine, oxaliplatin, and bevacizumab as first-line therapy [*16*]. Half the patients also received cetuximab. Twenty-nine percent of patients had high CTCs (≥3 CTCs/75. mL blood) and were also more likely to have stage IV disease, to not have received adjuvant chemotherapy, and to have abnormal serum LDH levels relative to other enrolled patients. Patients with hepatic metastasis only or metastasis to additional organs had elevated CTC levels (33%) relative to other patients (12%). The study confirmed previous findings by Cohen et al. [*12*••, *15*••] that higher CTC count at baseline or 1 to 2 weeks after treatment correlated with prolonged PFS and OS in both treatment groups.

Patients who converted from the low- to high-CTC group between baseline and a follow-up time point had significantly different median PFS and OS rates, between those of consistently high- and low-CTC patients. Previously, Cohen et al. [*12*••, *15*••] published data demonstrating that patients meeting this criterion had a median PFS similar to that of consistently CTC-negative patients. This difference might be the result of slight differences in CTC group classification time point or, more likely, patient treatment history. CTC count after 1 to 2 weeks of treatment appeared to have stronger-than-expected correlations with response by CT compared with baseline CTC count. In support of findings by Cohen et al. [*12*••, *15*••], CTC level and Response Evaluation Criteria in Solid Tumors (RECIST) classification by imaging (eg, CT) synergistically predicted OS.

The possibility that CTCs might predict metastasis before detection by conventional methods has considerable impetus. Garrigós et al. [*17* •] conducted a small-scale study to measure CTCs in 16 patients with stage III and IV CRC. The authors used immunomagnetic beads for EpCAM and subsequent flow cytometry to identify $CD45^-$ and $CK7^+$ or $CK8^+$ cells, as it was more sensitive at CTC detection and enumeration than other available methods. The authors of this study did not examine CellSearch for their comparison. Two of the 16 patients had tumor relapse following resection and had elevated CTCs before relapse relative to the patients without tumor relapse. The use of CTCs as a predictor of metastasis would be a powerful clinical tool; therefore, a study with standardized CTC detection methods and a large sample size is warranted.

The Search for New Markers

Although effort is being made to validate current CTC identification technology, several novel markers have been identified (Table 2). Markers of therapy-specific response are very useful for adjuvant therapy stratification. For instance, Ronzoni et al. [*18*] evaluated response to bevacizumab in CRC patients and the utility of circulating endothelial cells (CECs) and endothelial progenitor cells as response predictors. Resting CECs, defined as $CD45^-$, $CD146^+$, $CD34^+$, and $CD106^-$, had the greatest enrichment in CRC patients relative to benign controls.

Baseline CTCs had a strong correlation with response and PFS. No significant changes were found in the evaluated cell levels throughout treatment.

Table 2 Novel methods for circulating tumor cell identification and main conclusion(s)

Study	CTC enumeration method	Main conclusion
Antolovic et al. [*31*•]	Immunomagnetic enrichment and CK20 RT-PCR	The clone used as an antibody for EpCAM-based enrichment alters results significantly
Chen et al. [*28*]	KRAS membrane array	KRAS membrane array is sensitive and specific when used on CRC blood samples.
Findeisen et al. [*19*]	346 candidate genes	*SERPINB5* expression is elevated in CRC blood
Gervasoni et al. [*25*]	CK20, CK19, CEA, and GCC RT-PCR	CTCs can be predicted by CK20, CK19, CEA, and GCC together
Königsberg et al. [*27*]	MACS HEA MicroBeads,[a] RosetteSep,[b] density centrifugation	EpCAM-coupled antibodies are a better detection method than cytometric methods
Konyanagi et al. [*24*]	CK20 IHC and c-MET, MAGE-A3, hTERT, and GalNAc-T qRT-PCR	CK20 IHC and qRT-PCR strongly predict DFS
Shen et al. [*26*]	Survivin, CK20, CEA qRT-PCR	CK20 and CEA mRNA correlates with disease stage and LN
Uen et al. [*32*]	hTERT, CK19, CK20, and CEA RT-PCR	Persistently elevated CTCs, LN, and vascular invasion are independent predictors of postoperative relapse
Wong et al. [*22*]	CK20 positive, cell morphology, and cell size	CK20 may be detected in CRC patients and is associated with disease status and LN
Yang et al. [*30*]	*KRAS* membrane array	Can detect down to three colon tumor cells/mL of blood with membrane array
Yen et al. [*29*•]	*KRAS* membrane array	*KRAS* mutation status in CTCs predicts response to cetuximab and affects PFS and OS
Yie et al. [*20*]	Survivin RT-PCR ELISA	Survivin is elevated in CRCs and correlated with metastasis

CEA carcinoembryonic antigen, *CK* cytokine, *CRC* colorectal cancer, *CTC* circulating tumor cell, *DFS* disease-free survival, *ELISA* enzyme-linked immunosorbent assay, *EpCAM* epithelial cell adhesion molecule, *GalNAc-T* β-1,4-*N*-acetylgalactosaminyltransferase, *GCC* guanylyl cyclase C, hTERT human telomerase reverse transcriptase, IHC immunohistochemistry, LN lymph node, MAGE-A3 melanoma-associated antigen 3, OS overall survival, PFS progression-

free survival, qRT-PCR quantitative RT-PCR, RT-PCR reverse transcriptase polymerase chain reaction

[a]Registered trademark of Miltenyi Biotec, Auburn, CA

[b]Registered trademark of StemCell Technologies, Vancouver, Canada

Substantial evidence is emerging for detection of upregulated mRNA in patient blood samples and its correlation with CTCs and prognosis. Findeisen et al. [*19*] screened 346 genes that are upregulated and found *SERPINB5* to be significantly upregulated in patients with elevated CTCs compared with benign controls. This elevation was detected in cell-spiking experiments and validated in patient blood samples. Future work with *SERPINB5* should determine whether it is differentially expressed in mCRC and if any prognostic value can be gained. Yie et al. [*20*] have shown that survivin mRNA detected by RT-PCR enzyme-linked immunosorbent assay was correlated with the disease stage of CRC patients. Approximately half the CRC patients tested positive for survivin expression, and half of these patients eventually suffered relapse. Survivin expression was also shown to be a better risk factor ($P = 0.048$) for relapse than age, gender, disease stage, tumor penetration, nodal status, or plasma CEA.

Another study, by Wong et al. [*21*], found CK20 expression in LNs and blood of CRC patients. A follow-up study found that CK20-positive CTCs in CRC patients predicted metastasis ($P < 0.001$) and had a highly significant impact on OS ($P < 0.0001$) [*22*]. A randomized trial is being conducted to detect CTC levels by RT-PCR for CK20 and the impact of conventional versus anterior hepatic resection in mCRC patients [*23*]. The consequences of resection technique on tumor cell dissemination are discussed later in this review.

Koyanagi et al. [*24*] found that for LNs, CK immunohistochemistry (IHC; 30%) or measurement of CK blood levels by quantitative RT-PCR (qRT-PCR; 60%) was superior to conventional pathologic LN examination by hematoxylin and eosin staining (17%) in detecting relapse in 12 relapsed CRC patients. CK IHC and qRT-PCR together identified 70% of relapsed patients.

Combining mRNA markers for c-MET, melanoma-associated antigen 3 (MAGE-A3), β-1,4-*N*-acetylgalactosaminyltransferase (GalNAc-T), and CK20 showed a significant difference in PFS ($P = 0.014$), but not OS, in the same patients.

Because of the overwhelming diversity within tumors, it is unlikely that any single marker will yield optimal identification fidelity. Gervasoni et al. [*25*] published a preliminary report on the use of molecular signatures by RT-PCR to identify patients using epithelial-specific genes. CK20, CK19, CEA, and guanylyl cyclase G (CGG) were shown to identify cancer patients versus healthy patients. Shen et al. [*26*] showed that CK20, survivin, and CEA levels were all independently higher by qRT-PCR in CRC patients versus normal controls. Moreover, all Dukes stages were also found to correlate with survivin ($P < 0.001$), CK20 ($P = 0.011$), or CEA ($P < 0.001$) mRNA levels. Although these markers had increased sensitivity when combined, no data were shown for the markers in combination and their ability to predict any clinical outcomes. Future studies aiming to identify novel markers should corroborate the clinical significance using conventional detection methods (eg, CellSearch) and test in combination with conventional methods.

Improving CTC Detection Methods

With the availability of several methods for identification and enumeration of CTCs, investigators are faced with a difficult choice. Many methods that have higher sensitivity sacrifice accuracy and precision. Königsberg et al. [*27*] compared different nonautomated detection methods for CTC enrichment, including two density centrifugation methods, a density centrifugation and antibody-based method, and an immunomagnetic technique. Immunomagnetic enrichment using MACS HEA Microbeads (Miltenyi Biotec, Auburn, CA) that bind EpCAM had a superior recovery rate than the other methods in cell-spiking experiments and patient samples. CTC levels of ≥1 CTCs per 7.5 mL of blood were significantly correlated with PFS but not with OS. This disparity with other findings might be a result of shorter follow-up time points, a difference in CTC group

threshold numbers, a difference in detection methods, or patient composition, as this study included mCRC patients without specifying other factors.

A high-throughput method for detection of *KRAS* mutations by a membrane array has been developed [*28*] and recently applied in the clinic to mCRC patients treated with cetuximab and FOLFOX4 (oxaliplatin + leucovorin + fluorouracil) or FOLFIRI (leucovorin + fluorouracil + irinotecan) [*29* •]. This technique is carried out by amplification of total RNA from peripheral blood, cDNA synthesis, hybridization to membrane arrays, and quantification of resultant spot intensities. A strong correlation existed between *KRAS* mutation status in the tumor and that of peripheral blood samples using the membrane array, with high sensitivity (84.8%) and high specificity (95.3%). As expected, mutant *KRAS* in primary tumor samples correlated strongly with lack of response to cetuximab. This strong response correlation was extended to mutant *KRAS* detection in peripheral blood by the membrane array ($n = 86$; $P < 0.0001$). A multivariate analysis yielded a strong *KRAS* mutational status correlation with PFS and OS if detected in the tumor or in peripheral blood ($n = 86$; $P < 0.0001$).

This technique has been updated to utilize chemiluminescence to increase sensitivity [*30*]. Although the clinical study suggests a strong correlation with *KRAS* mutation status in the primary tumor and the peripheral blood, it cannot conclude that CTCs are the source. This is the case for all purely mRNA-based detection methods. Future experiments should determine whether the source of mutant *KRAS* in the peripheral blood is truly CTCs but may be complicated by limitations of current CTC enrichment methods. On the contrary, this may be an advantage, as this technique does not rely on selection techniques based on markers commonly used for CTC enrichment (eg, EpCAM).

Antolovic et al. [*31* •] recently reported on the importance of the chosen EpCAM epitope in antibody-based selection and its impact on CTC count. The study showed that the use of two different antibodies resulted in disparate CTC detection by a CK20 RT-PCR assay. Although RT-PCR may be more sensitive to error than multiparametric detection systems such as CellSearch,

EpCAM remains a widely used, exclusive selection factor in isolating CTCs. As such, evaluation of the significance of CTC detection dependency on EpCAM epitopes is warranted.

The Impact of Resection on CTCs

Disturbing tumor cells mechanically and causing shedding of tumor cells during resection have long been a concern. The question of whether these tumor cells remain viable and what they subsequently may do is still largely unanswered. CTC detection has allowed investigators to begin to reliably quantify this phenomenon. Uen et al. [*32*] published a large-scale study involving stage III and IV CRC patients undergoing curative resection. This study found that postoperative relapse was strongly correlated with LN metastases ($P < 0.001$), as well as CTC level if elevated at pre- and postoperative time points. Pre- and postoperative CTC levels were not analyzed separately as a predictor of relapse, but depth of invasion ($P = 0.032$), vascular invasion ($P = 0.001$), and perineural invasion ($P = 0.013$) were also found to predict relapse, although to a lesser extent. It should be noted that this study used a membrane array to detect human telomerase reverse transcriptase, CK19, CK20, and CEA mRNA levels for detecting CTCs.

Hepatic metastases in CRC were explored in a 20-patient study monitoring CRC patients before, during, and after resection or radiofrequency ablation (RFA) [*33*•]. This study found that preoperative and intraoperative CTC levels did not predict OS. Postoperative levels were predictive of OS and disease-free survival. It should be noted that the statistical analysis was performed using absolute CTC levels in contrast to the common categorical analysis by a threshold number of CTCs. An important observation is the sevenfold increase in intraoperative CTCs compared with preoperative levels. This enrichment was found to be in patients who underwent RFA (mean, 27 cells/7.5 mL blood) rather than resection (mean, 3 cells/7.5 mL blood). This finding is an important consideration in selecting a hepatic resection procedure in light of tumor dissemination. A lack of significant elevated CTC levels during resection also was reported by another study in patients with primary CRC or mCRC [*34*]. It should be noted that this study

analyzed CTCs by flow cytometry and did not use EpCAM as a selection criterion. Future studies should examine the clinical impact of significant tumor cell dissemination by RFA. As a whole, the literature strongly suggests that the choice of resection method plays a key role in tumor cell dissemination, but the consequence of this is unclear.

Conclusions

In the 1950s, CTC levels were observed in equal number in cancer patients with or without relapse and deemed useless as a prognostic factor. Today, CTC detection by CellSearch is FDA approved for patient prognosis in metastatic breast, prostate, or colorectal cancer. Clearly, future advancements in accurate detection of CTCs will be essential in assessing the utility of CTC levels as a patient prognostic factor. Detailed analyses of isolated CTCs need to be conducted to elucidate what properties are unique to these cells. For instance, do CTCs express epithelial–mesenchymal transition markers (eg, vimentin, twist, fibronectin)? Are the CTCs detected viable? Isolation of viable CTCs should be pursued for ex vivo analysis and in vivo investigation in animals models. Identification of CTC-specific properties may provide opportunities for therapeutic exploitation. For instance, insight could be gained from comparisons of disseminated tumor cells to intrinsic CTCs (eg, expression profiling). As for surgical method decisions in mCRC involving the liver, it is clear that RFA increases CTCs during the procedure. Data must be gathered on whether the disseminated tumor cells change clinical outcome.

The relationship of cancer stem cells (CSCs) with CTCs is entirely unclear at this point. In theory, CTCs must have tumor-initiating properties of CSCs but have additional intravasation and extravasation properties. Preliminary experiments should focus on the overlap with markers of CSCs and their levels in CTCs (ie, $CD133^+$). A recent finding indicates that a $CD26^+$subpopulation of $CD133^+$ CRC cells have unique metastatic potential in CRCs [*35*]. More specifically, this subpopulation exclusively forms liver metastasis when injected into the cecal wall

of mice. Furthermore, preliminary data from small groups of patients suggest that this marker may be useful in predicting metastasis.

Future efforts to improve CTC detection should explore the possibility of low EpCAM expression by CTCs, as this has been noted in epithelial–mesenchymal transitions, a process that CTCs may undergo during early stages of metastasis. The two large-scale patient studies by Cohen et al. [*12*••, *15*••] and Tol et al. [*16*] firmly place CTCs as an indicator of prognosis in mCRC. Examination of treatment regimen on CTC levels and the response of patients should be further explored to index therapeutic effects. Efforts to explore the role of CTCs in prediction of metastasis, as initiated by Garrigós et al. [*17*•], are highly warranted. Proof of CTCs as an indicator of future metastasis would be an extremely valuable tool in the clinic. With the available clinical data, CTC level should be incorporated with other traditional prognostic indicators to provide the best assessment possible for therapy stratification. The proven utility of CTCs needs to be integrated into clinics rather than viewed as a work in progress. In the spirit of Stephen Paget's metastasis model [*36*], which prevails more than a century later [*37*], with much effort we have found the "seeds"; now let us go to the field and stop them from being planted in the "soil."

Papers of particular interest, published recently, have been highlighted as: • Of importance •• Of major importance

1. Jemal A, Siegel R, Ward E, et al.: Cancer Statistics, 2009. CA Cancer J Clin 2009, 59:225–249

2. Lievre A, Bachet JB, Le Corre D, et al.: KRAS mutation status is predictive of response to cetuximab therapy in colorectal cancer. Cancer Res 2006, 66:3992–3995.

3. Ashworth T: A case of cancer in which cells similar to those in the tumours were seen in the blood after death. Aust Med J 1869.

4. Engell HC: Cancer cells in the circulating blood: a clinical study on the occurrence of cancer cells in the peripheral blood and in venous blood draining the tumour area at operation. Ugeskr Laeger 1955, 117:822–823.

5. Engell HC: Cancer cells in the blood: a five to nine year follow up study. Ann Surg 1959, 149:457–461.

6. Roberts S, Jonasson O, Long L, et al.: Clinical significance of cancer cells in the circulating blood: two to five-year survival. Ann Surg 1961, 154:362–370.

7. • Negin B, Cohen S: Circulating tumor cells in colorectal cancer: past, present, and future challenges. Curr Treat Options Oncol 2010 Feb 9 (Epub ahead of print)]. *This concise review describes current detection methods for CTCs*.

8. Allard WJ, Matera J, Miller MC, et al.: Tumor cells circulate in the peripheral blood of all major carcinomas but not in healthy subjects or patients with nonmalignant diseases. Clin Cancer Res 2004, 10:6897–6904.

9. Riethdorf S, Fritsche H, Müller V, et al.: Detection of circulating tumor cells in peripheral blood of patients with metastatic breast cancer: a validation study of the CellSearch System. Clin Cancer Res 2007, 13:920–928.

10. Hayes DF, Cristofanilli M, Budd G, et al.: Circulating tumor cells at each follow-up time point during therapy of metastatic breast cancer patients predict progression-free and overall survival. Clin Cancer Res 2006, 12:4218–4224.

11. Danila DC, Heller G, Gignac GA, et al.: Circulating tumor cell number and prognosis in progressive castration-resistant prostate cancer. Clin Cancer Res 2007, 13:7053–7058.

12. •• Cohen SJ, Punt CJA, Iannotti N, et al.: Prognostic significance of circulating tumor cells in patients with metastatic colorectal cancer. Ann Oncol 2009, 20:1223–1229. *This was the first large-scale mCRC patient study examining CTCs. CTC level was shown to correlate with PFS and OS*.

13. Sastre J, Maestro ML, Puente J, et al.: Circulating tumor cells in colorectal cancer: correlation with clinical and pathological variables. Ann Oncol 2008, 19:935–938.

14. Katsuno H, Zacharakis E, Aziz O, et al.: Does the presence of circulating tumor cells in the venous drainage of curative colorectal cancer resections determine prognosis? A meta-analysis. Ann Surg Oncol 2008, 15:3083–3091.

15. •• Cohen SJ, Punt CJA, Iannotti N, et al.: Relationship of circulating tumor cells to tumor response, progression-free survival, and overall survival in patients with metastatic colorectal cancer. J Clin Oncol 2008, 26:3213–3221. *This extended analysis of a previous study provides updated follow-up time points. The impact of CTCs on prognosis is examined in several subgroups of patients*.

16. Tol J, Koopman M, Miller MC, et al.: Circulating tumour cells early predict progression-free and overall survival in advanced colorectal cancer patients treated with chemotherapy and targeted agents. Ann Oncol 2009, 21:1006–1012

17. • Garrigós N, Gallego J, Guillén-Ponce C, et al.: Circulating tumour cell analysis as an early marker for relapse in stage II and III colorectal cancer patients: a pilot study. Clin Transl Oncol 2010, 12:142–147. *This small study demonstrated the potential of CTCs to predict metastasis in CRC*.

18. Ronzoni M, Manzoni M, Mariucci S, et al.: Circulating endothelial cells and endothelial progenitors as predictive markers of clinical response to bevacizumab-based first-line treatment in advanced colorectal cancer patients. Ann Oncol 2010 May 23 (Epub ahead of print).

19. Findeisen P, Matthias R, Matthias N, et al.: Systematic identification and validation of candidate genes for detection of circulating tumor cells in peripheral blood specimens of colorectal cancer patients. Int J Oncol 2008, 33:1001–1010.

20. Yie SM, Lou B, Ye S, et al.: Detection of survivin-expressing circulating cancer cells (CCCs) in peripheral blood of patients with gastric and colorectal cancer reveals high risks of relapse. Ann Surg Oncol 2008, 15:3073–3082.

21. Wong CSC, Cheung MT, Ma BBY, et al.: Isolated tumor cells and circulating CK20 mRNA in pN0 colorectal cancer patients. Int J Surg Pathol 2008, 16:119–126.

22. Wong SCC, Chan CML, Ma BBY, et al.: Clinical significance of cytokeratin 20-positive circulating tumor cells detected by a refined immunomagnetic enrichment assay in colorectal cancer patients. Clin Cancer Res 2009, 15:1005–1012.

23. Schmidt T, Koch M, Antolovic D, et al.: Influence of two different resection techniques (conventional liver resection versus anterior approach) of liver metastases from colorectal cancer on hematogenous tumor cell dissemination—prospective randomized multicenter trial. BMC Surg 2008, 8:6.

24. Koyanagi K, Bilchik AJ, Saha S, et al.: Prognostic relevance of occult nodal micrometastases and circulating tumor cells in colorectal cancer in a prospective multicenter trial. Clin Cancer Res 2008, 14:7391–7396.

25. Gervasoni A, Monasterio Muñoz RM, Wengler GS, et al.: Molecular signature detection of circulating tumor cells using a panel of selected genes. Cancer Lett 2008, 263:267–279.

26. Shen C, Hu L, Xia L, et al.: Quantitative real-time RT-PCR detection for survivin, CK20 and CEA in peripheral blood of colorectal cancer patients. Jpn J Clin Oncol 2008, 38:770–776.

27. Königsberg R, Gneist M, Jahn-Kuch D, et al.: Circulating tumor cells in metastatic colorectal cancer: efficacy and feasibility of different enrichment methods. Cancer Lett 2010, 293:117–123.

28. Chen YF, Wang JY, Wu CH, et al.: Detection of circulating cancer cells with K-ras oncogene using membrane array. Cancer Lett 2005, 229:115–122.

29. • Yen LC, Yeh YS, Chen CW, et al.: Detection of KRAS oncogene in peripheral blood as a predictor of the response to cetuximab plus chemotherapy in patients with metastatic colorectal cancer. Clin Cancer Res 2009, 15:4508–4513. *This study demonstrated the clinical feasibility of a novel membrane array for detecting CTCs and the importance of KRAS in*

CTCs for predicting cetuximab response.

30. Yang MJ, Chiu HH, Wang HW, et al.: Enhancing detection of circulating tumor cells with activating KRAS oncogene in patients with colorectal cancer by weighted chemiluminescent membrane array method. Ann Surg Oncol 2010, 17:624–633.

31. • Antolovic D, Galindo L, Carstens A, et al.: Heterogeneous detection of circulating tumor cells in patients with colorectal cancer by immunomagnetic enrichment using different EpCAM-specific antibodies. BMC Biotechnol 2010, 10:35. *This study demonstrated the significant impact of CTC identification method on CTC enumeration*.

32. Uen YH, Lu CY, Tsai HL, et al.: Persistent presence of postoperative circulating tumor cells is a poor prognostic factor for patients with stage I–III colorectal cancer after curative resection. Ann Surg Oncol 2008, 15:2120–2128.

33. • Papavasiliou P, Fisher T, Kuhn J, et al.: Circulating tumor cells in patients undergoing surgery for hepatic metastases from colorectal cancer. Proc (Bayl Univ Med Cent) 2010, 23:11–14. *This study found that RFA significantly increases the level of intraoperative CTCs*.

34. Tralhão JG, Hoti E, Serôdio M, et al.: Perioperative tumor cell dissemination in patients with primary or metastatic colorectal cancer. Eur J Surg Oncol (EJSO) 2010, 36:125–129.

35. Pang R, Law WL, Chu ACY: A subpopulation of $CD26^{+}$ cancer stem cells with metastatic capacity in human colorectal cancer. Cell Stem Cell 2010, 6:603–617.

36. Paget S: The distribution of secondary growths in cancer of the breast. Lancet 1889, 1:571–572.

37. Fidler IJ: The pathogenesis of cancer metastasis: the ‘seed and soil’ hypothesis revisited. Nat Rev Cancer 2003, 3:453–458.

Appendix 4 - Identification and enumeration of circulating tumor cells in the cerebrospinal fluid of breast cancer patients with central nervous system metastases

Akshal S. Patel[1,2,*], Joshua E. Allen[1,3,*], David T. Dicker[1], Kristi L. Peters[1], Jonas M. Sheehan[2], Michael J. Glantz[2] and Wafik S. El-Deiry[1,3]

[1]Laboratory of Translational Oncology and Experimental Cancer Therapeutics, Department of Medicine (Hematology/Oncology), Penn State Hershey Cancer Institute, Penn State College of Medicine, Hershey, PA, USA

[2]Department of Neurological Surgery, Penn State Hershey Medical Center, Hershey, PA, USA

[3]Biochemistry and Molecular Biophysics Graduate Group, University of Pennsylvania School of Medicine, Philadelphia, PA, USA

[*]Denotes equal contribution

ABSTRACT

The number of circulating tumor cells (CTCs) in the peripheral blood of metastatic breast cancer patients is now an established prognostic marker. While the central nervous system is a common site of metastasis in breast cancer, the standard marker for disease progression in this setting is cerebrospinal fluid (CSF) cytology. However, the significance of CSF cytology is unclear, requires large sample size, is insensitive and subjective, and sometimes yields equivocal results. Here, we report the detection of breast cancer cells in CSF using molecular markers by adapting the CellSearch system (Veridex). We used this platform to isolate and enumerate breast cancer cells in CSF of breast cancer patients with central nervous system (CNS) metastases. The number of CSF tumor cells correlated with tumor response to chemotherapy and were dynamically associated with disease burden. This CSF tumor cell detection method provides a semi-automated molecular analysis that vastly improves the sensitivity, reliability, objectivity, and accuracy of detecting CSF tumor cells compared to CSF cytology. CSF tumor cells may serve as a marker of disease progression and early-stage brain metastasis in breast cancer and potentiate further molecular analysis to elucidate the biology and significance of tumor cells in the CSF.

INTRODUCTION

In the modern era of oncology, cancer-related mortality is associated with metastatic spread rather than the voraciousness of the primary tumor [4]. Tumor seeding in secondary tissues therefore presents a major challenge in cancer treatment [5]. Therapeutic strategies are often focused on tumor containment in lieu of concerns for tumor cell dissemination into surrounding structures. The enumeration of circulating tumor cells (CTCs) can monitor the metastatic potential of some solid tumors, relate these cells to patient survival, and provide a surrogate marker of treatment response [6, 7]. Giving rise to the "liquid biopsy", peripheral blood can be analyzed for the presence of CTCs using a range of techniques that are in various stages of development [8]. The CellSearch system is a CTC detection method that utilizes several molecular parameters to isolate CTCs: immunomagnetic enrichment for epithelial cell adhesion molecule (EpCAM), nuclear staining with 4', 6-diamidino-2-phenylindole (DAPI), and immunofluorescence detection of cytokeratin and CD45 [9]. Due to its demonstrated reliability and prognostic value, the CellSearch system is the only CTC detection platform approved by the US Food and Drug Administration (FDA) for the enumeration of CTCs in metastatic colorectal, prostate, and breast cancers.

The cerebrospinal fluid (CSF) is an important, unique, and poorly understood compartment of the central nervous system (CNS). CSF often acts as a biologic sump for neurons and glia and is continuously produced and recycled much like blood or lymph, though never filtered. Cells from solid tumors can infiltrate the CSF by several mechanisms including blood-brain barrier penetration by circulating cells, directly through tumor extension along Vichow-Robin spaces, or through patterned secondary structures of Scherer [10, 11]. Tumor cells within the CSF represent a special subpopulation of malignant cells that have proven their metastatic potential in peripheral blood and may be a source of a number of devastating neurologic sequelae. Current methods for examining the CSF involve pathological identification of abnormal cells by Wright-Giemsa stain. With this method there is no quantification or characterization of these cells and clinicians must make judgments on the binary presence or absence of malignant cells as determined by cytology

[12]. This is the gold standard but lacks molecular analysis and sensitivity, often requiring repeat testing or high volume analysis [13].

The prognosis and therapeutic stratification of patients with CNS metastases is currently based on the integration of histopathologic data, the appearance and severity of neurologic symptoms, and magnetic resonance imaging (MRI) of the neuroaxis [14]. To overcome limitations of currently available clinical parameters, we developed a reliable detection method to enumerate CSF tumor cells (CSFTCs) using molecular tumor cell markers by adapting the CellSearch system. This report describes this detection method and demonstrates the feasibility and significance of CTC detection in a pilot study of metastatic breast cancer patients with CNS metastases.

RESULTS

Selective detection of breast cancer cells

One of the diagnostic criteria for CTCs as defined by the CellSearch system is to be $EpCAM^{+}$. We found that human glioblastoma cells do not express EpCAM contrary to breast cancer cells as expected (Figure 1A). Accordingly, spiking these cultured cells into normal human blood revealed that the CellSearch system detects breast cancer cells but not glioblastoma cells (Figure 1B-C). This suggests that the CellSearch system could be used to detect cancer cells in the CSF that are not of glial origin and therefore those with metastatic potential to the CNS.

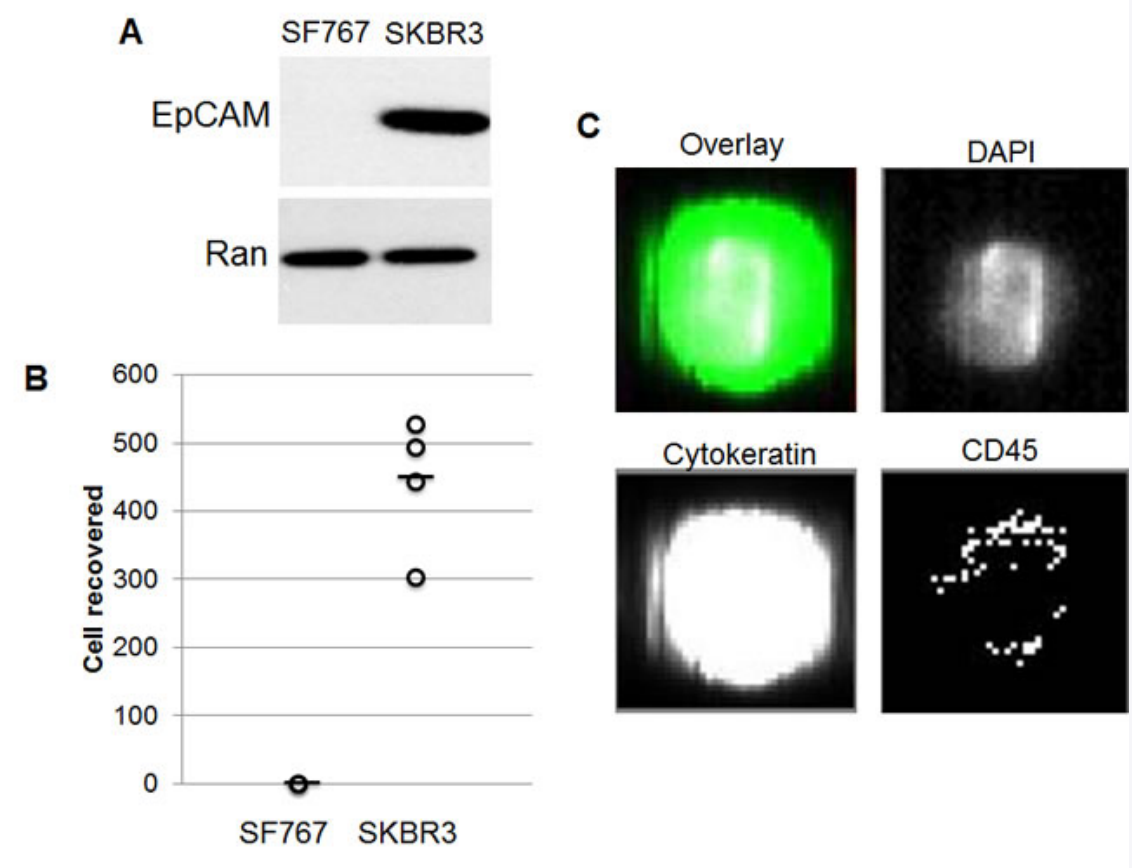

Figure 1: Detection by the CellSearch system of breast cancer cells but not glioblastoma cells present in human blood. (A) Western blot analysis of EpCAM expression in SF767 human glioblastoma cells and SKBR3 human breast cancer cells. Ran shown as a loading control. (B) Number of CTCs enumerated by CellSearch criteria in normal human blood spiked with 1,000 SF767 and SKBR3 cells from cell culture. (C) Exemplary image of an SKBR3 cell isolated by the CellSearch system.

Adapting the CellSearch system to detect CSFTCs

We aimed to develop a method of using the CellSearch system to detect tumor cells in CSF. The CellSearch uses 7.5 mL of peripheral blood for its standard detection method and relies on several checkpoints and caveats throughout its processing. One such caveat is that the tumor cells will be in the buffy coat following centrifugation of the sample. Due to this, CSF cannot be directly analyzed in the machine in lieu of blood. We circumvented this by spiking the cellular contents of the CSF sample into normal human blood for detection. This was accomplished by

centrifugation of the CSF and resuspension in a small volume of phosphate buffered saline (Figure 2). We regularly obtained normal blood for these assays by procuring leukocyte filters from blood drives and reconstituting normal blood with a physiological number of leukocytes. The CSF suspension was then spiked into the reconstituted blood and subjected to the standard CellSearch protocol. It is noteworthy that leukocytes are particularly important for this assay as the CellSearch system relies on CTCs and contaminating leukocytes when determining the focal plane for immunofluorescence analysis. Therefore if a sample with no CTCs is analyzed, the CellSearch system will abort the analysis if there are no remaining cells present for locating the focal plane.

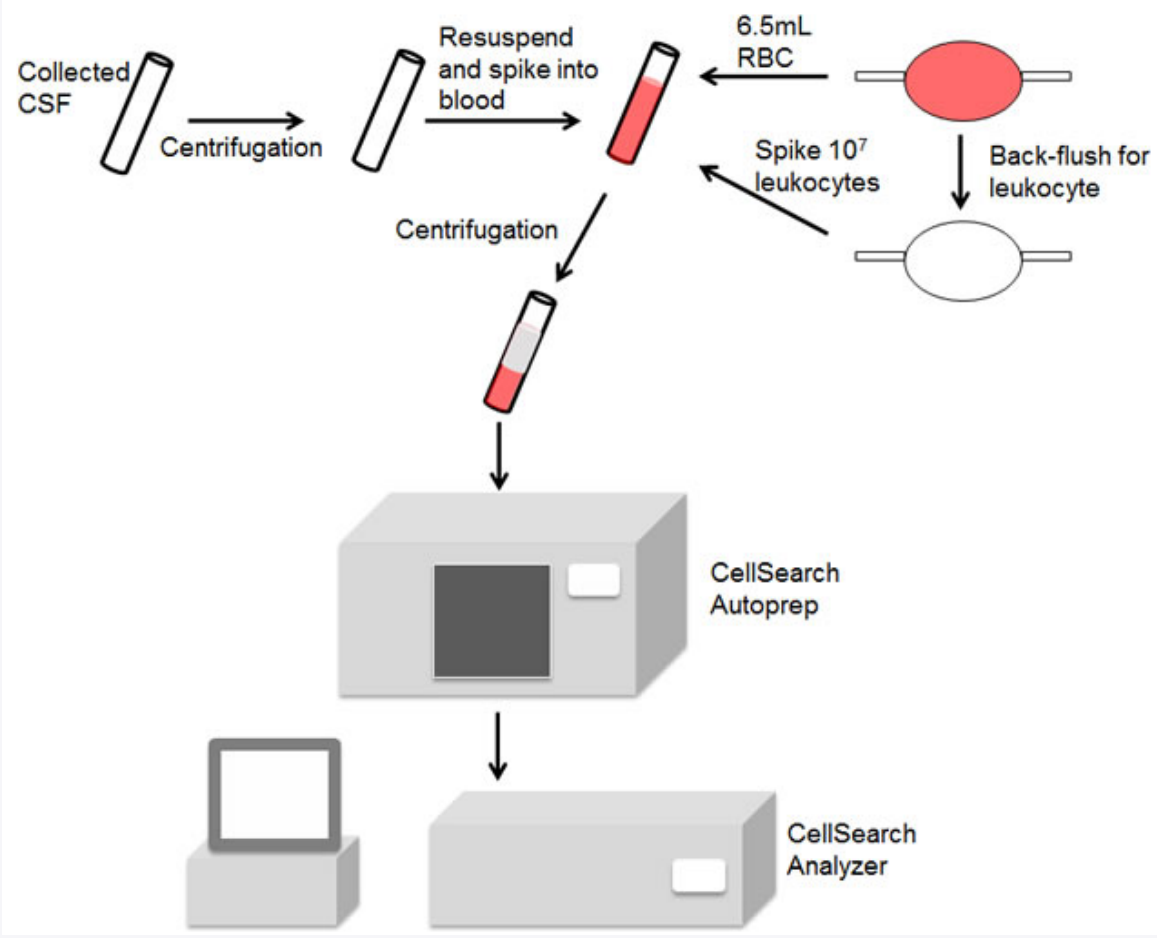

Figure 2: Schematic demonstrating use of the CellSearch system to detect breast cancer cerebrospinal fluid tumor cells.

Accuracy and reproducibility of detecting CSFTCs

To characterize the recovery rate and linearity of recovery, we spiked cultured breast cancer cells at varying cell numbers and determined the recovery rate at these various cell counts (Figure 3). We found that the recovery rate was ~38%, which is similar to that found in other recovery experiments where cultured human tumor cells are spiked directly into blood (data not shown). We also found this recovery rate to be reproducible and linear across the range of cell numbers tested (R^2 = .96).

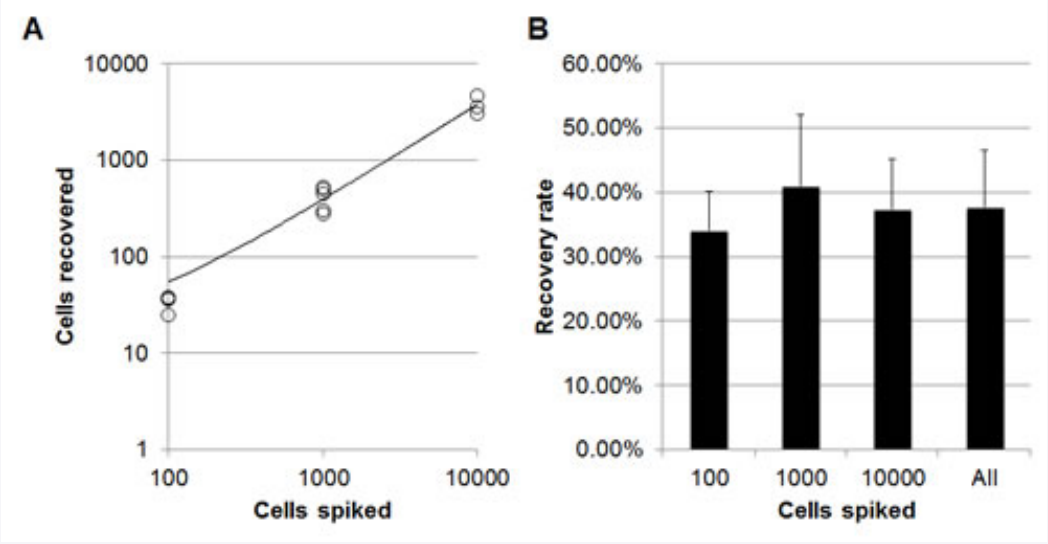

Figure 3: Recovery rate of breast cancer cells present in cerebrospinal fluid. (A) Enumeration and (B) recovery rate of cultured SKBR3 cells spiked into normal blood (n>3).

Detection of CSFTCs in breast cancer patients with CNS metastases and association with disease burden

Five patients with metastatic breast cancer involving the CNS were enrolled into a pilot study (Table 1). Detecting CSFTCs yielded a number of morphologically diverse species that included leukocytes, tumor cells, and significant amount of debris (Figure 4A). Note that debris is easily separable from tumor cells due to the immunostaining for a tumor cell marker and is an important advantage because tumor cells may be more difficult to distinguish by CSF cytology. Analyzing data at baseline and following treatment, there was a general inverse correlation between Karnofsky performance status (KPS) of and CSFTC number (r = -.66) (Figure 4B). There was a general trend toward a higher CSFTC count with positive CSF cytology (r = -.37)

(Figure 4B), though CSF cytology clearly does not reflect disease burden (Figure 4C). Subject 5 had >12,000 CSFTCs and on the same day of CSF collection developed status epilepticus and deceased. Interestingly this patient showed no gross abnormalities by MRI that suggested tumor burden and this underscores the importance of CSFTCs as a disease marker (Figure 4D). While the correlation between CSFTC number and Karnofsky performance shows significance in the pilot study, a large cohort of patients will likely reveal a stronger significance than can be demonstrated with this pilot study.

Table 1: Patient characteristics.

Subject	Age	Her2	Progesterone receptor	Estrogen receptor	Baseline KPS	Chemotherapy
1	54	+	-	-	80	Intrathecal trastuzumab, liposomal cytarabine, methotrexate
2	52	-	-	+	70	Intrathecal liposal cytarabine, methotrexate, thiotepa, topotecan
3	28	-	-	-	60	Intrathecal liposal cytarabine, methotrexate, thiotepa, topotecan
4	34	-	-	-	90	Intrathecal thiotepa, methotrexate, topotecan
5	35	-	-	-	60	Intrathecal thiotepa and topotecan

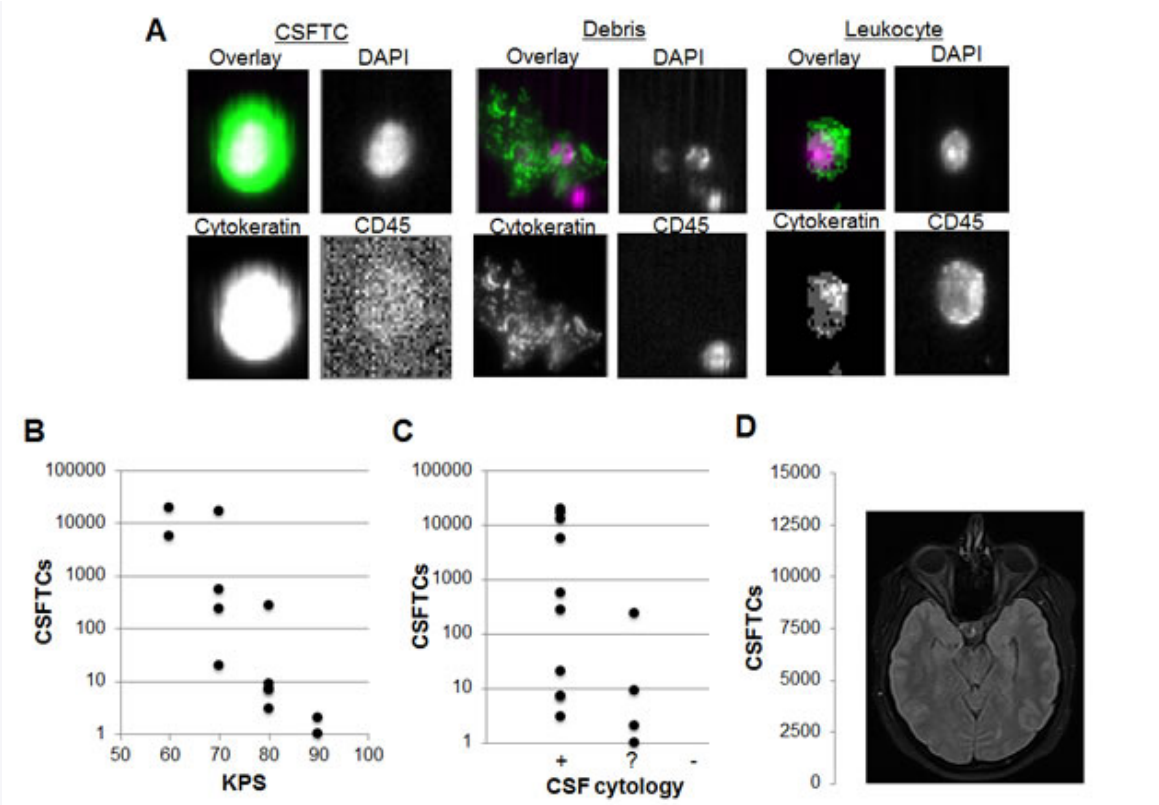

Figure 4: Detection of CSFTCs in breast cancer patients with CNS metastasis and correlation with Karnofsky performance status. (A) Exemplary images of species detected in CSF samples. (B) Correlation of Karnofsky performance status with CSF cytology versus CSFTC number in subjects 1,2, 3, and 5 throughout treatment. (C) Correlation of CSFTCs with CSF results that report positive (+), equivocal (?), or negative (-). (D) MRI of subject 5 on day of CSF withdrawal.

CSFTC count dynamically changes with treatment

Response to chemotherapy was evident in three patients that were followed over time in this pilot study (Figure 5). Subjects 1, 2, and 3 exhibited a significant decline in the number of CSFTCs following initiation of intrathecal therapy consisting of a combination of topotecan, liposomal cytarabine, thiotepa, methotrexate and/or trastuzumab (Table 1). It should be noted that at several time-points CSF cytology conducted by a blinded pathologist gave an equivocal result and that improvements in KPS tended to follow a decline in CSFTCs. This data clearly highlights the inability of CSF cytology to reflect dynamic changes in disease burden.

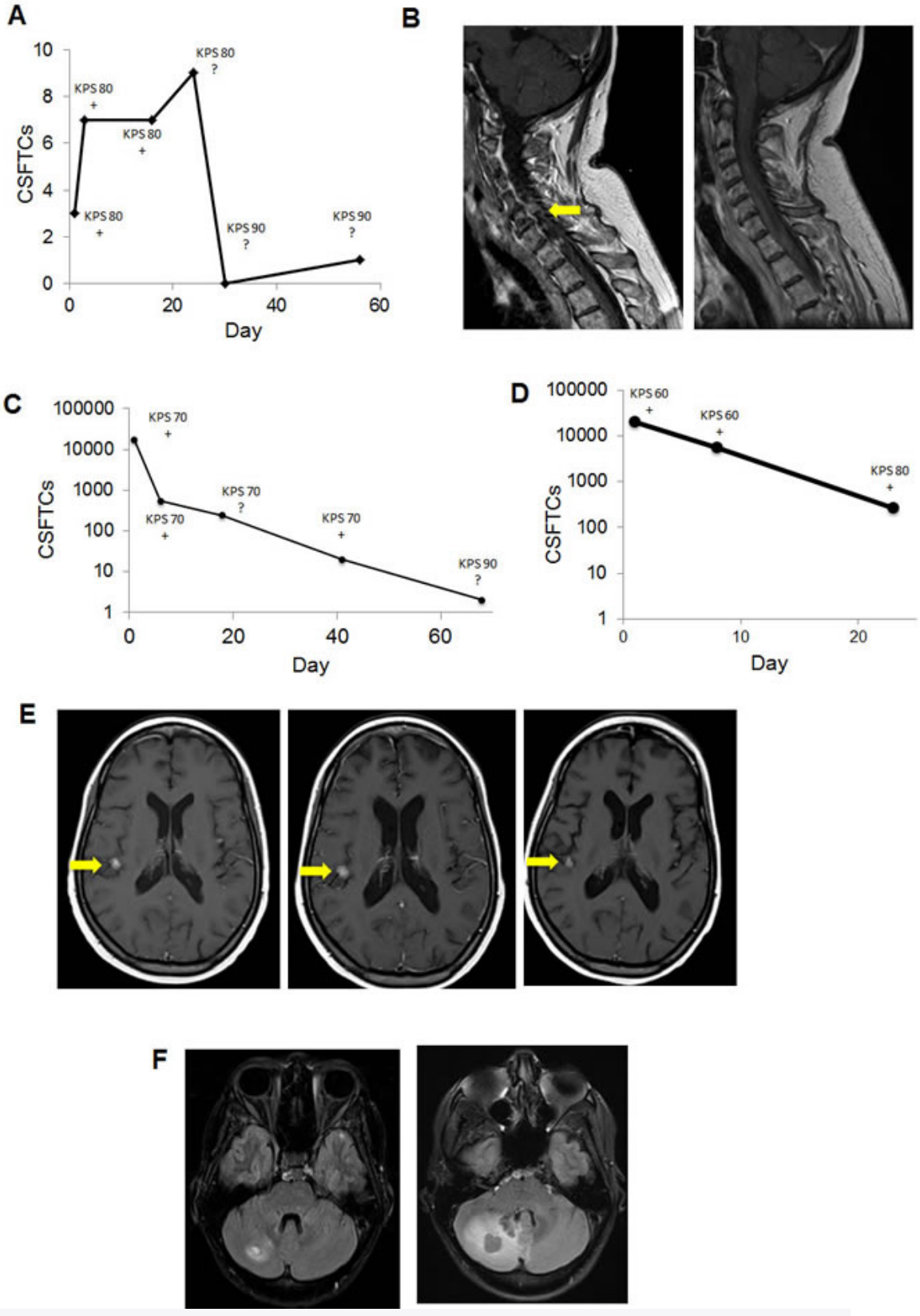

Figure 5: CSFTC counts dynamically change with chemotherapy. (A) CSFTC count over time and (B) MRI of subject 1 at baseline and days post-treatment initiation. CSFTC count over time in (C) subject 2 and (D) subject 3. (E) MRI of subject 3 at baseline (left panel), 42 (middle panel), and 68 days (right panel) post-treatment initiation. (F) MRI of subject 4 at baseline (left panel) and 57 days post-treatment initiation (right panel).

In addition to its general correlation with KPS, changes in CSFTC number tended to coincide with clinical deficits. Prior to treatment initiation, subject 2 had $>10^4$ CSFTCs and exhibited facial weakness and vertical diplopia. These symptoms were resolved approximately two months after treatment and was accompanied by a near complete disappearance of CSFTCs. Subject 3 also harbored $>10^4$ CSFTCs and suffered from severe vomiting, lethargy, and headaches. Following treatment this patient had a CSFTC count that declined significantly to 267 CSFTCs but still suffered from headaches, though other symptoms resolved. The clinical outcome of leptomeningeal or parenchymal CNS metastases varies greatly. Patients with an excess of 10,000 CSFTCs had cranial nerve deficits or mental status decline. Two patients showed an improvement in KPS after chemotherapy initiation and a concomitant decline in CSFTCs. Our findings from this small pilot study suggest a possible predictive role for CSFTCs and their quantification to serve as a reliable marker that reflects disease burden dynamically unlike CSF cytology and provides information regarding the magnitude of disease burden.

Gadolinium-enhanced MRI allows for the sensitive visualization of macroscopic changes with the brain, spine or leptomeninges. We found an inverse correlation with CSFTC count and the presence or enhancement pattern seen on such imaging. It should be noted that though neuroimaging is an indicator of CNS disease, it relies on the breakdown of the blood-brain barrier rather than a direct sign of response. Multi-modality imaging is an ever-advancing technology but is not sufficient to make judgments about cranial and spinal metastases. CSFTCs represent a novel marker of CNS disease that detects cancer at the single cell level and provides critical information to clinicians that attempt to combine cytology, imaging and neurologic examination as part and parcel of a treatment algorithm. While this study serves as a proof-of-principle and

shows promising significance, a larger cohort of patients with follow up studies will be required to concretely establish the prognostic significance of CSFTC enumeration and the ability of therapeutic agents to eliminate these cells.

DISCUSSION

The biology of metastases and their relationship to the microenvironment of the CNS remains unclear [15, 16]. The nature and purpose of malignant cells from extraneural sites within the CSF compartment also remains unexplored [17]. Our investigation suggests that the CSF is a viable source for detecting metastatic tumor cells in cancer patients with CNS involvement. Micrometastases to the cerebrospinal compartment and transmigration through the blood-brain barrier are poorly understood events[17-20]. Current anti-cancer therapies are relatively successful for local control of breast cancer at early stages. However, late-stage and recurrent breast cancer often metastasizes to the brain [21].

Accurate, early diagnosis and appropriate treatment decisions are likely to yield a better patient outcome and underscores the importance of accurately monitoring common secondary sites by a highly sensitive detection method. The ability to detect single cells at a metastatic site such as the brain may allow for therapeutic intervention that could prevent or destroy metastatic disease an early stage [22]. Delays in diagnosis can be disastrous from a neurologic standpoint and treatment decisions must weigh the risks of aggressive treatment with the extent of disease. As potentiated by the detection of CSFTCs, the knowledge that viable cancer remains in the CSF of patients is highly useful in making treatment decisions.

A number of techniques have been developed for the isolation of CTCs in peripheral blood since the first attempts in the late 1800s [23]. Investigational labs now use several different techniques for CTC detection including reverse transcriptase polymerase chain reaction, immunocytochemistry, flow cytometry, microchips, and size-based filtration methods [24-26]. The CellSearch system presents a platform that reliably captures CTCs in this setting and provides a semi-automated platform for enumerating CTCs based on multiple markers to yield high accuracy, recovery, and reproducibility. Several studies have demonstrated the clinical

significance of CTC number as a prognostic marker when enumerated by the CellSearch system in metastatic tumors of breast, colon and prostate [1, 27, 28]. The isolation and enumeration of CSFTCs may provide valuable information for patients with CNS metastasis and potentiate studies on the biology of these cells and how they differ from the primary and metastatic tumor as well as the CTCs found in peripheral blood.

The prognostic relevance of CSFTCs is correlated here with the clinical course of the patient and the CSFTC count. The biological significance of finding up to several thousand CSFTCs in a patient sample remains unclear though it is suggestive of and correlates with high disease burden. CNS metastases are often strategically located in close proximity to ventricular surfaces or CSF cisterns. However, natural circulation of CSF can be impaired, which may cause "loculations" of malignant CSF, thus lowering the diagnostic yield of lumbar puncture [29].

Our lab is currently pursuing post-isolation characterization of tumor cells isolated from peripheral blood as well as CSF [30]. There is an expanding though controversial body of evidence that cancer stem cells play a large role in the propagation of solid tumors, including critical mechanisms of metastasis [31-33]. The reliable, sensitive, and accurate isolation of CSFTCs enables such studies in conjunction with is potential as a novel marker that has clear advantages over CSF cytology.

METHODS

Cell culture experiments

Human SKBR3 breast cancer cells were obtained from ATCC and cultured in McCoy's 5A medium supplemented with 10% heat-inactivated fetal bovine serum and 1% penicillin and streptomycin. Human SF767 glioma cells were a kind gift from Akiva Mintz (Wake Forest University) and were cultured in RPMI under the same conditions. For Western blot analysis, cells were harvested by cell scraping, centrifuged, and lysed on ice for 2 hours. Lysates were harvested and the protein concentration was determined using the BioRad protein assay. Samples were electrophoresed on 4-12% Bis-Tris gels, transferred to PVDF, and blocked in 10% non-fat milk in TBST. Membranes were incubated with EpCAM (Cell Signaling) at 1:500 or Ran at

1:10,000 (BD biosciences) antibodies overnight at 4°C. Membranes were rinsed in TBST, incubated with an appropriate HRP-conjugated secondary antibody, and visualized using ECL-Plus and X-Ray film.

Cell spiking experiments

Tumor cells were harvested from log-phase growth by trypsinization and enumerated using a Cellometer (Nexcelom Biosciences) in triplicate. The appropriate volume of cell suspension was then added to a tube of CSF previously cleared of tumor cell contaminants by centrifugation. This CSF was then subjected to the standard CSFTC detection procedure described below.

Patients

The main inclusion criteria were newly discovered breast cancer with metastatic disease involving the CNS as confirmed with radiologic or cytologic findings and the commencement of intrathecal chemotherapy. All subjects provided informed consent for testing of their CSF as approved by the Institutional Review Board at the Penn State Hershey Medical Center. All subjects were diagnosed with primary breast cancer prior to enrollment into this study and had undergone neurosurgical intervention in terms of placement of a ventricular access device. All patients had involvement of the CNS, with combinations of parenchymal or leptomeningeal metastases. The ventricular access device provided a means to obtain CSF for testing. Prior to the onset of treatment, patients underwent thorough neurologic examination to identify any deficits and were stratified based on KPS. CSF was obtained every 2 to 3 weeks for each patient and often coincided with intrathecal chemotherapy deposition. The neuro-oncologist providing treatment and evaluating the patients was blinded to the CSFTC analysis.

Detection of CSFTCs

9mL of CSF was centrifuged at 500g for 10 minutes, the supernatant was removed, and the pellet was resuspended in 1mL of PBS. The suspension was then spiked into 6.5mL of reconstituted normal human blood. This blood was obtained from leukocyte filters that were generated from blood drives as approved by the Institutional Review Board at Penn State

Hershey Medical Center. 6.5mL of filtered blood was removed from the leukocyte trap, placed into a CellSave (Veridex) tube, and inverted 8 times. The leukocyte filter was rinsed with PBS and back-flushed to obtain leukocytes that were enumerated and spiked at 10^7 cells per 6.5mL sample of blood. Samples were analyzed within 3 days using the standard CellSearch protocol and the CTC Epithelial Cell Kit (Veridex). In brief, the CellSearch system qualifies a cell as a CTC if it has an evident nucleus by DAPI staining and is $EpCAM^+$, $cytokeratin^+$, and $CD45^-$. Analysis and enumeration of CTCs was conducted by a blinded, certified assay operator.

Statistics

Bivariate correlation calculated by Pearson's correlation.

ACKNOWLEDGEMENTS

We thank all enrolled patients for their involvement in this study. W.S.E-D. is an American Cancer Society Research Professor.

REFERENCES

1. Cristofanilli M, Budd GT, Ellis MJ, Stopeck A, Matera J, Miller MC, Reuben JM, Doyle GV, Allard WJ, Terstappen LW, Hayes DF. Circulating tumor cells, disease progression, and survival in metastatic breast cancer. New Engand Journal of Medicine. 2004; 351: 781-91.
2. Paterlini-Brechot P, Benali NL. Circulating tumor cells (CTC) detection: clinical impact and future directions. Cancer Letters. 2007; 253: 180-204.
3. Glantz MJ, Van Horn A, Fisher R, Chamberlain MC. Route of intracerebrospinal fluid chemotherapy administration and efficacy of therapy in neoplastic meningitis. Cancer. 2010; 116: 1947-52.
4. Heitz F, Rochon J, Harter P, Lueck HJ, Fisseler-Eckhoff A, Barinoff J, Traut A, Lorenz-Salehi F, du Bois A. Cerebral metastases in metastatic breast cancer: disease-specific risk factors and survival. Annals of Oncology. 2011; 22: 1571-81.

5. Mori T, Sugita K, Kimura K, Fuke T, Miura T, Kiyokawa N, Fujimoto J. Isolated central nervous system (CNS) relapse in a case of childhood systemic anaplastic large cell lymphoma without initial CNS involvement. Journal of Pediatric Hematology/Oncology. 2003; 25: 975-7.

6. Allen JE, El-Deiry WS. Circulating Tumor Cells and Colorectal Cancer. Current Colorectal Cancer Reports. 2010; 6: 212-20.

7. Criscitiello C, Sotiriou C, Ignatiadis M. Circulating tumor cells and emerging blood biomarkers in breast cancer. Current Opinions in Oncology. 2010; 22: 552-8.

8. Liu MC, Shields PG, Warren RD, Cohen P, Wilkinson M, Ottaviano YL, Rao SB, Eng-Wong J, Seillier-Moiseiwitsch F, Noone AM, Isaacs C. Circulating tumor cells: a useful predictor of treatment efficacy in metastatic breast cancer. Journal of Clinical Oncology. 2009; 27: 5153-9.

9. Hayes DF, Smerage JB. Circulating tumor cells. Progress in Molecular Biology and Translational Science. 2010; 95: 95-112.

10. Mammoser AG, Groves MD. Biology and therapy of neoplastic meningitis. Current Oncology Reports. 2010; 12: 41-9.

11. Weston CL, Glantz MJ, Connor JR. Detection of cancer cells in the cerebrospinal fluid: current methods and future directions. Fluids Barriers of the CNS. 2011; 8: 14.

12. Glantz MJ, Cole BF, Glantz LK, Cobb J, Mills P, Lekos A, Walters BC, Recht LD. Cerebrospinal fluid cytology in patients with cancer: minimizing false-negative results. Cancer. 1998; 82: 733-9.

13. Chamberlain MC, Glantz M, Groves MD, Wilson WH. Diagnostic tools for neoplastic meningitis: detecting disease, identifying patient risk, and determining benefit of treatment. Seminars in Oncology. 2009; 36, S35-45.

14. Straathof CS, de Bruin HG, Dippel DW, Vecht CJ. The diagnostic accuracy of magnetic resonance imaging and cerebrospinal fluid cytology in leptomeningeal metastasis. Journal of Neurology. 1999; 246: 810-4.

15. Zhang C, Yu D. Microenvironment determinants of brain metastasis. Cell & Bioscience. 2011; 1: 8.

16. Fidler IJ. The role of the organ microenvironment in brain metastasis. Seminars in Cancer Biology. 2011; 21: 107-12.

17. Melisko ME, Glantz M, Rugo HS. New challenges and opportunities in the management of brain metastases in patients with ErbB2-positive metastatic breast cancer. Nature Clinical Practice Oncology. 2009; 6: 25-33.

18. Eichler AF, Chung E, Kodack DP, Loeffler JS, Fukumura D, Jain RK. The biology of brain metastases-translation to new therapies. Nature Reviews Clinical Oncology. 2011; 8: 344-56.

19. Steeg PS, Camphausen KA, Smith QR. Brain metastases as preventive and therapeutic targets. Nature Reviews Cancer. 2011; 11: 352-63.

20. Lorger M, Lee H, Forsyth JS, Felding-Habermann B. Comparison of in vitro and in vivo approaches to studying brain colonization by breast cancer cells. Journal of Neurooncology. 2011; 104: 689-96.

21. Dieras V, Pierga JY. [Brain metastasis of breast tumors and blood brain barrier]. Bulletin du Cancer. 2011; 98: 385-9.

22. Oliveira M, Braga S, Passos-Coelho JL, Fonseca R, Oliveira J. Complete response in HER2+ leptomeningeal carcinomatosis from breast cancer with intrathecal trastuzumab. Breast Cancer Research and Treatment. 2011; 127: 841-4.

23. Wicha MS, Hayes DF. Circulating tumor cells: not all detected cells are bad and not all bad cells are detected. Journal of Clinical Oncology. 2011; 29: 1508-11.

24. Kojima T, Hashimoto Y, Watanabe Y, Kagawa S, Uno F, Kuroda S, Tazawa H, Kyo S, Mizuguchi H, Urata Y, Tanaka N, Fujiwara T. A simple biological imaging system for detecting viable human circulating tumor cells. Journal of Clincal Investigation. 2009; 119: 3172-81.

25. Nagrath S, Sequist LV, Maheswaran S, Bell DW, Irimia D, Ulkus L, Smith MR, Kwak EL, Digumarthy S, Muzikansky A, Ryan P, Balis UJ, Tompkins RG, Haber DA, Toner M. Isolation of rare circulating tumour cells in cancer patients by microchip technology. Nature. 2007; 450: 1235-9.

26. Diehl F, Schmidt K, Choti MA, Romans K, Goodman S, Li M, Thornton K, Agrawal N, Sokoll L, Szabo SA, Kinzler KW, Vogelstein B, Diaz LA Jr. Circulating mutant DNA to assess tumor dynamics. Nature Medicine. 2008; 14: 985-90.

27. de Bono JS, Scher HI, Montgomery RB, Parker C, Miller MC, Tissing H, Doyle GV, Terstappen LW, Pienta KJ, Raghavan D. Circulating tumor cells predict survival benefit from treatment in metastatic castration-resistant prostate cancer. Clinical Cancer Research. 2008; 14: 6302-9.

28. Cohen SJ, Punt CJ, Iannotti N, Saidman BH, Sabbath KD, Gabrail NY, Picus J, Morse M, Mitchell E, Miller MC, Doyle GV, Tissing H, Terstappen LW, Meropol NJ. Relationship of circulating tumor cells to tumor response, progression-free survival, and overall survival in patients with metastatic colorectal cancer. Journal of Clinical Oncology. 2008; 26: 3213-21.

29. Rogers LR, Duchesneau PM, Nunez C, Fishleder AJ, Weick JK, Bauer LJ, Boyett JM. Comparison of cisternal and lumbar CSF examination in leptomeningeal metastasis. Neurology. 1992; 42: 1239-41.

30. Faltas B, Zeidan A, Peters K, Das A, Joudeh J, Navaraj A, Dolloff NG, Harvey HA, Jiang Y, Allen JE, Dicker DT, El Deiry WS. Identifying Circulating Tumor Stem Cells That Matter: The Key to Prognostication and Therapeutic Targeting. Journal of Clinical Oncology. 2011; 29: 2946-7.

31. Boman BM, Wicha MS. Cancer stem cells: a step toward the cure. Journal of Clinical Oncology. 2008; 26: 2795-9.

32. Creighton CJ, Li X, Landis M, Dixon JM, Neumeister VM, Sjolund A, Rimm DL, Wong H, Rodriguez A, Herschkowitz JI, Fan C, Zhang X, He X, Pavlick A, Gutierrez MC,Renshaw L, et al. Residual breast cancers after conventional therapy display mesenchymal as well as

tumor-initiating features. Proceedings of the National Academy of Sciences of the United States of America. 2009; 106: 13820-5.

33. Iinuma H, Watanabe T, Mimori K, Adachi M, Hayashi N, Tamura J, Matsuda K, Fukushima R, Okinaga K, Sasako M, Mori M. Clinical significance of circulating tumor cells, including cancer stem-like cells, in peripheral blood for recurrence and prognosis in patients with Dukes' stage B and C colorectal cancer. Journal of Clinical Oncology. 2011; 20: 1547-55.

Appendix 5 - List of Abbreviations

Abbreviation or symbol	Term
5-FU	5-fluorouracil
AML	acute myeloid leukemia
AMPK	AMP-activated protein kinase
AP-1	activator protein 1
Bak	BCL2-antagonist/killer
Bax	Bcl-2–associated X protein
Bcl-2	B-cell lymphoma 2
BSA	bovine serum albumin
CBP	CREB-binding protein
CEBP	Ccaat-enhancer-binding protein
c-FLIP	cellular FLICE-like inhibitory protein
$C^{hi}P$	Calcein-high population
CHOP	CAAT/enhancer binding protein homologous transcription factor
cIAP	Cellular inhibitor of apoptosis
Cited 2	Cbp/p300-interacting transactivator 2
$C^{lo}P$	Calcein-low population
CSC	cancer stem cell
CSFTC	cerebrospinal fluid tumor cell
CT	computed tomography
CTC	circulating tumor cell
DAB	3,3-Diaminobenzidine
DcR1	decoy receptor 1
DcR2	decoy receptor 2
DD	death domain
DIABLO	direct IAP binding protein with low pI

DISC	death-inducing signaling complex
DMSO	dimethyl sulfoxide
DNA	deoxyribonucleic acid
DR4	death receptor 4
DR5	death receptor 5
EGFP	enhanced green fluorescent protein
EGFR	epidermal growth factor receptor
EMSA	Electrophoretic mobility shift assay
EMT	epithelial-mesenchymal transition
ER	endoplasmic reticulum
ERK	extracellular signal-related kinase
FADD	Fas-associated death domain
FasL	Fas ligand
FBS	fetal bovine serum
FOXO	Forkhead box O
gadd45	growth arrest and DNA damage
GAS	Inteferon-γ-activated sequence
GBM	glioblastoma multiforme
GR	gamma radiation
H&E	hematoxylin and eosin
HDAC	histone deacetylase
HDACi	HDAC inhibitor
HPLC	high-performance liquid chromatography
HSF-1	heat shock factor protein 1
HTLV-1	human T-cell leukemia virus type I
i.p.	intraperitoneal
i.v.	intravenous
IFN	interferon

IHC	immunohistochemistry
IL	interleukin
IRF	interferon regulatory transcription factor
IRSE	interferon-stimulated response element
JNK	c-Jun N-terminal kinase
LPS	lipopolysaccharide
MAPK	mitogen-activated protein kinase
Mcl-1	myeloid cell leukemia sequence 1
MDR	multi-drug resistance
MEK	mitogen-activated protein kinase/extracellular signal-regulated kinase
MRI	magnetic resonance imaging
mRNA	messenger RNA
MST1	macrophage stimulating 1
MTD	maximum tolerated dose
NCI	National Cancer Institute
NEMO	NF-kappa-B essential modulator
NFAT	Nuclear factor of activated T-cells
NFκB	Nuclear Factor-KappaB
NHL	non-Hodgkin's lymphoma
NK	natural killer
NSCLC	non-small cell lung cancer
PBS	phosphate buffered saline
PCG-1	Peroxisome proliferator-activated receptor gamma coactivator 1
PCR	polymerase chain reaction
PEDF	pigment epithelium-derived factor
PEGF	precursor epithelium growth factor

PET	positron emission tomography
PFS	progression-free survival
PI	propidium iodide
PML	Promyelocytic leukemia protein
PO	oral
PPAR	peroxisome proliferator-activated receptor
PTEN	Phosphatase and tensin homolog
qwk	once per week
RECIST	response evaluation criteria in solid tumors
rhTRAIL	recombinant human TRAIL
RIP1	receptor-interacting protein-1
RNA	ribonucleic acid
ROS	reactive oxygen species
RT	reverse transcription PCR
s.d.	standard deviation
SAHA	suberoylanilide hydroxamic acid
SCF	Skp, Cullin, F-box containing
SGK	Serum glucocorticoid kinase
shRNA	short hairpin RNA
siRNA	small interfering RNA
Sirt1	silent mating type information regulation 2
Smad	Sma and Mad homologue
SNP	single nucleotide polymorphism
SP-1	specificity protein 1
STAT	Signal Transducers and Activators of Transcription
TIC	TRAIL-inducing compound
TMZ	temozolomide

TNF	tumor necrosis factor
TRAF2	TNF receptor-associated factor 2
TRADD	TNF-R1-associated death domain
TRAIL	TNF-related apoptosis-inducing ligand
TTP	time to progression
TUNEL	Terminal deoxynucleotidyl transferase dUTP nick end labeling
UTR	untranslated region
VPA	valproic acid
Wnt	wingless
XIAP	X-linked inhibitor of apoptosis protein

BIBLIOGRAPHY

A. D. Baron, C. L. O. B., Y. Choi, S. Royer-Joo, C. C. Portera (2011). Phase Ib study of drozitumab combined with cetuximab (CET) plus irinotecan (IRI) or with FOLFIRI with or without bevacizumab (BV) in previously treated patients (pts) with metastatic colorectal cancer (mCRC). J Clin Oncol *29*.

Abdulghani, J., and El-Deiry, W. S. (2010). TRAIL receptor signaling and therapeutics. Expert Opinion on Therapeutic Targets *14*, 1091-1108.

Adams, C., Totpal, K., Lawrence, D., Marsters, S., Pitti, R., Yee, S., Ross, S., Deforge, L., Koeppen, H., Sagolla, M.*, et al.* (2008). Structural and functional analysis of the interaction between the agonistic monoclonal antibody Apomab and the proapoptotic receptor DR5. Cell Death Differ *15*, 751-761.

Albeck, J. G., Burke, J. M., Aldridge, B. B., Zhang, M., Lauffenburger, D. A., and Sorger, P. K. (2008). Quantitative Analysis of Pathways Controlling Extrinsic Apoptosis in Single Cells. Molecular Cell *30*, 11-25.

Allen, J. E., and El-Deiry, W. S. (2011). Oxaliplatin Uses JNK to Restore TRAIL Sensitivity in Cancer Cells Through Bcl-xL Inactivation. Gastroenterology *141*, 430-434.

Almeida, M., Han, L., Martin-Millan, M., O'Brien, C. A., and Manolagas, S. C. (2007). Oxidative Stress Antagonizes Wnt Signaling in Osteoblast Precursors by Diverting B-Catenin from T Cell Factor- to Forkhead Box O-mediated Transcription. Journal of Biological Chemistry *282*, 27298-27305.

Andreassen, C. N. (2005). Can risk of radiotherapy-induced normal tissue complications be predicted from genetic profiles? Acta Oncologica *44*, 801-815.

Armeanu, S., Lauer, U. M., Smirnow, I., Schenk, M., Weiss, T. S., Gregor, M., and Bitzer, M. (2003). Adenoviral Gene Transfer of Tumor Necrosis Factor-related Apoptosis-Inducing Ligand Overcomes an Impaired Response of Hepatoma Cells but Causes Severe Apoptosis in Primary Human Hepatocytes. Cancer Research *63*, 2369-2372.

Ashkenazi, A. (2002). Targeting death and decoy receptors of the tumour-necrosis factor superfamily. Nat Rev Cancer *2*, 420-430.

Ashkenazi, A., Pai, R. C., Fong, S., Leung, S., Lawrence, D. A., Marsters, S. A., Blackie, C., Chang, L., McMurtrey, A. E., Hebert, A.*, et al.* (1999a). Safety and antitumor activity of recombinant soluble Apo2 ligand. J Clin Invest *104*, 155 - 162.

Ashkenazi, A., Pai, R. C., Fong, S., Leung, S., Lawrence, D. A., Marsters, S. A., Blackie, C., Chang, L., McMurtrey, A. E., Hebert, A.*, et al.* (1999b). Safety and antitumor activity of recombinant soluble Apo2 ligand. The Journal of Clinical Investigation *104*, 155-162.

Austin, C. D., Lawrence, D. A., Peden, A. A., Varfolomeev, E. E., Totpal, K., De Maziere, A. M., Klumperman, J., Arnott, D., Pham, V., Scheller, R. H., and Ashkenazi, A. (2006). Death-receptor activation halts clathrin-dependent endocytosis. Proceedings of the National Academy of Sciences *103*, 10283-10288.

Avi Ashkenazi, R. C. P., Sharon Fong, Susan Leung, David A. Lawrence, Scot A. Marsters, Christine Blackie, Ling Chang, Amy E. McMurtrey, Andrea Hebert, Laura DeForge, Iphigenia L. Koumenis, Derf Lewis, Louise Harris, Jeanine Bussiere, Hartmut Koeppen, Zahra Shahrokh, Ralph H. Schwall (1999). Safety and antitumor activity of recombinant soluble Apo2 ligand. Journal of Clinical Investigations *102*, 155-162.

Aydin, C., Sanlioglu, A. D., Karacay, B., Ozbilim, G., Dertsiz, L., Ozbudak, O., Akdis, C. A., and Sanlioglu, S. (2007). Decoy Receptor-2 Small Interfering RNA (siRNA) Strategy Employing Three Different siRNA Constructs in Combination Defeats Adenovirus-Transferred Tumor Necrosis Factor-Related Apoptosis-Inducing Ligand Resistance in Lung Cancer Cells. Human Gene Therapy *18*, 39-50.

B. I. Sikic, H. A. W., M. von Mehren, N. Lewis, A. H. Calvert, E. R. Plummer, N. L. Fox, T. Howard, S. F. Jones, H. A. Burris (2007). A phase Ib study to assess the safety of lexatumumab, a human monoclonal antibody that activates TRAIL-R2, in combination with gemcitabine, pemetrexed, doxorubicin or FOLFIRI. Journal of Clinical Oncology *25*, 14006.

Baetu, T. M., Kwon, H., Sharma, S., Grandvaux, N., and Hiscott, J. (2001). Disruption of NF-κB Signaling Reveals a Novel Role for NF-κB in the Regulation of TNF-Related Apoptosis-Inducing Ligand Expression. The Journal of Immunology *167*, 3164-3173.

Bakker, W. J., Blazquez-Domingo, M., Kolbus, A., Besooyen, J., Steinlein, P., Beug, H., Coffer, P. J., Lowenberg, B., von Lindern, M., and van Dijk, T. B. (2004). FoxO3a regulates erythroid differentiation and induces BTG1, an activator of protein arginine methyl transferase 1. The Journal of Cell Biology *164*, 175-184.

Bayreuther, K., Rodemann, H. P., Hommel, R., Dittmann, K., Albiez, M., and Francz, P. I. (1988). Human skin fibroblasts in vitro differentiate along a terminal cell lineage. Proceedings of the National Academy of Sciences of the United States of America *85*, 5112-5116.

Bentzen, S. M. (2006). Preventing or reducing late side effects of radiation therapy: radiobiology meets molecular pathology. Nat Rev Cancer *6*, 702-713.

Bentzen, S. M., Thames, H. D., and Overgaard, M. (1989). Latent-time estimation for late cutaneous and subcutaneous radiation reactions in a single-follow-up clinical study. Radiotherapy and Oncology *15*, 267-274.

Beraza, N., Malato, Y., Sander, L. E., Al-Masaoudi, M., Freimuth, J., Riethmacher, D., Gores, G. J., Roskams, T., Liedtke, C., and Trautwein, C. (2009). Hepatocyte-specific NEMO deletion promotes NK/NKT cell- and TRAIL-dependent liver damage. The Journal of Experimental Medicine *206*, 1727-1737.

Biggs, W. H., Meisenhelder, J., Hunter, T., Cavenee, W. K., and Arden, K. C. (1999). Protein kinase B/Akt-mediated phosphorylation promotes nuclear exclusion of the winged helix transcription factor FKHR1. Proceedings of the National Academy of Sciences *96*, 7421-7426.

Bodmer, J.-L., Meier, P., Tschopp, J. r., and Schneider, P. (2000). Cysteine 230 Is Essential for the Structure and Activity of the Cytotoxic Ligand TRAIL. Journal of Biological Chemistry *275*, 20632-20637.

Bos, J. L., Fearon, E. R., Hamilton, S. R., Vries, M. V.-d., van Boom, J. H., van der Eb, A. J., and Vogelstein, B. (1987). Prevalence of ras gene mutations in human colorectal cancers. Nature *327*, 293-297.

Bos, P. D., Zhang, X. H. F., Nadal, C., Shu, W., Gomis, R. R., Nguyen, D. X., Minn, A. J., van de Vijver, M. J., Gerald, W. L., Foekens, J. A., and Massague, J. (2009). Genes that mediate breast cancer metastasis to the brain. Nature *459*, 1005-1009.

Bremer, E., and Helfrich, W. (2010). A Better TRAIL Variant for Tumor Cell-Specific Targeting? - Letter. Molecular Cancer Therapeutics *9*, 2853.

Brizel, D. M., Wasserman, T. H., Henke, M., Strnad, V., Rudat, V., Monnier, A., Eschwege, F., Zhang, J., Russell, L., Oster, W., and Sauer, R. (2000). Phase III Randomized Trial of Amifostine as a Radioprotector in Head and Neck Cancer. J Clin Oncol *18*, 3339-3345.

Brunet, A., Bonni, A., Zigmond, M. J., Lin, M. Z., Juo, P., Hu, L. S., Anderson, M. J., Arden, K. C., Blenis, J., and Greenberg, M. E. (1999). Akt Promotes Cell Survival by Phosphorylating and Inhibiting a Forkhead Transcription Factor. Cell *96*, 857-868.

Brunet, A., Kanai, F., Stehn, J., Xu, J., Sarbassova, D., Frangioni, J. V., Dalal, S. N., DeCaprio, J. A., Greenberg, M. E., and Yaffe, M. B. (2002). 14-3-3 transits to the nucleus and participates in dynamic nucleocytoplasmic transport. The Journal of Cell Biology *156*, 817-828.

Brunet, A., Sweeney, L. B., Sturgill, J. F., Chua, K. F., Greer, P. L., Lin, Y., Tran, H., Ross, S. E., Mostoslavsky, R., Cohen, H. Y.*, et al.* (2004). Stress-Dependent Regulation of FOXO Transcription Factors by the SIRT1 Deacetylase. Science *303*, 2011-2015.

Bunz, F., Hwang, P., Torrance, C., Waldman, T., Zhang, Y., Dillehay, L., Williams, J., Lengauer, C., Kinzler, K. W., and Vogelstein, B. (1999). Disruption of p53 in human cancer cells alters the responses to therapeutic agents. JCI *104*, 263–269.

Burns, T. F., and El-Deiry, W. S. (2001). Identification of Inhibitors of TRAIL-induced Death (ITIDs) in the TRAIL-sensitive Colon Carcinoma Cell Line SW480 Using a Genetic Approach. Journal of Biological Chemistry *276*, 37879-37886.

C Büneker, A. M., RM Zwacka (2009). The TRAIL-receptor-1: TRAIL-receptor-3 and -4 ratio is a predictor for TRAIL sensitivity of cancer cells. Oncol Rep *21*, 1289-1295.

C. S. Rocha Lima, J. C. B., J. Wallmark, Y. Choi, S. Royer-Joo, C. C. Portera (2011). Phase Ib study of drozitumab combined with first-line FOLFOX plus bevacizumab (BV) in patients (pts) with metastatic colorectal cancer (mCRC). J Clin Oncol *29*.

Calnan, D. R., and Brunet, A. (2008). The FoxO code. Oncogene *27*, 2276-2288.

Camidge, D., Herbst, R. S., Gordon, M., Eckhardt, S., Kurzroc, R., Durbin, B., Ing, J., Ling, J., Sager, J., and Mendelson, D. (2007). A phase I safety and pharmacokinetic study of apomab, a human DR5 agonist antibody, in patients with advanced cancer. J Clin Oncol (Meeting Abstracts) *25*, 3582-.

Cao, X., Yang, M., Wei, R. C., Zeng, Y., Gu, J. F., Huang, W. D., Yang, D. Q., Li, H. L., Ding, M., Wei, N.*, et al.* (2011). Cancer targeting Gene-Viro-Therapy of liver carcinoma by dual-regulated oncolytic adenovirus armed with TRAIL gene. Gene Ther *18*, 765-777.

Cassatella, M. A., Huber, V., Calzetti, F., Margotto, D., Tamassia, N., Peri, G., Mantovani, A., Rivoltini, L., and Tecchio, C. (2006). Interferon-activated neutrophils store a TNF-related apoptosis-inducing ligand (TRAIL/Apo-2 ligand) intracellular pool that is readily mobilizable following exposure to proinflammatory mediators. J Leukoc Biol *79*, 123-132.

Cha, S.-S., Kim, M.-S., Choi, Y. H., Sung, B.-J., Shin, N. K., Shin, H.-C., Sung, Y. C., and Oh, B.-H. (1999). 2.8 Å Resolution Crystal Structure of Human TRAIL, a Cytokine with Selective Antitumor Activity. Immunity *11*, 253-261.

Chan, J., Prado-Lourenco, L., Khachigian, L. M., Bennett, M. R., Di Bartolo, B. A., and Kavurma, M. M. (2010). TRAIL Promotes VSMC Proliferation and Neointima Formation in a FGF-2,Äì, Sp1 Phosphorylation,Äì, and NFŒ ∫ B-Dependent Manner. Circulation Research *106*, 1061-1071.

Chawla-Sarkar, M., Bae, S. I., Reu, F. J., Jacobs, B. S., Lindner, D. J., and Borden, E. C. (2004). Downregulation of Bcl-2, FLIP or IAPs (XIAP and survivin) by siRNAs sensitizes resistant melanoma cells to Apo2L//TRAIL-induced apoptosis. Cell Death Differ *11*, 915-923.

Chen, X., Kandasamy, K., and Srivastava, R. K. (2003). Differential Roles of RelA (p65) and c-Rel Subunits of Nuclear Factor kappa B in Tumor Necrosis Factor-related Apoptosis-inducing Ligand Signaling. Cancer Research *63*, 1059-1066.

Chinnaiyan, A. M., Prasad, U., Shankar, S., Hamstra, D. A., Shanaiah, M., Chenevert, T. L., Ross, B. D., and Rehemtulla, A. (2000). Combined effect of tumor necrosis factor-related apoptosis-inducing ligand and ionizing radiation in breast cancer therapy. Proc Natl Acad Sci U S A *97*, 1754 - 1759.

Choi, E. A., Lei, H., Maron, D. J., Wilson, J. M., Barsoum, J., Fraker, D. L., El-Deiry, W. S., and Spitz, F. R. (2003). Stat1-dependent Induction of Tumor Necrosis Factor-related Apoptosis-inducing Ligand and the Cell-Surface Death Signaling Pathway by Interferon beta in Human Cancer Cells. Cancer Research *63*, 5299-5307.

Chua, B., Olivotto, I. A., Weir, L., Kwan, W., Truong, P., and Ragaz, J. (2004). Increased Use of Adjuvant Regional Radiotherapy for Node-Positive Breast Cancer in British Columbia. Breast J *10*, 38 - 44.

Cippitelli, M., Fionda, C., Di Bona, D., Lupo, A., Piccoli, M., Frati, L., and Santoni, A. (2003). The Cyclopentenone-Type Prostaglandin 15-Deoxy-delta 12,14-Prostaglandin J2 Inhibits CD95 Ligand Gene Expression in T Lymphocytes: Interference with Promoter Activation Via Peroxisome Proliferator-Activated Receptor-gamma-Independent Mechanisms. The Journal of Immunology *170*, 4578-4592.

Clarke, N., Jimenez-Lara, A. M., Voltz, E., and Gronemeyer, H. (2004). Tumor suppressor IRF-1 mediates retinoid and interferon anticancer signaling to death ligand TRAIL. EMBO J *23*, 3051-3060.

Cohn, A. L., Tabernero, J., Maurel, J., Nowara, E., Dubey, S., Baker, N., Hei, Y. J., Galimi, F., and Choo, S. (2012). Conatumumab (CON) plus FOLFIRI (F) or ganitumab (GAN) plus F for second-line treatment of mutant (MT) KRAS metastatic colorectal cancer (mCRC). In 2012 Gastrointestinal Cancers Symposium, (J Clin Oncol).

Corallini, F., Celeghini, C., Rizzardi, C., Pandolfi, A., Di Silvestre, S., Vaccarezza, M., and Zauli, G. (2007). Insulin down-regulates TRAIL expression in vascular smooth muscle cells both in vivo and in vitro. Journal of Cellular Physiology *212*, 89-95.

Cretney, E., Takeda, K., Yagita, H., Glaccum, M., Peschon, J. J., and Smyth, M. J. (2002). Increased Susceptibility to Tumor Initiation and Metastasis in TNF-Related Apoptosis-Inducing Ligand-Deficient Mice. The Journal of Immunology *168*, 1356-1361.

Cummins, J. M., Kohli, M., Rago, C., Kinzler, K. W., Vogelstein, B., and Bunz, F. (2004). X-Linked Inhibitor of Apoptosis Protein (XIAP) Is a Nonredundant Modulator of Tumor Necrosis Factor-Related Apoptosis-Inducing Ligand (TRAIL)- Mediated Apoptosis in Human Cancer Cells. Cancer Research *64*, 3006-3008.

Daitoku, H., Hatta, M., Matsuzaki, H., Aratani, S., Ohshima, T., Miyagishi, M., Nakajima, T., and Fukamizu, A. (2004). Silent information regulator 2 potentiates Foxo1-mediated transcription through its deacetylase activity. Proceedings of the National Academy of Sciences of the United States of America *101*, 10042-10047.

de Vries, E. G. E., van der Graaf, W. T. A., Heijenbrok, F. J., Hoekstra, H. J., and de Jong, S. (2000). Don't blaze the trailblazer TRAIL too early. The Lancet *356*, 2014.

Degli-Esposti, M. A., Dougall, W. C., Smolak, P. J., Waugh, J. Y., Smith, C. A., and Goodwin, R. G. (1997a). The Novel Receptor TRAIL-R4 Induces NF-[kappa]B and Protects against TRAIL-Mediated Apoptosis, yet Retains an Incomplete Death Domain. Immunity *7*, 813-820.

Degli-Esposti, M. A., Smolak, P. J., Walczak, H., Waugh, J., Huang, C.-P., DuBose, R. F., Goodwin, R. G., and Smith, C. A. (1997b). Cloning and Characterization of TRAIL-R3, a Novel Member of the Emerging TRAIL Receptor Family. J Exp Med *186*, 1165-1170.

Demetri, G. D., Le Cesne, A., Chawla, S. P., Brodowicz, T., Maki, R. G., Bach, B. A., Smethurst, D. P., Bray, S., Hei, Y.-j., and Blay, J.-Y. (2012). First-line treatment of metastatic or locally advanced unresectable soft tissue sarcomas with conatumumab in combination with doxorubicin or doxorubicin alone: A Phase I/II open-label and double-blind study. European journal of cancer (Oxford, England : 1990) *48*, 547-563.

Desplat, V., Geneste, A., Begorre, M.-A., Fabre, S. B., Brajot, S., Massip, S., Thiolat, D., Mossalayi, D., Jarry, C., and Guillon, J. (2008). Synthesis of New Pyrrolo[1,2-a]quinoxaline Derivatives as Potential Inhibitors of Akt Kinase. Journal of Enzyme Inhibition and Medicinal Chemistry *23*, 648-658.

Doi, T., Murakami, H., Ohtsu, A., Fuse, N., Yoshino, T., Yamamoto, N., Boku, N., Onozawa, Y., Hsu, C. P., Gorski, K.*, et al.* (2011). Phase 1 study of conatumumab, a pro-apoptotic death receptor 5 agonist antibody, in Japanese patients with advanced solid tumors. Cancer Chemotherapy and Pharmacology *68*, 733-741.

Dolloff, N. G., Mayes, P. A., Hart, L. S., Dicker, D. T., Humphreys, R., and El-Deiry, W. S. (2011). Off-Target Lapatinib Activity Sensitizes Colon Cancer Cells Through TRAIL Death Receptor Up-Regulation. Science Translational Medicine *3*, 86ra50.

Dorr, J., Roth, K., Zurbuchen, U., Deisz, R., Bechmann, I., Lehmann, T.-N., Meier, S., Nitsch, R., and Zipp, F. (2005). Tumor-necrosis-factor-related apoptosis-inducing-ligand (TRAIL)-mediated death of neurons in living human brain tissue is inhibited by flupirtine-maleate. Journal of Neuroimmunology *167*, 204-209.

Dowell, P., Otto, T. C., Adi, S., and Lane, M. D. (2003). Convergence of Peroxisome Proliferator-activated Receptor gamma and Foxo1 Signaling Pathways. Journal of Biological Chemistry *278*, 45485-45491.

Dumont, N., and Arteaga, C. L. (2003). Targeting the TGF[beta] signaling network in human neoplasia. Cancer Cell *3*, 531-536.

Ebi, H., Corcoran, R. B., Singh, A., Chen, Z., Song, Y., Lifshits, E., Ryan, D. P., Meyerhardt, J. A., Benes, C., Settleman, J.*, et al.* (2011). Receptor tyrosine kinases exert dominant control over

PI3K signaling in human KRAS mutant colorectal cancers. Journal of Clinical Investigation *121*, 4311–4321.

Ehrhart, E. J., Segarini, P., Tsang, M. L., Carroll, A. G., and Barcellos-Hoff, M. H. (1997). Latent transforming growth factor beta1 activation in situ: quantitative and functional evidence after low-dose gamma-irradiation. FASEB J *11*, 991-1002.

Eimon, P. M., Kratz, E., Varfolomeev, E., Hymowitz, S. G., Stern, H., Zha, J., and Ashkenazi, A. (2006). Delineation of the cell-extrinsic apoptosis pathway in the zebrafish. Cell Death Differ *13*, 1619-1630.

El-Deiry, R. T. a. W. S. (2000). Wild-type p53 transactivates the KILLER/DR5 gene through an intronic sequence-specific DNA-binding site. Oncogene *19*, 1735-1743.

El-Deiry, W. S., Tokino, T., Velculescu, V. E., Levy, D. B., Parsons, R., Trent, J. M., Lin, D., Mercer, W. E., Kinzler, K. W., and Vogelstein, B. (1993). WAF1, a potential mediator of p53 tumor suppression. Cell *75*, 817-825.

Emery, J. G., McDonnell, P., Burke, M. B., Deen, K. C., Lyn, S., Silverman, C., Dul, E., Appelbaum, E. R., Eichman, C., DiPrinzio, R.*, et al.* (1998). Osteoprotegerin Is a Receptor for the Cytotoxic Ligand TRAIL. Journal of Biological Chemistry *273*, 14363-14367.

Essers, M. A. G., Weijzen, S., de Vries-Smits, A. M. M., Saarloos, I., de Ruiter, N. D., Bos, J. L., and Burgering, B. M. T. (2004). FOXO transcription factor activation by oxidative stress mediated by the small GTPase Ral and JNK. EMBO J *23*, 4802-4812.

Ewan, K. B., Henshall-Powell, R. L., Ravani, S. A., Pajares, M. J., Arteaga, C., Warters, R., Akhurst, R. J., and Barcellos-Hoff, M. H. (2002). Transforming Growth Factor-{beta}1 Mediates Cellular Response to DNA Damage in Situ. Cancer Res *62*, 5627-5631.

Fanger, N. A., Maliszewski, C. R., Schooley, K., and Griffith, T. S. (1999). Human Dendritic Cells Mediate Cellular Apoptosis via Tumor Necrosis Factor-Related Apoptosis-Inducing Ligand (Trail). J Exp Med *190*, 1155-1164.

Favata, M. F., Horiuchi, K. Y., Manos, E. J., Daulerio, A. J., Stradley, D. A., Feeser, W. S., Van Dyk, D. E., Pitts, W. J., Earl, R. A., Hobbs, F.*, et al.* (1998). Identification of a Novel Inhibitor of Mitogen-activated Protein Kinase Kinase. Journal of Biological Chemistry *273*, 18623-18632.

Fei, M., Zhao, Y., Wang, Y., Lu, M., Cheng, C., Huang, X., Zhang, D., Lu, J., He, S., and Shen, A. (2009). Low expression of Foxo3a is Associated with Poor Prognosis in Ovarian Cancer Patients. Cancer Investigation *27*, 52-59.

Feng, X.-H., and Derynck, R. (2005). SPECIFICITY AND VERSATILITY IN TGF-BETA SIGNALING THROUGH SMADS. Annual Review of Cell and Developmental Biology *21*, 659-693.

Finnberg, N., and El-Deiry, W. S. (2004). Activating FOXO3a, NF-kappaB and p53 by targeting IKKs: An effective multi-faceted targeting of the tumor-cell phenotype? Cancer Biology & Therapy *3*, 614-616.

Finnberg, N., Gruber, J. J., Fei, P., Rudolph, D., Bric, A., Kim, S.-H., Burns, T. F., Ajuha, H., Page, R., Wu, G. S.*, et al.* (2005). DR5 Knockout Mice Are Compromised in Radiation-Induced Apoptosis. Mol Cell Biol *25*, 2000-2013.

Finnberg, N., Klein-Szanto, A. J. P., and El-Deiry, W. S. (2008). TRAIL-R deficiency in mice promotes susceptibility to chronic inflammation and tumorigenesis. The Journal of Clinical Investigation *118*, 111-123.

Forrester, K., Almoguera, C., Han, K., Grizzle, W. E., and Perucho, M. (1987). Detection of high incidence of K-ras oncogenes during human colon tumorigenesis. Nature *327*, 298-303.

Fukuoka, M., Daitoku, H., Hatta, M., Matsuzaki, H., Umemura, S., and Fukamizu, A. (2003). Negative regulation of forkhead transcription factor AFX (Foxo4) by CBP-induced acetylation. International Journal of Molecular Medicine *12*, 503-508.

Furuyama, T., Nakazawa, T., Nakano, I., and Mori, N. (2000). Identification of the differential distribution patterns of mRNAs and consensus binding sequences for mouse DAF-16 homologues. Biochemical Journal *249*, 629-634.

Ganten, T. M., Koschny, R., Sykora, J., Schulze-Bergkamen, H., Buchler, P., Haas, T. L., Schader, M. B., Untergasser, A., Stremmel, W., and Walczak, H. (2006). Preclinical Differentiation between Apparently Safe and Potentially Hepatotoxic Applications of TRAIL Either Alone or in Combination with Chemotherapeutic Drugs. Clinical Cancer Research *12*, 2640-2646.

Gazitt, Y. (1999). TRAIL is a potent inducer of apoptosis in myeloma cells derived from multiple myeloma patients and is not cytotoxic to hematopoietic stem cells. Leukemia *13*, 1817–1824.

Gliniak, B., and Le, T. (1999). Tumor Necrosis Factor-related Apoptosis-inducing Ligand's Antitumor Activity in Vivo Is Enhanced by the Chemotherapeutic Agent CPT-11. Cancer Res *59*, 6153-6158.

Gobbi, G., Di Marcantonio, D., Micheloni, C., Carubbi, C., Galli, D., Vaccarezza, M., Bucci, G., Vitale, M., and Mirandola, P. (2012). TRAIL up-regulation must be accompanied by a reciprocal PKCε down-regulation during differentiation of colonic epithelial cell: Implications for colorectal cancer cell differentiation. Journal of Cellular Physiology *227*, 630-638.

Gong, B., and Almasan, A. (2000). Genomic Organization and Transcriptional Regulation of Human Apo2/TRAIL Gene. Biochemical and Biophysical Research Communications *278*, 747-752.

Gong, J., Yang, D., Kohanim, S., Humphreys, R., Broemeling, L., and Kurzrock, R. (2006). Novel in vivo imaging shows up-regulation of death receptors by paclitaxel and correlates with enhanced antitumor effects of receptor agonist antibodies. Molecular Cancer Therapeutics *5*, 2991-3000.

Gray, H. L., Sorensen, E. L., Hunt, J. S., and Ober, C. (2001). Three polymorphisms in the 3' UTR of the TRAIL (TNF-related apoptosis-inducing ligand) gene. Genes & Immunity *2*, 469-470.

Greco, F. A., Bonomi, P., Crawford, J., Kelly, K., Oh, Y., Halpern, W., Lo, L., Gallant, G., and Klein, J. (2008). Phase 2 study of mapatumumab, a fully human agonistic monoclonal antibody which targets and activates the TRAIL receptor-1, in patients with advanced non-small cell lung cancer. Lung Cancer *61*, 82-90.

Greer, E. L., Oskoui, P. R., Banko, M. R., Maniar, J. M., Gygi, M. P., Gygi, S. P., and Brunet, A. (2007). The Energy Sensor AMP-activated Protein Kinase Directly Regulates the Mammalian FOXO3 Transcription Factor. Journal of Biological Chemistry *282*, 30107-30119.

Griffith, T. S., and Broghammer, E. L. (2001). Suppression of Tumor Growth Following Intralesional Therapy with TRAIL Recombinant Adenovirus. Molecular Therapy *4*, 257–266.

Griffith, T. S., and Lynch, D. H. (1998). TRAIL: a molecule with multiple receptors and control mechanisms. Current Opinion in Immunology *10*, 559-563.

Griffith, T. S., Wiley, S. R., Kubin, M. Z., Sedger, L. M., Maliszewski, C. R., and Fanger, N. A. (1999). Monocyte-mediated Tumoricidal Activity via the Tumor Necrosis Factor-related Cytokine, TRAIL. J Exp Med *189*, 1343-1354.

Halaas, Vik, Ashkenazi, and Espevik (2000). Lipopolysaccharide Induces Expression of APO2 Ligand/TRAIL in Human Monocytes and Macrophages. Scandinavian Journal of Immunology *51*, 244-250.

Han, J., Hou, W., Goldstein, L. A., Lu, C., Stolz, D. B., Yin, X.-M., and Rabinowich, H. (2008). Involvement of Protective Autophagy in TRAIL Resistance of Apoptosis-defective Tumor Cells. Journal of Biological Chemistry *283*, 19665-19677.

He, C., Lao, W.-F., Hu, X.-T., Xu, X.-M., Xu, J., and Fang, B.-L. (2004). Anti-liver cancer activity of TNF-related apoptosis-inducing ligand gene and its bystander effects. World J Gastroenterol *10*, 654-659.

Herbst, R. S., Eckhardt, S. G., Kurzrock, R., Ebbinghaus, S., O'Dwyer, P. J., Gordon, M. S., Novotny, W., Goldwasser, M. A., Tohnya, T. M., Lum, B. L.*, et al.* (2006). Phase I Dose-Escalation Study of Recombinant Human Apo2L/TRAIL, a Dual Proapoptotic Receptor Agonist, in Patients With Advanced Cancer. Journal of Clinical Oncology *28*, 2839-2846.

Herbst, R. S., Eckhardt, S. G., Kurzrock, R., Ebbinghaus, S., O'Dwyer, P. J., Gordon, M. S., Novotny, W., Goldwasser, M. A., Tohnya, T. M., Lum, B. L.*, et al.* (2010a). Phase I Dose-Escalation Study of Recombinant Human Apo2L/TRAIL, a Dual Proapoptotic Receptor Agonist, in Patients With Advanced Cancer. Journal of Clinical Oncology *28*, 2839-2846.

Herbst, R. S., Kurzrock, R., Hong, D. S., Valdivieso, M., Hsu, C.-P., Goyal, L., Juan, G., Hwang, Y. C., Wong, S., Hill, J. S.*, et al.* (2010b). A First-in-Human Study of Conatumumab in Adult Patients with Advanced Solid Tumors. Clinical Cancer Research *16*, 5883-5891.

Herrero-Martin, G., Hoyer-Hansen, M., Garcia-Garcia, C., Fumarola, C., Farkas, T., Lopez-Rivas, A., and Jaattela, M. (2009). TAK1 activates AMPK-dependent cytoprotective autophagy in TRAIL-treated epithelial cells. EMBO J *28*, 677-685.

Herskind, C., Bentzen, S. M., Overgaard, J., Overgaard, M., Bamberg, M., and Rodemann, H. P. (1998). Differentiation state of skin fibroblast cultures versus risk of subcutaneous fibrosis after radiotherapy. Radiotherapy and Oncology *47*, 263-269.

Herskind, C., and Rodemann, H. P. (2000). Spontaneous and radiation-induced differentiationof fibroblasts. Experimental Gerontology *35*, 747-755.

Higuchi, H., Bronk, S. F., Taniai, M., Canbay, A., and Gores, G. J. (2002). Cholestasis Increases Tumor Necrosis Factor-Related Apoptotis-Inducing Ligand (TRAIL)-R2/DR5 Expression and Sensitizes the Liver to TRAIL-Mediated Cytotoxicity. Journal of Pharmacology and Experimental Therapeutics *303*, 461-467.

Hirose, T., Sowa, Y., Takahashi, S., Saito, S., Yasuda, C., Shindo, N., Furuichi, K., and Sakai, T. (2003). p53-independent induction of Gadd45 by histone deacetylase inhibitor: coordinate regulation by transcription factors Oct-1 and NF-Y. Oncogene *22*, 7762-7773.

Ho, T.-C., Chen, S.-L., Shih, S.-C., Chang, S.-J., Yang, S.-L., Hsieh, J.-W., Cheng, H.-C., Chen, L.-J., and Tsao, Y.-P. (2011). Pigment Epithelium-derived Factor (PEDF) Promotes Tumor Cell Death by Inducing Macrophage Membrane Tumor Necrosis Factor-related Apoptosis-inducing Ligand (TRAIL). Journal of Biological Chemistry *286*, 35943-35954.

Hoffmann, A., Levchenko, A., Scott, M. L., and Baltimore, D. (2002). The NFkB Signaling Module: Temporal Control and Selective Gene Activation. Science *298*, 1241-1245.

Hou, W., Han, J., Lu, C., Goldstein, L. A., and Rabinowich, H. (2008). Enhancement of tumor-TRAIL susceptibility by modulation of autophagy. Autophagy *4*, 940-943.

Hu, M. C. T., Lee, D.-F., Xia, W., Golfman, L. S., Ou-Yang, F., Yang, J.-Y., Zou, Y., Bao, S., Hanada, N., Saso, H., *et al.* (2004a). IkappaB Kinase Promotes Tumorigenesis through Inhibition of Forkhead FOXO3a. Cell *117*, 225-237.

Hu, M. C. T., Lee, D.-F., Xia, W., Golfman, L. S., Ou-Yang, F., Yang, J.-Y., Zou, Y., Bao, S., Hanada, N., Saso, H., *et al.* (2004b). IKB Kinase Promotes Tumorigenesis through Inhibition of Forkhead FOXO3a. Cell *117*, 225-237.

Huang, H., Regan, K. M., Wang, F., Wang, D., Smith, D. I., van Deursen, J. M. A., and Tindall, D. J. (2005). Skp2 inhibits FOXO1 in tumor suppression through ubiquitin-mediated degradation. Proceedings of the National Academy of Sciences of the United States of America *102*, 1649-1654.

Huang, W.-X., Huang, P., Gomes, A., and Hillert, J. (2000). Apoptosis mediators FasL and TRAIL are upregulated in peripheral blood mononuclear cells in MS. Neurology *55*, 928-934.

Huang, X., Lin, T., Gu, J., Zhang, L., Roth, J. A., Liu, J., and Fang, B. (2003). Cell to cell contact required for bystander effect of the TNF-related apoptosis-inducing ligand (TRAIL) gene. International Journal of Oncology *22*, 1241-1245.

Hymowitz, S. G., Christinger, H. W., Fuh, G., Ultsch, M., O'Connell, M., Kelley, R. F., Ashkenazi, A., and de Vos, A. M. (1999). Triggering Cell Death: The Crystal Structure of Apo2L/TRAIL in a Complex with Death Receptor 5. Molecular Cell *4*, 563-571.

Ikediobi, O. N., Davies, H., Bignell, G., Edkins, S., Stevens, C., O'Meara, S., Santarius, T., Avis, T., Barthorpe, S., Brackenbury, L., *et al.* (2006). Mutation analysis of 24 known cancer genes in the NCI-60 cell line set. Molecular Cancer Therapeutics *5*, 2606-2612.

Ishida, W., Mori, Y., Lakos, G., Sun, L., Shan, F., Bowes, S., Josiah, S., Lee, W.-C., Singh, J., Ling, L. E., and Varga, J. (2006). Intracellular TGF-[beta] Receptor Blockade Abrogates Smad-Dependent Fibroblast Activation In Vitro and In Vivo. J Invest Dermatol *126*, 1733-1744.

Iyer, S., Wang, Z., Akhtari, M., Zhao, W., and Seth, P. (2005). Targeting TGF Beta Signaling for Cancer Therapy. Cancer Biology and Therapy *4*, 260 - 265.

Jacobs, F. M. J., van der Heide, L. P., Wijchers, P. J. E. C., Burbach, J. P. H., Hoekman, M. F. M., and Smidt, M. P. (2003). FoxO6, a Novel Member of the FoxO Class of Transcription Factors with Distinct Shuttling Dynamics. Journal of Biological Chemistry *278*, 35959-35967.

Jeong, M., Kwon, Y.-S., Park, S.-H., Kim, C.-Y., Jeun, S.-S., Song, K.-W., Ko, Y., Robbins, P. D., Billiar, T. R., Kim, B.-M., and Seol, D.-W. (2009). Possible Novel Therapy for Malignant Gliomas with Secretable Trimeric TRAIL. PLoS ONE *4*, e4545.

Ji, Z., Flaherty, K. T., and Tsao, H. (2011). Targeting the RAS pathway in melanoma. Trends in Molecular Medicine.

Jiang, C. C., Chen, L. H., Gillespie, S., Kiejda, K. A., Mhaidat, N., Wang, Y. F., Thorne, R., Zhang, X. D., and Hersey, P. (2007). Tunicamycin Sensitizes Human Melanoma Cells to Tumor Necrosis Factor-Related Apoptosis-Inducing Ligand-Induced Apoptosis by Up-regulation of TRAIL-R2 via the Unfolded Protein Response. Cancer Research *67*, 5880-5888.

Jimbo, A., Fujita, E., Kouroku, Y., Ohnishi, J., Inohara, N., Kuida, K., Sakamaki, K., Yonehara, S., and Momoi, T. (2003). ER stress induces caspase-8 activation, stimulating cytochrome c release and caspase-9 activation. Experimental Cell Research *283*, 156-166.

Jin, Z., and El-Deiry, W. S. (2006). Distinct Signaling Pathways in TRAIL- versus Tumor Necrosis Factor-Induced Apoptosis. Molecular and Cellular Biology *26*, 8136-8148.

Jin, Z., McDonald, E. R., Dicker, D. T., and El-Deiry, W. S. (2004). Deficient Tumor Necrosis Factor-related Apoptosis-inducing Ligand (TRAIL) Death Receptor Transport to the Cell Surface in Human Colon Cancer Cells Selected for Resistance to TRAIL-induced Apoptosis. Journal of Biological Chemistry *279*, 35829-35839.

Jo, M., Kim, T.-H., Seol, D.-W., Esplen, J. E., Dorko, K., Billiar, T. R., and Strom, S. C. (2000). Apoptosis induced in normal human hepatocytes by tumor necrosis factor-related apoptosis-inducing ligand. Nat Med *6*, 564-567.

Jost, P. J., Grabow, S., Gray, D., McKenzie, M. D., Nachbur, U., Huang, D. C. S., Bouillet, P., Thomas, H. E., Borner, C., Silke, J.*, et al.* (2009). XIAP discriminates between type I and type II FAS-induced apoptosis. Nature *460*, 1035-1039.

Kagawa, S., He, C., Gu, J., Koch, P., Rha, S.-J., Roth, J. A., Curley, S. A., Stephens, L. C., and Fang, B. (2001). Antitumor Activity and Bystander Effects of the Tumor Necrosis Factor-related Apoptosis-inducing Ligand (TRAIL) Gene. Cancer Research *61*, 3330-3338.

Kalluri, R., and Neilson, E. G. (2003). Epithelial-mesenchymal transition and its implications for fibrosis. The Journal of Clinical Investigation *112*, 1776-1784.

Kang, Z., Chen, J.-J., Yu, Y., Li, B., Sun, S.-Y., Zhang, B., and Cao, L. (2011). Drozitumab, a Human Antibody to Death Receptor 5, Has Potent Antitumor Activity against Rhabdomyosarcoma with the Expression of Caspase-8 Predictive of Response. Clinical Cancer Research *17*, 3181-3192.

Kanzawa, T., Bedwell, J., Kondo, Y., Kondo, S., and Germano, I. M. (2003). Inhibition of DNA repair for sensitizing resistant glioma cells to temozolomide. Journal of Neurosurgery *99*, 1047-1052.

Kaplan-Lefko, P. J., Graves, J. D., Zoog, S. J., Pan, Y., Wall, J., Branstetter, D. G., Moriguchi, J., Coxon, A., Huard, J. N., Xu, R*., et al.* (2010). Conatumumab, a fully human agonist antibody to death receptor 5, induces apoptosis via caspase activation in multiple tumor types. Cancer Biology & Therapy *9*, 618-631.

Kau, T. R., Schroeder, F., Ramaswamy, S., Wojciechowski, C. L., Zhao, J. J., Roberts, T. M., Clardy, J., Sellers, W. R., and Silver, P. A. (2003). A chemical genetic screen identifies inhibitors of regulated nuclear export of a Forkhead transcription factor in PTEN-deficient tumor cells. Cancer cell *4*, 463-476.

Kayagaki, N., Yamaguchi, N., Nakayama, M., Eto, H., Okumura, K., and Yagita, H. (1999). Type I Interferons (IFNs) Regulate Tumor Necrosis Factor-related Apoptosis-inducing Ligand (TRAIL) Expression on Human T Cells: A Novel Mechanism for the Antitumor Effects of Type I IFNs. The Journal of Experimental Medicine *189*, 1451-1460.

Keane, M. M., Ettenberg, S. A., Nau, M. M., Russell, E. K., and Lipkowitz, S. (1999a). Chemotherapy augments TRAIL-induced apoptosis in breast cell lines. Cancer Res *59*, 734 - 741.

Keane, M. M., Ettenberg, S. A., Nau, M. M., Russell, E. K., and Lipkowitz, S. (1999b). Chemotherapy Augments TRAIL-induced Apoptosis in Breast Cell Lines. Cancer Res *59*, 734-741.

Kelley, S. K., Harris, L. A., Xie, D., DeForge, L., Totpal, K., Bussiere, J., and Fox, J. A. (2001). Preclinical Studies to Predict the Disposition of Apo2L/Tumor Necrosis Factor-Related Apoptosis-Inducing Ligand in Humans: Characterization of in Vivo Efficacy, Pharmacokinetics, and Safety. Journal of Pharmacology and Experimental Therapeutics *299*, 31-38.

Kemp, T. J., Ludwig, A. T., Earel, J. K., Moore, J. M., VanOosten, R. L., Moses, B., Leidal, K., Nauseef, W. M., and Griffith, T. S. (2005). Neutrophil stimulation with Mycobacterium bovis bacillus Calmette-Guerin (BCG) results in the release of functional soluble TRAIL/Apo-2L. Blood *106*, 3474-3482.

Kemp, T. J., Moore, J. M., and Griffith, T. S. (2004). Human B Cells Express Functional TRAIL/Apo-2 Ligand after CpG-Containing Oligodeoxynucleotide Stimulation. J Immunol *173*, 892-899.

Kikuchi, S., Miyagishi, R., Fukazawa, T., Yabe, I., Miyazaki, Y., and Sasaki, H. (2005). TNF-related apoptosis inducing ligand (TRAIL) gene polymorphism in Japanese patients with multiple sclerosis. Journal of Neuroimmunology *167*, 170-174.

Kikuchi, S., Nagai, T., Kunitama, M., Kirito, K., Ozawa, K., and Komatsu, N. (2007). Active FKHRL1 overcomes imatinib resistance in chronic myelogenous leukemia-derived cell lines via the production of tumor necrosis factor-related apoptosis-inducing ligand. Cancer Science *98*, 1949-1958.

Kim, K., Fisher, M. J., Xu, S.-Q., and El-Deiry, W. S. (2000). Molecular Determinants of Response to TRAIL in Killing of Normal and Cancer Cells. Clinical Cancer Research *6*, 335-346.

Kim, K.-B., Choi, Y.-H., Kim, I.-K., Chung, C.-W., Kim, B. J., Park, Y.-M., and Jung, Y.-K. (2002). POTENTIATION OF FAS- AND TRAIL-MEDIATED APOPTOSIS BY IFN-[gamma] IN A549 LUNG EPITHELIAL CELLS: ENHANCEMENT OF CASPASE-8 EXPRESSION THROUGH IFN-RESPONSE ELEMENT. Cytokine *20*, 283-288.

Kim, S. M., Lim, J. Y., Park, S. I., Jeong, C. H., Oh, J. H., Jeong, M., Oh, W., Park, S.-H., Sung, Y.-C., and Jeun, S.-S. (2008). Gene Therapy Using TRAIL-Secreting Human Umbilical Cord Blood-Derived Mesenchymal Stem Cells against Intracranial Glioma. Cancer Research *68*, 9614-9623.

Kirshner, J. R., Karpova, A. Y., Kops, M., and Howley, P. M. (2005). Identification of TRAIL as an Interferon Regulatory Factor 3 Transcriptional Target. J Virol *79*, 9320-9324.

Kischkel, F. C., Lawrence, D. A., Tinel, A., LeBlanc, H., Virmani, A., Schow, P., Gazdar, A., Blenis, J., Arnott, D., and Ashkenazi, A. (2001). Death Receptor Recruitment of Endogenous Caspase-10 and Apoptosis Initiation in the Absence of Caspase-8. Journal of Biological Chemistry *276*, 46639-46646.

Kitamura, T., Kitamura, Y. I., Funahashi, Y., Shawber, C. J., Castrillon, D. H., Kollipara, R., DePinho, R. A., Kitajewski, J., and Accili, D. (2007). A Foxo/Notch pathway controls myogenic differentiation and fiber type specification. The Journal of Clinical Investigation *117*, 2477-2485.

Kitamura, Y. I., Kitamura, T., Kruse, J.-P., Raum, J. C., Stein, R., Gu, W., and Accili, D. (2005). FoxO1 protects against pancreatic beta cell failure through NeuroD and MafA induction. Cell Metabolism *2*, 153-163.

Koga, Y., Matsuzaki, A., Suminoe, A., Hattori, H., and Hara, T. (2004). Neutrophil-Derived TNF-Related Apoptosis-Inducing Ligand (TRAIL): A Novel Mechanism of Antitumor Effect by Neutrophils. Cancer Res *64*, 1037-1043.

Kohlhaas, S. L., Craxton, A., Sun, X.-M., Pinkoski, M. J., and Cohen, G. M. (2007). Receptor-mediated Endocytosis Is Not Required for Tumor Necrosis Factor-related Apoptosis-inducing Ligand (TRAIL)-induced Apoptosis. Journal of Biological Chemistry *282*, 12831-12841.

Koornstra, J. J., Kleibeuker, J. H., van Geelen, C. M. M., Rijcken, F. E. M., Hollema, H., de Vries, E. G. E., and de Jong, S. (2003). Expression of TRAIL (TNF-related apoptosis-inducing ligand) and its receptors in normal colonic mucosa, adenomas, and carcinomas. The Journal of Pathology *200*, 327-335.

Kops, G. J. P. L., Ruiter, N. D. d., De Vries-Smits, A. M. M., Powell, D. R., Bos, J. L., and Burgering, B. M. T. (1999). Direct control of the Forkhead transcription factor AFX by protein kinase B. Nature *398*, 630-634.

Kornblau, S. M., Singh, N., Qiu, Y., Chen, W., Zhang, N., and Coombes, K. R. (2010). Highly Phosphorylated FOXO3A Is an Adverse Prognostic Factor in Acute Myeloid Leukemia. Clinical Cancer Research *16*, 1865-1874.

Krieg, A., Krieg, T., Wenzel, M., Schmitt, M., Ramp, U., Fang, B., Gabbert, H. E., Gerharz, C. D., and Mahotka, C. (2003). TRAIL-[beta] and TRAIL-[gamma]: two novel splice variants of the human TNF-related apoptosis-inducing ligand (TRAIL) without apoptotic potential. Br J Cancer *88*, 918-927.

Kuijlen, J. M. A., Mooij, J., Platteel, I., Hoving, E. W., van der Graaf, W., Span, M., Hollema, H., and den Dunnen, W. (2006). TRAIL-receptor expression is an independent prognostic factor for survival in patients with a primary glioblastoma multiforme. Journal of Neuro-Oncology *78*, 161-171.

Kuribayashi, K., Krigsfeld, G., Wang, W., Xu, J., Mayes, P., Dicker, D., Wu, G., and El-Deiry, W. (2008). TNFSF10 (TRAIL), a p53 target gene that mediates p53-dependent cell death. Cancer Biology and Therapy *7*, 2034-2038.

Laguinge, L. M., Samara, R. N., Wang, W., El-Deiry, W. S., Corner, G., Augenlicht, L., Mishra, L., and Jessup, J. M. (2008). DR5 Receptor Mediates Anoikis in Human Colorectal Carcinoma Cell Lines. Cancer Research *68*, 909-917.

Lamhamedi-Cherradi, S.-E., Zheng, S.-J., Maguschak, K. A., Peschon, J., and Chen, Y. H. (2003). Defective thymocyte apoptosis and accelerated autoimmune diseases in TRAIL-/- mice. Nat Immunol *4*, 255-260.

Lawrence, D., Shahrokh, Z., Marsters, S., Achilles, K., Shih, D., Mounho, B., Hillan, K., Totpal, K., DeForge, L., Schow, P.*, et al.* (2001). Differential hepatocyte toxicity of recombinant Apo2L/TRAIL versions. Nat Med *7*, 383-385.

Leask, A., and Abraham, D. J. (2004). TGF-{beta} signaling and the fibrotic response. FASEB J *18*, 816-827.

Lee, J., Hampl, M., Albert, P., and Fine, H. A. (2002). Antitumor activity and prolonged expression from a TRAIL-expressing adenoviral vector. Neoplasia *4*, 312-323.

Lee, S. H., Shin, M. S., Kim, H. S., Lee, H. K., Park, W. S., Kim, S. Y., Lee, J. H., Han, S. Y., Park, J. Y., Oh, R. R.*, et al.* (1999). Alterations of the DR5/TRAIL Receptor 2 Gene in Non-Small Cell Lung Cancers. Cancer Research *59*, 5683-5686.

Lee, S. H., Shin, M. S., Kim, H. S., Lee, H. K., Park, W. S., Kim, S. Y., Lee, J. H., Han, S. Y., Park, J. Y., Oh, R. R.*, et al.* (2001). Somatic mutations of TRAIL-receptor 1 and TRAIL-receptor 2 genes in non-Hodgkin's lymphoma. Oncogene *20*, 399-403.

Lehtinen, M. K., Yuan, Z., Boag, P. R., Yang, Y., Villen, J., Becker, E. B. E., DiBacco, S., de la Iglesia, N., Gygi, S., Blackwell, T. K., and Bonni, A. (2006). A Conserved MST-FOXO Signaling Pathway Mediates Oxidative-Stress Responses and Extends Life Span. Cell *125*, 987-1001.

Leong, S., Cohen, R. B., Gustafson, D. L., Langer, C. J., Camidge, D. R., Padavic, K., Gore, L., Smith, M., Chow, L. Q., von Mehren, M.*, et al.* (2009). Mapatumumab, an Antibody Targeting TRAIL-R1, in Combination With Paclitaxel and Carboplatin in Patients With Advanced Solid Malignancies: Results of a Phase I and Pharmacokinetic Study. J Clin Oncol *27*, 4413-4421.

Li, H., Zhu, H., Xu, C.-j., and Yuan, J. (1998). Cleavage of BID by Caspase 8 Mediates the Mitochondrial Damage in the Fas Pathway of Apoptosis. Cell *94*, 491-501.

Li, P., Lee, H., Guo, S., Unterman, T. G., Jenster, G., and Bai, W. (2003). AKT-Independent Protection of Prostate Cancer Cells from Apoptosis Mediated through Complex Formation between the Androgen Receptor and FKHR. Molecular and Cellular Biology *23*, 104-118.

Li, X., Monks, B., Ge, Q., and Birnbaum, M. J. (2007). Akt/PKB regulates hepatic metabolism by directly inhibiting PGC-1[alpha] transcription coactivator. Nature *447*, 1012-1016.

Lin, H.-H., Lai, S.-C., and Chau, L.-Y. (2011). Heme Oxygenase-1/Carbon Monoxide Induces Vascular Endothelial Growth Factor Expression via p38 Kinase-dependent Activation of Sp1. Journal of Biological Chemistry *286*, 3829-3838.

Lin, K., Baritaki, S., Militello, L., Malaponte, G., Bevelacqua, Y., and Bonavida, B. (2010). The Role of B-RAF Mutations in Melanoma and the Induction of EMT via Dysregulation of the NF-kB/Snail/RKIP/PTEN Circuit. Genes & Cancer *1*, 409-420.

Lin, Y., Devin, A., Cook, A., Keane, M. M., Kelliher, M., Lipkowitz, S., and Liu, Z.-g. (2000). The Death Domain Kinase RIP Is Essential for TRAIL (Apo2L)-Induced Activation of IκB Kinase and c-Jun N-Terminal Kinase. Molecular and Cellular Biology *20*, 6638-6645.

Lincz, L. F., Yeh, T. X., and Spencer, A. (2001). TRAIL-induced eradication of primary tumour cells from multiple myeloma patient bone marrows is not related to TRAIL receptor expression or prior chemotherapy. Leukemia : official journal of the Leukemia Society of America, Leukemia Research Fund, UK *15*, 1650-1657.

Lindegaard, J. C., and Grau, C. (2000). Has the outlook improved for amifostine as a clinical radioprotector? Radiotherapy and Oncology *57*, 113-118.

Liu, X., Yue, P., Khuri, F. R., and Sun, S.-Y. (2004). p53 Upregulates Death Receptor 4 Expression through an Intronic p53 Binding Site. Cancer Res *64*, 5078-5083.

Lluis, J. M., Nachbur, U., Cook, W. D., Gentle, I. E., Moujalled, D., Moulin, M., Wong, W. W.-L., Khan, N., Chau, D., Callus, B. A.*, et al.* (2010). TAK1 Is Required for Survival of Mouse

Fibroblasts Treated with TRAIL, and Does So by NF-κB Dependent Induction of cFLIPL. PLoS ONE *5*, e8620.

Lu, M., Ma, J., Xue, W., Cheng, C., Wang, Y., Zhao, Y., Ke, Q., Liu, H., Liu, Y., Li, P*., et al.* (2009). The Expression and Prognosis of FOXO3a and Skp2 in Human Hepatocellular Carcinoma. Pathology & Oncology Research *15*, 679-687.

Lu, M., Xiang, J., Xu, F., Wang, Y., Yin, Y., and Chen, D. (2011). The expression and significance of pThr32-FOXO3a in human ovarian cancer. Medical Oncology, 1-7.

Lub-de Hooge, M. N., de Vries, E. G. E., de Jong, S., and Bijl, M. (2005). Soluble TRAIL concentrations are raised in patients with systemic lupus erythematosus. Annals of the Rheumatic Diseases *64*, 854-858.

Ludwig, A. T., Moore, J. M., Luo, Y., Chen, X., Saltsgaver, N. A., O'Donnell, M. A., and Griffith, T. S. (2004). Tumor Necrosis Factor-Related Apoptosis-Inducing Ligand: A Novel Mechanism for Bacillus Calmette-Guerin-Induced Antitumor Activity. Cancer Res *64*, 3386-3390.

Lund, P., Kotova, I., Kedinger, V. r., Khanwalkar, H., Voltz, E., Hahn, W. C., and Gronemeyer, H. (2011). Transformation-Dependent Silencing of Tumor-Selective Apoptosis-Inducing TRAIL by DNA Hypermethylation Is Antagonized by Decitabine. Molecular Cancer Therapeutics *10*, 1611-1623.

Luo, J.-L., Maeda, S., Hsu, L.-C., Yagita, H., and Karin, M. (2004). Inhibition of NF- ∫ B in cancer cells converts inflammation- induced tumor growth mediated by TNF± to TRAIL-mediated tumor regression. Cancer cell *6*, 297-305.

Luo, X., Budihardjo, I., Zou, H., Slaughter, C., and Wang, X. (1998). Bid, a Bcl2 Interacting Protein, Mediates Cytochrome c Release from Mitochondria in Response to Activation of Cell Surface Death Receptors. Cell *94*, 481-490.

Luster, T. A., Carrell, J. A., McCormick, K., Sun, D., and Humphreys, R. (2009). Mapatumumab and lexatumumab induce apoptosis in TRAIL-R1 and TRAIL-R2 antibody-resistant NSCLC cell lines when treated in combination with bortezomib. Molecular Cancer Therapeutics *8*, 292-302.

M Saeed Sheikh, Y. H., Ester A Fernandez-Salas, Wafik S El-Deiry, Helmut Friess, Sally Amundson, Jing Yin, Stephen J Meltzer, Nikki J Holbrook and Albert J Fornace Jr (1999). The antiapoptotic decoy receptor TRID/TRAIL-R3 is a p53-regulated DNA damage-inducible gene that is overexpressed in primary tumors of the gastrointestinal tract. Oncogene *18*, 4153-4159.

Maas, C., Verbrugge, I., de Vries, E., Savich, G., van de Kooij, L. W., Tait, S. W. G., and Borst, J. (2010). Smac/DIABLO release from mitochondria and XIAP inhibition are essential to limit clonogenicity of Type I tumor cells after TRAIL receptor stimulation. Cell Death Differ *17*, 1613-1623.

MacFarlane, M., Ahmad, M., Srinivasula, S. M., Fernandes-Alnemri, T., Cohen, G. M., and Alnemri, E. S. (1997). Identification and Molecular Cloning of Two Novel Receptors for the Cytotoxic Ligand TRAIL. Journal of Biological Chemistry *272*, 25417-25420.

Marini, P., Denzinger, S., Schiller, D., Kauder, S., Welz, S., Humphreys, R., Daniel, P. T., Jendrossek, V., Budach, W., and Belka, C. (2006). Combined treatment of colorectal tumours with agonistic TRAIL receptor antibodies HGS-ETR1 and HGS-ETR2 and radiotherapy: enhanced effects in vitro and dose-dependent growth delay in vivo. Oncogene *25*, 5145-5154.

Marini, P., Schmid, A., Jendrossek, V., Faltin, H., Daniel, P., Budach, W., and Belka, C. (2005). Irradiation specifically sensitises solid tumour cell lines to TRAIL mediated apoptosis. BMC Cancer *5*, 5.

Marsters, S. A., Sheridan, J. P., Pitti, R. M., Huang, A., Skubatch, M., Baldwin, D., Yuan, J., Gurney, A., Goddard, A. D., Godowski, P., and Ashkenazi, A. (1997). A novel receptor for Apo2L/TRAIL contains a truncated death domain. Current Biology *7*, 1003-1006.

Martin, G., Sprague, C., Norwood, T., and Pendergrass, W. (1974). Clonal Selection, Attenuation and Differentiation in an In Vitro Model of Hyperplasia. Am J Pathol *74*, 137–154.

Matsuda, T., Almasan, A., Tomita, M., Uchihara, J.-n., Masuda, M., Ohshiro, K., Takasu, N., Yagita, H., Ohta, T., and Mori, N. (2005). Resistance to Apo2 Ligand (Apo2L)/Tumor Necrosis Factor-Related Apoptosis-Inducing Ligand (TRAIL)-Mediated Apoptosis and Constitutive Expression of Apo2L/TRAIL in Human T-Cell Leukemia Virus Type 1-Infected T-Cell Lines. Journal of Virology *79*, 1367-1378.

Matsuzaki, H., Daitoku, H., Hatta, M., Aoyama, H., Yoshimochi, K., and Fukamizu, A. (2005). Acetylation of Foxo1 alters its DNA-binding ability and sensitivity to phosphorylation. Proceedings of the National Academy of Sciences of the United States of America *102*, 11278-11283.

Matsuzaki, H., Daitoku, H., Hatta, M., Tanaka, K., and Fukamizu, A. (2003). Insulin-induced phosphorylation of FKHR (Foxo1) targets to proteasomal degradation. Proceedings of the National Academy of Sciences *100*, 11285-11290.

Matysiak, M., Jurewicz, A., Jaskolski, D., and Selmaj, K. (2002). TRAIL induces death of human oligodendrocytes isolated from adult brain. Brain *125*, 2469-2480.

Meng, X. W., Lee, S.-H., Dai, H., Loegering, D., Yu, C., Flatten, K., Schneider, P., Dai, N. T., Kumar, S. K., Smith, B. D.*, et al.* (2007). MCL-1 as a Buffer for Proapoptotic BCL-2 Family Members during TRAIL-induced Apoptosis. Journal of Biological Chemistry *282*, 29831-29846.

Micheau, O., Thome, M., Schneider, P., Holler, N., Tschopp, J., Nicholson, D. W., Briand, C., and Gr√ºtter, M. G. (2002). The Long Form of FLIP Is an Activator of Caspase-8 at the Fas Death-inducing Signaling Complex. Journal of Biological Chemistry *277*, 45162-45171.

Michowitz, Y., Goldstein, E., Roth, A., Afek, A., Abashidze, A., Ben Gal, Y., Keren, G., and George, J. (2005). The involvement of tumor necrosis factor-related apoptosis-inducing ligand (TRAIL) in atherosclerosis. Journal of the American College of Cardiology *45*, 1018-1024.

Mills, K. R., Reginato, M., Debnath, J., Queenan, B., and Brugge, J. S. (2004). Tumor necrosis factor-related apoptosis-inducing ligand (TRAIL) is required for induction of autophagy during lumen formation in vitro. Proceedings of the National Academy of Sciences of the United States of America *101*, 3438-3443.

Mizutani, Y., Yoshida, O., Miki, T., and Bonavida, B. (1999). Synergistic Cytotoxicity and Apoptosis by Apo-2 Ligand and Adriamycin against Bladder Cancer Cells. Clinical Cancer Research *5*, 2605-2612.

Modur, V., Nagarajan, R., Evers, B. M., and Milbrandt, J. (2002). FOXO Proteins Regulate Tumor Necrosis Factor-related Apoptosis Inducing Ligand Expression. Journal of Biological Chemistry *277*, 47928-47937.

Mohr, A., Henderson, G., Dudus, L., Herr, I., Kuerschner, T., Debatin, K. M., Weiher, H., Fisher, K. J., and Zwacka, R. M. (2004). AAV-encoded expression of TRAIL in experimental human colorectal cancer leads to tumor regression. Gene Ther *11*, 534-543.

Mom, C. H., Verweij, J., Oldenhuis, C. N. A. M., Gietema, J. A., Fox, N. L., Miceli, R. e., Eskens, F. A. L. M., Loos, W. J., de Vries, E. G. E., and Sleijfer, S. (2009). Mapatumumab, a Fully Human Agonistic Monoclonal Antibody That Targets TRAIL-R1, in Combination with Gemcitabine and Cisplatin: a Phase I Study. Clinical Cancer Research *15*, 5584-5590.

Mongkolsapaya, J., Cowper, A. E., Xu, X.-N., Morris, G., McMichael, A. J., Bell, J. I., and Screaton, G. R. (1998). Cutting Edge: Lymphocyte Inhibitor of TRAIL (TNF-Related Apoptosis-Inducing Ligand): A New Receptor Protecting Lymphocytes from the Death Ligand TRAIL. J Immunol *160*, 3-6.

Mongkolsapaya, J., Grimes, J. M., Chen, N., Xu, X.-N., Stuart, D. I., Jones, E. Y., and Screaton, G. R. (1999). Structure of the TRAIL-DR5 complex reveals mechanisms conferring specificity in apoptotic initiation. Nat Struct Mol Biol *6*, 1048-1053.

Nakae, J., Park, B.-C., and Accili, D. (1999). Insulin Stimulates Phosphorylation of the Forkhead Transcription Factor FKHR on Serine 253 through a Wortmannin-sensitive Pathway. Journal of Biological Chemistry *274*, 15982-15985.

Nawrocki, S. T., Carew, J. S., Douglas, L., Cleveland, J. L., Humphreys, R., and Houghton, J. A. (2007). Histone Deacetylase Inhibitors Enhance Lexatumumab-Induced Apoptosis via a p21Cip1-Dependent Decrease in Survivin Levels. Cancer Research *67*, 6987-6994.

Nebbioso, A., Clarke, N., Voltz, E., Germain, E., Ambrosino, C., Bontempo, P., Alvarez, R., Schiavone, E. M., Ferrara, F., Bresciani, F., *et al.* (2005). Tumor-selective action of HDAC inhibitors involves TRAIL induction in acute myeloid leukemia cells. Nat Med *11*, 77-84.

Nemoto, S., Fergusson, M. M., and Finkel, T. (2004). Nutrient Availability Regulates SIRT1 Through a Forkhead-Dependent Pathway. Science *306*, 2105-2108.

Nesterov, A., Nikrad, M., Johnson, T., and Kraft, A. S. (2004). Oncogenic Ras Sensitizes Normal Human Cells to Tumor Necrosis Factor-alpha-Related Apoptosis-Inducing Ligand-Induced Apoptosis. Cancer Research *64*, 3922-3927.

Nimmanapalli, R., Perkins, C. L., Orlando, M., O'Bryan, E., Nguyen, D., and Bhalla, K. N. (2001). Pretreatment with Paclitaxel Enhances Apo-2 Ligand/Tumor Necrosis Factor-related Apoptosis-inducing Ligand-induced Apoptosis of Prostate Cancer Cells by Inducing Death Receptors 4 and 5 Protein Levels. Cancer Res *61*, 759-763.

Nitsch, R., Bechmann, I., Deisz, R. A., Haas, D., Lehmann, T. N., Wendling, U., and Zipp, F. (2000). Human brain-cell death induced by tumour-necrosis-factor-related apoptosis-inducing ligand (TRAIL). The Lancet *356*, 827-828.

Obsilova, V., Vecer, J., Herman, P., Pabianova, A., Sulc, M., Teisinger, J., Boura, E., and Obsil, T. (2005). 14-3-3 Protein Interacts with Nuclear Localization Sequence of Forkhead Transcription Factor FoxO4. Biochemistry *44*, 11608-11617.

Oh, S. W., Mukhopadhyay, A., Svrzikapa, N., Jiang, F., Davis, R. J., and Tissenbaum, H. A. (2005). JNK regulates lifespan in Caenorhabditis elegans by modulating nuclear translocation of forkhead transcription factor/DAF-16. Proceedings of the National Academy of Sciences of the United States of America *102*, 4494-4499.

Ou, D., Wang, X., Metzger, D. L., Robbins, M., Huang, J., Jobin, C., Chantler, J. K., James, R. F. L., Pozzilli, P., and Tingle, A. J. (2005). Regulation of TNF-Related Apoptosis-Inducing Ligand-Mediated Death-Signal Pathway in Human beta Cells by Fas-Associated Death Domain and Nuclear Factor κB. Human Immunology *66*, 799-809.

Ozoren, N., and El-Deiry, W. (2002). Heat Shock Protects HCT116 and H460 Cells from TRAIL-Induced Apoptosis. Experimental Cell Research *281*, 175-181.

Ozoren, N., Kim, K., Burns, T. F., Dicker, D. T., Moscioni, A. D., and El-Deiry, W. S. (2000). The Caspase 9 Inhibitor Z-LEHD-FMK Protects Human Liver Cells while Permitting Death of Cancer Cells Exposed to Tumor Necrosis Factor-related Apoptosis-inducing Ligand. Cancer Research *60*, 6259-6265.

Pai, S. I., Wu, G. S., √ ñz√ ∂ ren, N., Wu, L., Jen, J., Sidransky, D., and El-Deiry, W. S. (1998). Rare Loss-of-Function Mutation of a Death Receptor Gene in Head and Neck Cancer. Cancer Research *58*, 3513-3518.

Pal, R., Gochhait, S., Chattopadhyay, S., Gupta, P., Prakash, N., Agarwal, G., Chaturvedi, A., Husain, N., Husain, S., and Bamezai, R. (2011). Functional implication of TRAIL −716 C/T promoter polymorphism on its in vitro and in vivo expression and the susceptibility to sporadic breast tumor. Breast Cancer Research and Treatment *126*, 333-343.

Pan, G., Ni, J., Wei, Y.-F., Yu, G.-l., Gentz, R., and Dixit, V. M. (1997a). An Antagonist Decoy Receptor and a Death Domain-Containing Receptor for TRAIL. Science *277*, 815-818.

Pan, G., Ni, J., Wei, Y. F., Yu, G., Gentz, R., and Dixit, V. M. (1997b). An antagonist decoy receptor and a death domain-containing receptor for TRAIL. Science *277*, 815 - 818.

Pan, G., Ni, J., Yu, G.-l., Wei, Y.-F., and Dixit, V. M. (1998). TRUNDD, a new member of the TRAIL receptor family that antagonizes TRAIL signalling. FEBS Letters *424*, 41-45.

Pan, G., O'Rourke, K., Chinnaiyan, A. M., Gentz, R., Ebner, R., Ni, J., and Dixit, V. M. (1997c). The receptor for the cytotoxic ligand TRAIL. Science *276*, 111 - 113.

Pan, G., O'Rourke, K., Chinnaiyan, A. M., Gentz, R., Ebner, R., Ni, J., and Dixit, V. M. (1997d). The Receptor for the Cytotoxic Ligand TRAIL. Science *276*, 111-113.

Park, K.-J., Lee, S.-H., Kim, T.-I., Lee, H.-W., Lee, C.-H., Kim, E.-H., Jang, J.-Y., Choi, K. S., Kwon, M.-H., and Kim, Y.-S. (2007). A Human scFv Antibody against TRAIL Receptor 2 Induces Autophagic Cell Death in Both TRAIL-Sensitive and TRAIL-Resistant Cancer Cells. Cancer Research *67*, 7327-7334.

Pascal, S. (2000). Production of recombinant TRAIL and TRAIL receptor: Fc chimeric proteins. In Methods in Enzymology, C.R. John, ed. (Academic Press), pp. 325-345.

Pitti, R. M., Marsters, S. A., Ruppert, S., Donahue, C. J., Moore, A., and Ashkenazi, A. (1996). Induction of Apoptosis by Apo-2 Ligand, a New Member of the Tumor Necrosis Factor Cytokine Family. Journal of Biological Chemistry *271*, 12687-12690.

Plas, D. R., and Thompson, C. B. (2003). Akt Activation Promotes Degradation of Tuberin and FOXO3a via the Proteasome. Journal of Biological Chemistry *278*, 12361-12366.

Plummer, R., Attard, G., Pacey, S., Li, L., Razak, A., Perrett, R., Barrett, M., Judson, I., Kaye, S., Fox, N. L.*, et al.* (2007). Phase 1 and Pharmacokinetic Study of Lexatumumab in Patients with Advanced Cancers. Clinical Cancer Research *13*, 6187-6194.

Pollack, I. F., Erff, M., and Ashkenazi, A. (2001). Direct Stimulation of Apoptotic Signaling by Soluble Apo2L/Tumor Necrosis Factor-related Apoptosis-inducing Ligand Leads to Selective Killing of Glioma Cells. Clinical Cancer Research *7*, 1362-1369.

Rades, D., Fehlauer, F., Bajrovic, A., Mahlmann, B., Richter, E., and Alberti, W. (2004). Serious adverse effects of amifostine during radiotherapy in head and neck cancer patients. Radiotherapy and Oncology *70*, 261-264.

Reiss, M. (1997). Transforming growth factor-β in breast cancer: A working hypothesis Breast Cancer Research and Treatment *45*, 81-95.

Rena, G., Woods, Y. L., Prescott, A. R., Peggie, M., Unterman, T. G., Williams, M. R., and Cohen, P. (2002). Two novel phosphorylation sites on FKHR that are critical for its nuclear exclusion. EMBO J *21*, 2263-2271.

Ricci, M. S., Jin, Z., Dews, M., Yu, D., Thomas-Tikhonenko, A., Dicker, D. T., and El-Deiry, W. S. (2004). Direct Repression of FLIP Expression by c-myc Is a Major Determinant of TRAIL Sensitivity. Molecular and Cellular Biology *24*, 8541-8555.

Ricci, M. S., Kim, S.-H., Ogi, K., Plastaras, J. P., Ling, J., Wang, W., Jin, Z., Liu, Y. Y., Dicker, D. T., Chiao, P. J.*, et al.* (2007). Reduction of TRAIL-Induced Mcl-1 and cIAP2 by c-Myc or Sorafenib Sensitizes Resistant Human Cancer Cells to TRAIL-Induced Death. Cancer cell *12*, 66-80.

Ringborg, U., Bergqvist, D., Brorsson, B., Eva, C. S., Ceberg, J., Einhorn, N., Frodin, J.-E., Jarhult, J., Lamnevik, G., Lindholm, C.*, et al.* (2003). The Swedish Council on Technology Assessment in Health Care (SBU) Systematic Overview of Radiotherapy for Cancer including a Prospective Survey of Radiotherapy Practice in Sweden 2001--Summary and Conclusions. Acta Oncologica *42*, 1.

Roberts, A. B., Tian, F., Byfield, S. D., Stuelten, C., Ooshima, A., Saika, S., and Flanders, K. C. Smad3 is key to TGF-[beta]-mediated epithelial-to-mesenchymal transition, fibrosis, tumor suppression and metastasis. Cytokine & Growth Factor Reviews *17*, 19-27.

Rodemann, H., Peterson, H., Schwenke, K., and von Wangenheim, K. (1991). Terminal differentiation of human fibroblasts is induced by radiation. Scanning Microscopy *5*, 1135-1142.

Rosato, R. R., Almenara, J. A., Coe, S., and Grant, S. (2007). The Multikinase Inhibitor Sorafenib Potentiates TRAIL Lethality in Human Leukemia Cells in Association with Mcl-1 and cFLIPL Down-regulation. Cancer Res *67*, 9490-9500.

Rossin, A. l., Derouet, M., Abdel-sater, F., and Hueber, A.-O. (2009). Palmitoylation of the TRAIL receptor DR4 confers an efficient TRAIL-induced cell death signalling. Biochem J *419*, 185-192.

Roth, W., Isenmann, S., Naumann, U., Kugler, S., Bahr, M., Dichgans, J., Ashkenazi, A., and Weller, M. (1999). Locoregional Apo2L/TRAIL Eradicates Intracranial Human Malignant Glioma Xenografts in Athymic Mice in the Absence of Neurotoxicity. Biochemical and Biophysical Research Communications *265*, 479-483.

Samara, R. N., Laguinge, L. M., and Jessup, J. M. (2007). Carcinoembryonic Antigen Inhibits Anoikis in Colorectal Carcinoma Cells by Interfering with Trail-R2 (DR5) Signaling. Cancer Research *67*, 4774-4782.

Sanlioglu, A., Dirice, E., Aydin, C., Erin, N., Koksoy, S., and Sanlioglu, S. (2005). Surface TRAIL decoy receptor-4 expression is correlated with TRAIL resistance in MCF7 breast cancer cells. BMC Cancer *5*, 54.

Sanlioglu, A. D., Karacay, B., Koksal, I. T., Griffith, T. S., and Sanlioglu, S. (2007). DcR2 (TRAIL-R4) siRNA and adenovirus delivery of TRAIL (Ad5hTRAIL) break down in vitro tumorigenic potential of prostate carcinoma cells. Cancer Gene Ther *14*, 976-984.

Sasportas, L. S., Kasmieh, R., Wakimoto, H., Hingtgen, S., van de Water, J. A. J. M., Mohapatra, G., Figueiredo, J. L., Martuza, R. L., Weissleder, R., and Shah, K. (2009). Assessment of therapeutic efficacy and fate of engineered human mesenchymal stem cells for cancer therapy. Proceedings of the National Academy of Sciences.

Saulle, E., Petronelli, A., Pasquini, L., Petrucci, E., Mariani, G., Biffoni, M., Ferretti, G., Scambia, G., Benedetti-Panici, P., Cognetti, F.*, et al.* (2007). Proteasome inhibitors sensitize ovarian cancer cells to TRAIL induced apoptosis. Apoptosis *12*, 635-655.

Schilling, M. M., Oeser, J. K., Boustead, J. N., Flemming, B. P., and O'Brien, R. M. (2006). Gluconeogenesis: Re-evaluating the FOXO1-PGC-1[alpha] connection. Nature *443*, E10-E11.

Schoppet, M., Sattler, A. M., Schaefer, J. R., and Hofbauer, L. C. (2006). Osteoprotegerin (OPG) and tumor necrosis factor-related apoptosis-inducing ligand (TRAIL) levels in atherosclerosis. Atherosclerosis *184*, 446-447.

Senf, S. M., Sandesara, P. B., Reed, S. A., and Judge, A. R. (2011). p300 Acetyltransferase activity differentially regulates the localization and activity of the FOXO homologues in skeletal muscle. American Journal of Physiology - Cell Physiology *300*, C1490-C1501.

Seoane, J., Le, H.-V., Shen, L., Anderson, S. A., and Massague, J. (2004). Integration of Smad and Forkhead Pathways in the Control of Neuroepithelial and Glioblastoma Cell Proliferation. Cell *117*, 211-223.

Seol, J. Y., Park, K.-H., Hwang, C.-I., Park, W.-Y., Yoo, C.-G., Kim, Y. W., Han, S. K., Shim, Y.-S., and Lee, C.-T. (2003). Adenovirus-TRAIL can overcome TRAIL resistance and induce a bystander effect. Cancer Gene Ther *10*, 540-548.

Shao, R.-G., Shimizu, T., and Pommier, Y. (1996). Brefeldin A Is a Potent Inducer of Apoptosis in Human Cancer Cells Independently of p53. Experimental Cell Research *227*, 190-196.

Shapiro, M. B., and Senapathy, P. (1987). RNA splice junctions of different classes of eukaryotes: sequence statistics and functional implications in gene expression. Nucleic Acids Research *15*, 7155-7174.

Shareef, M. M., Cui, N., Burikhanov, R., Gupta, S., Satishkumar, S., Shajahan, S., Mohiuddin, M., Rangnekar, V. M., and Ahmed, M. M. (2007). Role of Tumor Necrosis Factor-α and TRAIL in High-Dose Radiation-Induced Bystander Signaling in Lung Adenocarcinoma. Cancer Research *67*, 11811-11820.

Sheikh, M. S., Burns, T. F., Huang, Y., Wu, G. S., Amundson, S., Brooks, K. S., Fornace, A. J., and el-Deiry, W. S. (1998). p53-dependent and -independent regulation of the death receptor KILLER/DR5 gene expression in response to genotoxic stress and tumor necrosis factor alpha. Cancer Res *58*, 1593 - 1598.

Sheridan, J. P., Marsters, S. A., Pitti, R. M., Gurney, A., Skubatch, M., Baldwin, D., Ramakrishnan, L., Gray, C. L., Baker, K., Wood, W. I.*, et al.* (1997). Control of TRAIL-Induced Apoptosis by a Family of Signaling and Decoy Receptors. Science *277*, 818-821.

Shin, M. S., Kim, H. S., Lee, S. H., Park, W. S., Kim, S. Y., Park, J. Y., Lee, J. H., Lee, S. K., Lee, S. N., Jung, S. S.*, et al.* (2001). Mutations of Tumor Necrosis Factor-related Apoptosis-inducing Ligand Receptor 1 (TRAIL-R1) and Receptor 2 (TRAIL-R2) Genes in Metastatic Breast Cancers. Cancer Research *61*, 4942-4946.

Siegel, P. M., and Massague, J. (2003). Cytostatic and apoptotic actions of TGF-[beta] in homeostasis and cancer. Nat Rev Cancer *3*, 807-820.

Siegel, P. M., Shu, W., Cardiff, R. D., Muller, W. J., and Massague, J. (2003). Transforming growth factor beta signaling impairs Neu-induced mammary tumorigenesis while promoting pulmonary metastasis. Proceedings of the National Academy of Sciences of the United States of America *100*, 8430-8435.

Simons, M. P., Leidal, K. G., Nauseef, W. M., and Griffith, T. S. (2008). TNF-related apoptosis-inducing ligand (TRAIL) is expressed throughout myeloid development, resulting in a broad distribution among neutrophil granules. J Leukoc Biol *83*, 621-629.

Simons, M. P., Moore, J. M., Kemp, T. J., and Griffith, T. S. (2007). Identification of the Mycobacterial Subcomponents Involved in the Release of Tumor Necrosis Factor-Related Apoptosis-Inducing Ligand from Human Neutrophils. Infect Immun *75*, 1265-1271.

Singh, A., Ye, M., Bucur, O., Zhu, S., Tanya Santos, M., Rabinovitz, I., Wei, W., Gao, D., Hahn, W. C., and Khosravi-Far, R. (2010). Protein Phosphatase 2A Reactivates FOXO3a through a Dynamic Interplay with 14-3-3 and AKT. Molecular Biology of the Cell *21*, 1140-1152.

Smith, M. R., Jin, F., and Joshi, I. (2007). Bortezomib Sensitizes Non-Hodgkin's Lymphoma Cells to Apoptosis Induced by Antibodies to Tumor Necrosis Factor-Related Apoptosis-Inducing Ligand (TRAIL) Receptors TRAIL-R1 and TRAIL-R2. Clinical Cancer Research *13*, 5528s-5534s.

Solis, M., Goubau, D., Romieu-Mourez, R. I., Genin, P., Civas, A., and Hiscott, J. (2006). Distinct functions of IRF-3 and IRF-7 in IFN-alpha gene regulation and control of anti-tumor activity in primary macrophages. Biochemical Pharmacology *72*, 1469-1476.

Sprick, M. R., Rieser, E., Stahl, H., Grosse-Wilde, A., Weigand, M. A., and Walczak, H. (2002). Caspase-10 is recruited to and activated at the native TRAIL and CD95 death-inducing signalling complexes in a FADD-dependent manner but can not functionally substitute caspase-8. EMBO J *21*, 4520-4530.

Su, Z., Xin, S., Xu, L., Cheng, J., Guo, J., Li, L., and Wei, Q. (2012). The calcineurin B subunit induces TNF-related apoptosis-inducing ligand (TRAIL) expression via CD11b-NF-κB pathway in RAW264.7 macrophages. Biochemical and Biophysical Research Communications *417*, 777-783.

Subramanian, A., Tamayo, P., Mootha, V. K., Mukherjee, S., Ebert, B. L., Gillette, M. A., Paulovich, A., Pomeroy, S. L., Golub, T. R., Lander, E. S., and Mesirov, J. P. (2005). Gene set enrichment analysis: A knowledge-based approach for interpreting genome-wide expression profiles. Proceedings of the National Academy of Sciences of the United States of America *102*, 15545-15550.

Sun, S.-Y., Yue, P., Zhou, J.-Y., Wang, Y., Choi Kim, H.-R., Lotan, R., and Sheng Wu, G. (2001). Overexpression of Bcl2 Blocks TNF-Related Apoptosis-Inducing Ligand (TRAIL)-Induced Apoptosis in Human Lung Cancer Cells. Biochemical and Biophysical Research Communications *280*, 788-797.

Sun, X.-M., Bratton, S. B., Butterworth, M., MacFarlane, M., and Cohen, G. M. (2002). Bcl-2 and Bcl-xL Inhibit CD95-mediated Apoptosis by Preventing Mitochondrial Release of Smac/DIABLO and Subsequent Inactivation of X-linked Inhibitor-of-Apoptosis Protein. Journal of Biological Chemistry *277*, 11345-11351.

Sun, X.-Y., Nong, J., Qin, K., Lu, H., Moniri, M. R., Dai, L.-J., and Warnock, G. L. (2011). MSCTRAIL-mediated HepG2 Cell Death in Direct and Indirect Co-cultures. Anticancer Research *31*, 3705-3712.

Tartaglia, L. A., Ayres, T. M., Wong, G. H. W., and Goeddel, D. V. (1993). A novel domain within the 55 kd TNF receptor signals cell death. Cell *74*, 845-853.

Tecchio, C., Huber, V., Scapini, P., Calzetti, F., Margotto, D., Todeschini, G., Pilla, L., Martinelli, G., Pizzolo, G., Rivoltini, L., and Cassatella, M. A. (2004). IFN{alpha}-stimulated neutrophils and monocytes release a soluble form of TNF-related apoptosis-inducing ligand (TRAIL/Apo-2 ligand) displaying apoptotic activity on leukemic cells. Blood *103*, 3837-3844.

Thome, M., and Tschopp, J. r. (2001). Regulation of lymphocyte proliferation and death by flip. Nat Rev Immunol *1*, 50-58.

Tiwary, R., Yu, W., Li, J., Park, S.-K., Sanders, B. G., and Kline, K. (2010). Role of Endoplasmic Reticulum Stress in α-TEA Mediated TRAIL/DR5 Death Receptor Dependent Apoptosis. PLoS ONE *5*, e11865.

Trarbach, T., Moehler, M., Heinemann, V., Kohne, C. H., Przyborek, M., Schulz, C., Sneller, V., Gallant, G., and Kanzler, S. (2010). Phase II trial of mapatumumab, a fully human agonistic monoclonal antibody that targets and activates the tumour necrosis factor apoptosis-inducing ligand receptor-1 (TRAIL-R1), in patients with refractory colorectal cancer. Br J Cancer *102*, 506-512.

Tsai, K.-L., Sun, Y.-J., Huang, C.-Y., Yang, J.-Y., Hung, M.-C., and Hsiao, C.-D. (2007). Crystal structure of the human FOXO3a-DBD/DNA complex suggests the effects of post-translational modification. Nucleic Acids Research *35*, 6984-6994.

Tu, Z., Hamalainen-Laanaya, H. K., Crispe, I. N., and Orloff, M. S. (2011). Synergy between TLR3 and IL-18 promotes IFN-γ dependent TRAIL expression in human liver NK cells. Cellular Immunology *271*, 286-291.

Unnithan, J., and Macklis, R. M. (2004). TRAIL Induction by Radiation in Lymphoma Patients. Cancer Investigation *22*, 522-525.

Unoki, M., Furuta, S., Onouchi, Y., Watanabe, O., Doi, S., Fujiwara, H., Miyatake, A., Fujita, K., Tamari, M., and Nakamura, Y. (2000). Association studies of 33 single nucleotide polymorphisms (SNPs) in 29 candidate genes for bronchial asthma: positive association of a T924C polymorphism in the thromboxane A2 receptor gene. Human Genetics *106*, 440-446.

van der Horst, A., de Vries-Smits, A. M. M., Brenkman, A. B., van Triest, M. H., van den Broek, N., Colland, F., Maurice, M. M., and Burgering, B. M. T. (2006). FOXO4 transcriptional activity is regulated by monoubiquitination and USP7/HAUSP. Nat Cell Biol *8*, 1064-1073.

van der Horst, A., Tertoolen, L. G. J., de Vries-Smits, L. M. M., Frye, R. A., Medema, R. H., and Burgering, B. M. T. (2004). FOXO4 Is Acetylated upon Peroxide Stress and Deacetylated by the Longevity Protein hSir2SIRT1. Journal of Biological Chemistry *279*, 28873-28879.

van der Sloot, A. M., Mullally, M. M., Fernandez-Ballester, G., Serrano, L., and Quax, W. J. (2004). Stabilization of TRAIL, an all-B-sheet multimeric protein, using computational redesign. Protein Engineering Design and Selection *17*, 673-680.

van der Sloot, A. M., Tur, V., Szegezdi, E., Mullally, M. M., Cool, R. H., Samali, A., Serrano, L., and Quax, W. J. (2006). Designed tumor necrosis factor-related apoptosis-inducing ligand variants initiating apoptosis exclusively via the DR5 receptor. Proceedings of the National Academy of Sciences *103*, 8634-8639.

van Grevenynghe, J., Cubas, R. A., Noto, A., DaFonseca, S., He, Z., Peretz, Y., Filali-Mouhim, A., Dupuy, F. P., Procopio, F. A., Chomont, N.*, et al.* (2011). Loss of memory B cells during chronic HIV infection is driven by Foxo3a- and TRAIL-mediated apoptosis. The Journal of Clinical Investigation *121*, 3877-3888.

Varfolomeev, E., Maecker, H., Sharp, D., Lawrence, D., Renz, M., Vucic, D., and Ashkenazi, A. (2005). Molecular Determinants of Kinase Pathway Activation by Apo2 Ligand/Tumor Necrosis Factor-related Apoptosis-inducing Ligand. Journal of Biological Chemistry *280*, 40599-40608.

Voelkel-Johnson, C., King, D. L., and Norris, J. S. (2002). Resistance of prostate cancer cells to soluble TNF-related apoptosis-inducing ligand (TRAIL/Apo2L) can be overcome by doxorubicin or adenoviral delivery of full-length TRAIL. Cancer Gene Ther *9*, 164-172.

Vogelstein, B., Fearon, E. R., Hamilton, S. R., Kern, S. E., Preisinger, A. C., Leppert, M., Smits, A. M. M., and Bos, J. L. (1988). Genetic Alterations during Colorectal-Tumor Development. New England Journal of Medicine *319*, 525-532.

Wagner, K. W., Punnoose, E. A., Januario, T., Lawrence, D. A., Pitti, R. M., Lancaster, K., Lee, D., von Goetz, M., Yee, S. F., Totpal, K.*, et al.* (2007). Death-receptor O-glycosylation controls tumor-cell sensitivity to the proapoptotic ligand Apo2L/TRAIL. Nat Med *13*, 1070-1077.

Wakefield, L. M., and Roberts, A. B. (2002). TGF-[beta] signaling: positive and negative effects on tumorigenesis. Current Opinion in Genetics & Development *12*, 22-29.

Wakelee, H. A., Patnaik, A., Sikic, B. I., Mita, M., Fox, N. L., Miceli, R., Ullrich, S. J., Fisher, G. A., and Tolcher, A. W. (2010). Phase I and pharmacokinetic study of lexatumumab (HGS-ETR2) given every 2 weeks in patients with advanced solid tumors. Annals of Oncology *21*, 376-381.

Walczak, H., Degli-Esposti, M. A., Johnson, R. S., Smolak, P. J., Waugh, J. Y., Boiani, N., Timour, M. S., Gerhart, M. J., Schooley, K. A., Smith, C. A.*, et al.* (1997). TRAIL-R2: a novel apoptosis-mediating receptor for TRAIL. EMBO J *16*, 5386-5397.

Walczak, H., Miller, R. E., Ariail, K., Gliniak, B., Griffith, T. S., Kubin, M., Chin, W., Jones, J., Woodward, A., Le, T.*, et al.* (1999a). Tumoricidal activity of tumor necrosis factor-related apoptosis-inducing ligand in vivo. Nat Med *5*, 157 - 163.

Walczak, H., Miller, R. E., Ariail, K., Gliniak, B., Griffith, T. S., Kubin, M., Chin, W., Jones, J., Woodward, A., Le, T.*, et al.* (1999b). Tumoricidal activity of tumor necrosis factor-related apoptosis-inducing ligand in vivo. Nat Med *5*, 157-163.

Wandinger, K.-P., Lunemann, J. D., Wengert, O., Bellmann-Strobl, J., Aktas, O., Weber, A., Grundstrom, E., Ehrlich, S., Wernecke, K.-D., Volk, H.-D., and Zipp, F. (2003). TNF-related apoptosis inducing ligand (TRAIL) as a potential response marker for interferon-beta treatment in multiple sclerosis. The Lancet *361*, 2036-2043.

Wang, F., Chan, C. H., Chen, K., Guan, X., Lin, H. K., and Tong, Q. (2011a). Deacetylation of FOXO3 by SIRT1 or SIRT2 leads to Skp2-mediated FOXO3 ubiquitination and degradation. Oncogene.

Wang, J., Chun, H. J., Wong, W., Spencer, D. M., and Lenardo, M. J. (2001). Caspase-10 is an initiator caspase in death receptor signaling. Proceedings of the National Academy of Sciences *98*, 13884-13888.

Wang, P., Lu, Y., Li, C., Li, N., Yu, P., and Ma, D. (2011b). Novel transcript variants of TRAIL show different activities in activation of NF-Œ ∫ B and apoptosis. Life Sciences *89*, 839-846.

Wang, Q., Ji, Y., Wang, X., and Evers, B. M. (2000). Isolation and Molecular Characterization of the 5'-Upstream Region of the Human TRAIL Gene. Biochemical and Biophysical Research Communications *276*, 466-471.

Wang, Q., Zhou, Y., Weiss, H. L., Chow, C.-W., and Evers, B. M. (2011c). NFATc1 Regulation of TRAIL Expression in Human Intestinal Cells. PLoS ONE *6*, e19882.

Wang, S., and El-Deiry, W. S. (2003). Requirement of p53 targets in chemosensitization of colonic carcinoma to death ligand therapy. Proceedings of the National Academy of Sciences *100*, 15095-15100.

Wang, W., and El-Deiry, W. S. (2004). Targeting FOXO Kills Two Birds with One Stone. Chemistry & biology *11*, 16-18.

Wang, W., Kim, S.-H., and El-Deiry, W. S. (2006). Small-molecule modulators of p53 family signaling and antitumor effects in p53-deficient human colon tumor xenografts. Proceedings of the National Academy of Sciences *103*, 11003-11008.

Weber, A., Wandinger, K.-P., Mueller, W., Aktas, O., Wengert, O., Grundstrom, E., Ehrlich, S., Windemuth, C., Kuhlmann, T., Wienker, T.*, et al.* (2004). Identification and functional characterization of a highly polymorphic region in the human TRAIL promoter in multiple sclerosis. Journal of Neuroimmunology *149*, 195-201.

Wiley, S., Schooley, K., Smolak, P., Din, W., Huang, C., Nicholl, J., Sutherland, G., Smith, T., Rauch, C., and Smith, C. e. a. (1995). Identification and characterization of a new member of the TNF family that induces apoptosis. Immunity *3*, 673–682.

Wiley SR, S. K., Smolak PJ, Din WS, Huang CP, Nicholl JK, Sutherland GR, Smith TD, Rauch C, Smith CA, et al. (1995). Identification and characterization of a new member of the TNF family that induces apoptosis. Immunity *3*, 673–682.

Woods, D. C., Alvarez, C., and Johnson, A. L. (2008). Cisplatin-mediated sensitivity to TRAIL-induced cell death in human granulosa tumor cells. Gynecologic Oncology *108*, 632-640.

Wosik, K., Biernacki, K., Khouzam, M.-P., and Prat, A. (2007). Death receptor expression and function at the human blood brain barrier. Journal of the neurological sciences *259*, 53-60.

Wu, G. S., Burns, T. F., McDonald, E. R., Jiang, W., Meng, R., Krantz, I. D., Kao, G., Gan, D.-D., Zhou, J.-Y., Muschel, R.*, et al.* (1997). KILLER/DR5 is a DNA damage-inducible p53-regulated death receptor gene. Nat Genet *17*, 141-143.

Wu, G. S., Burns, T. F., Zhan, Y., Alnemri, E. S., and El-Deiry, W. S. (1999). Molecular Cloning and Functional Analysis of the Mouse Homologue of the KILLER/DR5 Tumor Necrosis Factor-related Apoptosis-inducing Ligand (TRAIL) Death Receptor. Cancer Res *59*, 2770-2775.

Wu, J., Lee, S. W., Zhang, X., Han, F., Kwan, S. Y., Yuan, X., Yang, W. L., Jeong, Y. S., Rezaeian, A. H., Gao, Y.*, et al.* (2012). Foxo3a transcription factor is a negative regulator of Skp2 and Skp2 SCF complex. Oncogene.

Wu, X.-X., Jin, X.-H., Zeng, Y., El Hamed, A. M. A., and Kakehi, Y. (2007). Low concentrations of doxorubicin sensitizes human solid cancer cells to tumor necrosis factor-related apoptosis-inducing ligand (TRAIL)-receptor (R) 2-mediated apoptosis by inducing TRAIL-R2 expression. Cancer Science *98*, 1969-1976.

Wu, X.-X., and Kakehi, Y. (2009). Enhancement of Lexatumumab-Induced Apoptosis in Human Solid Cancer Cells by Cisplatin in Caspase-Dependent Manner. Clinical Cancer Research *15*, 2039-2047.

Xavier, S., Piek, E., Fujii, M., Javelaud, D., Mauviel, A., Flanders, K. C., Samuni, A. M., Felici, A., Reiss, M., Yarkoni, S.*, et al.* (2004). Amelioration of Radiation-induced Fibrosis. Journal of Biological Chemistry *279*, 15167-15176.

Xuan, Z., and Zhang, M. Q. (2005). From worm to human: bioinformatics approaches to identify FOXO target genes. Mechanisms of Ageing and Development *126*, 209-215.

Yamaguchi, H., and Wang, H.-G. (2004). CHOP Is Involved in Endoplasmic Reticulum Stress-induced Apoptosis by Enhancing DR5 Expression in Human Carcinoma Cells. Journal of Biological Chemistry *279*, 45495-45502.

Yamamura, Y., Lee, W. L., Inoue, K.-i., Ida, H., and Ito, Y. (2006). RUNX3 Cooperates with FoxO3a to Induce Apoptosis in Gastric Cancer Cells. Journal of Biological Chemistry *281*, 5267-5276.

Yan, X., Xu, L., Qi, J., Liang, X., Ma, C., Guo, C., Zhang, L., Sun, W., Zhang, J., Wei, X., and Gao, L. (2009). sTRAIL levels and TRAIL gene polymorphisms in Chinese patients with fatty liver disease. Immunogenetics *61*, 551-556.

Yanase, N., Hata, K., Shimo, K., Hayashida, M., Evers, B. M., and Mizuguchi, J. (2005). Requirement of c-Jun NH2-terminal kinase activation in interferon-alpha-induced apoptosis through upregulation of tumor necrosis factor-related apoptosis-inducing ligand (TRAIL) in Daudi B lymphoma cells. Experimental Cell Research *310*, 10-21.

Yang, J.-Y., Zong, C. S., Xia, W., Yamaguchi, H., Ding, Q., Xie, X., Lang, J.-Y., Lai, C.-C., Chang, C.-J., Huang, W.-C.*, et al.* (2008a). ERK promotes tumorigenesis by inhibiting FOXO3a via MDM2-mediated degradation. Nat Cell Biol *10*, 138-148.

Yang, W., Dolloff, N. G., and El-Deiry, W. S. (2008b). ERK and MDM2 prey on FOXO3a. Nat Cell Biol *10*, 125-126.

Yang, Y., Zhu, Y.-q., Jiang, L., Li, L.-f., and Ge, J.-p. (2011). Thalidomide induces apoptosis in human oral squamous cell carcinoma cell line with altered expression of tumor necrosis factor-related apoptosis-inducing ligand (TRAIL). Oral Oncology *47*, 927-928.

Yoshida, T., Shiraishi, T., Horinaka, M., Wakada, M., and Sakai, T. (2007). Glycosylation modulates TRAIL-R1/death receptor 4 protein: different regulations of two pro-apoptotic receptors for TRAIL by tunicamycin. Oncology Reports *18*, 1239-1242.

Yoshida, T., Shiraishi, T., Nakata, S., Horinaka, M., Wakada, M., Mizutani, Y., Miki, T., and Sakai, T. (2005). Proteasome Inhibitor MG132 Induces Death Receptor 5 through CCAAT/Enhancer-Binding Protein Homologous Protein. Cancer Research *65*, 5662-5667.

Yoshimochi, K., Daitoku, H., and Fukamizu, A. (2010). PCAF represses transactivation function of FOXO1 in an acetyltransferase-independent manner. Journal of Receptors and Signal Transduction *30*, 43-49.

Zamai, L., Ahmad, M., Bennett, I. M., Azzoni, L., Alnemri, E. S., and Perussia, B. (1998). Natural Killer (NK) Cell-mediated Cytotoxicity: Differential Use of TRAIL and Fas Ligand by Immature and Mature Primary Human NK Cells. J Exp Med *188*, 2375-2380.

Zhao, X., Gan, L., Pan, H., Kan, D., Majeski, M., Adam, S. A., and Unterman, T. G. (2004). Multiple elements regulate nuclear/cytoplasmic shuttling of FOXO1: characterization of phosphorylation- and 14-3-3-dependent and -independent mechanisms. Biochem J *378*, 839-849.

Zou, W., Yue, P., Khuri, F. R., and Sun, S.-Y. (2008). Coupling of Endoplasmic Reticulum Stress to CDDO-Me-Induced Up-regulation of Death Receptor 5 via a CHOP-Dependent Mechanism Involving JNK Activation. Cancer Research *68*, 7484-7492.